ELSEVIER

Physics Reports 374 (2003) 165–270

PHYSICS REPORTS

www.elsevier.com/locate/physrep

# Physics at CPLEAR

## CPLEAR Collaboration

A. Angelopoulos[a], A. Apostolakis[a,1], E. Aslanides[b], G. Backenstoss[c], P. Bargassa[d], C.P. Bee[b], O. Behnke[e], A. Benelli[c], V. Bertin[b], F. Blanc[d,f], P. Bloch[g], P. Carlson[h], M. Carroll[i], E. Cawley[i], M.B. Chertok[j], M. Danielsson[h], M. Dejardin[k], J. Derre[k], A. Ealet[b], C. Eleftheriadis[l], R. Ferreira-Marques[m], W. Fetscher[e], M. Fidecaro[g], A. Filipčič[n], D. Francis[j], J. Fry[i], E. Gabathuler[i], R. Gamet[i], H.-J. Gerber[e], A. Go[g], A. Haselden[i], P.J. Hayman[i], F. Henry-Couannier[b], R.W. Hollander[o], K. Jon-And[h], P.-R. Kettle[d], P. Kokkas[g], R. Kreuger[o], R. Le Gac[b], F. Leimgruber[c], I. Mandić[n], N. Manthos[p], G. Marel[k], M. Mikuž[n], J. Miller[j], F. Montanet[b], A. Muller[k], T. Nakada[d], B. Pagels[e], I. Papadopoulos[l], P. Pavlopoulos[c,*], A. Policarpo[m], G. Polivka[c], R. Rickenbach[c], B.L. Roberts[j], T. Ruf[g], L. Sakeliou[a], M. Schäfer[e], L.A. Schaller[f], T. Schietinger[c], A. Schopper[g], L. Tauscher[c], C. Thibault[q], F. Touchard[b], C. Touramanis[i], C.W.E. Van Eijk[o], S. Vlachos[c], P. Weber[e], O. Wigger[d], M. Wolter[e], C. Yèche[k], D. Zavrtanik[n], D. Zimmerman[j]

[a] *University of Athens, Greece*
[b] *CPPM, IN2P3-CNRS et Université d'Aix-Marseille II, France*
[c] *University of Basle, Switzerland*
[d] *Paul Scherrer Institut (PSI), Switzerland*
[e] *ETH-IPP Zürich, Switzerland*
[f] *University of Fribourg, Switzerland*
[g] *CERN, Geneva, Switzerland*
[h] *Royal Institute of Technology, Stockholm, Sweden*
[i] *University of Liverpool, UK*
[j] *Boston University, USA*
[k] *CEA, DSM/DAPNIA, CE-Saclay, France*
[l] *University of Thessaloniki, Greece*
[m] *LIP and University of Coimbra, Portugal*
[n] *J. Stefan Inst. and Phys. Dep., University of Ljubljana, Slovenia*
[o] *Delft University of Technology, Netherlands*

[*] Corresponding author. P. Pavlopoulos, CERN, CH-1211 Geneva 23, Switzerland.
*E-mail address:* noulis.pavlopoulos@cern.ch (P. Pavlopoulos).
[1] Deceased.


PII: S0370-1573(02)00367-8

[p] University of Ioannina, Greece
[q] CSNSM, IN2P3-CNRS, Orsay, France

Accepted 29 July 2002
editor: J.V. Allaby

**Abstract**

LEAR offered unique opportunities to study the symmetries which exist between matter and antimatter. At variance with other approaches at this facility, CPLEAR was an experiment devoted to the study of $\mathscr{CP}$, $\mathscr{T}$ and $\mathscr{CPT}$ symmetries in the neutral-kaon system. A variety of measurements allowed us to determine with high precision the parameters which describe the time evolution of the neutral kaons and their antiparticles, including decay amplitudes, and the related symmetry properties. Limits concerning quantum-mechanical predictions (EPR, coherence of the wave function) or the equivalence principle of general relativity have been obtained. An account of the main features of the experiment and its performances is given here, together with the results achieved.


*PACS:* 11.30.−j; 13.20.Eb

**Contents**

## 1. Introduction

The CPLEAR experiment at CERN [1] has performed measurements concerning a vast variety of subjects, such as symmetry properties of weak interactions ($\mathscr{T}, \mathscr{CP}, \mathscr{CPT}$), quantum coherence of the wave function, Bose–Einstein correlations in multipion states, regeneration of the short-lived kaon component in matter, the Einstein–Rosen–Podolski paradox using entangled neutral-kaon pair states, and the equivalence principle of general relativity.

To this end, 12 Tbytes of measured information were recorded (on 50 000 magnetic tapes), and 200 million productions and decays of neutral kaons have been reconstructed. In a most general analysis, the values of more than two dozens of parameters, mainly describing neutral kaons and their weak and electromagnetic decays, have been deduced, some with unprecedented precision, some for the first time.

The main reason that many experiments in nuclear and particle physics have focused on the study of symmetry properties of physical laws, is, that these properties lead, in a very direct way, to symmetries in experimentally observable quantities. This is exemplified in Table 1, below, where the relation of a particular symmetry of the Hamiltonian of the weak interaction to the corresponding asymmetry parameter, as measured by CPLEAR, is shown.

The main reason that the CPLEAR experiment has been able to contribute to so many fields of physics lies in the properties of the neutral kaons, paired with the high-intensity antiproton beam at CERN [2] and with the high-speed detector [3], which is able to visualize the complete event and to measure the locations, the momenta, and the charges of all the accompanying (charged) tracks, as well at the production of the neutral kaon, as at its decay. This allows one to know the quantum numbers of the kaon at its production and, in principle, at its decay.

A neutral kaon has the remarkable property [4,5] that the one physical quantity, strangeness, which could possibly distinguish it from its antiparticle, is not conserved, owing to the weak interaction. As a consequence, it becomes a very sensitive two-state system, ($|K_S\rangle$ and $|K_L\rangle$), which has a behaviour analogous to a (slowly decaying) particle of spin $1/2$ in a magnetic field, with which an NMR precession experiment is being performed. It is described by a wave function with an oscillation between the two states of strangeness $+1$, ($|K^0\rangle$), and of strangeness $-1$, ($|\bar{K}^0\rangle$). The oscillation frequency can conveniently be observed, as it happens to be comparable to the decay rate of the short-lived state, $|K_S\rangle$. Its magnitude ($\omega = 5.3 \times 10^9\ s^{-1}$) and the wave length of the resulting visible interference pattern in space (some cm, for CPLEAR energies), corresponding to the interfering wave functions, fit perfectly well to the technical performances of high-energy physics measuring equipment.

The tiny energy difference between the two states $|K_S\rangle$ and $|K_L\rangle$, $\hbar\omega = 3.5 \times 10^{-12}$ MeV, sets the scale for the sensitivity of the detection of a possible energy difference between $|K^0\rangle$ and $|\bar{K}^0\rangle$. Such a difference could e.g. occur from a $\mathscr{CPT}$-violating interaction or from a gravitational field which would act differently on a particle than on an antiparticle. It has also been conceived that quantum mechanics might be apparently violated by gravitation in such a way that pure states may develop into mixed states, which is highly forbidden otherwise. This would reduce the phase coherence of the wave functions and thus diminish the observable interference effects. CPLEAR has given limits to parameters describing these situations.

The neutral kaons used by the CPLEAR experiment are produced by antiproton annihilations in a high-pressure hydrogen gas. Sometimes, a pair of a neutral kaon and a neutral antikaon, $K^0\bar{K}^0$, is also produced. These happen to be (mostly) in an odd angular momentum state ($L = 1$), and, due to Bose statistics, are governed by a two-particle wave function, which is antisymmetric with respect to particle–antiparticle interchange. In this way, quantum mechanics predicts a high correlation in the behaviour of the two particles, even after they have gone far apart from each other, reminiscent of the EPR paradox. CPLEAR presents a measurement of this effect.

CPLEAR results and analyses were published timely [3,6–32]. As a completion of 15-years' work, we wish to present here a global and coherent view of the CPLEAR experiment.

The history of symmetry violations, in particular the one of neutral kaons, is full of beautiful surprises. Appendix A gives a summary of facts and literature [4,5,33–60]. These matters were dealt with in textbooks, see Refs. [61–65] and the most recent Refs. [66–68], and review papers, see e.g. [69–71]. The present study is limited to the neutral-kaon states, as encountered in the experiments, without any attempt to interpret the results at the quark level, see, however, Appendix B.

## 2. Description of the neutral-kaon system

### 2.1. Time evolution

The time evolution of a neutral kaon and of its decay products may be represented by the state vector

$$|\psi\rangle = \psi_{\mathrm{K}^0}(t)|\mathrm{K}^0\rangle + \psi_{\bar{\mathrm{K}}^0}(t)|\bar{\mathrm{K}}^0\rangle + \sum_m c_m(t)|m\rangle \tag{1}$$

which satisfies the Schrödinger equation

$$\mathrm{i}\,\frac{\mathrm{d}|\psi\rangle}{\mathrm{d}t} = \mathscr{H}|\psi\rangle\ . \tag{2}$$

In the Hamiltonian, $\mathscr{H} = \mathscr{H}_0 + \mathscr{H}_{\mathrm{wk}}$, $\mathscr{H}_0$ governs the strong and electromagnetic interactions. It is invariant with respect to the transformations $\mathscr{C}$, $\mathscr{P}$, $\mathscr{T}$, and it conserves the strangeness $S$. The states $|\mathrm{K}^0\rangle$ and $|\bar{\mathrm{K}}^0\rangle$ are common stationary eigenstates of $\mathscr{H}_0$ and $S$, with the mass $m_0$ and with opposite strangeness: $\mathscr{H}_0|\mathrm{K}^0\rangle = m_0|\mathrm{K}^0\rangle$, $\mathscr{H}_0|\bar{\mathrm{K}}^0\rangle = m_0|\bar{\mathrm{K}}^0\rangle$, $S|\mathrm{K}^0\rangle = |\mathrm{K}^0\rangle$, $S|\bar{\mathrm{K}}^0\rangle = -|\bar{\mathrm{K}}^0\rangle$. The states $|m\rangle$ are continuum eigenstates of $\mathscr{H}_0$ and represent the decay products. They are absent at the instant of production ($t = 0$) of the neutral kaon. The initial condition is thus

$$|\psi_0\rangle = \psi_{\mathrm{K}^0}(0)|\mathrm{K}^0\rangle + \psi_{\bar{\mathrm{K}}^0}(0)|\bar{\mathrm{K}}^0\rangle\ . \tag{3}$$

$\mathscr{H}_{\mathrm{wk}}$ governs the weak interactions. Since these do not conserve strangeness, a neutral kaon will, in general, change its strangeness as time evolves.

The symmetry properties of $\mathscr{H}_{\mathrm{wk}}$ with respect to the transformations $\mathscr{CPT}$, $\mathscr{T}$, and $\mathscr{CP}$ are the main subjects of the CPLEAR experiment.

Eq. (2) may be solved for the unknown functions $\psi_{\mathrm{K}^0}(t)$ and $\psi_{\bar{\mathrm{K}}^0}(t)$, by using a generalized Weisskopf–Wigner approximation [41] with the result [39,47]

$$\psi = \mathrm{e}^{-\mathrm{i}\Lambda t}\psi_0 \tag{4}$$

which also satisfies

$$\mathrm{i}\,\frac{\mathrm{d}\psi}{\mathrm{d}t} = \Lambda\psi\ , \tag{5}$$

where $\psi$ is the column vector with components $\psi_{\mathrm{K}^0}(t)$ and $\psi_{\bar{\mathrm{K}}^0}(t)$, $\psi_0$ equals $\psi$ at $t = 0$, and $\Lambda$ is the time-independent $2 \times 2$ matrix $(\Lambda_{\alpha\alpha'})$. All components refer to the two-dimensional basis $(|\mathrm{K}^0\rangle, |\bar{\mathrm{K}}^0\rangle)$. Expressed in terms of $\mathscr{H}_{\mathrm{wk}}$ (including second order in $\mathscr{H}_{\mathrm{wk}}$), and with the notation

$$\Lambda = \mathrm{M} - \frac{\mathrm{i}}{2}\Gamma\ , \tag{6a}$$

$$\mathrm{M} = \mathrm{M}^\dagger, \quad \Gamma = \Gamma^\dagger\ , \tag{6b}$$

Table 1
Relation between properties of $\mathscr{H}_{\rm wk}$ and observable quantities

| If $\mathscr{H}_{\rm wk}$ has the property | called | then | or |
|---|---|---|---|
| $\mathscr{T}^{-1}\mathscr{H}_{\rm wk}\mathscr{T}=\mathscr{H}_{\rm wk}$ | $\mathscr{T}$ invariance | $\Lambda_{\rm K^0\bar{K}^0}=\Lambda_{\rm \bar{K}^0K^0}$ | $A_{\rm T}=0$ |
| $(\mathscr{CPT})^{-1}\mathscr{H}_{\rm wk}(\mathscr{CPT})=\mathscr{H}_{\rm wk}$ | $\mathscr{CPT}$ invariance | $\Lambda_{\rm K^0K^0}=\Lambda_{\rm \bar{K}^0\bar{K}^0}$ | $A_{\rm CPT}=0$ |
| $(\mathscr{CP})^{-1}\mathscr{H}_{\rm wk}(\mathscr{CP})=\mathscr{H}_{\rm wk}$ | $\mathscr{CP}$ invariance | $\Lambda_{\rm K^0K^0}=\Lambda_{\rm \bar{K}^0\bar{K}^0}$ and | |
| | | $\Lambda_{\rm K^0\bar{K}^0}=\Lambda_{\rm \bar{K}^0K^0}$ | $A_{\rm CP}=0$ |

The last column indicates asymmetries of quantities which are measured in the CPLEAR experiment, as explained below. The relation $\Lambda_{\rm K^0\bar{K}^0}=\Lambda_{\rm \bar{K}^0K^0}$ is obtained by adopting a convenient phase convention (see later).

they are

$$\mathrm{M}_{\alpha\alpha'}=m_0\delta_{\alpha\alpha'}+\langle\alpha|\mathscr{H}_{\rm wk}|\alpha'\rangle+\mathscr{P}\sum_{\beta}\left(\frac{\langle\alpha|\mathscr{H}_{\rm wk}|\beta\rangle\langle\beta|\mathscr{H}_{\rm wk}|\alpha'\rangle}{m_0-E_\beta}\right)\ , \tag{7a}$$

$$\Gamma_{\alpha\alpha'}=2\pi\sum_{\beta}\langle\alpha|\mathscr{H}_{\rm wk}|\beta\rangle\langle\beta|\mathscr{H}_{\rm wk}|\alpha'\rangle\delta(m_0-E_\beta)\ , \tag{7b}$$

$$(\alpha,\alpha'=\mathrm{K}^0,\bar{\mathrm{K}}^0)\ .$$

Eqs. (7a) and (7b) enable one now to state directly the symmetry properties of $\mathscr{H}_{\rm wk}$ in terms of experimentally observable relations among the elements of $\Lambda$, see Table 1. We remark that $\mathscr{CPT}$ invariance imposes no restrictions on the off-diagonal elements, and that $\mathscr{T}$ invariance imposes no restrictions on the diagonal elements of $\Lambda$. $\mathscr{T}$ invariance implies $\Lambda_{\rm K^0\bar{K}^0}=\Lambda_{\rm \bar{K}^0K^0}$ within a convenient phase convention.

A speciality of this experiment is that each neutral kaon is produced with known strangeness, i.e. as $|\mathrm{K}^0\rangle$, or as $|\bar{\mathrm{K}}^0\rangle$. Due to certain rules governing the decay mechanisms or due to properties of the decay products, information of the neutral kaon state at the moment of its decay becomes known, e.g. the decay into two pions indicates a $\mathscr{CP}$ eigenstate with a positive eigenvalue, or the semileptonic decay indicates an eigenstate of definite strangeness with an eigenvalue equal to the value of the charge of the accompanying lepton. In order to interpret experimental results, we thus need to calculate the amplitudes for a strangeness eigenstate to develop into the same or into another eigenstate of strangeness, or into an eigenstate of $\mathscr{CP}$. The decay processes themselves are characterized by the amplitudes indicated in Eq. (7b). They are also used to measure properties of $\mathscr{H}_{\rm wk}$.

The probability amplitude for a state $|A\rangle$, produced at $t=0$, to become the state $|B\rangle$ at time $t$ equals

$$\langle B|\mathrm{e}^{-\mathrm{i}\Lambda t}|A\rangle\ . \tag{8}$$

We apply this to one of the most interesting manifestations of $\mathscr{T}$ violation [53,72,73]: the non-vanishing of the asymmetry $A_{\rm T}$, the first time measured by the CPLEAR experiment (see Section 5.3). The observation is that

the probability for a $\bar{\mathrm{K}}^0$ to become a $\mathrm{K}^0$ during the time interval $t$ is *different* from
the probability for the reverse development, namely *different* from
the probability for a $\mathrm{K}^0$ to become a $\bar{\mathrm{K}}^0$ during $t$.

The numerator of $A_T$ measures this difference:

$$A_T \equiv \frac{|\langle K^0|e^{-i\Lambda t}|\bar{K}^0\rangle|^2 - |\langle \bar{K}^0|e^{-i\Lambda t}|K^0\rangle|^2}{|\langle K^0|e^{-i\Lambda t}|\bar{K}^0\rangle|^2 + |\langle \bar{K}^0|e^{-i\Lambda t}|K^0\rangle|^2} = \frac{|\Lambda_{K^0\bar{K}^0}|^2 - |\Lambda_{\bar{K}^0K^0}|^2}{|\Lambda_{K^0\bar{K}^0}|^2 + |\Lambda_{\bar{K}^0K^0}|^2} \ . \tag{9}$$

$A_T$ is constant in time. The last term of Eq. (9) is the formal expression that a non-vanishing $A_T$ is necessary and sufficient for $\mathscr{T}$ violation in $\mathscr{H}_{wk}$. A direct way to calculate an equivalent term is presented in Ref. [73]. In the CPLEAR experiment $|K^0\rangle$ and $|\bar{K}^0\rangle$ states are produced by $\bar{p}p$ annihilations as mentioned in Section 1. The final states $\langle K^0|$ and $\langle \bar{K}^0|$ are tagged by the semileptonic decays.

The question whether the asymmetry $A_T \neq 0$ measured by CPLEAR constitutes direct evidence for time-reversal violation has been discussed in Refs. [74,75].

It has been explicitly proven [73] that the doubts expressed in Refs. [74,75] are not justified and that the asymmetry measured by CPLEAR is indeed directly related to the definition of $\mathscr{T}$ violation and not affected by time or decay processes. Moreover, the CPLEAR method of measuring $A_T$ (see Section 5.3) makes the result independent of any $\mathscr{CPT}$ or unitarity assumptions for the mixing matrix, or even possible invisible decay modes. We conclude therefore that CPLEAR indeed made the first direct measurement of $\mathscr{T}$ violation.

The measurement of $A_{CPT}$ has been performed as a test of $\mathscr{CPT}$ symmetry of $\mathscr{H}_{wk}$. The numerator of $A_{CPT}$ compares the probability for an antikaon to stay an antikaon with the probability for a kaon to stay a kaon:

$$A_{CPT} \equiv \frac{|\langle \bar{K}^0|e^{-i\Lambda t}|\bar{K}^0\rangle|^2 - |\langle K^0|e^{-i\Lambda t}|K^0\rangle|^2}{|\langle \bar{K}^0|e^{-i\Lambda t}|\bar{K}^0\rangle|^2 + |\langle K^0|e^{-i\Lambda t}|K^0\rangle|^2} \ . \tag{10}$$

$A_{CPT}$ has the property to vanish if $\Lambda_{K^0K^0} = \Lambda_{\bar{K}^0\bar{K}^0}$.

The measurement of the asymmetry $A_{CP}$ detects $\mathscr{CP}$ violation, and allows one to determine parameters which describe this violation. The numerator of $A_{CP}$ compares the development of an antikaon into an eigenstate of $\mathscr{CP}$, ($|f\rangle = 2^{-1/2}(|K^0\rangle \pm |\bar{K}^0\rangle)$), with that of a kaon:

$$A_{CP} \equiv \frac{|\langle f|e^{-i\Lambda t}|\bar{K}^0\rangle|^2 - |\langle f|e^{-i\Lambda t}|K^0\rangle|^2}{|\langle f|e^{-i\Lambda t}|\bar{K}^0\rangle|^2 + |\langle f|e^{-i\Lambda t}|K^0\rangle|^2} \ . \tag{11}$$

The formal expression for $A_{CP}$ has the property to depend on all four elements $\Lambda_{\alpha\alpha'}$, and $A_{CP} = 0$ if both conditions, $\Lambda_{K^0K^0} = \Lambda_{\bar{K}^0\bar{K}^0}$ *and* $\Lambda_{K^0\bar{K}^0} = \Lambda_{\bar{K}^0K^0}$, are fulfilled. (With a suitable choice of the phases in $\Lambda_{K^0\bar{K}^0}$ and $\Lambda_{\bar{K}^0K^0}$ it is sufficient to fulfill $|\Lambda_{K^0\bar{K}^0}|^2 = |\Lambda_{\bar{K}^0K^0}|^2$. See also Eq. (18) below.)

We wish to remark that these conclusions, as summarized in Table 1, have been reached without using any eigenstates from non-hermitian operators.

By solving Eq. (5), we obtain

$$\psi = e^{-i\Lambda t}\psi_0 = \begin{pmatrix} f_+ + 2\delta f_- & 2(\varepsilon - \sigma)f_- \\ -2(\varepsilon + \sigma)f_- & f_+ - 2\delta f_- \end{pmatrix} \psi_0 \tag{12}$$

with

$$f_{\pm}(t) = \frac{e^{-i\lambda_S t} \pm e^{-i\lambda_L t}}{2} \ , \tag{13}$$

$$\delta \equiv (\Lambda_{\bar{K}^0\bar{K}^0} - \Lambda_{K^0K^0})/(2\Delta\lambda) \ , \tag{14a}$$

$$\varepsilon \equiv (\Lambda_{\bar{K}^0K^0} - \Lambda_{K^0\bar{K}^0})/(2\Delta\lambda) \ , \tag{14b}$$

$$\sigma \equiv (\Lambda_{\bar{K}^0K^0} + \Lambda_{K^0\bar{K}^0})/(2\Delta\lambda) \ , \tag{14c}$$

where

$$\lambda_{L,S} = \tfrac{1}{2}(\Lambda_{K^0K^0} + \Lambda_{\bar{K}^0\bar{K}^0} \pm \sqrt{(\Lambda_{K^0K^0} - \Lambda_{\bar{K}^0\bar{K}^0})^2 + 4\Lambda_{K^0\bar{K}^0}\Lambda_{\bar{K}^0K^0}}) \tag{15}$$

and

$$\Delta\lambda = \lambda_L - \lambda_S \ . \tag{16}$$

The time evolutions of initial $|K^0\rangle$ and $|\bar{K}^0\rangle$ become

$$|K^0(t)\rangle = \left[f_+(t) + \frac{\Lambda_{\bar{K}^0\bar{K}^0} - \Lambda_{K^0K^0}}{\Delta\lambda} f_-(t)\right] |K^0\rangle - 2\frac{\Lambda_{\bar{K}^0K^0}}{\Delta\lambda} f_-(t)|\bar{K}^0\rangle \ ,$$

$$|\bar{K}^0(t)\rangle = \left[f_+(t) - \frac{\Lambda_{\bar{K}^0\bar{K}^0} - \Lambda_{K^0K^0}}{\Delta\lambda} f_-(t)\right] |\bar{K}^0\rangle - 2\frac{\Lambda_{K^0\bar{K}^0}}{\Delta\lambda} f_-(t)|K^0\rangle \ .$$

We recognize from Eq. (14a) and Table 1 that $\mathscr{CPT}$ invariance requires $\delta = 0$.

The interpretation of $\varepsilon$ is complicated by the fact, that it is defined in terms of non-observable quantities, $\Lambda_{K^0\bar{K}^0}$ and $\Lambda_{\bar{K}^0K^0}$. Since the vectors of the basis, $|K^0\rangle$ and $|\bar{K}^0\rangle$, as defined as common eigenstates of $\mathscr{H}_0$ and $S$, are indetermined by an arbitrary phase factor, each, it follows that $\Lambda_{K^0\bar{K}^0} = \langle K^0|\Lambda|\bar{K}^0\rangle$ and $\Lambda_{\bar{K}^0K^0} = \langle\bar{K}^0|\Lambda|K^0\rangle$ are both indetermined by the appropriate ratio of these factors. *The phase angles of these factors will now be fixed such as to give $\varepsilon$ a meaning with respect to $\mathscr{T}$ invariance*. Referring to Eq. (6b), we set $M_{K^0\bar{K}^0} = |M_{K^0\bar{K}^0}| \exp(i\phi_M)$ and $\Gamma_{K^0\bar{K}^0} = |\Gamma_{K^0\bar{K}^0}| \exp(i\phi_\Gamma)$, and we find

$$\varepsilon = 0 \quad \text{follows from } A_T = 0 \tag{17}$$

if the choice

$$\phi_\Gamma = \pm n\pi, \quad n = 0, 1, \ldots \tag{18}$$

is made. Then, $\mathscr{T}$ invariance requires $\varepsilon = 0$. Explicitly, we obtain

$$|\Lambda_{K^0\bar{K}^0}|^2 - |\Lambda_{\bar{K}^0K^0}|^2 = 2|M_{K^0\bar{K}^0}|\,|\Gamma_{K^0\bar{K}^0}| \sin(\phi_\Gamma - \phi_M) \ , \tag{19}$$

from which we see that $\mathscr{T}$ invariance requires also

$$(\phi_M - \phi_\Gamma) = \pm n\pi, \quad n = 0, 1, \ldots$$

and

$$\varepsilon = i\,(|\Lambda_{K^0\bar{K}^0}|^2 - |\Lambda_{\bar{K}^0K^0}|^2)/(2\Delta\lambda|\Gamma_{K^0\bar{K}^0}|) \ . \tag{20}$$

The phases of $\varepsilon$ and $\Delta\lambda$ are now simply related.

For $\varepsilon = |\varepsilon| e^{i\phi_\varepsilon}$,

$$\pm \tan(\phi_\varepsilon) = 2\Delta m/\Delta\Gamma \equiv \tan(\phi_{SW}) \ , \tag{21}$$

where we consider $\Delta m$ and $\Delta\Gamma$ as directly measured quantities related to $\Delta\lambda$ as $\Delta\lambda \equiv \lambda_L - \lambda_S = \Delta m + i\Delta\Gamma/2$, and the positive or negative sign holds depending on whether $|\Lambda_{K^0\bar{K}^0}|$ is greater or smaller than $|\Lambda_{\bar{K}^0K^0}|$. The quantity $\phi_{SW}$ is called the superweak phase.

We wish to emphasize that the conclusion expressed in Eq. (9), however, has been reached *without* any assumption on the phases of $\Lambda_{\bar{K}^0K^0}$ or $\Lambda_{K^0\bar{K}^0}$ or on the smallness of symmetry violations.

We now choose

$$\phi_\Gamma = 0.$$

*From now on this condition is required to be fulfilled.* Since violations of $\mathscr{T}$, $\mathscr{CP}$, and possibly $\mathscr{CPT}$, are small, we also assume

$$|\varepsilon| \ll 1 \quad \text{and} \quad |2\delta| \ll 1 \ . \tag{22}$$

This allows

$$\phi_M \approx \pi \ ,$$

$$\Delta\lambda \equiv \lambda_L - \lambda_S \approx 2\sqrt{\Lambda_{K^0\bar{K}^0}\Lambda_{\bar{K}^0K^0}} = 2(|M_{K^0\bar{K}^0}| + \frac{i}{2}|\Gamma_{K^0\bar{K}^0}|) \ ,$$

$$\Delta m = m_L - m_S \simeq 2|M_{K^0\bar{K}^0}|, \quad \Delta\Gamma = \Gamma_S - \Gamma_L \simeq 2|\Gamma_{K^0\bar{K}^0}| \ ,$$

$$2\bar{m} = m_L + m_S = M_{K^0K^0} + M_{\bar{K}^0\bar{K}^0}, \quad 2\bar{\Gamma} = \Gamma_L + \Gamma_S = \Gamma_{K^0K^0} + \Gamma_{\bar{K}^0\bar{K}^0} \ .$$

The parameters $m_{L,S}$ and $\Gamma_{L,S}$ signify the masses and decay widths of the eigenstates $|K_{L,S}\rangle$, respectively. The eigenvectors of $\Lambda$, whose time developments are expressed by the exponentials $\exp(-i\lambda_S t)$ and $\exp(-i\lambda_L t)$, respectively, are

$$|K_S\rangle = \frac{1}{\sqrt{2(1+|\varepsilon_S|^2)}}[(1+\varepsilon_S)|K^0\rangle + (1-\varepsilon_S)|\bar{K}^0\rangle] \ , \tag{23a}$$

$$|K_L\rangle = \frac{1}{\sqrt{2(1+|\varepsilon_L|^2)}}[(1+\varepsilon_L)|K^0\rangle - (1-\varepsilon_L)|\bar{K}^0\rangle] \ , \tag{23b}$$

where

$$\varepsilon_S = \varepsilon + \delta \quad \text{and} \quad \varepsilon_L = \varepsilon - \delta \ . \tag{24}$$

The time evolutions of an initial $K^0$ or $\bar{K}^0$ are then expressed, in the $(K^0, \bar{K}^0)$ basis (first line) or in the $(K_S, K_L)$ basis (second line), by the two following equations:

$$\begin{aligned} |\bar{K}^0(t)\rangle &= [f_+(t) + 2\delta f_-(t)]|K^0\rangle + (1-2\varepsilon)f_-(t)|\bar{K}^0\rangle \\ &= \frac{1}{\sqrt{2}}[(1-\varepsilon+\delta)e^{-i\lambda_S t}|K_S\rangle + (1-\varepsilon-\delta)e^{-i\lambda_L t}|K_L\rangle] \ , \end{aligned} \tag{25a}$$

$$|\bar{\mathrm{K}}^0(t)\rangle = [f_+(t) - 2\delta f_-(t)]|\bar{\mathrm{K}}^0\rangle + (1+2\varepsilon) f_-(t)|\mathrm{K}^0\rangle$$
$$= \frac{1}{\sqrt{2}}[(1+\varepsilon-\delta)\mathrm{e}^{-\mathrm{i}\lambda_S t}|\mathrm{K_S}\rangle - (1+\varepsilon+\delta)\mathrm{e}^{-\mathrm{i}\lambda_L t}|\mathrm{K_L}\rangle] \ . \tag{25b}$$

Finally, we derive the probabilities

$$\mathscr{P}_+(\tau) = \mathscr{P}(\mathrm{K}^0_{t=0} \to \mathrm{K}^0_{t=\tau})$$
$$= \tfrac{1}{4}[(1+4\,\mathrm{Re}(\delta))\mathrm{e}^{-\Gamma_S\tau} + (1-4\,\mathrm{Re}(\delta))\mathrm{e}^{-\Gamma_L\tau} + 2(\cos(\Delta m\tau) - 4\,\mathrm{Im}(\delta)\sin(\Delta m\tau))\mathrm{e}^{-\bar{\Gamma}\tau}] \ ,$$

$$\bar{\mathscr{P}}_+(\tau) = \mathscr{P}(\bar{\mathrm{K}}^0_{t=0} \to \mathrm{K}^0_{t=\tau})$$
$$= \tfrac{1}{4}[1+4\,\mathrm{Re}(\varepsilon)][\mathrm{e}^{-\Gamma_S\tau} + \mathrm{e}^{-\Gamma_L\tau} - 2\cos(\Delta m\tau)\mathrm{e}^{-\bar{\Gamma}\tau}] \ ,$$

$$\mathscr{P}_-(\tau) = \mathscr{P}(\mathrm{K}^0_{t=0} \to \bar{\mathrm{K}}^0_{t=\tau})$$
$$= \tfrac{1}{4}[1-4\,\mathrm{Re}(\varepsilon)][\mathrm{e}^{-\Gamma_S\tau} + \mathrm{e}^{-\Gamma_L\tau} - 2\cos(\Delta m\tau)\mathrm{e}^{-\bar{\Gamma}\tau}] \ ,$$

$$\bar{\mathscr{P}}_-(\tau) = \mathscr{P}(\bar{\mathrm{K}}^0_{t=0} \to \bar{\mathrm{K}}^0_{t=\tau})$$
$$= \tfrac{1}{4}[(1-4\,\mathrm{Re}(\delta))\mathrm{e}^{-\Gamma_S\tau} + (1+4\,\mathrm{Re}(\delta))\mathrm{e}^{-\Gamma_L\tau} + 2(\cos(\Delta m\tau) + 4\,\mathrm{Im}(\delta)\sin(\Delta m\tau))\mathrm{e}^{-\bar{\Gamma}\tau}] \ .$$

In order to base the analysis of experimental data on the relations presented above we need to know the strangeness or the $\mathscr{CP}$ parity of the neutral kaon at the moment just before its decay. The following sections quantify in how far this information can be gained from the decay processes, and describe the possibility to study the decay processes themselves.

### 2.2. Semileptonic and pionic decays as time and strangeness markers

In the CPLEAR experiment, pionic and semileptonic decays are the main tools to define a time $\tau$ subsequent to the production time ($t=0$): thus we can establish which symmetries are valid in the interaction responsible for the neutral-kaon time evolution. The choice of the decay mode depends on more factors than the simple decay-time definition. Pionic ($\pi\pi$ and $\pi\pi\pi$) final states (which are $\mathscr{CP}$ eigenstates or a superposition of them) are suitable for $\mathscr{CP}$ studies. Semileptonic ($\mathrm{e}\pi\nu$ and $\mu\pi\nu$) final states (which allow $\mathrm{K}^0$ to be differentiated from $\bar{\mathrm{K}}^0$ at the decay time) are convenient for $\mathscr{T}$ and $\mathscr{CPT}$ studies. These points will be made clear in the following sections where we give the explicit expressions of the decay rates. The measurement of the decay rates as a function of $\tau$ allows us to determine $\mathscr{T}$ and $\mathscr{CPT}$ parameters as well as $\mathscr{CP}$ parameters. This is best achieved by forming rate asymmetries (thus allowing the contribution of some systematic errors to be reduced).

#### 2.2.1. Decays to $\mathrm{e}\pi\nu$ and $\mu\pi\nu$

Firstly we introduce semileptonic decays, i.e. decays to $\ell\pi\nu$ ($\ell = \mathrm{e}, \mu$). Here, owing to the absence of final-state strong interactions, the dynamic situation is less complex than in the case of non-leptonic decays, i.e. decays to $\pi\pi$ and to $\pi\pi\pi$. Moreover, in the limit that the $\Delta S = \Delta Q$ rule holds [70,71], the charge-sign of the lepton $\ell$ in the final state is a tag of the strangeness of the neutral kaon at the decay time. We refer explicitly to $\mathrm{e}\pi\nu$ decays as these are relevant for the CPLEAR experiment.

The $\mu\pi\nu$ decays only play a subsidiary role in the experiment, and their phenomenological description is the same as that of $e\pi\nu$ decays, once the different kinematic conditions are taken into account.

For the instant decay of a $K^0$ or a $\bar{K}^0$ to a final state $e\pi\nu$, we can define four amplitudes,

$$\mathscr{A}_+ = \langle e^+\pi^-\nu|\mathscr{H}_{wk}|K^0\rangle, \quad \bar{\mathscr{A}}_- = \langle e^-\pi^+\bar{\nu}|\mathscr{H}_{wk}|\bar{K}^0\rangle \ , \tag{26a}$$

$$\mathscr{A}_- = \langle e^-\pi^+\bar{\nu}|\mathscr{H}_{wk}|K^0\rangle, \quad \bar{\mathscr{A}}_+ = \langle e^+\pi^-\nu|\mathscr{H}_{wk}|\bar{K}^0\rangle \ , \tag{26b}$$

each one being a function of the kinematical configuration (including spin) of the final state. Of these amplitudes, $\mathscr{A}_+$ and $\bar{\mathscr{A}}_-$ respect the $\Delta S = \Delta Q$ rule, $\mathscr{A}_-$ and $\bar{\mathscr{A}}_+$ violate it. Each amplitude can be further decomposed in two terms, of which one is $\mathscr{CPT}$ invariant and the other is $\mathscr{CPT}$ non-invariant [70,71].

$$\mathscr{A}_+ = a + b, \quad \bar{\mathscr{A}}_- = a^* - b^* \ , \tag{27a}$$

$$\mathscr{A}_- = c + d, \quad \bar{\mathscr{A}}_+ = c^* - d^* \ . \tag{27b}$$

The $\mathscr{CPT}$-invariant and -violating terms are given by $a$ and $b$, respectively, if the $\Delta S = \Delta Q$ rule holds, and by $c$ and $d$ if it is violated. As for $\mathscr{T}$, the imaginary parts of all amplitudes are $\mathscr{T}$ violating. It is further convenient to introduce the quantities

$$x = \frac{\bar{\mathscr{A}}_+}{\mathscr{A}_+}, \quad \bar{x} = \left(\frac{\mathscr{A}_-}{\bar{\mathscr{A}}_-}\right)^*, \quad y = \frac{\bar{\mathscr{A}}_-^* - \mathscr{A}_+}{\bar{\mathscr{A}}_-^* + \mathscr{A}_+} \ , \tag{28}$$

where $x$ and $\bar{x}$ parametrize the violation of the $\Delta S = \Delta Q$ rule in decays to positive and negative leptons, respectively, and $y = -b/a$ parametrizes $\mathscr{CPT}$ violation when the $\Delta S = \Delta Q$ rule holds. $\mathrm{Re}(a)$ is $\mathscr{T}$, $\mathscr{CPT}$ and $\mathscr{CP}$ invariant and dominates all other terms, hence $x$, $\bar{x}$ and $y$ are all $\ll 1$. The parameters $x_+ = (x + \bar{x})/2$ and $x_- = (x - \bar{x})/2$ describe the violation of the $\Delta S = \Delta Q$ rule in $\mathscr{CPT}$-conserving and $\mathscr{CPT}$-violating amplitudes, respectively.

Finally, neutral-kaon decays to $e\pi\nu$ are described by four independent decay rates, depending on the strangeness of the kaon ($K^0$ or $\bar{K}^0$) at the production time, $t = 0$, and on the charge of the decay lepton ($e^+$ or $e^-$):

$$R_+(\tau) \equiv R[K^0_{t=0} \to (e^+\pi^-\nu)_{t=\tau}], \quad \bar{R}_-(\tau) \equiv R[\bar{K}^0_{t=0} \to (e^-\pi^+\bar{\nu})_{t=\tau}] \ , \tag{29a}$$

$$R_-(\tau) \equiv R[K^0_{t=0} \to (e^-\pi^+\bar{\nu})_{t=\tau}], \quad \bar{R}_+(\tau) \equiv R[\bar{K}^0_{t=0} \to (e^+\pi^-\nu)_{t=\tau}] \ . \tag{29b}$$

The dependence of the rates on the decay eigentime $\tau$ and on various parameters is obtained by making use of Eqs. (26) and (27) and integrating over the phase space $\Omega$ of the final states:

$$R_+(\tau) = \int_\Omega |[f_+(\tau) + 2\delta f_-(\tau)].\mathscr{A}_+ + (1 - 2\varepsilon) f_-(\tau).\bar{\mathscr{A}}_+|^2 \, d\Omega \ , \tag{30a}$$

$$\bar{R}_-(\tau) = \int_\Omega |[f_+(\tau) - 2\delta f_-(\tau)].\bar{\mathscr{A}}_- + (1 + 2\varepsilon) f_-(\tau).\mathscr{A}_-|^2 \, d\Omega \ , \tag{30b}$$

$$R_-(\tau) = \int_\Omega |[f_+(\tau) + 2\delta f_-(\tau)].\mathscr{A}_- + (1 - 2\varepsilon) f_-(\tau).\bar{\mathscr{A}}_-|^2 \, d\Omega \ , \tag{30c}$$

$$\bar{R}_+(\tau) = \int_\Omega |[f_+(\tau) - 2\delta f_-(\tau)].\bar{\mathscr{A}}_+ + (1 + 2\varepsilon) f_-(\tau).\mathscr{A}_+|^2 \, d\Omega \ . \tag{30d}$$

If the decay amplitudes in Eqs. (26) and (27) do depend on the phase-space configuration of the final state, it is convenient to redefine the parameters $x$, $\bar{x}$ and $y$ through the following equations:

$$\mathscr{F}_+ = \int_\Omega |\mathscr{A}_+|^2 \,\mathrm{d}\Omega, \quad \mathscr{F}_- = \int_\Omega |\bar{\mathscr{A}}_-|^2 \,\mathrm{d}\Omega, \quad \mathscr{F} = \int_\Omega |\bar{\mathscr{A}}^*_- + \mathscr{A}_+|^2 \,\mathrm{d}\Omega \ ,$$

$$x = \frac{\int_\Omega \mathscr{A}^*_+ \bar{\mathscr{A}}_+ \,\mathrm{d}\Omega}{\mathscr{F}_+} \ , \quad \bar{x} = \frac{\int_\Omega \bar{\mathscr{A}}^*_- \mathscr{A}_- \,\mathrm{d}\Omega}{\mathscr{F}_-} \ , \quad \mathrm{Re}(y) = -\frac{1}{2}\frac{\mathscr{F}_+ - \mathscr{F}_-}{\mathscr{F}_+ + \mathscr{F}_-} \ . \tag{31}$$

If the decay amplitudes of Eqs. (26) and (27) are constant over the phase space, these definitions are essentially the same as Eq. (28)—more common in the current literature. The same conclusion is reached if the kinematical dependence can be factorized as a factor common to all four amplitudes (as is usual in $K^0_{e3}$ form-factor studies [15]).

Keeping only first-order terms in all parameters, the four independent decay rates can now be written as

$$\begin{aligned} R_+(\tau) = \frac{\mathscr{F}}{4}([1 + 2\,\mathrm{Re}(x) + 4\,\mathrm{Re}(\delta) - 2\,\mathrm{Re}(y)]\mathrm{e}^{-\Gamma_S\tau} + [1 - 2\,\mathrm{Re}(x) - 4\,\mathrm{Re}(\delta) - 2\,\mathrm{Re}(y)]\mathrm{e}^{-\Gamma_L\tau} \\ + \{2[1 - 2\,\mathrm{Re}(y)]\cos(\Delta m\tau) - [8\,\mathrm{Im}(\delta) + 4\,\mathrm{Im}(x)]\sin(\Delta m\tau)\}\mathrm{e}^{-(1/2)(\Gamma_S+\Gamma_L)\tau}) \ , \end{aligned} \tag{32a}$$

$$\begin{aligned} \bar{R}_-(\tau) = \frac{\mathscr{F}}{4}([1 + 2\,\mathrm{Re}(\bar{x}) - 4\,\mathrm{Re}(\delta) + 2\,\mathrm{Re}(y)]\mathrm{e}^{-\Gamma_S\tau} + [1 - 2\,\mathrm{Re}(\bar{x}) + 4\,\mathrm{Re}(\delta) + 2\,\mathrm{Re}(y)]\mathrm{e}^{-\Gamma_L\tau} \\ + \{2[1 + 2\,\mathrm{Re}(y)]\cos(\Delta m\tau) + [8\,\mathrm{Im}(\delta) + 4\,\mathrm{Im}(\bar{x})]\sin(\Delta m\tau)\}\mathrm{e}^{-(1/2)(\Gamma_S+\Gamma_L)\tau}) \ , \end{aligned} \tag{32b}$$

$$\begin{aligned} R_-(\tau) = \frac{\mathscr{F}}{4}([1 + 2\,\mathrm{Re}(\bar{x}) - 4\,\mathrm{Re}(\varepsilon) + 2\,\mathrm{Re}(y)]\mathrm{e}^{-\Gamma_S\tau} + [1 - 2\,\mathrm{Re}(\bar{x}) - 4\,\mathrm{Re}(\varepsilon) + 2\,\mathrm{Re}(y)]\mathrm{e}^{-\Gamma_L\tau} \\ - \{2[1 - 4\,\mathrm{Re}(\varepsilon) + 2\,\mathrm{Re}(y)]\cos(\Delta m\tau) + 4\,\mathrm{Im}(\bar{x})\sin(\Delta m\tau)\}\mathrm{e}^{-(1/2)(\Gamma_S+\Gamma_L)\tau}) \ , \end{aligned} \tag{32c}$$

$$\begin{aligned} \bar{R}_+(\tau) = \frac{\mathscr{F}}{4}([1 + 2\,\mathrm{Re}(x) + 4\,\mathrm{Re}(\varepsilon) - 2\,\mathrm{Re}(y)]\mathrm{e}^{-\Gamma_S\tau} + [1 - 2\,\mathrm{Re}(x) + 4\,\mathrm{Re}(\varepsilon) - 2\,\mathrm{Re}(y)]\mathrm{e}^{-\Gamma_L\tau} \\ - \{2[1 + 4\,\mathrm{Re}(\varepsilon) - 2\,\mathrm{Re}(y)]\cos(\Delta m\tau) - 4\,\mathrm{Im}(x)\sin(\Delta m\tau)\}\mathrm{e}^{-(1/2)(\Gamma_S+\Gamma_L)\tau}) \ . \end{aligned} \tag{32d}$$

Using the above rates, the asymmetries corresponding to Eqs. (9) and (10) are then written as

$$\begin{aligned} A_T(\tau) &= \frac{\bar{R}_+(\tau) - R_-(\tau)}{\bar{R}_+(\tau) + R_-(\tau)} \\ &= 4\,\mathrm{Re}(\varepsilon) - 2(\mathrm{Re}(y) + \mathrm{Re}(x_-)) + 2\,\frac{\mathrm{Re}(x_-)(\mathrm{e}^{-(1/2)\Delta\Gamma\tau} - \cos(\Delta m\tau)) + \mathrm{Im}(x_+)\sin(\Delta m\tau)}{\cosh(\frac{1}{2}\Delta\Gamma\tau) - \cos(\Delta m\tau)} \\ &\to 4\,\mathrm{Re}(\varepsilon) - 2(\mathrm{Re}(x_-) + \mathrm{Re}(y)) \quad \text{for } \tau \gg \tau_S \ , \end{aligned} \tag{33}$$

$$\begin{aligned} A_{CPT}(\tau) &= \frac{\bar{R}_-(\tau) - R_+(\tau)}{\bar{R}_-(\tau) + R_+(\tau)} \\ &= 2\frac{(2\,\mathrm{Re}(\delta) + \mathrm{Re}(x_-))\sinh(\frac{1}{2}\Delta\Gamma\tau)}{\cosh(\frac{1}{2}\Delta\Gamma\tau) + \cos(\Delta m\tau)} + 2\,\mathrm{Re}(y) + 2\,\frac{(2\,\mathrm{Im}(\delta) + \mathrm{Im}(x_+))\sin(\Delta m\tau)}{\cosh(\frac{1}{2}\Delta\Gamma\tau) + \cos(\Delta m\tau)} \\ &\to 4\,\mathrm{Re}(\delta) + 2(\mathrm{Re}(x_-) + \mathrm{Re}(y)) \quad \text{for } \tau \gg \tau_S \ . \end{aligned} \tag{34}$$

*2.2.2. Decays to $\pi\pi$*

In the neutral-kaon decays to $\pi\pi$, the two pions have a relative angular momentum $l=0$ and a $\mathscr{CP}$ eigenvalue $(-1)^l=+1$. These final states can be decomposed into a superposition of isospin eigenstates: here the isospin $I$ can take only values which are even and not greater than 2. The instant decay of a neutral kaon to two pions is then described by the amplitudes $\mathscr{A}_I$, $\bar{\mathscr{A}}_I$,

$$\mathscr{A}_I=\langle\pi\pi,I|\mathscr{H}_{\rm wk}|\mathrm{K}^0\rangle,\quad \bar{\mathscr{A}}_I=\langle\pi\pi,I|\mathscr{H}_{\rm wk}|\bar{\mathrm{K}}^0\rangle\ ,$$
$$\mathscr{A}_I=(A_I+B_I)\mathrm{e}^{\mathrm{i}\delta_I},\quad \bar{\mathscr{A}}_I=(A_I^*-B_I^*)\mathrm{e}^{\mathrm{i}\delta_I}\ , \tag{35}$$

where $I=0,2$. The amplitudes $A_I$ and $B_I$ are $\mathscr{CPT}$ symmetric and antisymmetric, respectively. The factor $\mathrm{e}^{\mathrm{i}\,\delta_I}$ represents the $\pi\pi$ final-state interaction: $\langle\pi\pi,I;out|\pi\pi,I;in\rangle=\mathrm{e}^{\mathrm{i}\delta_I}$, i.e. $\delta_I$ is the phase of the $\pi\pi$ S-wave scattering amplitude computed for the energy $m_{\rm K}$ and the isospin $I$. Using amplitudes (35) the rates of decays to $\pi\pi$ can be calculated along the same lines as the rates of decays to $e\pi\nu$.

Alternatively we can express the rates in terms of $\mathrm{K_S}$ and $\mathrm{K_L}$ decay amplitudes to the final state $f=\pi\pi$ (this approach is common when $f$ is a $\mathscr{CP}$ eigenstate—the relation between the two parametrizations is given in Section 8.3):

$$\mathscr{A}_{f\mathrm{S}}=\langle f|\mathscr{H}_{\rm wk}|\mathrm{K_S}\rangle\ ,\quad \mathscr{A}_{f\mathrm{L}}=\langle f|\mathscr{H}_{\rm wk}|\mathrm{K_L}\rangle\ . \tag{36}$$

Then for the decay rates, at a time $t=\tau$, of an initially pure $\mathrm{K}^0$ or $\bar{\mathrm{K}}^0$ state,

$$R_f(\tau)\equiv R[\mathrm{K}^0_{t=0}\to f_{t=\tau}],\quad \bar{R}_f(\tau)\equiv R[\bar{\mathrm{K}}^0_{t=0}\to f_{t=\tau}]\ , \tag{37}$$

we obtain from Eqs. (2.13)

$$\begin{aligned}\frac{R_f(\tau)}{\bar{R}_f(\tau)}&=\frac{[1\mp 2\,\mathrm{Re}(\varepsilon)]}{2}\{[1\pm 2\,\mathrm{Re}(\delta)]|\mathscr{A}_{f\mathrm{S}}|^2\mathrm{e}^{-\Gamma_{\mathrm{S}}\tau}+[1\mp 2\,\mathrm{Re}(\delta)]|\mathscr{A}_{f\mathrm{L}}|^2\mathrm{e}^{-\Gamma_{\mathrm{L}}\tau}\\&\quad\pm\mathrm{e}^{-(1/2)(\Gamma_{\mathrm{S}}+\Gamma_{\mathrm{L}})\tau}([1\pm 2\mathrm{i}\,\mathrm{Im}(\delta)]\mathscr{A}^*_{f\mathrm{L}}\mathscr{A}_{f\mathrm{S}}\mathrm{e}^{\mathrm{i}\Delta m\tau}+[1\mp 2\mathrm{i}\,\mathrm{Im}(\delta)]\mathscr{A}^*_{f\mathrm{S}}\mathscr{A}_{f\mathrm{L}}\mathrm{e}^{-\mathrm{i}\Delta m\tau})\}\ .\end{aligned} \tag{38}$$

In this context it is convenient to introduce the $\mathscr{CP}$-violating parameters $\eta_{\pi\pi}$,

$$\eta_{\pi\pi}=|\eta_{\pi\pi}|\mathrm{e}^{\mathrm{i}\phi_{\pi\pi}}=\left.\frac{\mathscr{A}_{f\mathrm{L}}}{\mathscr{A}_{f\mathrm{S}}}\right|_{\pi\pi}=\frac{\langle\pi\pi|\mathscr{H}_{\rm wk}|\mathrm{K_L}\rangle}{\langle\pi\pi|\mathscr{H}_{\rm wk}|\mathrm{K_S}\rangle}\ , \tag{39}$$

which are experimentally known to have a magnitude $|\eta_{\pi\pi}|\ll 1$. The parameter $\eta_{\pi\pi}$ becomes $\eta_{+-}$ or $\eta_{00}$ when the $\pi\pi$ state refers specifically to $\pi^+\pi^-$ and $\pi^0\pi^0$, respectively. With these definitions and $f=\pi^+\pi^-$, the rates become (again assuming the $\mathscr{CP}$-violating parameters to be small)

$$\begin{aligned}\frac{R_{\pi^+\pi^-}(\tau)}{\bar{R}_{\pi^+\pi^-}(\tau)}&=\frac{[1\mp 2\,\mathrm{Re}(\varepsilon-\delta)]}{2}\Gamma_{\mathrm{S}}^{\pi^+\pi^-}\\&\quad\times[\mathrm{e}^{-\Gamma_{\mathrm{S}}\tau}+|\eta_{+-}|^2\mathrm{e}^{-\Gamma_{\mathrm{L}}\tau}\pm 2|\eta_{+-}|\mathrm{e}^{-(1/2)(\Gamma_{\mathrm{S}}+\Gamma_{\mathrm{L}})\tau}\cos(\Delta m\tau-\phi_{+-})]\ ,\end{aligned} \tag{40}$$

where $\Gamma_{\mathrm{S}}^{\pi^+\pi^-}$ is the $\mathrm{K_S}\to\pi^+\pi^-$ partial decay width. Analogous expressions hold for the decay rates to $\pi^0\pi^0$. For decays to $\mathscr{CP}$ eigenstates, a difference between $\mathrm{K}^0$ and $\bar{\mathrm{K}}^0$ decay rates is an indication of $\mathscr{CP}$ violation. To study $\mathscr{CP}$-violation effects, it is then convenient to form the following rate

asymmetry:

$$A_{\mathrm{CP}}^{f}(\tau)=\frac{\bar{R}_f(\tau)-R_f(\tau)}{\bar{R}_f(\tau)+R_f(\tau)}$$

$$=2\,\mathrm{Re}(\varepsilon-\delta)-2\frac{|\eta_f|\mathrm{e}^{(1/2)(\Gamma_{\mathrm{S}}-\Gamma_{\mathrm{L}})\tau}\cos(\Delta m\tau-\phi_f)}{1+|\eta_f|^2\mathrm{e}^{(\Gamma_{\mathrm{S}}-\Gamma_{\mathrm{L}})\tau}}\ , \tag{41}$$

where $f=\pi^+\pi^-$ (and $\eta_f=\eta_{+-}$) or $f=\pi^0\pi^0$ (and $\eta_f=\eta_{00}$).

*2.2.3. Decays to $\pi\pi\pi$*

The description of the decay is more complex for the $\pi\pi\pi$ final states as a consequence of the variety of possible kinematic and isospin configurations. The $\pi\pi\pi$ final states can be decomposed into a superposition of states with definite total isospin $I$, and the amplitudes of a neutral-kaon decaying to $\pi\pi\pi$ can be written as a sum of products containing the isospin, angular momentum and energy–momentum dependencies [76,77].

The isospin can take all integer values between 0 and 3 for a $\pi^+\pi^-\pi^0$ state, and the values 1 and 3 for a $\pi^0\pi^0\pi^0$ state since the even isospin configurations of $\pi^0\pi^0\pi^0$ do not satisfy Bose statistics. The angular momentum dependence is defined in the $\pi^+\pi^-\pi^0$ state by the relative angular momentum $l$ between the two charged pions. This is also the relative angular momentum between the $\pi^+\pi^-$ subsystem and the $\pi^0$ owing to the zero spin of the neutral kaon. In the $\pi^0\pi^0\pi^0$ state, $l=0$ is the relative angular momentum between any two of the three $\pi^0$. The angular momentum also fixes the $\mathscr{CP}$ eigenvalue which is equal to $(-1)^l$.

The dependence of the amplitudes on the pion momenta is expressed as a function of the pion kinetic energies $E^*(\pi)$ in the kaon centre-of-mass, through the Dalitz variables $X$ and $Y$ with $X=(2m_{\mathrm{K}}/m_\pi^2)(E^*(\pi^+)-E^*(\pi^-))$ and $Y\simeq(2m_{\mathrm{K}}/m_\pi^2)(m_{\mathrm{K}}/3-E^*(\pi^0))$ in $\pi^+\pi^-\pi^0$ decays, and through equivalent quantities in $\pi^0\pi^0\pi^0$ decays (each of the kinetic energies entering $X$ and $Y$ refers to a different $\pi^0$). The probability to find a given momentum configuration for the $\pi^+\pi^-\pi^0$ state is given by the Dalitz distribution function (Dalitz plot).

The instant decay to three pions, in a state of isospin $I$ and angular momentum $l$, is described in general by the following amplitudes:

$$\mathscr{A}_{I,l}^{3\pi}=\langle\pi\pi\pi,I,l|\mathscr{H}_{\mathrm{wk}}|\mathrm{K}^0\rangle,\quad \bar{\mathscr{A}}_{I,l}^{3\pi}=\langle\pi\pi\pi,I,l|\mathscr{H}_{\mathrm{wk}}|\bar{\mathrm{K}}^0\rangle\ ,$$

$$\mathscr{A}_{I,l}^{3\pi}=a_{l,I}\mathrm{e}^{\mathrm{i}\delta_I}\ ,\quad \bar{\mathscr{A}}_{I,l}^{3\pi}=(-1)^{(l+1)}a_{l,I}^*\mathrm{e}^{\mathrm{i}\delta_I}\ , \tag{42}$$

where $a_{l,I}$ describes the part of the decay amplitude coming from the weak interaction (here assumed to be $\mathscr{CPT}$ invariant) and $\delta_I$ is the phase of the scattering amplitude describing the interaction of the final-state pions. The latter is expected to be small owing to the small phase-space available to these pions, in contrast to the two-pion decays. The $\mathrm{K_L}$ and $\mathrm{K_S}$ amplitudes are given by

$$\mathscr{A}_{\mathrm{L}}^{l,I}=\frac{1}{\sqrt{2}}[(1+\varepsilon_{\mathrm{L}})a_{l,I}-(-1)^{l+1}(1-\varepsilon_{\mathrm{L}})a_{l,I}^*]\mathrm{e}^{\mathrm{i}\delta_I}\ ,$$

$$\mathscr{A}_{\mathrm{S}}^{l,I}=\frac{1}{\sqrt{2}}[(1+\varepsilon_{\mathrm{S}})a_{l,I}+(-1)^{l+1}(1-\varepsilon_{\mathrm{S}})a_{l,I}^*]\mathrm{e}^{\mathrm{i}\delta_I}\ . \tag{43}$$

These amplitudes, properly summed over the possible values of $I$ and $l$, give the $\mathrm{K_S}$ and $\mathrm{K_L}$ decay amplitudes $\mathscr{A}_{\mathrm{S}}^{3\pi}(X,Y)$ and $\mathscr{A}_{\mathrm{L}}^{3\pi}(X,Y)$, as shown in Eq. (60). They are different depending on whether

the decay is to $\pi^+\pi^-\pi^0$ or to $\pi^0\pi^0\pi^0$. The rates corresponding to decays at the point $(X,Y)$ of the phase space at time $\tau$ are then expressed as

$$\begin{matrix} R_{3\pi}(X,Y,\tau) \\ \bar{R}_{3\pi}(X,Y,\tau) \end{matrix} \propto [1 \mp 2\,\mathrm{Re}(\varepsilon+\delta)]\mathrm{e}^{-\Gamma_\mathrm{L}\tau}\,|\mathscr{A}_\mathrm{L}^{3\pi}(X,Y)|^2 \pm \mathrm{e}^{-(\Gamma_\mathrm{S}+\Gamma_\mathrm{L})\tau/2} \times\{\mathrm{Re}[\mathscr{A}_\mathrm{S}^{3\pi}(X,Y)\mathscr{A}_\mathrm{L}^{3\pi}(X,Y)^*]\cos(\Delta m\tau) - \mathrm{Im}[\mathscr{A}_\mathrm{S}^{3\pi}(X,Y)\mathscr{A}_\mathrm{L}^{3\pi}(X,Y)^*]\sin(\Delta m\tau)\}\,. \tag{44}$$

(These are the rates of Eq. (38) when, as shown later, $|\mathscr{A}_\mathrm{S}^{3\pi}(X,Y)|^2 \ll |\mathscr{A}_\mathrm{L}^{3\pi}(X,Y)|^2$.) Furthermore we may consider the $\mathscr{CP}$ symmetry of the final state:

$$\begin{aligned} \mathscr{A}_\mathrm{S}^{3\pi}(X,Y) &= \mathscr{A}_\mathrm{S}^{3\pi(\mathrm{CP}=+1)}(X,Y) + \mathscr{A}_\mathrm{S}^{3\pi(\mathrm{CP}=-1)}(X,Y)\,, \\ \mathscr{A}_\mathrm{L}^{3\pi}(X,Y) &= \mathscr{A}_\mathrm{L}^{3\pi(\mathrm{CP}=+1)}(X,Y) + \mathscr{A}_\mathrm{L}^{3\pi(\mathrm{CP}=+1)}(X,Y)\,. \end{aligned} \tag{45}$$

Since weak transitions with $\Delta I = 1/2$ are known [71] to be dominant, only the decays to $\pi^+\pi^-\pi^0$ ($I = 0,1$) and to $\pi^0\pi^0\pi^0$ ($I = 1$) are relevant here. In addition, the kaon mass is very close to the total mass of the three pions, thus their kinetic energy is small in the kaon centre-of-mass, large angular momenta are suppressed due to the centrifugal barrier and only the values $l = 0$ and $l = 1$ need to be considered. Hence, the amplitudes of $\pi^0\pi^0\pi^0$ decays, $\mathscr{A}_\mathrm{S}^{000}(X,Y)$ and $\mathscr{A}_\mathrm{L}^{000}(X,Y)$, contain only $\mathscr{CP} = -1$ ($l = 0$) terms and are symmetric in $X$. Since $\mathrm{K_S}$ and $\mathrm{K_L}$ are mainly $\mathscr{CP}$ even and odd, respectively, these amplitudes are in turn $\mathscr{CP}$ non-invariant and $\mathscr{CP}$ invariant.

As for the decay to $\pi^+\pi^-\pi^0$, the $\mathrm{K_L}$ decay amplitude to a $l = 1$ state is suppressed both by $\mathscr{CP}$ violation and centrifugal barrier, thus $\mathscr{A}_\mathrm{L}^{+-0}(X,Y) \simeq \mathscr{A}_\mathrm{L}^{3\pi(\mathrm{CP}=-1)}(X,Y)$, again symmetric in $X$. The $\mathrm{K_S}$ decay amplitude instead contains both ($l = 0$) and ($l = 1$) terms—the first is suppressed by $\mathscr{CP}$ violation and the second, allowed by $\mathscr{CP}$, is suppressed by centrifugal barrier—with the property that $\mathscr{A}_\mathrm{S}^{+-0}(-X,Y) = -\mathscr{A}_\mathrm{S}^{3\pi(\mathrm{CP}=+1)}(X,Y) + \mathscr{A}_\mathrm{S}^{3\pi(\mathrm{CP}=-1)}(X,Y)$.

The integration over the Dalitz plot between the $Y$ boundaries and over $X > 0$ or $X < 0$ leads from Eq. (44) to the following integrated rates for the decays to $\pi\pi\pi$:

$$\begin{matrix} R_{3\pi}(X>0,\tau) \\ \bar{R}_{3\pi}(X>0,\tau) \end{matrix} \propto [1 \mp 2\,\mathrm{Re}(\varepsilon+\delta)]\mathrm{e}^{-\Gamma_\mathrm{L}\tau} \pm 2[\mathrm{Re}(\eta_{\pi\pi\pi}+\lambda)\cos(\Delta m\tau) - \mathrm{Im}(\eta_{\pi\pi\pi}+\lambda)\sin(\Delta m\tau)]\mathrm{e}^{-(\Gamma_\mathrm{S}+\Gamma_\mathrm{L})\tau/2}\,,$$

$$\begin{matrix} R_{3\pi}(X<0,\tau) \\ \bar{R}_{3\pi}(X<0,\tau) \end{matrix} \propto [1 \mp 2\,\mathrm{Re}(\varepsilon+\delta)]\mathrm{e}^{-\Gamma_\mathrm{L}\tau} \pm 2[\mathrm{Re}(\eta_{\pi\pi\pi}-\lambda)\cos(\Delta m\tau) - \mathrm{Im}(\eta_{\pi\pi\pi}-\lambda)\sin(\Delta m\tau)]\mathrm{e}^{-(\Gamma_\mathrm{S}+\Gamma_\mathrm{L})\tau/2}\,.$$

Here, using a similar approach to that for $\pi\pi$ decays, we have introduced the $\mathscr{CP}$-violating parameter $\eta_{\pi\pi\pi}$ and the $\mathscr{CP}$-conserving parameter $\lambda$ defined as

$$\lambda = \frac{\int_{X>0} \mathscr{A}_\mathrm{L}^{*\,3\pi(\mathrm{CP}=-1)}(X,Y)\mathscr{A}_\mathrm{S}^{3\pi(\mathrm{CP}=-1)}(X,Y)\,\mathrm{d}X\,\mathrm{d}Y}{\int_{X>0} |\mathscr{A}_\mathrm{L}^{3\pi(\mathrm{CP}=-1)}(X,Y)|^2\,\mathrm{d}X\,\mathrm{d}Y}\,, \tag{46}$$

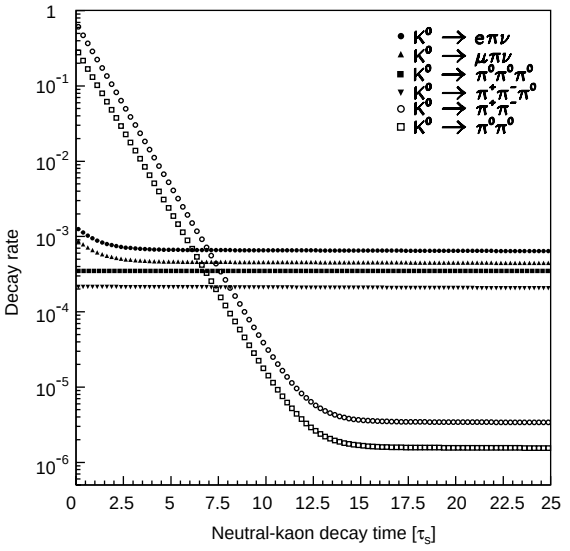


Fig. 1. Neutral-kaon decay rates for the main decay modes, versus the decay time $\tau$ (in units of the $K_S$ mean lifetime $\tau_S$). The rates are averaged over an equal number of initial $K^0$ and $\bar{K}^0$; their sum is normalized to unity.

$$\eta_{\pi\pi\pi} = \frac{\int_\Omega \mathscr{A}_L^{*\,3\pi(CP=-1)}(X,Y)\mathscr{A}_S^{3\pi(CP=-1)}(X,Y)\,dX\,dY}{\int_\Omega |\mathscr{A}_L^{3\pi(CP=-1)}(X,Y)|^2\,dX\,dY}\ , \tag{47}$$

where $\Omega$ is the phase space of the final states. There is no $\lambda$ contribution in the $\pi^0\pi^0\pi^0$ decay rates since $\lambda \equiv 0$ for these decays. This is in contrast to $\pi^+\pi^-\pi^0$ decays where the $\lambda$ term cancels in the rates only if they are integrated over the whole phase space ($X \lessgtr 0$). The $\mathscr{CP}$-violation effects are conveniently extracted, forming the following decay rate asymmetry:

$$A_{CP}^f(\tau) = \frac{\bar{R}_f(\tau) - R_f(\tau)}{\bar{R}_f(\tau) + R_f(\tau)} = 2\,\mathrm{Re}(\varepsilon+\delta) - 2|\eta_f|e^{-(1/2)(\Gamma_S-\Gamma_L)\tau}\cos(\Delta m\tau + \phi_f)\ , \tag{48}$$

where $f = \pi^+\pi^-\pi^0$ (and $\eta_f = \eta_{+-0}$) or $f = \pi^0\pi^0\pi^0$ (and $\eta_f = \eta_{000}$). Note that the expressions of the rate asymmetries in the case of decay to $\pi\pi$ and to $\pi\pi\pi$ are equal except for an opposite sign in front of $\delta$ and $\phi_f$.

### 2.2.4. Summary of neutral-kaon decay rates

The decay rates averaged over an equal number of initial $K^0$ and $\bar{K}^0$ are shown in Fig. 1 for the main decay modes. These rates depend more or less explicitly on the validity of the symmetries under study. Such dependence is summarized separately for the parameters of the time evolution (Table 2) and the decay amplitudes (Table 3 for decays to $e\pi\nu$ and Table 4 for decays to $\pi\pi$). It should be noted that since the decay amplitudes can be rephased, only the ratios between these amplitudes are relevant.

From the measured rates we extract the symmetry-breaking parameters by forming decay-rate asymmetries. The use of the asymmetries is discussed in detail in the following sections. We will

Table 2
The properties of the $\Lambda$-matrix elements under the assumption of $\mathscr{CPT}$, $\mathscr{T}$ and $\mathscr{CP}$ invariance and the parameters which describe the breaking of these symmetries. (As mentioned in Table 1 $|\Lambda_{K^0\bar{K}^0}| = |\Lambda_{\bar{K}^0K^0}|$ becomes equivalent to $\Lambda_{K^0\bar{K}^0} = \Lambda_{\bar{K}^0K^0}$ under a certain phase convention)

| Symmetry | $\Lambda$-matrix properties | Parameters |
|---|---|---|
| $\mathscr{CPT}$ | $\Lambda_{K^0K^0} = \Lambda_{\bar{K}^0\bar{K}^0}$ | $\delta$ |
| $\mathscr{T}$ | $\lvert\Lambda_{K^0\bar{K}^0}\rvert = \lvert\Lambda_{\bar{K}^0K^0}\rvert$ | $\varepsilon$ |
| $\mathscr{CP}$ | $\Lambda_{K^0K^0} = \Lambda_{\bar{K}^0\bar{K}^0}$ | $\varepsilon_L = \varepsilon - \delta$ |
| | and | $\varepsilon_S = \varepsilon + \delta$ |
| | $\lvert\Lambda_{K^0\bar{K}^0}\rvert = \lvert\Lambda_{\bar{K}^0K^0}\rvert$ | |

Table 3
The properties of the e$\pi\nu$ decay amplitudes under the assumption of $\mathscr{CPT}$, $\mathscr{T}$ and $\mathscr{CP}$ invariance: the sign + (−) stands for different from (equal to) zero. $\mathscr{T}$ invariance implies that the amplitudes are real, thus $x$, $\bar{x}$, and $y$ are real; $\mathscr{CP}$ invariance requires that $x = \bar{x}^*$ and $y$ are imaginary; $\mathscr{CPT}$ invariance results in $y = 0$ and $x = \bar{x}$

| Symmetry | Re($a$), Re($c$) | Im($a$), Im($c$) | Re($b$), Re($d$) | Im($b$), Im($d$) |
|---|---|---|---|---|
| $\mathscr{CPT}$ | + | − | − | + |
| $\mathscr{T}$ | + | − | + | − |
| $\mathscr{CP}$ | + | + | − | − |

Table 4
The properties of the $\pi\pi$ decay amplitudes under the assumption of $\mathscr{CPT}$, $\mathscr{T}$ and $\mathscr{CP}$ invariance: the sign + (−) stands for different from (equal to) zero

| Symmetry | Re($A_I$) | Im($A_I$) | Re($B_I$) | Im($B_I$) |
|---|---|---|---|---|
| $\mathscr{CPT}$ | + | − | − | + |
| $\mathscr{T}$ | + | − | + | − |
| $\mathscr{CP}$ | + | + | − | − |

show how to handle the complications arising from theory because of the decay amplitudes (see above), and from experimental constraints (leading to the measurement of $A_T^{exp}$, $A_\delta^{exp}$ for $A_{CPT}$, and $A_f^{exp}$ for $A_{CP}^f$. Some of the rate asymmetries are sensitive to $\Delta m$, one of the time-evolution parameters, which was also measured (using e$\pi\nu$ and $\pi^+\pi^-$ decays). The other parameter $\Delta\Gamma$ was obtained from external measurements [78]. The physics content of each asymmetry will be discussed later together with the results of our measurements.

The measurements of the decay rates also give access to other quantities not directly related to the discrete symmetries, such as the $K^0_{e3}$ form factor or the parameters describing the Dalitz plot in the neutral-kaon decay to three pions. For these, somewhat different analyses were required [9,15].

### 2.3. Regeneration effects

Regeneration of neutral kaons [79,80] plays an important role in most experiments that measure $\mathscr{CP}$ violation in the neutral-kaon system, either because regeneration is employed to produce a $K_S$ beam or because $K_S$ regenerated in detector material can fake $\mathscr{CP}$-violating $K_L$ decays.

The regenerating power of a medium is given by the difference, $\Delta f = f(0) - \bar{f}(0)$, between the nuclear forward scattering amplitudes of $K^0$ and $\bar{K}^0$, which is also called the *regeneration amplitude* [81]. In the neutral-kaon time evolution, regeneration appears as an effective $\mathscr{CPT}$ violation as the following equation holds:

$$i\frac{\partial}{\partial\tau}\psi(\tau) = \left[\Lambda - \frac{2\pi N}{m}\begin{pmatrix} f(0) & 0 \\ 0 & \bar{f}(0) \end{pmatrix}\right]\psi(\tau)\ .$$

When the asymmetry, for instance the asymmetry of the decay rates to $\pi^+\pi^-$, is measured in a regenerating medium, additional terms of the form

$$|\varrho|\cos(\Delta m\tau - \phi_{+-} + \arg(\varrho))$$

appear, where $\varrho$ depends on the properties of the medium and is proportional to $\Delta f$ [23]. The result is a pronounced change of the oscillation pattern of Eq. (41). This can be regarded as due to an additional interference, between inherent and regenerated $K_S$ amplitudes, or as an amplification of the asymmetry caused by the unequal interaction of $K^0$ and $\bar{K}^0$ in the medium. If the regenerating medium is only present in a limited range of lifetimes (i.e. neutral kaons of a given momentum cross an absorber of a certain thickness), there will be a sharp step in the asymmetry in that range (cf. Ref. [23]).

### 2.4. Strong interactions as time and strangeness markers

The conservation of strangeness in strong interactions dictates that the strangeness of the final state is equal to that of the initial state. This fact is practically exploitable with exclusive reactions containing only a few particles, thus in the low energy range. It allows neutral kaons of known strangeness to be produced starting from beams of positive or negative kaons. For instance, in Ref. [82] opposite-sign kaon beams were used to produce $K^0$ and $\bar{K}^0$ by elastic charge-exchange in carbon (thus $K^0$ and $\bar{K}^0$ decay rates to $\pi^+\pi^-$ could be compared). Similarly, in Ref. [83] $K^0$ were obtained by inelastic charge-exchange of positive kaons in hydrogen. CPLEAR instead produced concurrently $K^0$ and $\bar{K}^0$ starting from $\bar{p}p$ annihilations, by selecting two convenient channels as shown in Section 3.1. In these annihilation channels a $K^0$ is accompanied by a $K^-$, and a $\bar{K}^0$ by a $K^+$. The kaon strangeness at production is thus tagged by measuring the charge sign of the accompanying charged kaon.

In order to identify the strangeness at a later time $t = \tau$, the neutral kaon could be allowed to interact in a thin slab of matter (in most cases bound nucleons), for instance in one of the following reactions:

$$K^0 + p \to K^+ + n, \quad \bar{K}^0 + n \to K^+ + p, \quad \bar{K}^0 + n \to \pi^0 + \Lambda(\to \pi^- p)\ .$$

CPLEAR made use of this option with the set-up modified for the measurement of the regeneration amplitude, see Section 7.

## 3. CPLEAR: the experiment

### 3.1. Experimental method

The method chosen by CPLEAR was to make use of the charge-conjugate particles $K^0$ and $\bar{K}^0$ produced in $\bar{p}p$ collisions, which have a flavour of strangeness different for particles ($K^0$) and antiparticles ($\bar{K}^0$). The strangeness, properly monitored, is an ideal tool to label (tag) $K^0$ and $\bar{K}^0$, whose subsequent evolution in time under weak interaction can thus be analysed and compared.

Initially-pure $K^0$ and $\bar{K}^0$ states were produced concurrently by antiproton annihilation at rest in a hydrogen target via the *golden* channels:

$$\bar{p}p \rightarrow \begin{matrix} K^-\pi^+K^0 \\ K^+\pi^-\bar{K}^0 \end{matrix} , \tag{49}$$

each having a branching ratio of $\approx 2\times 10^{-3}$. The conservation of strangeness in the strong interaction dictates that a $K^0$ is accompanied by a $K^-$, and a $\bar{K}^0$ by a $K^+$. Hence, the strangeness of the neutral kaon at production was tagged by measuring the charge sign of the accompanying charged kaon, and was therefore known event by event. The momentum of the produced $K^0$ ($\bar{K}^0$) was obtained from measurement of the $\pi^{\pm}K^{\mp}$ pair kinematics. If the neutral kaon subsequently decayed to $e\pi\nu$, its strangeness could also be tagged at the decay time by the charge of the decay electron: in the limit that only transitions with $\Delta S = \Delta Q$ take place, neutral kaons decay to $e^+$ if the strangeness is positive at the decay time and to $e^-$ if it is negative. This clearly was not possible for neutral-kaon decays to two or three pions.

For each initial strangeness, the number of neutral-kaon decays was measured as a function of the decay time $\tau$. These numbers, $N_f(\tau)$ and $\bar{N}_f(\tau)$ for a non-leptonic final state $f$, or $N_{\pm}(\tau)$ and $\bar{N}_{\mp}(\tau)$ for an $e\pi\nu$ final state, were combined to form asymmetries—thus dealing mainly with ratios between measured quantities. However, the translation of measured numbers of events into decay rates requires (a) acceptance factors which do not cancel in the asymmetry, (b) residual background, and (c) regeneration effects to be taken into account. These experimental complications were handled essentially with the same procedure in the different asymmetries. Thus, here we exemplify the procedure referring to $e\pi\nu$ decays: the changes which are in order for other decays are discussed when reporting these measurements.

(a) Detecting and strangeness-tagging neutral kaons at production and decay relied on measuring, at the production (primary) vertex, a $K^{\pm}\pi^{\mp}$ track-pair and the corresponding momenta $\vec{p}_{K^{\pm}}$ and $\vec{p}_{\pi^{\mp}}$, and, at the decay (secondary) vertex, an $e^{\mp}\pi^{\pm}$ track-pair and the corresponding momenta $\vec{p}_{e^{\mp}}$ and $\vec{p}_{\pi^{\pm}}$. The detection (tagging) efficiencies of the $K^{\pm}\pi^{\mp}$ track-pairs depend on the pair charge configuration and momenta, and are denoted by $\epsilon(\vec{p}_{K^{\pm}}, \vec{p}_{\pi^{\mp}})$. A similar dependence exists for the detection efficiencies of the $e^{\mp}\pi^{\pm}$ track-pairs, $\epsilon(\vec{p}_{e^{\mp}}, \vec{p}_{\pi^{\pm}})$. Since the detection efficiencies of primary and secondary track-pairs were mostly uncorrelated, the acceptance of a signal ($e\pi\nu$) event was factorized as $\varrho_S \times \epsilon(\vec{p}_{K^{\pm}}, \vec{p}_{\pi^{\mp}}) \times \epsilon(\vec{p}_{e^{\mp}}, \vec{p}_{\pi^{\pm}})$. The factor $\varrho_S$ represents the portion of the acceptance which does not depend on the charge configuration of either primary or secondary particles. The acceptances of the events corresponding to different charge

configurations were then equalized (or normalized) by introducing two functions:

$$\xi(\vec{p}_{\mathrm{K}}, \vec{p}_{\pi}) \equiv \frac{\epsilon(\vec{p}_{\mathrm{K}^+}, \vec{p}_{\pi^-})}{\epsilon(\vec{p}_{\mathrm{K}^-}, \vec{p}_{\pi^+})} ,$$

$$\eta(\vec{p}_{\mathrm{e}}, \vec{p}_{\pi}) \equiv \frac{\epsilon(\vec{p}_{\mathrm{e}^-}, \vec{p}_{\pi^+})}{\epsilon(\vec{p}_{\mathrm{e}^+}, \vec{p}_{\pi^-})} .$$

These functions, referred to as *primary-vertex normalization factor* and *secondary-vertex normalization factor*, respectively, are weights applied event by event, $\xi$ to $\mathrm{K}^0$ events and $\eta$ to the events with a neutral kaon decaying to $\mathrm{e}^+\pi^-$.

(b) The background events mainly consist of neutral-kaon decays to final states other than the signal. Their number depends on the decay time $\tau$. To a high degree of accuracy the amount of background is the same for initial $\mathrm{K}^0$ and $\bar{\mathrm{K}}^0$ and hence cancels in the numerator but not in the denominator of any asymmetry: thus it is a dilution factor of the asymmetry. To account for these events, the analytic expressions of the asymmetries were modified by adding to the signal rates $R$ and $\bar{R}$ the corresponding background rates $B$ and $\bar{B}$:

$$B(\tau) = \sum_i R_{Bi} \times \varrho_{Bi}/\varrho_S, \quad \bar{B}(\tau) = \sum_i \bar{R}_{Bi} \times \varrho_{Bi}/\varrho_S , \tag{50}$$

where $R_{Bi}, \bar{R}_{Bi}$ are the rates of the background source $i$ for initial $\mathrm{K}^0$ and $\bar{\mathrm{K}}^0$, respectively, $\varrho_S$ is defined above and $\varrho_{Bi}$ is the corresponding term for the acceptance of events from the background source $i$. The quantities $\varrho_{Bi}$ and $\varrho_S$ were obtained by Monte Carlo simulation. Experimental asymmetries were formed from event rates including signal and background: $R^* = R + B$ and $\bar{R}^* = \bar{R} + \bar{B}$. These asymmetries were then fitted to the asymmetries of the *measured rates* (see below), which included residual background.

(c) The regeneration probabilities of $\mathrm{K}^0$ and $\bar{\mathrm{K}}^0$ propagating through the detector material are not the same, thus making the measured ratio of initial $\bar{\mathrm{K}}^0$ to $\mathrm{K}^0$ decay events at time $\tau$ different from that expected in vacuum. A correction was performed by giving each $\mathrm{K}^0$ ($\bar{\mathrm{K}}^0$) event a weight $w_r$ ($\bar{w}_r$) equal to the ratio of the decay probabilities for an initial $\mathrm{K}^0$ ($\bar{\mathrm{K}}^0$) propagating in vacuum and through the detector.

Finally, when $\mathrm{e}\pi\nu$ decays were considered, each initial-$\mathrm{K}^0$ event was given a total weight $w_+ = \xi \times \eta \times w_r$ or $w_- = \xi \times w_r$ if the final state was $\mathrm{e}^+\pi^-\nu$ or $\mathrm{e}^-\pi^+\bar{\nu}$, respectively. The summed weights in a decay-time bin are $N_{w+}(\tau)$ and $N_{w-}(\tau)$. In the same way, each initial-$\bar{\mathrm{K}}^0$ event was given a total weight $\bar{w}_+ = \eta \times \bar{w}_r$ or $\bar{w}_- = \bar{w}_r$ if the final state was $\mathrm{e}^+\pi^-\nu$ or $\mathrm{e}^-\pi^+\bar{\nu}$. The corresponding summed weights are $\bar{N}_{w+}(\tau)$ and $\bar{N}_{w-}(\tau)$. Instead, in the case of decays to two or three pions, each initial-$\mathrm{K}^0$ event was given a total weight $\bar{w} = \xi \times \bar{w}_r$, and each initial-$\bar{\mathrm{K}}^0$ event a total weight $\bar{w} = \bar{w}_r$. The corresponding summed weights are $N_w(\tau)$ and $\bar{N}_w(\tau)$. In the following the summed weights are referred to as the *measured decay rates*.

Two points are worth mentioning with regard to this method. Effects related to a possible violation of charge asymmetry in the reactions of Eq. (49) are taken into account by the weighting procedure at the primary vertex. When comparing the measured asymmetries with the phenomenological ones we take advantage of the fact that those reactions are strangeness conserving. A small strangeness violation (not expected at a level to be relevant in the CPLEAR experiment) would result in a dilution of the asymmetry and affect only some of the parameters.

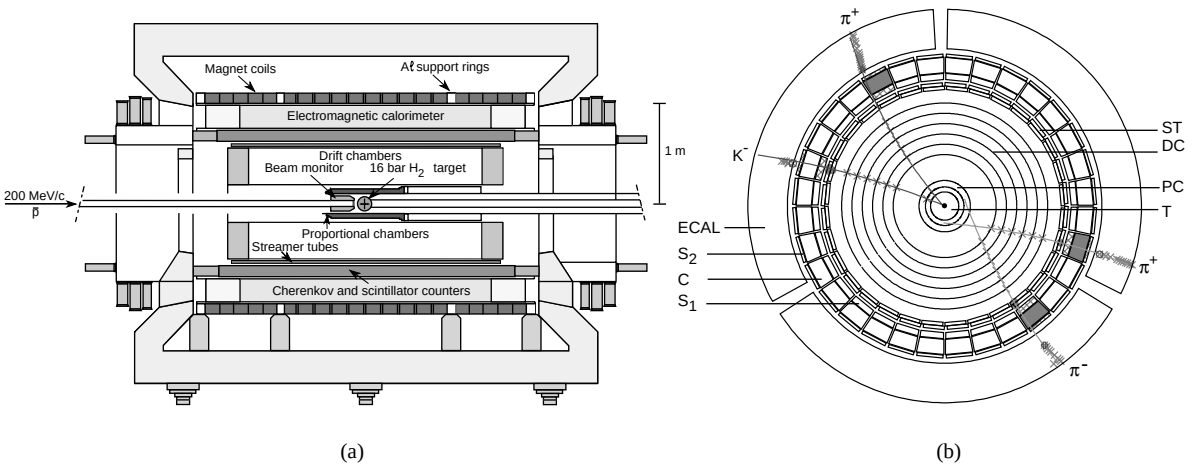


Fig. 2. CPLEAR detector: (a) longitudinal view, and (b) transverse view and display of an event, $\bar{p}p$ (not shown) $\rightarrow K^-\pi^+K^0$ with the neutral kaon decaying to $\pi^+\pi^-$. View (b) is magnified twice with respect to (a) and does not show the magnet coils and outer detector components. In both views the central region refers to the early data taking without the innermost proportional chamber PC0.

### 3.2. The detector

The detector specifications were based on the experimental requirements, which were the following.

- To select reaction (49) from the (very) large number of multi-pion annihilation channels. In particular, a very efficient kaon identification is essential.
- To distinguish between the various neutral-kaon decay channels.
- To measure the decay proper time between 0 and $\approx 20\,K_S$ mean lives. At the highest $K^0$ momentum measured in our experiment (750 MeV/$c$), the $K_S$ mean decay length is 4 cm. This sets the size of the cylindrical $K^0$ decay volume to a radius of $\approx 60$ cm.
- To acquire a large quantity of statistics, which required both a high rate capability (1 MHz annihilation rate) and large geometrical coverage.

An important aspect in the design of the experiment was the need to minimize neutral-kaon regeneration effects in the decay volume by minimizing the amount of matter in the detector. The regeneration effects modify the time evolution of initial $K^0$ and $\bar{K}^0$ differently. The regeneration amplitude had not been measured in our $K^0$ momentum range and at first had to be inferred from previous measurements of charged-kaon cross-sections. Later, however, we could measure it in the same detector.

Since the antiproton reactions of Eq. (49) were observed at rest, the particles were produced isotropically, thus the detector had a typical near-4$\pi$ geometry. The whole detector was embedded in a (3.6 m long, 2 m diameter) warm solenoidal magnet which provided a 0.44 T uniform field.

The general layout of the CPLEAR experiment is shown in Fig. 2; a comprehensive description of the detector is found in Ref. [3]. The incoming $\bar{p}$ beam was delivered by the Low Energy

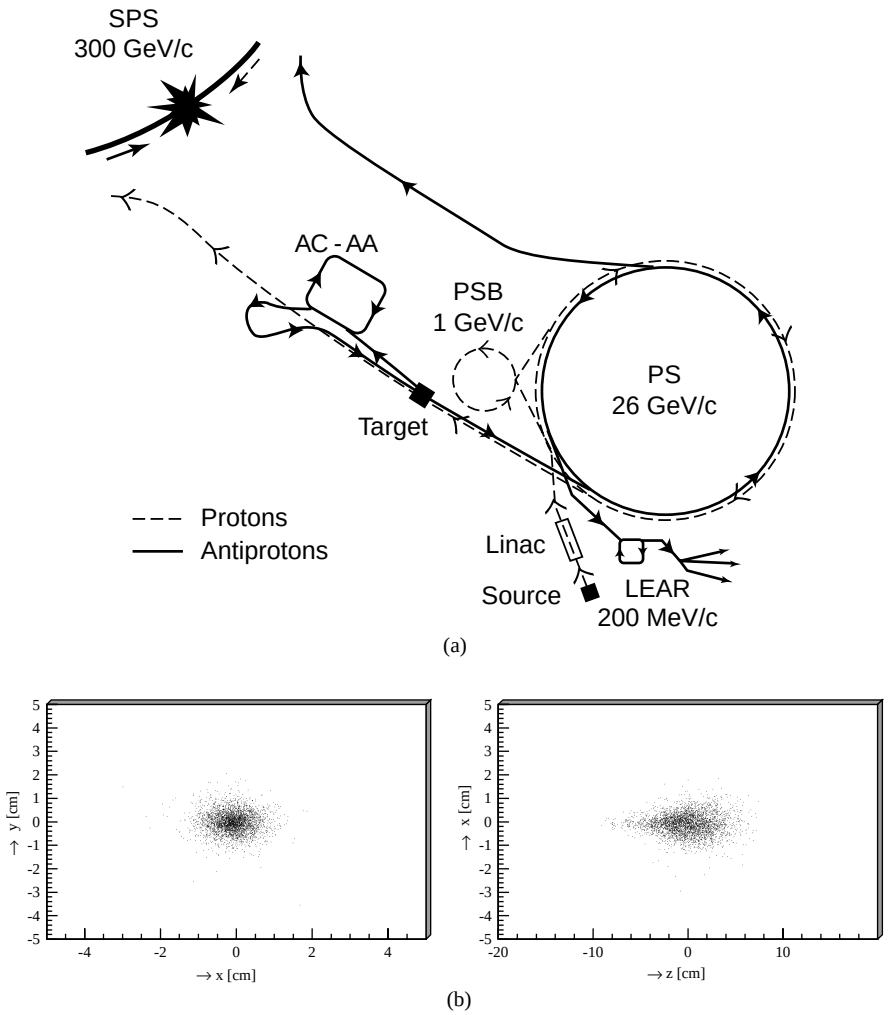


Fig. 3. (a) The complex of accelerators providing the 200 MeV/$c$ antiproton beam to the CPLEAR experiment. (b) The distribution of the vertices for $\bar{p}p$ annihilation channels containing four visible tracks: transverse $(x, y)$ and longitudinal $(x, z)$ projections. The annihilations take place in gaseous hydrogen at 16 bar.

Antiproton Ring (LEAR) facility at CERN. The beam had a momentum of 200 MeV/$c$ and a rate of $\approx$1 MHz. The antiprotons were made by a complex of accelerators shown in Fig. 3a, see Ref. [2]. First a proton beam was accelerated to 26 GeV/$c$ in the proton synchrotron (PS) and bombarded into an iridium target. A magnetic spectrometer selected the emerging antiprotons (3.6 GeV/$c$) and injected them into an antiproton collector (AC). Here they stayed for 4.8 s to reduce their momentum spread by means of stochastic cooling before being stored for a long time in the antiproton accumulator (AA). Whenever the LEAR machine was ready to take a shot ($\approx 5\times 10^9$) of $\bar{p}$, the AA released a part of its stack to the PS, where the $\bar{p}$'s were decelerated to 609 MeV/$c$, injected into LEAR, and stochastically cooled down to a momentum spread of $\sigma_p/p = 10^{-3}$ for

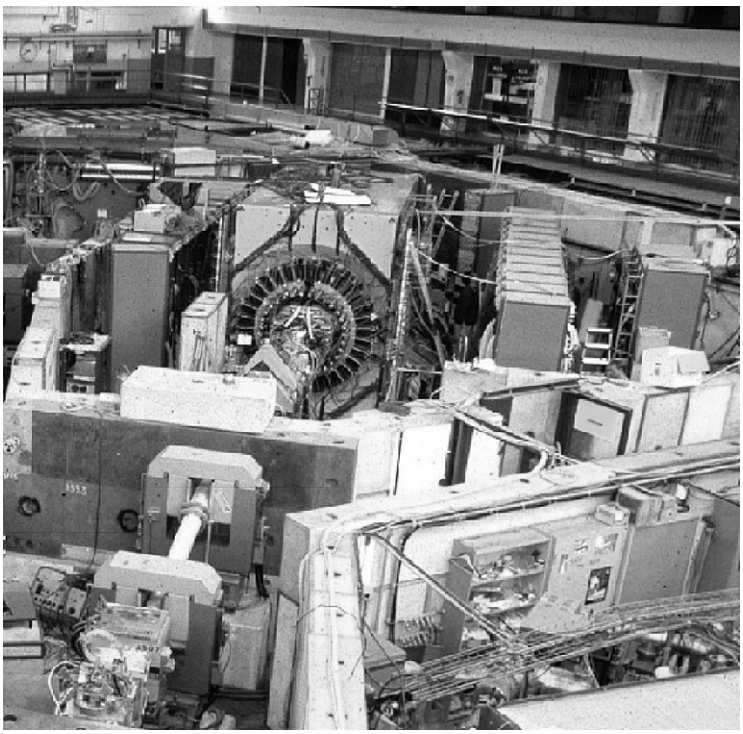

Fig. 4. View of the CPLEAR detector in the South Hall at CERN. The last elements of the antiproton-beam transport system are also visible.

another 5 min. This was followed by electron cooling, resulting in a relative momentum spread of only $5 \times 10^{-4}$. After the cooling had been finished, the LEAR machine would extract the 200 MeV/$c$ stack at a rate of 1 MHz in spills of about 1 h. The whole procedure of refilling LEAR and cooling took about 15 min between the spills. The last part of the beam line comprised two horizontal and two vertical bending magnets followed by a quadrupole doublet. These components were used to align and focus the beam on the target in the centre of the detector (Fig. 4). The size of the beam spot on the target had a FWHM of about 3 mm.

The antiprotons were stopped in a pressurized hydrogen gas target. The use of liquid hydrogen was ruled out in order to minimize the amount of matter in the decay volume. The high pressure of the hydrogen and the low momentum of the incoming $\bar{p}$ beam helped to keep the size of the stopping region small, see Fig. 3b. For data taken up to mid-1994 the target was a sphere of 7 cm radius at 16 bar pressure. After that date it was replaced by a 1.1 cm radius cylindrical target at 27 bar pressure.

A series of cylindrical tracking detectors provided information about the trajectories of charged particles in order to determine their charge signs, momenta and positions. There were two proportional chambers (9.5 and 12.7 cm in radius, measuring $r\phi$), six drift chambers (from 25 to 60 cm, measuring $r\phi, z$) and two layers of streamer tubes (for a fast $z$ determination within 600 ns). The total material in the target and tracking chambers amounted to $\approx 300$ mg cm$^{-2}$ and $\approx 10^{-2}$ equivalent

radiation length ($X_0$). After track fit the resolution was better than 350 μm in $r$ and $r\phi$, and 2 mm in $z$. A moderate momentum resolution ($\Delta p/p$ between 5% and 10%) was sufficient to perform the experiment. These detectors enabled the annihilation vertex to be located, as well as the decay vertex for $K^0$ decays to charged particles. To calculate the decay proper time $\tau$, a precision of the order of a few millimetres in the vertex positions was required in the transverse plane (perpendicular to the beam axis) since $\tau = m_{K^0} \times d_T/p_T$, $d_T$ being the distance between the two vertices, $p_T$ the momentum of the $K^0$, both projected onto this plane, and $m_{K^0}$ the neutral-kaon mass. Such a precision could only be obtained when the decay final state included charged particles.

The tracking detectors were followed by the particle-identification detector (PID), which carried out the charged-kaon identification. The PID comprised a threshold Cherenkov detector, which was mainly effective for $K/\pi$ separation above 350 MeV/$c$ momentum, and scintillators which measured the energy loss ($dE/dx$) and the time of flight of charged particles. The PID recognized in $\approx 60$ ns the presence of a charged kaon out of a background 250 times higher. The Cherenkov threshold was 300 MeV/$c$ for pions and 700 MeV/$c$ for kaons. The total thickness was 0.5 $X_0$. The PID was also used to separate electrons from pions below 350 MeV/$c$.

The outermost detector was a lead/gas sampling calorimeter (ECAL) used to detect the photons produced in $\pi^0$ decays. It consisted of 18 layers of 1.5 mm lead converters and high-gain tubes, the latter sandwiched between two layers of pick-up strips ($\pm 30°$ with respect to the tubes), for a total of 64 000 readout channels. The design criteria of the calorimeter were mainly dictated by the required accuracy on the reconstruction of the $K^0 \to 2\pi^0$ or $3\pi^0$ decay vertices. The calorimeter provided $e/\pi$ separation at higher momenta ($p > 300$ MeV/$c$) complementary to the PID.

The small value of the branching ratio for reaction (49) and the necessary high annihilation rate placed stringent requirements on the experiment. To reduce the dead-time due to data acquisition and to limit the amount of recorded data, the unwanted events needed to be removed efficiently. A set of hardwired processors (HWP) was specially designed to achieve this task. The role of the processors was to provide full event reconstruction in a few microseconds (charged-track pattern-recognition and kinematics, particle identification and shower counting in the calorimeter) with sufficient precision to allow event selection.

### 3.3. The trigger

The trigger system aimed at the selection of $K^0$ and $\bar{K}^0$ in identifying a primary $K^{\pm}\pi^{\mp}$ pair and at the observation of the $K^0(\bar{K}^0)$ decay inside the fiducial volume of the detector. Nearly half of the produced neutral kaons (96% of the $K_L$ component) decayed outside this volume.

The decisions were based on fast recognition of the charged kaon (using the PID hit maps), the number and topology of the charged tracks, the particle identification (using energy-loss, time-of-flight and Cherenkov light response) and kinematic constraints, as well as the number of showers in the ECAL. Fig. 5 shows the trigger decision steps in chronological order taking into account the availability in real time of the relevant detector information. The rate reductions achieved by the different processor steps given in Fig. 5 depend on the particular detailed logic conditions set at each level.

We shall just mention that the first decision step (early decision logic—EDL) selected candidate events with at least two charged tracks (at least two hits in the inner scintillator S1), one of which must be a kaon, defined by the coincidence of the two scintillator layers and no Cherenkov response, S1$\bar{C}$S2. This first identification of charged kaons was further improved by requesting a minimum

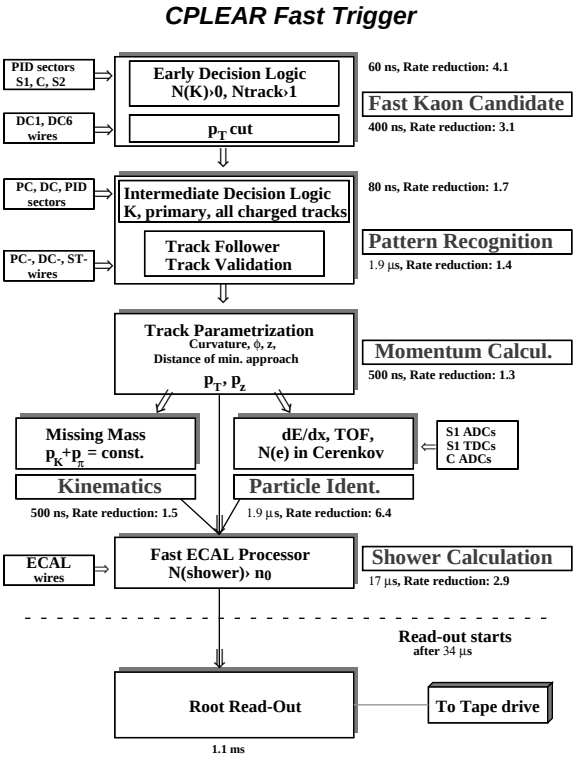


Fig. 5. Logic and data flow diagram of the trigger system. Typically $0.8 \times 10^6$ $\bar{p}p$ annihilations/s, including 3200 events/s as in Eq. (49), of which 1600/s were observed. The acquisition rate was 1 MB/s on 200-MB cartridges (one every 4 min) with 100 cartridges per shift of 8 h.

transverse momentum ($p_T$ cut) in order to eliminate false kaon candidates due to slow pions. For data taken from 1995 onwards a cylindrical proportional chamber PC0 of 1.5 cm radius, 10 cm length, which had been installed together with the new target, was incorporated into the trigger. The decay of the neutral kaon outside this chamber was guaranteed by demanding not more than two hits in the chamber. This eliminated a large number of unwanted, very short decay-time $K_S$ decays as well as background multikaon and multipion annihilations, and hence, allowed the rate of useful events being recorded to be increased significantly. For candidate 'neutral' events, i.e. events with only two primary ($K\pi$) tracks, the requirement for a minimum number of showers eliminated all $K_L$ events decaying outside the fiducial volume of the detector, or interacting strongly with ECAL.

The overall rejection factor of the trigger was about $10^3$, allowing a read-out rate of $\approx 450$ events per second at an average beam rate of 800 kHz. The global acceptance for $K^0$ or $\bar{K}^0$ produced in reaction (49) and decaying inside the fiducial volume of the detector was about 7%, mainly determined by geometrical factors. The decision time of each stage of the trigger varied from 60 ns (EDL) to 17 μs (when showers were calculated). The read-out strobe was delivered to the front-end electronics 34 μs after the arrival of the beam-counter signal.

The multilevel processor system was controlled using a pipelined logic (sequencer) unit. A trigger control system provided all the signals required by the detector front-end electronics and initiated the transfer of information to the Root Read-out system. It was capable of rejecting a wrong candidate

event as soon as it was possible following its identification. After a 'clear time' of 350 ns the trigger system was ready to accept the next candidate event. This minimized the trigger dead-time caused by the large number of rejected events. The overall dead-time of the trigger was about 25% at a 1 MHz antiproton rate. Monitoring the trigger operation was very important also from the point of view of the systematic errors. The trigger system contained a dedicated interface called 'SPY'. This collected the data input to the processors (the hit maps and front-end data from the detectors) and all intermediate and final data and logic decisions generated by the trigger system. By using SPY data and the full trigger simulation, we could on the one hand verify that the simulation reproduced perfectly (at the bit level) the functionality of each trigger stage, and on the other detect any misfunctioning of the hardware.

Primary K$\pi$ pairs found by the trigger had to be confirmed by the primary K$\pi$ pairs found by the offline reconstruction. This matching procedure was achieved by running the trigger simulation on the selected events, requiring the event to pass the trigger criteria with which the data were written, and rejecting events where the trigger and offline reconstruction disagreed on primary tracks.

The trigger system did not allow to record concurrently physics events and down-scaled minimum-bias events. However, minimum-bias data (T1), requiring only the coincidence between a $\bar{p}$ signal and a signal in the S1 scintillator, were collected at least three times a day, thus providing a representative set of the overall data to be used for calibration purposes. Whenever possible these data were also used for trigger studies. We also generated a large number of events to produce an unbiased simulated sample: real and simulated unbiased samples were useful to study specific points; however, they could not cope with the fact that the scaling factor of the real trigger was larger than a thousand.

The detector response to electrons and pions was particularly important in relation to e$\pi\nu$ decays. The quality of this response was verified with electrons and pions obtained with the current trigger throughout the data-taking: electrons were assembled (at the analysis level) in the so-called T$\gamma$ sample by selecting $e^+e^-$ pairs produced by $\gamma$-conversion, with the $\gamma$ in turn resulting from a $\pi^0$ decay. The pions were part of the $\pi^+\pi^-$ decay sample. A detailed investigation of the various contributions to the secondary-vertex normalization factor $\eta$ was performed using electrons of the T$\gamma$ sample and pions either of the $\pi^+\pi^-$ decay sample or of a four-pion sample. This four-pion sample was selected off-line from the data collected with the minimum-bias T1 trigger.

We stress that the analysis had to rely on simulation only for the purpose of computing the residual background and decay-time resolutions. In other cases simulated data allowed us to verify with higher statistics the results obtained with real calibration samples. The simulation results are independent of the general properties of the simulated sample (such as phase space) and are entirely governed by the trigger simulation which is an exact bit-to-bit reproduction of the hardware. For real data the method of *trigger simulation* which handles real data on an event-by-event basis is much more powerful than the use of down-scaled triggers which could only give global information.

### 3.4. The detector performance

The CPLEAR detector was fully operational between 1992 and 1996, collecting a total number of antiprotons equal to $1.1 \times 10^{13}$ (20 pg!) and data contained in 12 Tbytes of recorded information. All the subdetectors—beam monitors, tracking devices, particle-identification detector, electromagnetic calorimeter—achieved their expected performance, which is summarized below.

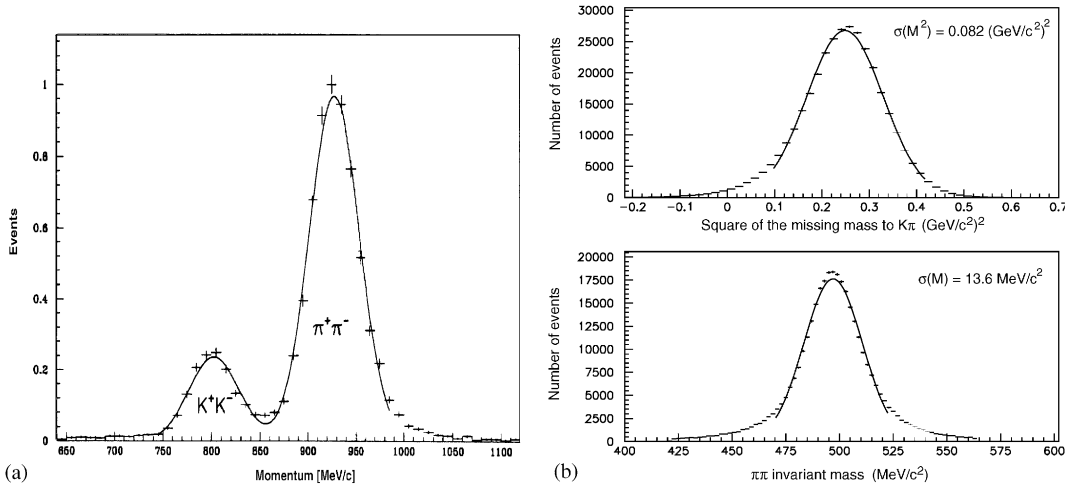


Fig. 6. (a) Alignment quality with back-to-back tracks: the two annihilation channels to $\pi^+\pi^-$ and $K^+K^-$ pairs are clearly shown. (b—top) Square of the missing mass to the primary K$\pi$ pair for selected $p\bar{p} \to \pi KK^0$ events, and (b—bottom) invariant mass of $\pi^+\pi^-$ pair for $K^0 \to \pi^+\pi^-$ decays.

- Interaction rate of 1 MHz.
- Magnetic field of 0.44 T, stable to a few parts in $10^{-4}$.
- Tracking chambers (proportional and drift chambers, streamer tubes) with a spatial resolution of $\sigma \approx 300$ μm in the transverse plane and $\sigma \approx 5$ mm for $z$, and a momentum resolution of $\sigma_p/p \approx$ 5–10%, see also Fig. 6a.
- Particle identification with pion/kaon separation $> 4\sigma$ above 350 MeV/$c$, see Figs. 7 and 8, and electron/pion separation.
- Photon detection in ECAL with spatial resolution $\sigma(x) \approx 5$ mm, energy resolution $\sigma(E) \approx 15\%/\sqrt{E(\mathrm{GeV})}$, and efficiency shown in Fig. 9.
- Multilevel trigger system allowing an event to be reconstructed in $\approx 6$ μs.
- $\pi\pi$ invariant mass ($\sigma(m_{K^0}) \approx 13$ MeV/$c^2$) and K$\pi$ missing-mass distributions shown in Fig. 6b; decay-time resolution: for charged decays $\sigma(\tau) \approx (5\text{–}10)\times 10^{-12}$ s, see Fig. 10, for $\pi^0\pi^0$ FWHM $\approx 70 \times 10^{-12}$ s.

The detector ran smoothly for 5 years and accumulated (on 50 000 tapes containing 100 000 events each with 2 kbyte per event) nearly $2 \times 10^8$ decays of strangeness-tagged neutral kaons entering our final data sample, of which $7 \times 10^7$ decays are to $\pi^+\pi^-$ with a decay time greater than 1 $\tau_S$ [7], $1.3 \times 10^6$ to e$\pi\nu$ [11–14], $2.0 \times 10^6$ to $\pi^0\pi^0$ [8], $5.0 \times 10^5$ to $\pi^+\pi^-\pi^0$ [9], and $1.7 \times 10^4$ to $\pi^0\pi^0\pi^0$ [10].

With these data CPLEAR achieved a number of results on the discrete symmetries in the neutral-kaon system [7–10,12,13] and measured other relevant quantities [9,11,15,16]. Calibration data were used to study $\bar{p}p$ annihilation channels, relative branching ratios [17–19] and Bose–Einstein correlations in multipion final states [20–22]. The set-up was slightly modified to measure neutral-kaon forward scattering cross-sections in carbon and evaluate the regeneration effects [23,24] and also to perform an Einstein–Podolski–Rosen-type experiment [25]. Some of the measurements led

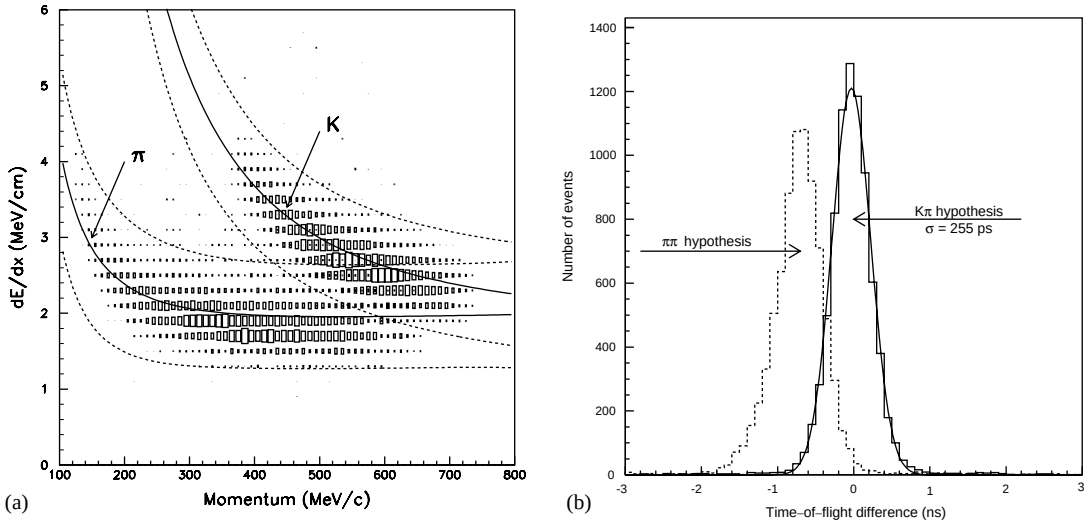


Fig. 7. (a) Energy loss measured in S1 as a function of momentum. For both kaons and pions, the solid line shows the expected average energy loss and the dashed lines form a band containing 92% of the events. (b) Time-of-flight difference between kaons and pions for the whole accepted phase space of $K\pi K^0$ events. The solid line corresponds to the correct particle assignment, the dashed histogram to the case where both particles are assumed to be pions.

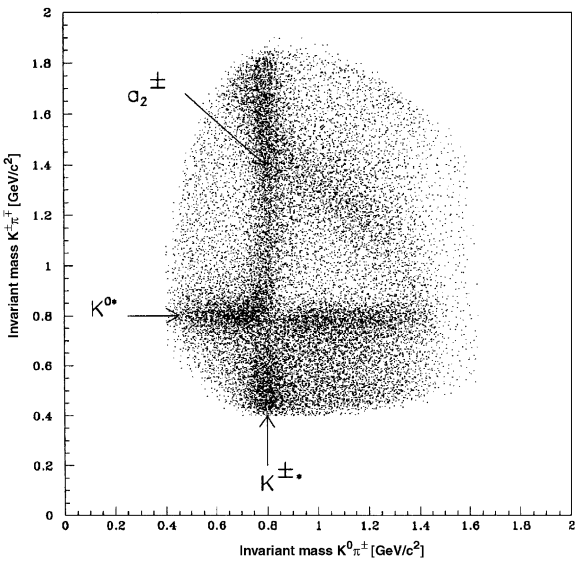


Fig. 8. Scatter plot of golden events: $K^{\pm}\pi^{\mp}$ invariant mass versus $K^0\pi^{\pm}$ invariant mass.

to publications with a phenomenological flavour [27–32]. These covered global, optimal evaluations of the parameters measured and related quantities [27–30] and also tests of quantum mechanics [31] and of the equivalence principle [32]. Over the years, 52 PhD students were involved, at different times, and contributed to the success of the experiment.

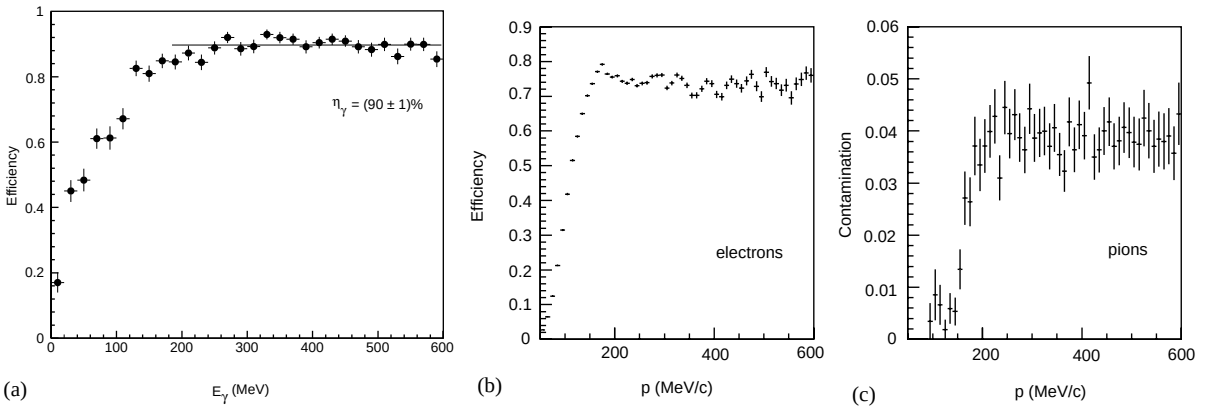


Fig. 9. ECAL performance: (a) photon detection efficiency as a function of the energy $E_\gamma$ ($\eta_\gamma$ is the plateau value of this efficiency), and (b) electron detection efficiency (at 4% pion contamination) and pion contamination as a function of particle momentum $p$.

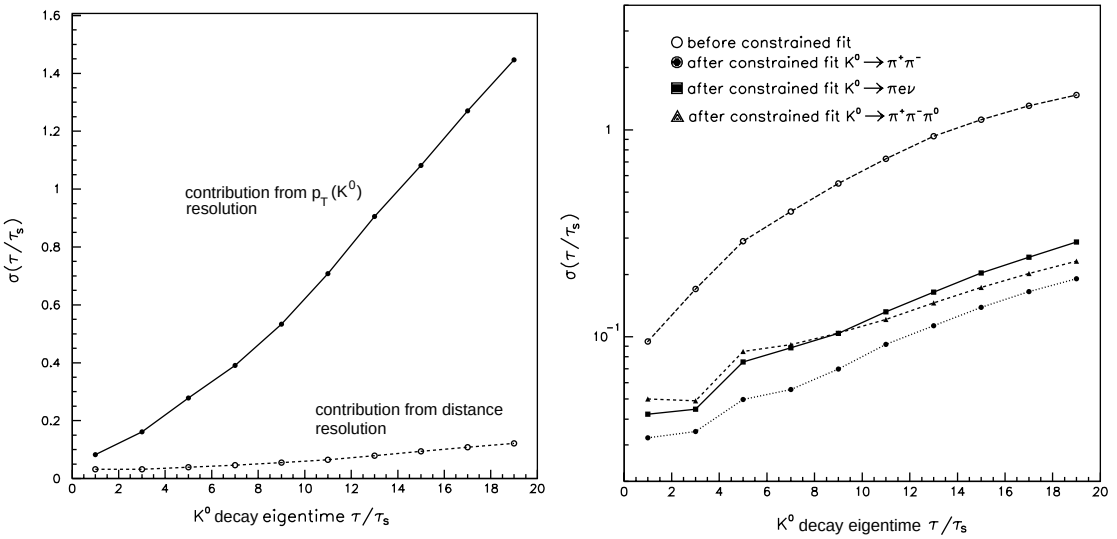


Fig. 10. (a) Decay-time resolution before constrained fit (simulated data). The two curves show separately the contributions due to the uncertainty in the neutral-kaon transverse momentum $p_T$ and in the distance $d_T$ between the annihilation and decay vertices. (b) Decay-time resolution before and after constrained fit (simulated data). The improvement after the fit shown in (b) is expected because of the important contribution to the decay-time resolution resulting from the momentum resolution, shown in (a).

### 3.5. Event selection and analysis

The selection of events corresponding to $\bar{p}p$ annihilations in the golden channels (49), followed by the decay of the neutral kaon to one of the final states previously mentioned, was performed by a set of topological cuts and by kinematic and geometric constrained fits. The kinematic boundaries

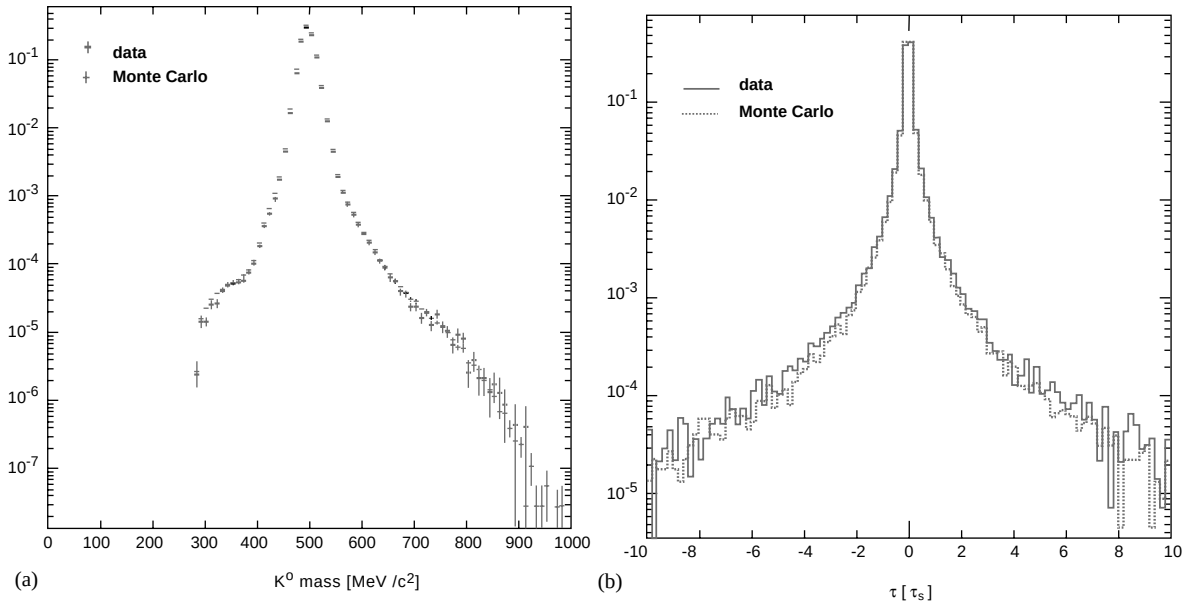


Fig. 11. Data-simulation quality checks: (a) $K^0$ reconstructed mass for selected $\pi^+\pi^-$ decays, and (b) $K^0$ reconstructed lifetime: the data points are the pseudo-lifetimes obtained for the events of the four-pion sample ($\bar{p}p \to \pi^+\pi^-\pi^+\pi^-$, see Section 3.3) fitted as golden events accompanied by a $K^0$ decay to $\pi^+\pi^-$.

of Eq. (49) and the improvement in momentum measurement brought in by constrained fits to $\pi^+\pi^-$ decay events are shown in Fig. 12.

The fits reduced the number of background events associated with $\bar{p}p$ annihilation channels and neutral-kaon decay modes other than the ones under study. They also improved considerably the decay-time resolution, see Fig. 10b. Simulated data were produced with high statistics (at least one order of magnitude larger than the real data)—they allowed a precise monitoring of efficiencies and losses in all the selections, and the evaluation of the residual background. The quality of the simulation is demonstrated by the comparison with real data when measuring the $\pi^+\pi^-$ invariant mass in the neutral-kaon decays to $\pi^+\pi^-$ and the time resolution in the four-pion production with a minimum-bias trigger, see Figs. 11a and b.

Before entering the decay-rate asymmetries, the events finally selected in each channel were weighted on an event-by-event basis, following the method outlined in Section 3.1. The determination of primary- and secondary-vertex normalization factors and of regeneration weights is described elsewhere [7,14,24]. The following points should be recalled in view of later analyses.

- $K^0$ to $\bar{K}^0$ rate normalization (primary vertex). For the same production flux, at $(t = 0)$ we would detect different numbers of $K^0$ and $\bar{K}^0$: owing to different strong interactions the ratio $\xi$ of $\bar{K}^0$ to $K^0$ tagging (detection) efficiency is different from one. As $\xi$ is independent of the decay mode—which was verified with high-statistics simulated data—we selected $\pi^+\pi^-$ events with a decay time between 1 and 4 $\tau_S$: here high statistics is available with a very small background, and the $\mathscr{CP}$-violating contribution to the rates is known with sufficient accuracy. From the ratio of observed $K^0$ to $\bar{K}^0$ events, we could then determine $\alpha\xi = [1 + 4\,\mathrm{Re}(\varepsilon_L)]\xi$. When $\xi$ alone was

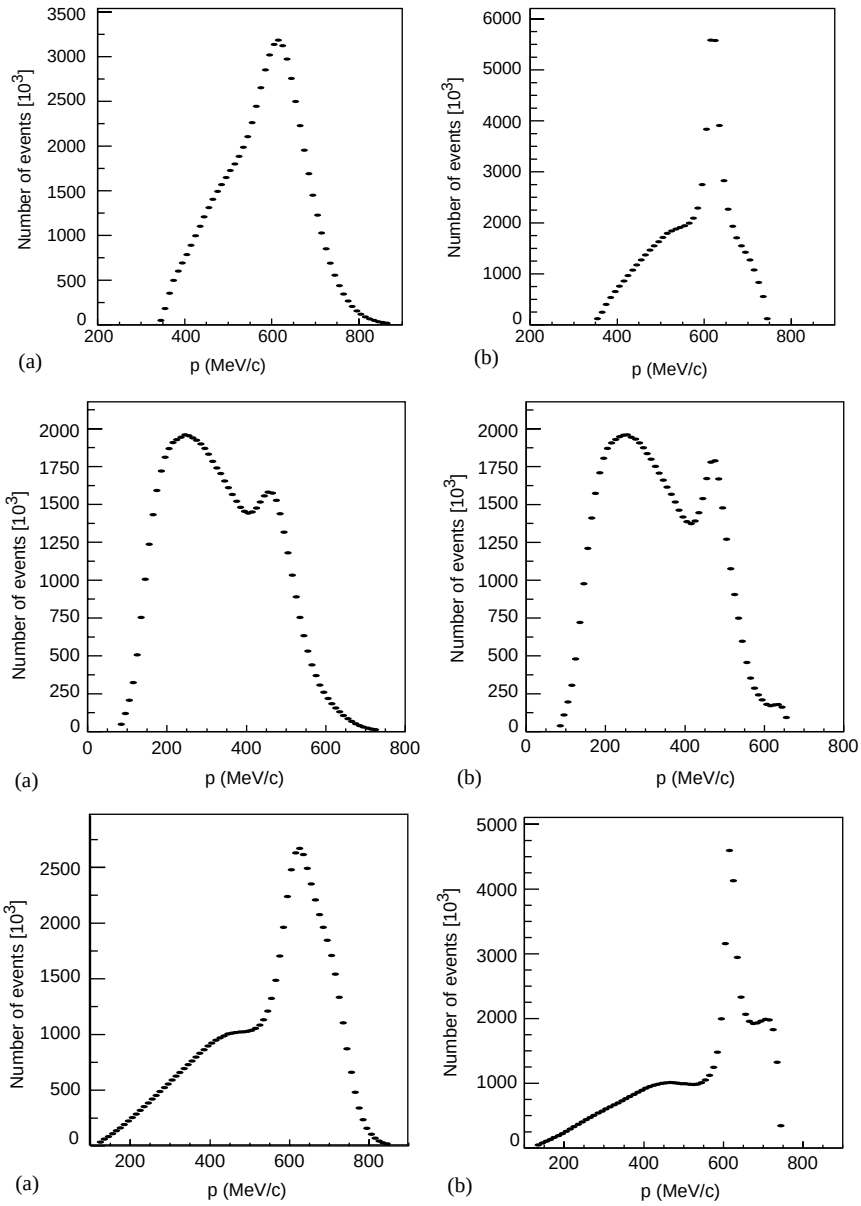


Fig. 12. Momentum distribution for real data after (a) track fit and (b) kinematic and geometric constrained fit: primary pions (top), charged kaons (centre), neutral kaons (bottom).

needed, we used the value of the charge asymmetry $\delta_\ell$ measured with neutral-kaon decays to $\ell\pi\nu$: $\delta_\ell = 2\,\mathrm{Re}(\varepsilon_\mathrm{L}) - 2[\mathrm{Re}(x_-) + \mathrm{Re}(y)] = (3.27 \pm 0.12) \times 10^{-3}$ [78]—in the limit that these decays are $\mathscr{CPT}$ invariant, the simple relation $2\,\mathrm{Re}(\varepsilon_\mathrm{L}) = \delta_\ell$ holds.

The quantity $\alpha\xi$ was given through look-up tables as a function of charged-kaon transverse and longitudinal momentum, pion momentum, and magnetic-field polarity, and the phase-space

differences between primary K$\pi$ pairs of different decay channels were taken into account. Averaging over the phase space of the e$\pi\nu$ channel, we obtained typically $\langle\alpha\xi\rangle = 1.12756 \pm 0.00034$. Whenever possible, the measured asymmetries were defined such as to incorporate $\alpha\xi$, see below, Eqs. (51a), (51d) and (51e). No assumption on (direct) $\mathscr{CPT}$ violation in $\pi^+\pi^-$ decays is needed, since a possible $\mathscr{CPT}$ violation is contained in the experimental value of $\eta_{+-}$, thus the primary-vertex normalization is performed for these asymmetries using only quantities measured in the same experiment. With some variants in the procedure, to be seen later, the same holds for the asymmetries of Eq. (51b).

This is in contrast to the $\mathscr{T}$-violation analysis, see Eq. (51c), where only $\xi$ enters: there, in order to account for $\alpha$, the value of $\delta_\ell$ was used, at the cost of introducing additional direct $\mathscr{CPT}$-violating terms in the asymmetry.

- Final-state relative efficiency (secondary vertex): $\eta$ is given as a function of pion momentum, from $\pi^-$ and $\pi^+$ tracks of minimum-bias data, and electron momentum, from electrons of $e^+e^-$ conversion pairs selected from decays of $K^0(\bar{K}^0) \to 2\pi^0$, with $\pi^0 \to 2\gamma$. On average we found $\langle\eta\rangle = 1.014 \pm 0.002$.

Various *measured* asymmetries were then formed with the summed weights of events obtained as a function of the decay time for each decay channel.

### 3.6. Physics analysis and fits

The measured asymmetries were formed with the measured decay rates as defined in Section 3.1. The asymmetries considered in the present study were

$$A_{+-}^{\exp}(\tau) = \frac{\bar{N}_w(\tau) - \alpha N_w(\tau)}{\bar{N}_w(\tau) + \alpha N_w(\tau)}\,, \tag{51a}$$

$$A_f^{\exp}(\tau) = \frac{\bar{N}_w(\tau) - N_w(\tau)}{\bar{N}_w(\tau) + N_w(\tau)}\,, \tag{51b}$$

$$A_{\mathrm{T}}^{\exp}(\tau) = \frac{\bar{N}_{w+}(\tau) - N_{w-}(\tau)}{\bar{N}_{w+}(\tau) + N_{w-}(\tau)}\,, \tag{51c}$$

$$A_\delta^{\exp}(\tau) = \frac{\bar{N}_{w+}(\tau) - \alpha N_{w-}(\tau)}{\bar{N}_{w+}(\tau) + \alpha N_{w-}(\tau)} + \frac{\bar{N}_{w-}(\tau) - \alpha N_{w+}(\tau)}{\bar{N}_{w-}(\tau) + \alpha N_{w+}(\tau)}\,, \tag{51d}$$

$$A_{\Delta m}^{\exp}(\tau) = \frac{[\bar{N}_{w-}(\tau) + \alpha N_{w+}(\tau)] - [\bar{N}_{w+}(\tau) + \alpha N_{w-}(\tau)]}{[\bar{N}_{w-}(\tau) + \alpha N_{w+}(\tau)] + [\bar{N}_{w+}(\tau) + \alpha N_{w-}(\tau)]}\,. \tag{51e}$$

The form of each of these asymmetries optimizes a specific measurement: $\mathscr{CP}$ violation with $\pi^+\pi^-$ decays for Eq. (51a), and with other pionic final states $f$ for Eq. (51b); $\mathscr{T}$ violation for Eq. (51c); $\mathscr{CPT}$ invariance for Eq. (51d); and $\Delta m$ for Eq. (51e).

The reason for the factor $\alpha = 1 + 4\,\mathrm{Re}(\varepsilon_{\mathrm{L}})$ in some of the asymmetries goes back to the previous discussion on the primary-vertex normalization factor $\xi$, and to the fact that the quantities $\alpha\xi$ could be measured using Eq. (51a) with a high-statistics, low-background sample of $\pi^+\pi^-$ decays [7].

Other asymmetries contain simply $\xi$ (in the summed weight of $K^0$ events): either because it is imposed by the physics content of the asymmetry ($A_T$) or because of the analysis method that was chosen ($A_f$).[2]

In order to extract the parameters of interest from each experimental asymmetry, we have to consider the corresponding phenomenological asymmetry function, which includes background rates, see Section 3.1, for instance in the case of $\pi^+\pi^-$ decays:

$$A^*_{+-}(\tau) = \frac{\bar{R}^*(\tau) - \alpha R^*(\tau)}{\bar{R}^*(\tau) + \alpha R^*(\tau)} \ . \tag{52}$$

Explicit expressions of the phenomenological asymmetries, in the limit of negligible background, will be given in Sections 4 and 5.

The phenomenological asymmetries folded with time resolution, as given by the simulation, were fitted to the measured asymmetries in the decay-time interval between 1 and 20 $\tau_S$. In all cases the parameters $\Gamma_S = \hbar/\tau_S$ and $\Gamma_L = \hbar/\tau_L$ were given world-average values with $\tau_S = (89.34 \pm 0.08) \times 10^{-12}$ s, and $\tau_L = (5.17 \pm 0.04) \times 10^{-8}$ s [78]. The parameter $\Delta m$, when not considered a free parameter of the fit, was given the world-average value $\Delta m = (530.1 \pm 1.4) \times 10^7\ \hbar/\text{s}$ [78] which includes a subset of the CPLEAR measurements.

These asymmetry data were taken in eight separate data-taking periods between 1992 and 1995. To check the internal consistency of the data, fits were performed for each data-taking period separately, and the results are also shown.

### 3.7. Systematic errors

Most of the sources of systematic errors and their uncertainties are common to the various asymmetries. (However, they have different impacts on the various analyses, as shown in the corresponding sections.) They are as follows.

- *The amount and shape of background:* they are estimated by comparing the decay-time distributions of real and simulated data. This determination is limited by the accuracy of our simulation. However, a more favourable situation is found in the case of the decay to $\pi^+\pi^-$, where the data itself allows a determination of the background.
- *The error on the normalization factors:* this is dominated by statistics. The normalization procedures were the subject of extensive studies: varying the cuts, using parallel analyses from different teams, subdividing the data in periods, etc. The results were found to be stable, therefore not hinting at any additional errors beyond the statistical uncertainty. To compute the systematic error on the parameters following from it, we have performed an error propagation, repeating the fit with the value of the normalization factor varied statistically around its central value. The standard deviations of the parameter values returned by the fits are assumed as the systematic error

[2] Eq. (51a) is in fact a variant of Eq. (51b) which was singled out because of its role in the experiment. More variants concern the other asymmetries $A_f$ depending on whether the weights $\xi$ were determined using only the information contained in the data sample itself ($\pi^0\pi^0$ and $\pi^0\pi^0\pi^0$ decays), or using as well the $\pi^+\pi^-$ information ($\pi^+\pi^-\pi^0$ decays). In all these procedures, the weights $\xi$ eventually translate into an offset of the phenomenological asymmetry, which becomes a free parameter of the fit.

contributions from this entry. A similar procedure has been followed to calculate the systematic error induced by the secondary-vertex normalization $\eta$ (in the case of e$\pi\nu$ decays).

- *The error of the regeneration correction:* The systematic uncertainties on the regeneration corrections were determined by simultaneously varying the real and imaginary parts of the neutral-kaon forward scattering amplitudes within their combined statistical and systematic uncertainties, as determined by our own measurement [24]. Contributions to the systematic errors due to uncertainties in the positions, thicknesses and densities of the various elements of the detector traversed by the neutral kaons were found to be negligible.
- *Decay-time resolution:* it is determined using simulated data. The quality of the simulation is shown in Fig. 11b.
- *The absolute time-scale:* it was the subject of a study combining hardware and software information with dedicated simulations. The details are given in Refs. [3,84]. After the kinematic constrained fits, the absolute time-scale measured in the experiment is known with a precision of $\pm 0.2$ parts per million. Changing the absolute time-scale by this factor produces the shifts in the fitted parameters which contribute to the systematic error.

By varying the quantities parametrizing the sources of systematic errors within their estimated uncertainties, the corresponding systematic errors on the fitted parameters were then determined.

## 4. The pionic decay channels ($\mathscr{CP}$)

When a neutral kaon decays to pions exclusively, this final state is a $\mathscr{CP}$ eigenstate. The final states $\pi^+\pi^-$ and $\pi^0\pi^0$ have a $\mathscr{CP}$ eigenvalue equal to $+1$, $\pi^0\pi^0\pi^0$ a $\mathscr{CP}$ eigenvalue equal to $-1$, and that of $\pi^+\pi^-\pi^0$ is $+1$ or $-1$ depending on the kinematical configuration. Any difference in the rates of $\mathrm{K}^0$ and $\bar{\mathrm{K}}^0$ decaying to one of these eigenstates is a sign of $\mathscr{CP}$ violation.

### 4.1. $\pi^+\pi^-$—Measurement of $|\eta_{+-}|$, $\phi_{+-}$, and $\Delta m$ (method a) [7]

The measured decay rate (acceptance corrected) for $\mathrm{K}^0$ and $\bar{\mathrm{K}}^0$ is shown in Fig. 13a: as expected, the dependence on decay time is not described by a simple exponential. The total rate can be decomposed according to the initial strangeness of the neutral kaons. These measured rates are displayed in Fig. 13b separately for initial $\mathrm{K}^0$ and $\bar{\mathrm{K}}^0$, after acceptance correction and background subtraction, and clearly show the expected $\mathscr{CP}$-violation effect. The $\mathscr{CP}$ parameters are best measured by isolating the interference term in the decay rates through the asymmetry $A_{+-}^{\exp}$ of Eq. (51a) fitted by the asymmetry $A_{+-}^{*}$, see Eq. (52). The asymmetry $A_{+-}^{*}$ is constructed with the rates of Eq. (40) and the background rates:

$$A_{+-}^{*}(\tau) = -2\frac{|\eta_{+-}|\mathrm{e}^{(1/2)(\Gamma_S-\Gamma_L)\tau}\cos(\Delta m\tau - \phi_{+-})}{1+[|\eta_{+-}|^2 + B(\tau)]\mathrm{e}^{(\Gamma_S-\Gamma_L)\tau}}\ , \tag{53}$$

where the term $B(\tau)\mathrm{e}^{(\Gamma_S-\Gamma_L)\tau}$ results from the background contribution to the decay rates of either $\mathrm{K}^0$ or $\bar{\mathrm{K}}^0$. The decay-time dependence of the background, $B(\tau)$, is parametrized, and its absolute level fixed to the mean value obtained as the average of three different methods (see Ref. [7] for details). To account for the statistical uncertainties in the normalization weights and for the

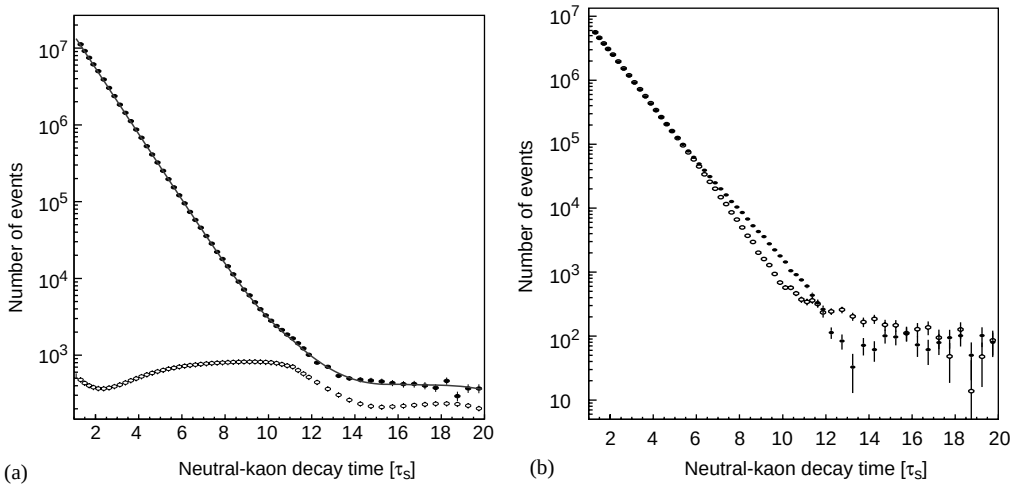


Fig. 13. Decay to $\pi^+\pi^-$: (a) The measured decay rate (acceptance corrected) as a function of the decay time $\tau$, when $K^0$ and $\bar{K}^0$ decays are not separated. The continuous curve is a fit to the real data (•). The open circles show the calculated background level. (b) The measured decay rates displayed separately for $K^0$ (○) and $\bar{K}^0$ (•) after acceptance correction and background subtraction.

correlations between the magnitudes of these weights and the fitted $\mathscr{CP}$-violation parameters, we allow for a further, overall normalization factor $k$, with the asymmetry $A^*_{+-}(\tau)$ of Eq. (53) set equal to $[\bar{N}_w(\tau) - k\alpha N_w(\tau)]/[\bar{N}_w(\tau) + k\alpha N_w(\tau)]$. Equivalently, the measured asymmetry $A^{\rm exp}_{+-}(\tau)$ satisfies the equality

$$A^{\rm exp}_{+-}(\tau) = \frac{(k-1) + (k+1)A^*_{+-}(\tau)}{(k+1) + (k-1)A^*_{+-}(\tau)} \ . \tag{54}$$

The measured decay-rate asymmetry $A^{\rm exp}_{+-}(\tau)$ was then fitted by the right-hand side of Eq. (53). The parameters left free in the fit were $\phi_{+-}$ and $|\eta_{+-}|$, which are contained in the phenomenological expression of the asymmetry, $A^*_{+-}(\tau)$, and $k$. Fits were also performed with $\Delta m$ as an additional free parameter.

The value obtained for $\phi_{+-}$ depends on the value of $\Delta m$—varying as

$$\phi^{\Delta m}_{+-} = \phi^{\langle \Delta m \rangle}_{+-} + 0.300(\Delta m - \langle \Delta m \rangle) \ ,$$

with $\phi_{+-}$ in degrees and $\Delta m$ in units of $10^7\ \hbar/\mathrm{s}$—but has negligible dependence on the value of $\tau_S$. The value of $|\eta_{+-}|$ depends on the value of $\tau_S$ as

$$|\eta_{+-}|^{\tau_S} = |\eta_{+-}|^{\langle \tau_S \rangle} + 0.091(\tau_S - \langle \tau_S \rangle) \times 10^{-3} \ ,$$

where $\tau_S$ is in ps, and has negligible dependence on the value of $\Delta m$. Neither $|\eta_{+-}|$ nor $\phi_{+-}$ have any significant dependence on the value of $\Gamma_L$ used in the fit.

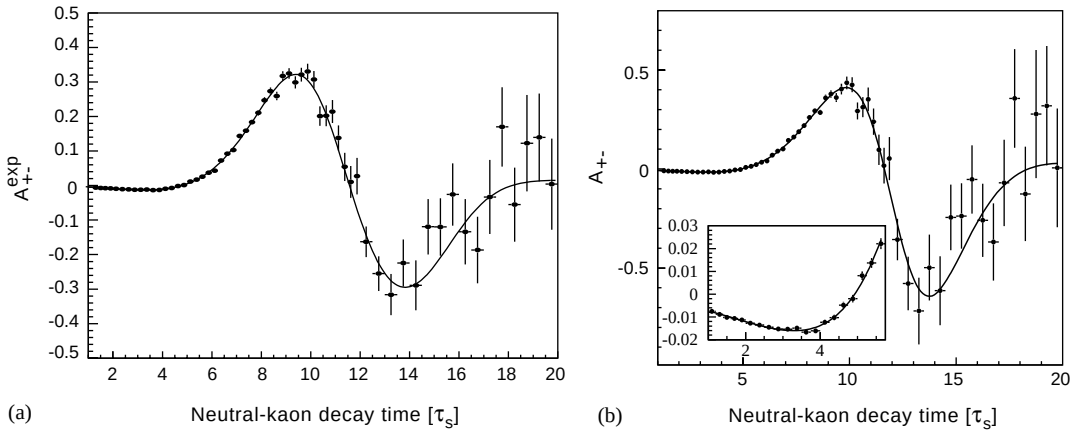


Fig. 14. (a) The measured decay-rate asymmetry, $A^{\rm exp}_{+-}(\tau)$: the data points (•) include residual background. (b) The decay-rate asymmetry $A_{+-}(\tau)$: the data points (•) are background subtracted. In both cases the continuous curve is the result of our fit.

Table 5
Correlation coefficients for the fitted values in the case of fixed $\Delta m$

| | $\phi_{+-}$ | $\lvert\eta_{+-}\rvert$ | $k$ |
|---|---|---|---|
| $\phi_{+-}$ | 1 | 0.17 | 0.37 |
| $\lvert\eta_{+-}\rvert$ | | 1 | 0.65 |
| $k$ | | | 1 |

Using for $\langle\Delta m\rangle$ and $\langle\tau_S\rangle$ the world averages [78], $\langle\Delta m\rangle = (530.1 \pm 1.4) \times 10^7\ \hbar/\mathrm{s}$ and $\langle\tau_S\rangle = (89.34 \pm 0.08)$ ps, the results of the fit are

$$|\eta_{+-}| = (2.264 \pm 0.023) \times 10^{-3}\ ,$$

$$\phi_{+-} = 43.19^\circ \pm 0.53^\circ\ ,$$

$$k = 0.9997 \pm 0.0004\ ,$$

where the errors are purely statistical and $\chi^2/\mathrm{ndf} = 1.2$. The result of the fit is shown as a solid line in Fig. 14a. The dilution effect caused by the background becomes apparent when compared to Fig. 14b where the background is subtracted. Table 5 shows the correlation coefficients between $\phi_{+-}$, $|\eta_{+-}|$ and $k$, given by the fit. An alternative way of presenting the data is given by the 'reduced asymmetry', $A_{\rm red}(\tau) = A^{\rm exp}_{+-}(\tau) \times \mathrm{e}^{-(1/2)(\Gamma_S - \Gamma_L)\tau}$, as shown in Fig. 15. The physics content of Fig. 15 is identical to that of Fig. 14, but it emphasizes the low/medium decay-time region where statistics are high and to which the fit is sensitive, at the expense of the high decay-time region where statistics are low and to which the fit has little or no sensitivity.

If the value of $\Delta m$ is left free in the fit, the result is $\Delta m = (524.0 \pm 4.4_{\rm stat} \pm 3.3_{\rm syst}) \times 10^7\ \hbar/\mathrm{s}$, in agreement with the value $(529.5 \pm 2.0_{\rm stat} \pm 0.3_{\rm syst}) \times 10^7\ \hbar/\mathrm{s}$ obtained from the complete sample of CPLEAR semileptonic data [11]; the correlation coefficient between $\Delta m$ and $\phi_{+-}$ is 0.92.

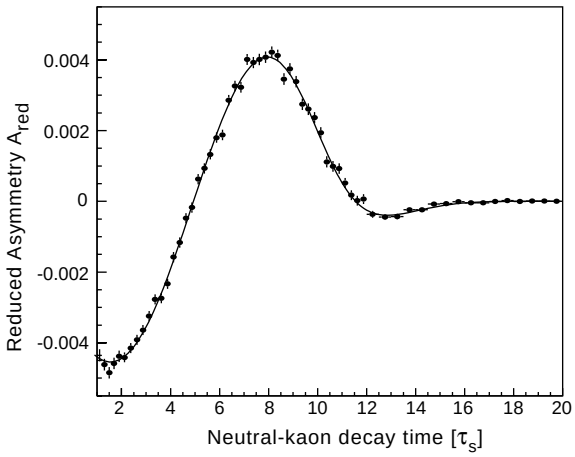


Fig. 15. The 'reduced asymmetry' $A_{\mathrm{red}}(\tau)$ (see text). The continuous curve is calculated from the result of our fit.

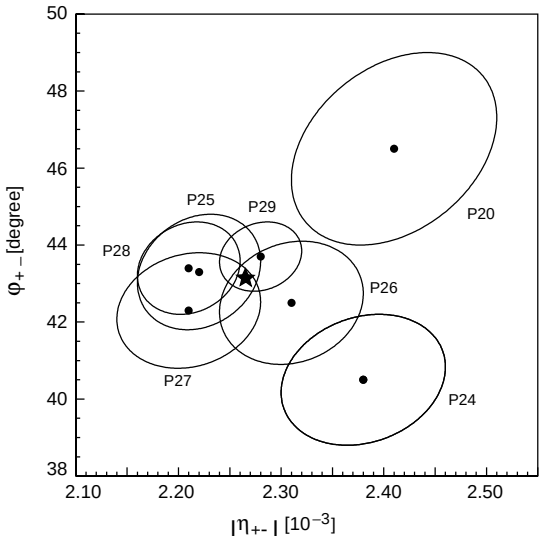


Fig. 16. The one-sigma error ellipses for $\phi_{+-}$ versus $|\eta_{+-}|$ for each data-taking period (P20 and from P24 to P29). The final result (★) is also shown.

The results from the different data-taking periods are shown in Fig. 16, together with the one-standard-deviation ellipses of $\phi_{+-}$ versus $|\eta_{+-}|$, taking into account their correlations. The value of the overall $\chi^2$ is 10.3 for 12 ndf, showing that the results for each period are internally consistent within their statistical errors.

The sources of systematic errors specific to these results are the following.

The level of background is fixed to the mean value of its three separate determinations. The scatter of these values indicates an uncertainty on this mean level of 6%. The uncertainty on the decay-time

Table 6
Systematic errors on the fitted values of $\phi_{+-}$ and $|\eta_{+-}|$ (for $\Delta m$ fixed) and of $\Delta m$ (for $\phi_{+-}$ fixed)

| Source | $\phi_{+-}$ (°) | $\lvert\eta_{+-}\rvert$ ($10^{-3}$) | $\Delta m$ ($10^7$ $\hbar$/s) |
|---|---|---|---|
| Background level | 0.09 | 0.010 | 0.9 |
| Background shape | 0.04 | 0.005 | 0.5 |
| Changes in cuts | 0.16 | 0.008 | 3.0 |
| Decay time | 0.06 | 0.010 | 0.2 |
| Normalization | 0.07 | 0.001 | 0.3 |
| Absolute time-scale | 0.03 | 0.001 | 0.1 |
| Regeneration | 0.19 | 0.019 | 0.7 |
| Total | 0.28 | 0.026 | 3.3 |
| $\Delta m$ | 0.42 | 0.001 | |
| $\tau_S$ | 0.03 | 0.007 | |

dependence of the background is determined from the errors on the parameters obtained from the fit.

The level and decay-time dependence of the background at late decay times was varied by changing the values of the fit-probability cuts at these decay times. These changes in background level and shape led to small variations in the values of the fitted parameters. This is particularly true for $\Delta m$ which has much greater sensitivity than $\phi_{+-}$ or $|\eta_{+-}|$ to data beyond 10–12 $\tau_S$. The values of other cuts were also varied and found to give very small changes in the values of the fitted parameters.

The measured values of $\phi_{+-}$, $|\eta|$ and $\Delta m$, stated earlier, were corrected for the finite resolution of the neutral-kaon decay-time measurement. The sizes of these corrections, determined using high-statistics simulated data, are $-0.18°$, $+0.042 \times 10^{-3}$ and $+0.7 \times 10^7$ $\hbar$/s respectively. The systematic errors due to these corrections were obtained by varying the resolution correction, as a function of decay time, by its statistical uncertainty.

The primary-vertex normalization procedure of applying event weights changed the fitted value of $\phi_{+-}$ by $+0.65°$, of $|\eta_{+-}|$ by $+0.02 \times 10^{-3}$ and of $\Delta m$ by $-1.3 \times 10^7$ $\hbar$/s. As for the systematic errors induced by this procedure, we refer to Section 3.7.

The systematic errors of $\phi_{+-}$ and $|\eta_{+-}|$ are shown in Table 6 for $\Delta m$ and $\tau_S$ fixed to the world-average values [79], and also for $\Delta m$ when $\phi_{+-}$ and $\tau_S$ are instead fixed to their world-average values [78]. The systematic error due to regeneration effects is discussed in Section 4.2.

Our final results for $\eta_{+-}$, with $\Delta m$ and $\tau_S$ fixed at the world-average values from [78], are

$$|\eta_{+-}| = (2.264 \pm 0.023_{\text{stat}} \pm 0.026_{\text{syst}} \pm 0.007_{\tau_S}) \times 10^{-3} \ ,$$

$$\phi_{+-} = 43.19° \pm 0.53°_{\text{stat}} \pm 0.28°_{\text{syst}} \pm 0.42°_{\Delta m} \ .$$

These values agree with the results of earlier experiments [86–93] as displayed later in Fig. 22a. Our errors are smaller (even if only slightly) than the errors quoted in any earlier experiment.

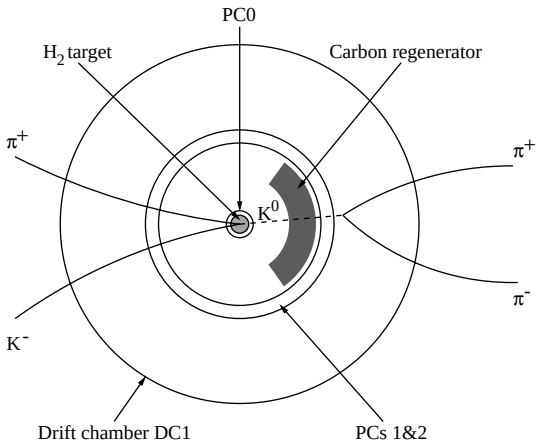


Fig. 17. The topology of a typical regeneration event in an expanded view of the inner detector.

### 4.2. $\pi^+\pi^-$—Measurement of regeneration amplitudes [24], and sign of $\Delta m$

In the CPLEAR experiment, the $K_S$ amplitude that is regenerated in the detector interferes with the inherent one from the produced $K^0(\bar{K}^0)$ states causing a small but not always negligible change in the decay rates. Carbon nuclei account for about two-thirds of the regeneration effect, and other contributions are mainly due to nitrogen and oxygen which have very similar nuclear properties. Since prior to CPLEAR direct measurements of the regeneration amplitudes $\Delta f$ were available only for kaon momenta above 2 GeV/$c$ [81,94], the regeneration amplitude in carbon was determined by CPLEAR at momenta between 250 and 750 MeV/$c$ by measuring in a dedicated data-taking the interference of inherent and coherently regenerated $K_S$ amplitudes (Section 2.3).

For this purpose the set-up was modified, as shown in Fig. 17, by the insertion of a carbon absorber (regenerator) shaped as a segment of a hollow cylinder with a thickness of 2.5 cm, a length of 25.5 cm and an opening angle of 115°. To maximize the regenerating effect within the constraints of the detector design the regenerator was positioned close to the inner wall of the first large proportional chamber (PC1). The opening angle was chosen to enable the selection of events with neutral kaons regenerated in the carbon but no charged primary tracks ($K^\pm$ and $\pi^\mp$) that crossed the absorber. The topology of a typical regeneration event is depicted schematically in Fig. 17.

To isolate the interference terms arising from regeneration, we used two sets of $\pi^+\pi^-$ events:

(a) the actual regeneration data taken with the absorber installed,
(b) a reference set containing data obtained before installing the absorber.

The two sets of data were taken under the same detector and trigger conditions, the only difference being the presence of the absorber, and they were also subject to exactly the same selection procedure. The reference data set contained more than three times the number of events of the regeneration data set so that the statistical error is almost entirely given by the statistics of the latter.

In addition to the standard selection of $K^0$ and $\bar{K}^0$ events we required, in both data sets, that the direction of the neutral kaon be in the absorber sector and rejected events in which one or both

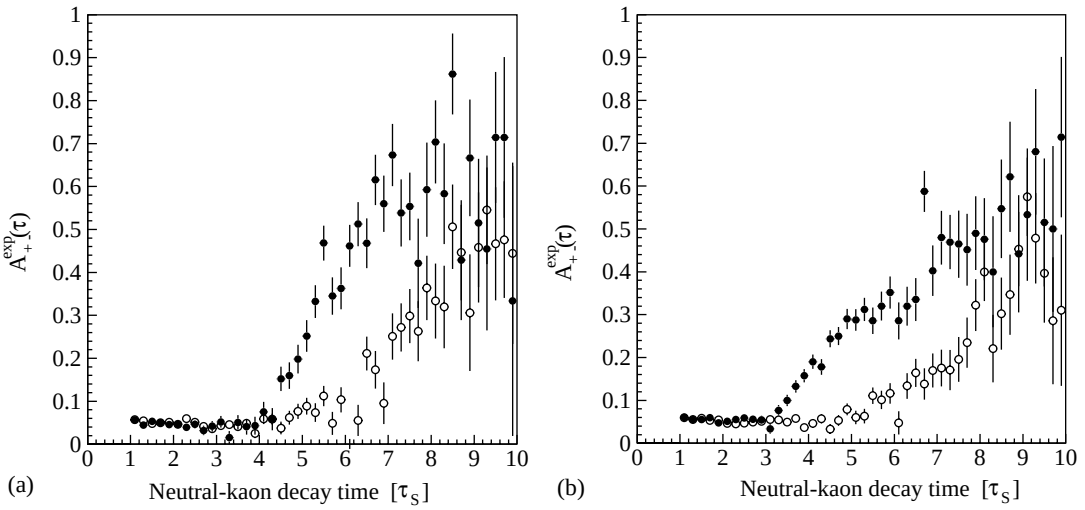


Fig. 18. Measured decay-rate asymmetries $A_{+-}^{\exp}$: (•) with absorber and (○) without absorber, for two momentum intervals centred around (a) 300 and (b) 400 MeV/$c$.

of the charged primary tracks crossed the volume occupied by the absorber. Furthermore we only accepted neutral kaons with momenta greater than 250 MeV/$c$. Within the regeneration data set, $3 \times 10^6$ events satisfy all selection criteria. In two-thirds of these events, however, the neutral kaon decays before reaching the absorber, thus yielding no information on the regeneration amplitude. About $10^7$ events of the reference data set remain after applying identical selection cuts. The gain in statistical precision at higher momenta is in part compensated for by a loss of sensitivity caused by the decreasing evolution time of the neutral kaon before reaching the absorber.

To account for the variation of the regeneration amplitude $\Delta f$ as a function of neutral-kaon momentum we divided the data of both sets into five momentum intervals of 100 MeV/$c$ width each, and decay-rate asymmetries were formed separately for each momentum interval. These asymmetries were constructed as in Eq. (51a), with the qualification that no weight was applied to the events. Fig. 18 shows two typical asymmetries. The step in the regenerator asymmetries is smeared out because the effective distance and thickness of the absorber as encountered by the neutral kaon varied from event to event depending on its emission angle. Furthermore, the neutral kaons were not mono-energetic but had a finite range of momenta.

Because of smearing effects, it was not possible to extract the desired information by a fit to an analytical function. Instead, we performed a numerical fit. For most neutral-kaon momenta, the inherent $K_S$ amplitude by far outweighs the regenerated one at the time of the decay. This means that the spatial vertex distribution of $\pi^+\pi^-$ decays in the regeneration set is well approximated by the data of the reference set and the weights applied to simulate the regeneration effects are close to one. At very low momenta, however, we find that almost all $K_S$ decay before reaching the absorber and hence our method is not applicable. We therefore restricted the analysis to neutral kaon momenta above 250 MeV/$c$, where the decay rates after the absorber are still dominated by the inherent $K_S$ amplitude.

Table 7
Systematic errors on $\Delta f$ due to the uncertainty in the normalization of $K^0$ and $\bar{K}^0$ rates

| Mom. range (MeV/$c$) | Re($\Delta f$) (fm) | Im($\Delta f$) (fm) |
|---|---|---|
| 250–550 | $< 0.05$ | $< 0.05$ |
| 550–650 | 0.06 | 0.2 |
| 650–750 | 0.06 | 0.6 |

An offset appears in the measured asymmetries of Fig. 18, as expected since the events were not weighted by a primary-vertex normalization factor. This factor is expected to be of the same magnitude in both the regeneration and the reference data set, i.e. the *relative* normalization factor $\xi_{\mathrm{rel}}$ should be close to one. We measured this factor by comparing the observed ratios of $K^0$ and $\bar{K}^0$ decays before the absorber in both data sets and obtained $\xi_{\mathrm{rel}} = 1.0028 \pm 0.0016$, constant in phase space. In the analysis, we applied this factor as a correction to the reference data set and deduced the systematic errors by varying it in its range of statistical uncertainty, see Table 7.

A further systematic error is caused by the uncertainty of $\pm 0.5$ mm in the distance between the absorber and the $K^0(\bar{K}^0)$ production point. This uncertainty propagates to differences in the regeneration amplitudes that do not exceed 0.05 fm in both the real and imaginary parts of the amplitudes.

Any difference in running conditions between the collection of the two data samples used for the analysis could constitute a further source of systematic error. In addition to ensuring that all detector and trigger parameters remained the same, we verified that neither the presence of the absorber nor the time difference of 1 year between the two runs affected the data in any unpredictable way. This was done by analysing events in which no particle came close to the absorber. The asymmetries constructed from these events are equal for the two data sets within statistical fluctuations.

We also carefully studied the effect of incoherent (diffractive) regeneration which is not taken into account in our analysis. It can be shown that in $K^0$–$\bar{K}^0$ asymmetry experiments the influence of incoherent regeneration is very small for measurements in the $K_S$-dominated decay region and may be neglected in our analysis.

Furthermore we looked at the systematics already considered for the $\eta_{+-}$ precision measurement (Section 4.1), namely background level, decay time resolution, regeneration in other detector components and the uncertainties in $\Delta m$ and $\tau_S$. These effects were all found to be negligible in this analysis.

Our results are summarized in Table 8 and Fig. 19. They represent the first experimental data on both the real and imaginary parts of the regeneration amplitude for kaon momenta below 1 GeV/$c$ and are in accordance with the predictions of Eberhard and Uchiyama [81] as well as with more recent calculations done for the $\phi$-factory at Frascati [95].

The optical theorem relates total cross-sections to the imaginary parts of the corresponding forward scattering amplitudes. Under the assumption of isospin invariance in kaon–nucleon scattering, measurements of the difference between $K^+$ and $K^-$ total cross-sections may therefore be employed to put further constraints on our results and possibly resolve their large correlation present in some momentum bins. However, in our momentum range only the measurements of Bugg et al. [96] on $K^+$ and $K^-$ total cross-sections in carbon at momenta between 655 and 2606 MeV/$c$ are available.

Table 8
The CPLEAR results on $\Delta f$ with standard errors in the Gaussian approximation in comparison with the optical model calculations of Ref. [81] where available; the last row shows the combined result of Ref. [96] and CPLEAR

| $p_{K^0}$ (MeV/$c$) | CPLEAR | | Correl. coeff. | Optical model [81] | |
|---|---|---|---|---|---|
| | $\langle \mathrm{Re}(\Delta f)\rangle$ (fm) | $\langle \mathrm{Im}(\Delta f)\rangle$ (fm) | | $\langle \mathrm{Re}(\Delta f)\rangle$ (fm) | $\langle \mathrm{Im}(\Delta f)\rangle$ (fm) |
| 250–350 | $-3.8 \pm 1.3$ | $-2.4 \pm 1.2$ | $-0.76$ | | |
| 350–450 | $-4.9 \pm 0.5$ | $-1.2 \pm 1.6$ | $-0.76$ | $-3.48$ | $-3.88$ |
| 450–550 | $-4.2 \pm 0.3$ | $-4.9 \pm 2.0$ | 0.60 | $-4.03$ | $-3.38$ |
| 550–650 | $-5.1 \pm 0.6$ | $-2.8 \pm 1.9$ | 0.96 | $-5.26$ | $-3.81$ |
| 650–750 | $-5.7 \pm 1.8$ | $-4.3 \pm 3.6$ | 0.99 | $-6.38$ | $-4.59$ |
| 650–750 | $-5.5 \pm 0.3$ | $-4.1 \pm 0.2$ | | | |

The values of Refs. [81,96] are weighted according to the neutral-kaon momentum spectrum measured at the entrance of the absorber.

(Krauss et al. [97] obtained data at lower momenta, but only for $K^+$.) We interpolated the values of Ref. [96] to compare them with our measurement in the momentum range 650–750 MeV/$c$ and found excellent agreement. The combination of the two measurements reduces the error on the real part of $\Delta f$ in this momentum bin by more than a factor of 6 (see Fig. 19e and Table 8). For a comprehensive evaluation of all available data on regeneration in carbon we refer to our dispersion relation analysis, Ref. [30].

Our results on $\Delta f$ allow us to reduce the systematic error on our measurement of the $\mathscr{CP}$-violation parameter $\phi_{+-}$ due to regeneration to below 0.2°, less than half of the statistical error (see Table 8).

It is worth pointing out that the CPLEAR regeneration experiment also provided information on the sign of $\Delta m$, i.e. on the question of which of the two mass eigenstates, $K_L$ and $K_S$ is the heavier. In fact, without a priori knowledge of the sign of $\Delta m$, the experimental data determine the complex regeneration amplitude only up to a sign ambiguity in the real part. In that case, the results of Table 8 must be interpreted as $\mathrm{Im}(\Delta f)$, sign $\times$ $\mathrm{Re}(\Delta f)$.

While the optical-model based extrapolation of kaon-nucleon scattering data to the regeneration amplitude for various materials is not accurate enough for the systematic correction of our precision measurement of $\phi_{+-}$, it is certainly adequate to establish, with very high confidence, that $\mathrm{Re}(\Delta f) < 0$ over the energy range of interest. Therefore, the CPLEAR data clearly imply $\Delta m > 0$, i.e. that $K_L$ is heavier than $K_S$. For literature concerning earlier determinations of the sign of $\Delta m$, see Refs. [98–100].

### 4.3. $\pi^0\pi^0$—*Measurement of* $|\eta_{00}|$ *and* $\phi_{00}$ *[8]*

The decay $K^0(\bar{K}^0) \to \pi^0\pi^0 \to 4\gamma$ is selected by requiring exactly two charged tracks that have been identified as a kaon and a pion, and exactly four electromagnetic showers in the calorimeter [6]. A typical event display is shown in Fig. 20, together with its reconstruction.

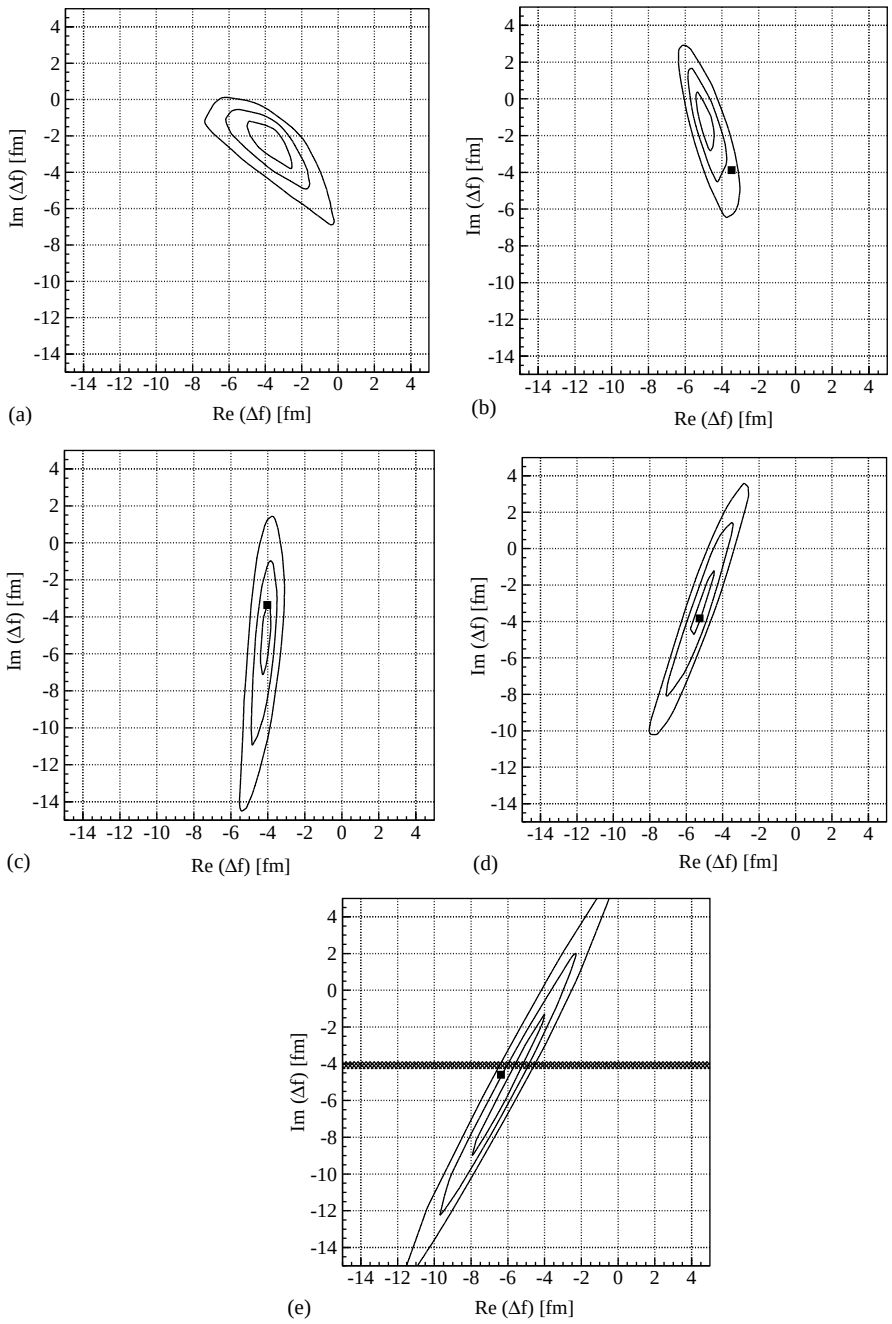


Fig. 19. The $\Delta f$ complex plane for the five momentum intervals centred around 300 (a), 400 (b), 500 (c), 600 (d) and 700 MeV/$c$ (e). The curves with $\chi^2 = \chi^2_{\min} + s^2$ are shown for $s = 1, 2, 3$, marking confidence regions that approximately correspond to 1, 2 and 3 standard deviations. The results of the optical model calculation of Ref. [81] are inserted for comparison (small squares). In (e), the total cross-section measurement of Ref. [96] is also shown (dashed region).

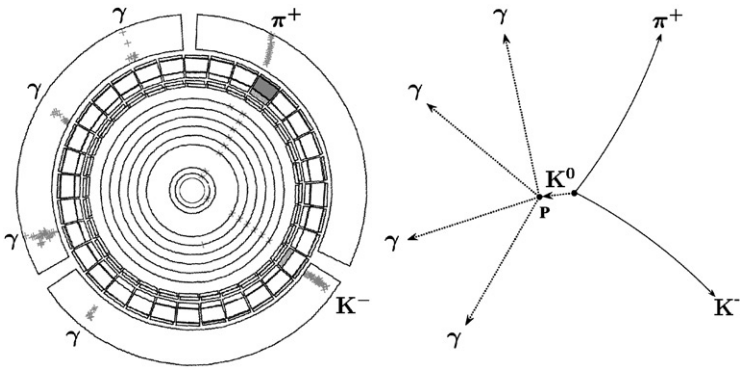


Fig. 20. Display of an event, $\bar{p}p$ (not shown) $\rightarrow K^- \pi^+ K^0$ with $K^0 \rightarrow \pi^0\pi^0 \rightarrow 4\gamma$ and its reconstruction. P is the decay point.

The decay time $\tau$ of the neutral kaon is determined from a constrained fit to the data using the momenta obtained from the charged tracks, the $\bar{K}^0(K^0)$ production vertex, the photon conversion points and the photon energies in the electromagnetic calorimeter. The decay-time resolution function is equally determined by the precision of the neutral-kaon four-momentum as by the precision of the photon conversion-point positions.

Three criteria based on the invariant masses of all $\gamma\gamma$-pair combinations, on a detailed study of the shape of the $\chi^2$ function of the decay-time distribution and on the measured shower directions of the four photons are further applied to the data in order to improve the experimental decay-time resolution. The selection criteria have been optimized by providing the best sensitivity to the measured parameters and not to the decay-time resolution or background rejection [101].

Fig. 21a shows the measured decay-time distribution for $\bar{K}^0$ and $K^0$ overlayed with the simulated decay-time distribution taking into account the acceptance, the decay-time resolution, and sources of background. The acceptance for the signal events varies only very slowly as a function of the decay time and is constant up to $\approx 10\,\tau_S$. The resolution function has been determined according to Ref. [8] and gives a value of $0.77\,\tau_S$ (FWHM).

Sources of background are the kaonic annihilation channels $\bar{p}p \rightarrow \bar{K}^0(K^0)K^{\pm}\pi^{\mp} + \pi^0$ and $\bar{p}p \rightarrow K^+K^- + n\pi^0$ ($n \geqslant 0$), the pionic annihilation channel $\bar{p}p \rightarrow \pi^+\pi^- + n\pi^0$ ($n \geqslant 0$) and the neutral-kaon decay $K_L \rightarrow \pi^0\pi^0\pi^0$. The contributions from kaons are determined from simulation, while the contributions from the pionic annihilation are determined from the data by studying the energy loss distribution of the charged particles in the inner scintillator of the particle-identification detector. Table 9 summarizes the background channels contributing to the final data sample in the decay-time interval $0$–$20\,\tau_S$. In the interference region the total background does not exceed 2.5%.

Here, to properly account for the primary-vertex normalization $\xi$, we divided the full data set into subsamples as a function of the momentum of the neutral kaon in such a way that the influence from a varying $\xi$ and a varying decay-time acceptance within each subsample become negligible. The values of $|\eta_{00}|$ and $\phi_{00}$ were extracted from a global likelihood fit to the asymmetries constructed from these different data samples as in Eq. (51b), with the summed weights $N_w$ and $\bar{N}_w$ calculated using the regeneration weights alone. The phenomenological expression to be used in the fit is then

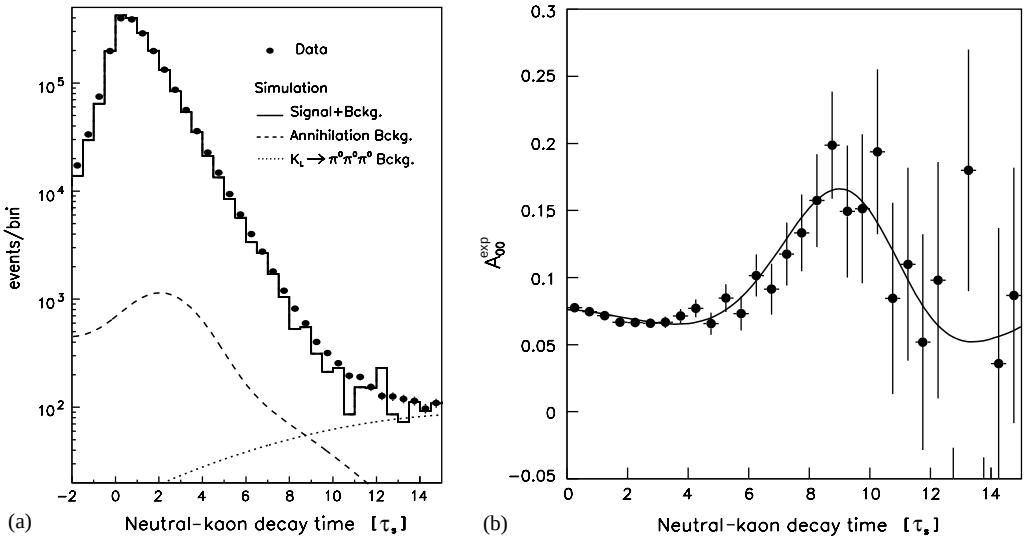


Fig. 21. (a) The measured decay-time distribution for $\bar{K}^0(K^0) \to \pi^0\pi^0$, overlayed with the result of the simulation of this decay (solid line) and the different background channels according to Table 9. The background is shown separately for contributions from $\bar{p}p$ annihilations (dashed line) and $K_L \to \pi^0\pi^0\pi^0$ decays (dotted line). (b) The measured asymmetry $A_{00}^{exp}(\tau)$. The solid line shows the result of the fit.

Table 9
Background contributions to the final data sample in the decay-time interval 0–20 $\tau_S$

| Background channel | Contribution (%) |
|---|---|
| $K_L \to \pi^0\pi^0\pi^0$ | $0.137 \pm 0.005$ |
| $\bar{p}p \to \bar{K}^0(K^0)K^{\pm}\pi^{\mp} + \pi^0$ | $0.065 \pm 0.017$ |
| $\bar{p}p \to \pi^+\pi^- + n\pi^0$ $(n \geqslant 0)$ | $0.511 \pm 0.020$ |

The quoted errors are statistical.

written as

$$A_{00}(\tau) = \frac{\alpha\xi - 1}{\alpha\xi + 1} - 2\,\frac{|\eta_{00}|e^{(1/2)(\Gamma_S-\Gamma_L)\tau}\cos(\Delta m\tau - \phi_{00})}{1 + |\eta_{00}|^2 e^{(\Gamma_S-\Gamma_L)\tau}}\ . \tag{55}$$

The decay-time resolution, the remaining background contributions and the regeneration correction were taken into account individually for each neutral-kaon momentum interval. The measured decay-rate asymmetry $A_{00}^{exp}$ is shown in Fig. 21b. The oscillation of the $\mathscr{CP}$-violation interference term is clearly visible, diluted by the decay-time resolution and by the $K_L \to \pi^0\pi^0\pi^0$ background at late decay times.

The $\alpha\xi$ values of the different momentum subsamples were free parameters in the fit, together with $|\eta_{00}|$ and $\phi_{00}$. The result of the fit is shown as a solid line in Fig. 21b. The correlation coefficient between $\phi_{00}$ and $|\eta_{00}|$ given by the fit is 0.03. The $\xi$ values have a weighted average of

Table 10
Summary of the systematic errors on $\phi_{00}$ and $|\eta_{00}|$

| Source | $\phi_{00}$ (°) | $\lvert\eta_{00}\rvert$ ($10^{-3}$) |
|---|---|---|
| Decay-time resolution | 0.6 | 0.16 |
| $\bar{K}^0/K^0$ identification efficiencies | 0.29 | 0.01 |
| Photons from secondary interactions | 1.4 | 0.13 |
| *Backgrounds* | | |
| $\bar{p}p \to \pi^+\pi^- + n\pi^0$ $(n \geqslant 0)$ | 1.1 | 0.07 |
| $\bar{p}p \to \bar{K}^0(K^0)K^\pm\pi^\mp + \pi^0$ | 0.16 | 0.05 |
| $K_L \to 3\pi^0$ | 0.26 | 0.06 |
| Regeneration | 0.2 | 0.07 |
| Total | 1.9 | 0.24 |
| $\Delta m$ | 0.34 | 0.003 |
| $\tau_S$ | 0.036 | 0.001 |

$\langle\xi\rangle = 1.178 \pm 0.003$, where the error is statistical, and $\mathrm{Re}(\varepsilon_L)$ is set equal to twice the world-average value of $\delta_\ell$ [78].

The contributions to the systematic errors are summarized in Table 10. Some comments are in order with respect to the other asymmetries.

- The systematic uncertainties in the values of $\phi_{00}$ and $|\eta_{00}|$ due to uncertainties in the parametrization of the resolution function have been determined from the decay-time distribution of Fig. 21a by varying the resolution function so that the resulting decay curve agrees within statistics with the observed one, and are given in Table 10. A possible variation in the decay-time resolution as a function of the decay time has also been studied by simulation. No evidence for such a dependence has been found and variations within the statistical limits have a negligible effect on $\phi_{00}$ and $|\eta_{00}|$.
- Systematic uncertainties introduced by a possible deviation of the relative tagging efficiencies $\xi$ from a constant and by a different decay-time acceptance, have been determined within each neutral-kaon momentum subsample.
- In a small number of events one undetected photon from the decay of $\bar{K}^0(K^0) \to \pi^0\pi^0$ is replaced by a photon that originates from the strong interaction or the decay of the accompanying charged particles in the calorimeter. For such events the reconstruction of the neutral-kaon decay time is affected. According to simulations such events contribute to about 0.7% of the data and the relative tagging efficiency for these events is 10% smaller than for correctly reconstructed events. The uncertainty in determining the number of such events has been evaluated from a fit to the measured decay-time distribution of Fig. 21a. The systematic errors as given in Table 10 were obtained by varying the number of such secondary photons by 50% and the relative identification efficiency for $\bar{K}^0$ and $K^0$ by 5%.
- Uncertainties in the determination of the background channels were estimated from various fits to the measured decay-time distribution of Fig. 21a. For each channel the amount of background as

given in Table 9 was varied by up to 50% and the relative contribution to the $\bar{K}^0$ and $K^0$ signal by 5%. For $K_L \to \pi^0\pi^0\pi^0$ and for $\bar{p}p \to \bar{K}^0(K^0)K^{\pm}\pi^{\mp} + \pi^0$, the relative amount of background in $\bar{K}^0$ and $K^0$ is identical to the relative tagging efficiency $\xi$ for the signal events. However, for the pionic background $\bar{p}p \to \pi^+\pi^- + n\pi^0$ $(n \geqslant 0)$ it is 15% smaller.

Our final result from $2 \times 10^6$ reconstructed $K^0(\bar{K}^0) \to \pi^0\pi^0$ events is

$$\phi_{00} = 42.0^\circ \pm 5.6^\circ_{\text{stat}} \pm 1.9^\circ_{\text{syst}} ,$$

$$|\eta_{00}| = [2.47 \pm 0.31_{\text{stat}} \pm 0.24_{\text{syst}}] \times 10^{-3} .$$

The dependence of $\phi_{00}$ and $|\eta_{00}|$ on $\Delta m$ (in units of $10^7\ \hbar/\text{s}$) and $\tau_S$ (in units of ps) is given by

$$\phi_{00} = [42.0 + 0.24(\Delta m - 530.7) + 0.40(\tau_S - 89.22)]^\circ ,$$

$$|\eta_{00}| = [2.47 - 0.002(\Delta m - 530.7) + 0.015(\tau_S - 89.22)] \times 10^{-3}$$

with correlation coefficients between $\phi_{00}$ and $\Delta m$ and $|\eta_{00}|$ and $\Delta m$ of 0.88 and $-0.25$, respectively. These values agree with other results [88,102–104], however in this case our errors are not as small as quoted by some earlier experiment, see Fig. 22b. A direct comparison between the decays to $\pi^0\pi^0$ and $\pi^+\pi^-$ is performed in the experiments of Refs. [88–90] with the measurement of $\phi_{+-} - \phi_{00}$, see Fig. 22c, and Refs. [105–109] with the measurement of $|\eta_{00}/\eta_{+-}|$, see Fig. 22d.

### 4.4. $\pi^+\pi^-\pi^0$—*Measurement of* $Re(\eta_{+-0})$ *and* $Im(\eta_{+-0})$ *[9]*

The parameter $\eta_{+-0}$ measures $\mathscr{CP}$ violation of $K_S \to \pi^+\pi^-\pi^0$, and is defined by Eq. (47) referred to that decay. This violation is expected to be as large as $\mathscr{CP}$ violation of $K_L \to \pi^+\pi^-$, with $\eta_{+-0} \approx \eta_{+-}$. The $\eta_{+-0}$ contribution to the interference term in the decay rates of Eq. (44) is isolated by forming the asymmetry of Eq. (48),

$$A_{+-0}(\tau) = \frac{\bar{R}_{+-0}(\tau) - R_{+-0}(\tau)}{\bar{R}_{+-0}(\tau) + R_{+-0}(\tau)}$$

$$= 2\,\text{Re}(\varepsilon + \delta) - 2e^{-(\Gamma_S - \Gamma_L)\tau/2}[\text{Re}(\eta_{+-0})\cos(\Delta m\tau) - \text{Im}(\eta_{+-0})\sin(\Delta m\tau)] . \quad (56)$$

The expected $\mathscr{CP}$-violating asymmetry is plotted in Fig. 23a and shows that the maximum sensitivity on the real and imaginary parts of the $\mathscr{CP}$ parameter is obtained at early decay time.

For $\pi^+\pi^-\pi^0$ decays, the events selected contained four charged-particle tracks, with zero total charge, and one or more electromagnetic shower in the calorimeter, well separated from any charged tracks. The latter requirement considerably reduced the background from $\bar{p}p$ annihilations to $K^+K^-\pi^+\pi^-$ as well as $\pi^+\pi^-$ and semileptonic decays of neutral kaons. At the output of the topological filter we requested that the invariant mass of the secondary particles $\pi^+\pi^-\pi^0$ be smaller than $600\ \text{MeV}/c^2$, see Fig. 24a—the charged-pion momenta were given by the track-fit procedure while the $K^0$ momentum was defined as the total missing momentum in the $\bar{p}p$ annihilation. The remaining background was estimated from the difference between data and simulated $\pi^+\pi^-\pi^0$ events properly normalized, see Fig. 24b. Since a background, not associated with semileptonic events, is clearly seen below 4 $\tau_S$, we chose to normalize the simulated data to real data above 6 $\tau_S$ where the background is only contributed by semileptonic events. We concluded that with our selections the

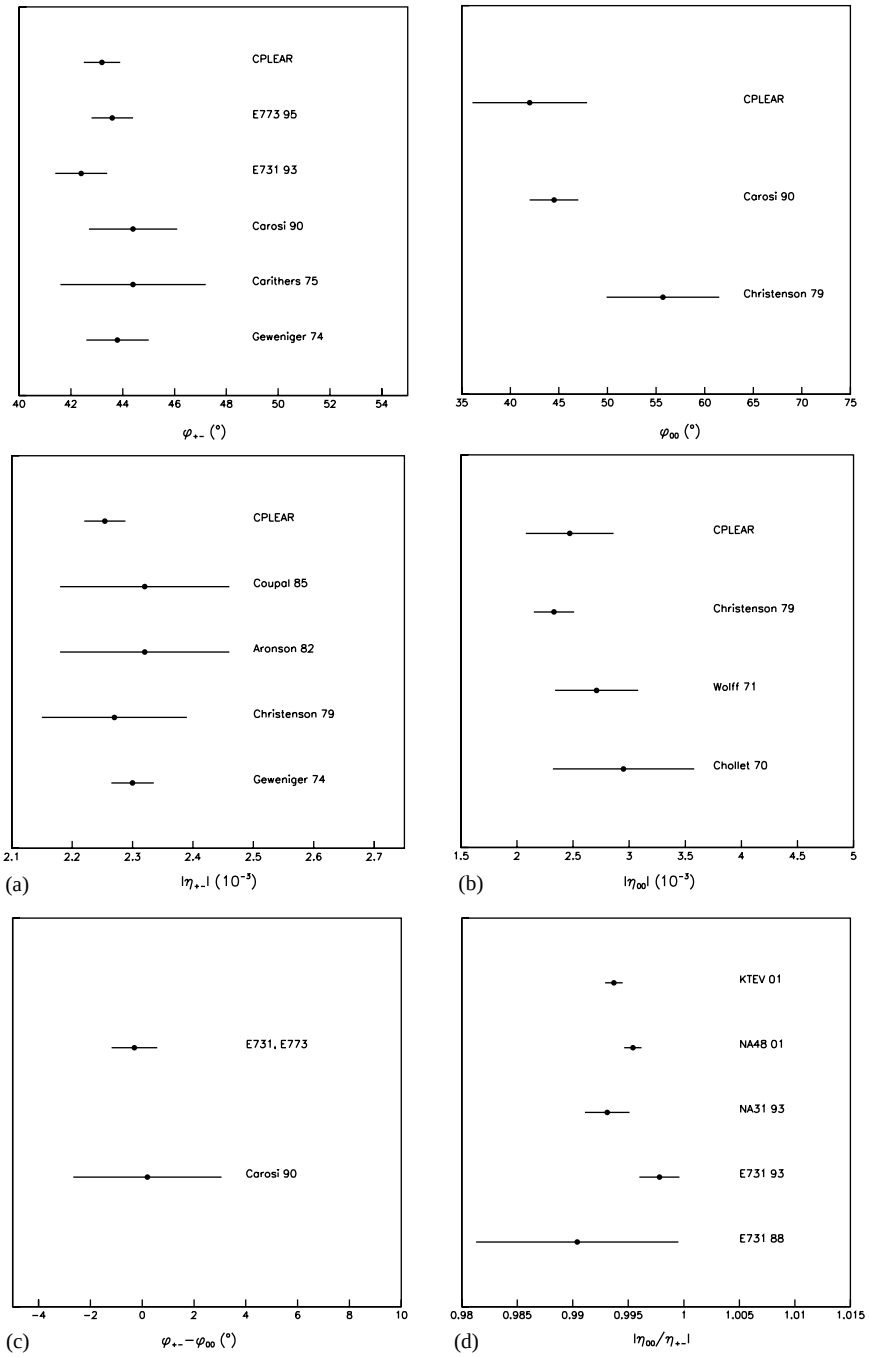


Fig. 22. CPLEAR measurements of neutral-kaon decays to $\pi\pi$ compared to previous experiments for $\Delta m = (530.0 \pm 1.2) \times 10^7\ \hbar/\mathrm{s}$ and $\tau_S = 89.35 \pm 0.08$ ps [85]: (a) $\phi_{+-}$ and $|\eta_{+-}|$ from Refs. [7,86–93]; (b) $\phi_{00}$ and $|\eta_{00}|$ from Refs. [8,88,102–104]. In some of these experiments decays to $\pi^+\pi^-$ are directly compared with decays to $\pi^0\pi^0$, (c) $\phi_{+-} - \phi_{00}$ from Refs. [88–90] and (d) $|\eta_{00}/\eta_{+-}|$ from Refs. [105–109].

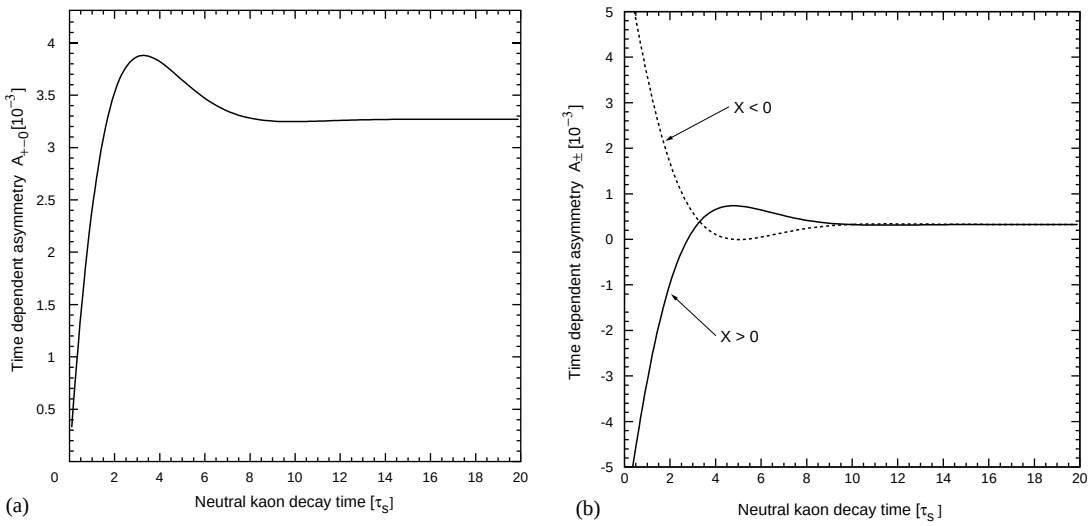


Fig. 23. The expected time-dependent decay-rate asymmetries (a) $A_{+-0}(\tau)$ and (b) $A_{\pm}(\tau) = A_{+-0}(X \lessgtr 0, \tau)$ computed by assuming $\eta_{+-0} = \eta_{+-}$. The expected value of $\lambda$ and the world-average values of $\eta_{+-}$ and other parameters are also used [78].

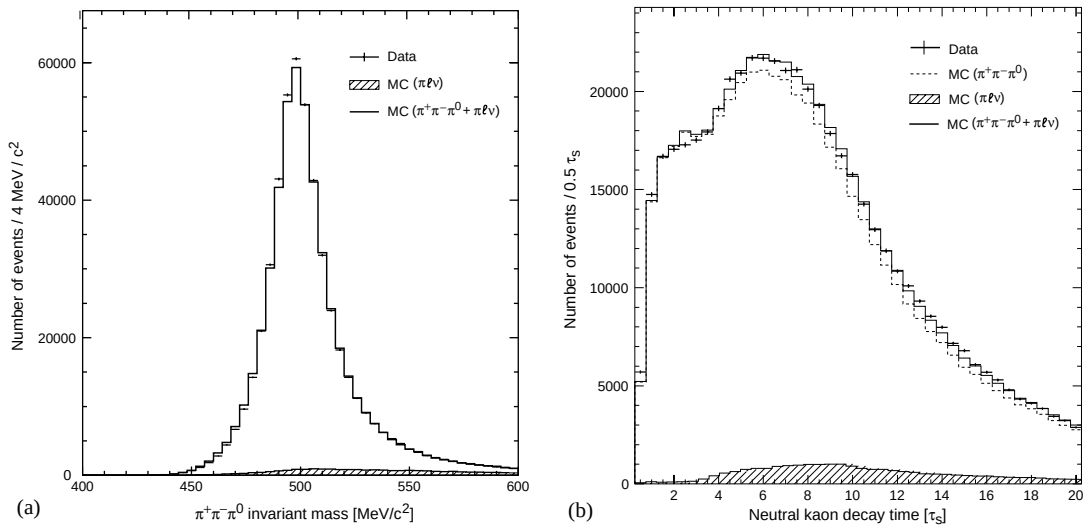


Fig. 24. (a) The $\pi^+\pi^-\pi^0$ invariant mass distribution for real and simulated data after the full selection. The plain histogram shows the simulated distribution built from the $\pi^+\pi^-\pi^0$ and the semileptonic decays of neutral kaons, normalized to the real data set above 6 $\tau_S$. The background contribution due to semileptonic decay events alone is given by the shaded area. (b) The decay-time distribution of the sum of initial $K^0$ and $\bar{K}^0$ decaying into $\pi^+\pi^-\pi^0$ for real and simulated data after applying the final selection. The full line shows the simulated distribution built from the sum of the $\pi^+\pi^-\pi^0$ and the semileptonic decays of neutral kaons, normalized to the real data set above 6 $\tau_S$. The distribution of the signal events is shown by the dashed line, while the background contribution from the semileptonic events is given by the shaded area.

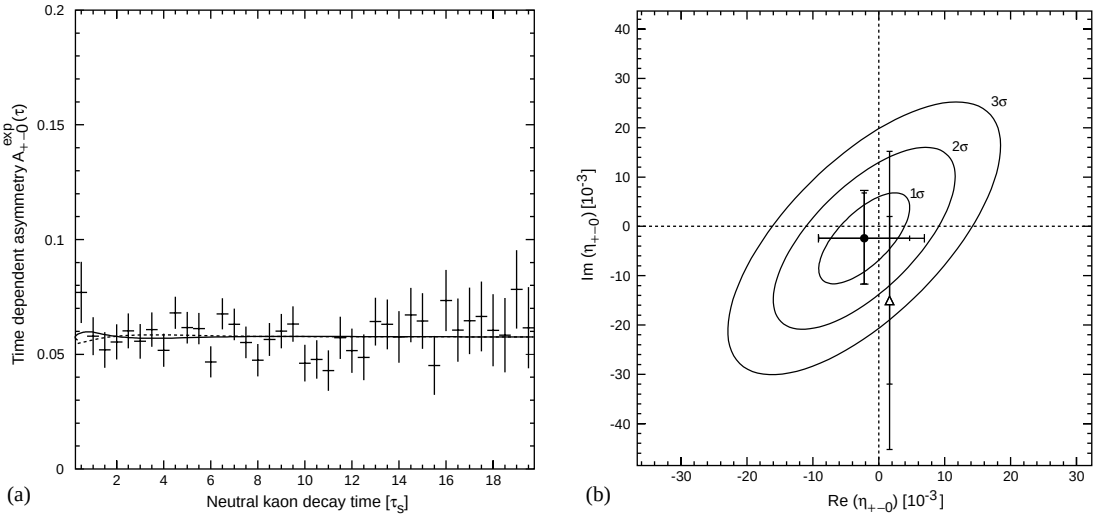


Fig. 25. (a) The measured decay-rate asymmetry $A^{\rm exp}_{+-0}(\tau)$. The solid line is the fit result. The broken line shows the asymmetry expected when assuming $\eta_{+-0}=\eta_{+-}$. (b) The real and imaginary parts of $\eta_{+-0}$: the central value (•) with its statistical and total uncertainties, and the statistical correlation ellipses as obtained in this work. For comparison, the result of Zou et al. [111] on $\mathrm{Im}(\eta_{+-0})$, obtained by fixing $\mathrm{Re}(\eta_{+-0})=\mathrm{Re}(\varepsilon)$, is also shown (△) with its statistical and total errors.

data sample was dominantly composed of neutral-kaon decays to $\pi^+\pi^-\pi^0$ with a 4% contamination of late decay-time background coming from semileptonic decays, and an 8% contamination of other, early decay-time, background.

The experimental decay-rate asymmetries are written here as

$$A_k^{\rm exp}(\tau)=\frac{\bar N_k(\tau)-N_k(\tau)}{\bar N_k(\tau)+N_k(\tau)}$$
$$\approx\left(\frac{\xi_{\rm N}-1}{\xi_{\rm N}+1}\right)+\frac{4\xi_{\rm N}[1-\zeta_{\rm B}(\tau)]}{(\xi_{\rm N}+1)^2}A_k(\tau)\ , \qquad (57)$$

where the subscript $k$ refers to the Dalitz-plot integration domain, $\xi_{\rm N}$ is the primary-vertex mean normalization factor, and $\zeta_{\rm B}(\tau)$ is the parametrization of the total-background distribution, defined as the relative difference between the data and the simulated $\pi^+\pi^-\pi^0$ events, as a function of the decay time. The quantities $N_k(\tau)$ and $\bar N_k(\tau)$ denote the event summed weights (see Section 3.1), and $A_k$ the phenomenological expressions of the asymmetries. If the integration extends to all the $X$ values, $A_k(\tau)$ becomes $A_{+-0}(\tau)$ and is given by Eq. (56). In the fitting procedure the $\mathscr{CP}$ parameters of $A_k$, and the mean normalization factor $\xi_{\rm N}$ were left to vary freely—however the dependence of the normalization on the primary K$\pi$ pair kinematic was obtained in the standard way from $\pi^+\pi^-$ decays in the range 1–4 $\tau_{\rm S}$. The quantity $\mathrm{Re}(\varepsilon_{\rm S})$ contained in $A_k$, see Eqs. (56) and (58), was taken to be equal to $\mathrm{Re}(\varepsilon_{\rm L})$ and fixed to $\delta_\ell/2$. This approximation has no consequence on the result.

The experimental asymmetry $A^{\rm exp}_{+-0}(\tau)$ obtained from the complete data set is shown in Fig. 25a together with the result of the fit to the data. The fit, performed using Eqs. (57) and (56), yielded

Table 11
Statistical correlation coefficients between $\eta_{+-0}$ and $\xi_N$ in the fit to the complete data set

| | $\mathrm{Re}(\eta_{+-0})$ | $\mathrm{Im}(\eta_{+-0})$ | $\xi_N$ |
|---|---|---|---|
| $\mathrm{Re}(\eta_{+-0})$ | 1 | | |
| $\mathrm{Im}(\eta_{+-0})$ | +0.68 | 1 | |
| $\xi_N$ | −0.21 | −0.51 | 1 |

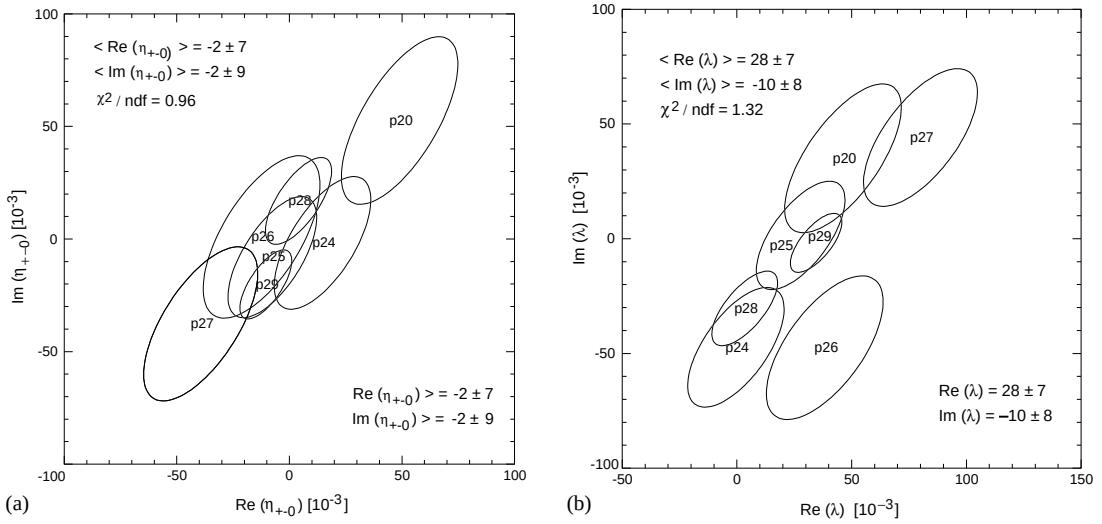


Fig. 26. The values of (a) $\mathrm{Re}(\eta_{+-0})$ and $\mathrm{Im}(\eta_{+-0})$, and (b) $\mathrm{Re}(\lambda)$ and $\mathrm{Im}(\lambda)$ fitted for each data-taking period (P20 and from P24 to P29) and the resulting mean values. The projection of the measured values in the complex plane are shown with their statistical correlation ellipses. The area of the ellipses depends on the recorded statistics. The mean values obtained are given in the top left corner and the values of the standard analysis in the bottom right corner, see Sections 4.4 and 4.5, respectively.

a value of $\chi^2/\mathrm{ndf} = 0.86$, and the statistical correlation coefficients of Table 11. The results for the various data-taking periods are reported in Fig. 26a.

The systematic errors which affect the determination of $\eta_{+-0}$ are summarized in Table 12. They mainly come from differences in the background content between the $K^0$ and $\bar{K}^0$ data sets which are not described by the background parametrization $\zeta_B$: the background component at early decay times was isolated by adding together $K^0$ and $\bar{K}^0$ data, to eliminate, to first order, any $\mathscr{CP}$-conserving or $\mathscr{CP}$-violating effects coming from $K_S$ decays. Our final result on $\eta_{+-0}$ is

$$\mathrm{Re}(\eta_{+-0}) = \left(-2 \pm 7_{\mathrm{stat}} \begin{matrix}+4\\-1\end{matrix}{}_{\mathrm{syst}}\right) \times 10^{-3} ,$$

$$\mathrm{Im}(\eta_{+-0}) = \left(-2 \pm 9_{\mathrm{stat}} \begin{matrix}+2\\-1\end{matrix}{}_{\mathrm{syst}}\right) \times 10^{-3} .$$

Table 12
Summary of the systematic errors on the real and imaginary parts of $\eta_{+-0}$

| Source | $\mathrm{Re}(\eta_{+-0})$ $(10^{-3})$ | $\mathrm{Im}(\eta_{+-0})$ $(10^{-3})$ |
|---|---|---|
| Pionic and kaonic background—amount and normalization | $\begin{pmatrix}+1.5\\-0.7\end{pmatrix}$ | $\begin{pmatrix}+0.7\\-0.2\end{pmatrix}$ |
| $\Lambda(1115)$ background | $+4.1$ | $+1.9$ |
| $\mathscr{CP}$-conserving $K_S$ decay amplitude | $-0.1$ | — |
| Decay-time dependence of normalization[a] | $\pm0.2$ | $\pm0.4$ |
| Decay-time resolution | $\pm0.2$ | $\pm0.2$ |
| Regeneration | $<0.1$ | $<0.1$ |
| $\Delta m$, $\Gamma_S$, $\Gamma_L$ and $\mathrm{Re}(\varepsilon_S)$ | — | — |
| Total | $\begin{pmatrix}+4\\-1\end{pmatrix}$ | $\begin{pmatrix}+2\\-1\end{pmatrix}$ |

[a]Error determination limited by statistics.

These quantities are displayed in Fig. 25b. Compared to the published values of Barmin et al. [110] and Zou et al. (only $\mathrm{Im}(\eta_{+-0})$) [111] our errors are smaller by more than one order of magnitude and by a factor of four, respectively. Assuming no correlation between the systematic errors, we obtain $|\eta_{+-0}| < 0.017$ at the 90% CL.

### 4.5. $\pi^+\pi^-\pi^0$—*Measurement of* $Re(\lambda)$ *and* $Im(\lambda)$ *[9]*

In a different analysis, the two asymmetries obtained by separating the rates according to whether the Dalitz variable $X$ is negative or positive,

$$A_{+-0}(X \lessgtr 0,\tau) = \frac{\bar{R}_{+-0}(X \lessgtr 0,\tau) - R_{+-0}(X \lessgtr 0,\tau)}{\bar{R}_{+-0}(X \lessgtr 0,\tau) + R_{+-0}(X \lessgtr 0,\tau)}$$
$$= 2\,\mathrm{Re}(\varepsilon+\delta) - 2e^{-(\Gamma_S-\Gamma_L)\tau/2}$$
$$\times[\mathrm{Re}(\eta_{+-0}\mp\lambda)\cos(\Delta m\tau) - \mathrm{Im}(\eta_{+-0}\mp\lambda)\sin(\Delta m\tau)]\ , \tag{58}$$

are used to determine the $\mathscr{CP}$-conserving parameter $\lambda$, defined by Eq. (46). The upper and lower signs correspond to rates integrated over positive and negative values of $X$. The expected $\mathscr{CP}$-conserving asymmetries are displayed in Fig. 23b.

For this measurement the data set is split into two parts according to the sign of the Dalitz variable $X$. The experimental asymmetries $A^{\mathrm{exp}}_{+-0}(X>0,\tau)$ and $A^{\mathrm{exp}}_{+-0}(X<0,\tau)$ are formed from the corresponding samples. Their time dependences, given by Eq. (57), are fitted to the data in two steps. Firstly, a simultaneous six-parameter fit of the functions $A^{\mathrm{exp}}_{+-0}(X>0,\tau)$ and $A^{\mathrm{exp}}_{+-0}(X<0,\tau)$ to the relevant data set gives the following results:

$$\mathrm{Re}(\eta_{+-0}) = [-2\pm7_{\mathrm{stat}}]\times10^{-3}\ ,$$
$$\mathrm{Im}(\eta_{+-0}) = [-2\pm9_{\mathrm{stat}}]\times10^{-3}\ ,$$

Table 13
Statistical correlation coefficients between $\eta_{+-0}$, $\lambda$ and $\xi_N$ when the mean primary-vertex normalization $\xi_N$ is assumed to be different for the regions of the Dalitz plot with $X \lessgtr 0$

| | $\mathrm{Re}(\eta_{+-0})$ | $\mathrm{Im}(\eta_{+-0})$ | $\xi_N^{X>0}$ | $\xi_N^{X<0}$ | $\mathrm{Re}(\lambda)$ | $\mathrm{Im}(\lambda)$ |
|---|---|---|---|---|---|---|
| $\mathrm{Re}(\eta_{+-0})$ | 1 | | | | | |
| $\mathrm{Im}(\eta_{+-0})$ | +0.677 | 1 | | | | |
| $\xi_N^{X>0}$ | −0.149 | −0.364 | 1 | | | |
| $\xi_N^{X<0}$ | −0.147 | −0.362 | 0 | 1 | | |
| $\mathrm{Re}(\lambda)$ | +0.008 | +0.003 | −0.149 | +0.147 | 1 | |
| $\mathrm{Im}(\lambda)$ | +0.003 | +0.004 | −0.364 | +0.362 | 0.677 | 1 |

$$\mathrm{Re}(\lambda) = [+27 \pm 7_{\mathrm{stat}}] \times 10^{-3} ,$$

$$\mathrm{Im}(\lambda) = [-12 \pm 9_{\mathrm{stat}}] \times 10^{-3} ,$$

$$\xi_N^{X<0} = 1.118 \pm 0.005_{\mathrm{stat}} ,$$

$$\xi_N^{X>0} = 1.114 \pm 0.005_{\mathrm{stat}} ,$$

with a $\chi^2/\mathrm{ndf} = 0.88$ and the statistical correlation matrix of Table 13. The results on $\mathrm{Re}(\eta_{+-0})$ and $\mathrm{Im}(\eta_{+-0})$ are identical to those obtained by fitting the experimental asymmetry integrated over the whole Dalitz plot. Since there is almost no correlation between $\lambda$ and $\eta_{+-0}$, $\eta_{+-0}$ was fixed to the known value of $\eta_{+-}$ [78], thus increasing the statistical accuracy without any implicit assumption on direct $\mathscr{CP}$ violation in the decay or $\mathscr{CPT}$-invariance in the mixing matrix. In addition, since $\xi_N^{X>0}$ and $\xi_N^{X<0}$ are statistically compatible, the equality $\xi_N^{X>0} = \xi_N^{X<0} = \xi_N$ was assumed. Therefore, in the second step, a simultaneous fit of the asymmetries $A_{+-0}^{\mathrm{exp}}(X > 0, \tau)$ and $A_{+-0}^{\mathrm{exp}}(X < 0, \tau)$ was performed by varying freely $\lambda$ and $\xi_N$ and by fixing $\eta_{+-}$ to the world average value [78]. The results of our measurements are shown in Fig. 27 with the result of the fit. The fit yields a value of $\chi^2/\mathrm{ndf} = 0.85$, and statistical correlation coefficients of 0.68 between $\mathrm{Re}(\lambda)$ and $\mathrm{Im}(\lambda)$, and zero between these two quantities and $\xi_N$.

Table 14 summarizes the systematic errors which affect the determination of $\lambda$. They are largely the same as those affecting the determination of $\eta_{+-0}$. We note, however, that the sensitivity to the normalization is weak in the simultaneous fit (there is no correlation between $\lambda$ and $\xi_N$) and the uncertainty on the background normalization also cancels in first order. On the other hand, the difference between the two halves, $X > 0$ and $X < 0$, of the Dalitz plot, and the difference in the background normalization lead to the dominant systematic error on $\lambda$.

As a final value for $\lambda$ we obtain

$$\mathrm{Re}(\lambda) = [+28 \pm 7_{\mathrm{stat}} \pm 3_{\mathrm{syst}}] \times 10^{-3} ,$$

$$\mathrm{Im}(\lambda) = [-10 \pm 8_{\mathrm{stat}} \pm 2_{\mathrm{syst}}] \times 10^{-3} .$$

The CPLEAR measurements are reported in Fig. 27a together with the result of the fit. The fitted value of $\lambda$ is compared to the best earlier experiment [112] in Fig. 27b. The results of the fits for the various data-taking periods are shown in Fig. 26b. Although $\lambda$ is determined without any theoretical

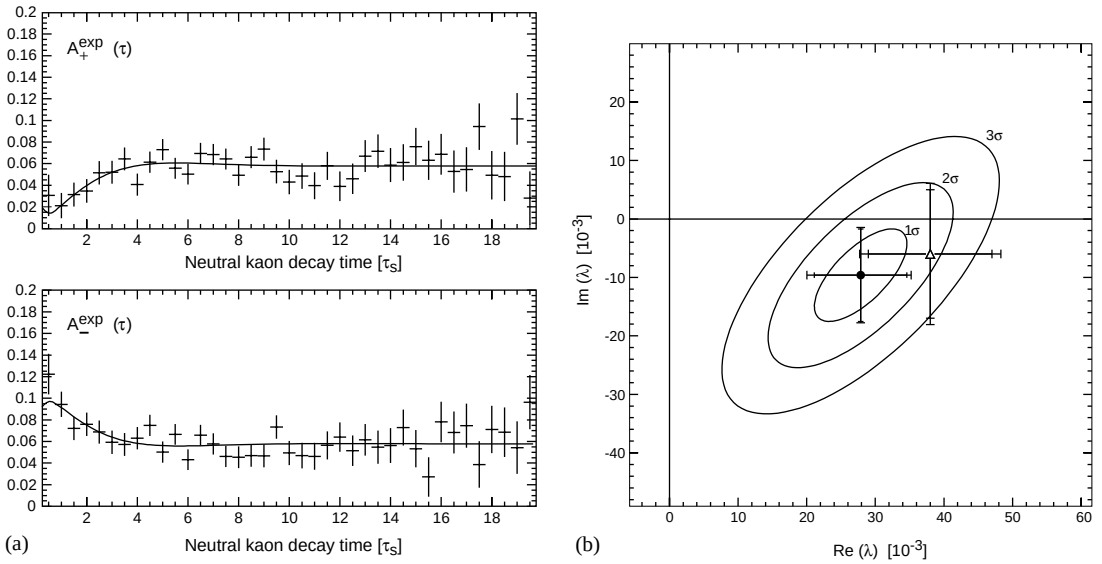


Fig. 27. (a) The measured decay-rate asymmetries for $X > 0$ and $X < 0$. The solid curves are the result of the simultaneous fit of Eq. (57) assuming common $\lambda$ and $\xi$. In this determination, we fixed $\eta_{+-0} = \eta_{+-}$. (b) The real and imaginary parts of $\lambda$: the central value (●) with its statistical and total uncertainties, and the correlation ellipses as obtained in this work. For comparison, the result of Zou et al. [112] is also shown (△) with its statistical and total error.

Table 14
Summary of the systematic errors on the real and imaginary parts of $\lambda$

| Source | Re($\lambda$) ($10^{-3}$) | Im($\lambda$) ($10^{-3}$) |
|---|---|---|
| Pionic and kaonic background—amount and $X$ asymmetry | $\begin{pmatrix}+1.3\\-1.4\end{pmatrix}$ | $\begin{pmatrix}+0.5\\-0.3\end{pmatrix}$ |
| $\Lambda(1115)$ background—amount and $X$ asymmetry | $\begin{pmatrix}+0.7\\-2.3\end{pmatrix}$ | $\begin{pmatrix}+0.2\\-0.8\end{pmatrix}$ |
| Decay-time dependence of normalization[a] | $\pm 0.2$ | $\pm 0.2$ |
| Decay-time resolution | $+1.1$ | $+0.7$ |
| Regeneration | $< 0.1$ | $< 0.1$ |
| $\Delta m$ and $\Gamma_S$ | $\pm 0.1$ | $\begin{pmatrix}+0.1\\-0.2\end{pmatrix}$ |
| Acceptance | $\pm 2.0$ | $\pm 1.8$ |
| Total | $\pm 3$ | $\pm 2$ |

[a]Error determination limited by statistics.

inputs, the determination of the branching ratio of the $\mathscr{CP}$-conserving $K_S \to \pi^+\pi^-\pi^0$ decay requires the phenomenological parametrization of the amplitudes of the neutral-kaon decay to $\pi^+\pi^-\pi^0$. This will be discussed in the next section.

### 4.6. $\pi^+\pi^-\pi^0$—Measurement of the Dalitz plot slope parameters and other decay parameters [9]

The probability to find a given momentum configuration for the $\pi^+\pi^-\pi^0$ state is given by the distribution function of the Dalitz variables $X$ and $Y$ (Dalitz plot), see Section 2.2.3. Since the sum of the masses of the three pions is close to the kaon mass, $X$ and $Y$ are small, and the corresponding decay amplitudes can be expanded as polynomials in $X$ and $Y$, limiting the expansion up to quadratic terms in $X$ and $Y$.

Following the literature [113–118] we express the $K_S$ and $K_L$ decay amplitudes as follows:

$$\begin{aligned}
&\mathscr{A}_S^{3\pi(CP=-1)}(X,Y) \approx \varepsilon_S \mathscr{A}_L^{3\pi(CP=-1)}(X,Y)\ ,\\
&\mathscr{A}_S^{3\pi(CP=+1)}(X,Y) \approx \gamma X(1+i\delta_2) - \xi_{XY} XY\ ,\\
&\mathscr{A}_L^{3\pi(CP=-1)}(X,Y) \approx \alpha(1+i\delta_1) - \beta Y(1+i\delta_{1M}) + \xi(Y^2 - \tfrac{1}{3}X^2) + \zeta(Y^2 + \tfrac{1}{3}X^2)\ ,\\
&\mathscr{A}_L^{3\pi(CP=+1)}(X,Y) \approx \varepsilon_L \mathscr{A}_S^{3\pi(CP=+1)}(X,Y)\ .
\end{aligned} \tag{59}$$

The parameters contained in the above functions, shortly denoted as isospin components, are related to the isospin amplitudes $a_{0,1}$ and $a_{1,2}$ of Eqs. (43), and have equal weak phases (that is direct $\mathscr{CP}$ violation is not included). The $\pi\pi$ interaction in the final states (rescattering) gives the phases $\delta_1$ and $\delta_{1M}$ if the state isospin is $I=1$ [113], and $\delta_2$ if $I=2$. The amplitudes $\xi$, $\xi_{XY}$ and $\zeta$ correspond to angular momenta $l>1$ and final-state interactions. These terms are small, and their rescattering phases are neglected [118].

The isospin components may also be determined through the energy dependence of the Dalitz distribution for $K_L \to \pi^+\pi^-\pi^0$, which is usually parametrized as

$$|\mathscr{A}_L^{3\pi}(X,Y)|^2 \propto 1 + gY + hY^2 + jX + kX^2 + fXY\ . \tag{60}$$

The so-called slope parameters $g$, $h$, $j$, $k$, and $f$ are expressed in terms of the isospin amplitudes of Eqs. (59) as

$$\begin{aligned}
&g = -2\frac{\beta}{\alpha},\quad h = 2\frac{\zeta+\xi}{\alpha} + \left(\frac{\beta}{\alpha}\right)^2,\quad k = \frac{2}{3}\frac{\zeta-\xi}{\alpha}\ ,\\
&j = 2\,\mathrm{Re}(\varepsilon_L)\frac{\gamma}{\alpha},\quad f = 2\,\mathrm{Re}(\varepsilon_L)\frac{\gamma\beta}{\alpha^2}\ .
\end{aligned} \tag{61}$$

(A non-zero value of the slope parameters $j$ and $f$ would indicate $\mathscr{CP}$ violation in $K_L$ decays to $\pi^+\pi^-\pi^0$.)

Previous to CPLEAR, the isospin components $\alpha$, $\beta$, $\gamma$, $\xi$, $\xi_{XY}$ and $\zeta$ were determined by a fit to all known neutral-and charged-kaon decay rates [113,117] and also estimated by fits to data using chiral perturbation theory (ChPT) at next-to-leading order [117,118]. In these calculations both $\Delta I = 1/2$ and $\Delta I = 3/2$ transitions were taken into account, while the rescattering phases and their kinematical dependence were only considered in Ref. [118].

By using the parametrizations of Eqs. (59), we deduce the following relations:

$$\begin{aligned}
&\eta_{+-0} = \varepsilon_S\ ,\\
&\mathrm{Re}(\lambda) = \frac{\gamma(\alpha I_{1,0} - \beta I_{1,1}) - \alpha\xi_{XY} I_{1,1}}{\alpha^2 I_{0,0} - 2\alpha\beta I_{0,1} + \beta^2 I_{0,2}}\ ,
\end{aligned} \tag{62}$$

Table 15
The real and imaginary parts of the $\mathscr{CP}$-conserving parameter $\lambda$

| | K expts. [117] | ChPT [117] | ChPT [118] | E621 [112] | CPLEAR |
|---|---|---|---|---|---|
| Re($\lambda$) | $0.028 \pm 0.003$ | 0.031 | $+0.031$ | $+0.038 \pm 0.010$ | $+0.028 \pm 0.008$ |
| Im($\lambda$) | — | — | $-0.006$ | $-0.006 \pm 0.012$ | $-0.010 \pm 0.008$ |

The values of the first three columns were evaluated from the isospin components displayed, respectively, in the first three columns of Table 20 using Eqs. (62) and (63). For comparison, the values measured directly by E621 and CPLEAR are shown in the last two columns.

$$\mathrm{Im}(\lambda) = \frac{\gamma(\alpha(\delta_2 - \delta_1)I_{1,0} - \beta(\delta_2 - \delta_{1\mathrm{M}})I_{1,1}) + \alpha\xi_{XY}\delta_1 I_{1,1}}{\alpha^2 I_{0,0} - 2\alpha\beta I_{0,1} + \beta^2 I_{0,2}} \ , \tag{63}$$

where the coefficient $I_{n,m}$ represents the integral, over the Dalitz plot, of the quantity $X^n Y^m$. We note that for the parameter $\lambda$ describing the interference between the $K_S$ and $K_L$ $\mathscr{CP}$-allowed decay amplitudes, an imaginary part could exist only because of the rescattering phase or a possible direct $\mathscr{CP}$-violation contribution. Both, however, are small, and $\lambda$ is expected to be almost real.

Table 15 shows a comparison between the values of $\lambda$ obtained by entering in Eqs. (62) and (63) the isospin components given in Refs. [117,118], as mentioned above, and the results of direct measurements by CPLEAR and the best earlier experiment [112].

Within this context, we have measured directly the isospin components $\gamma$ and $\xi_{XY}$ of the $K_S$ decay amplitudes, and the slope parameters of the $K_L$ decay to $\pi^+\pi^-\pi^0$. Besides being of intrinsic interest, these measurements provide, by comparison with those of previous experiments, an overall consistency check of our systematic errors.

*4.6.1. $K_S$ decay: the isospin components of the amplitude, $\gamma$ and $\xi_{XY}$*

CPLEAR has measured directly the isospin components $\gamma$ and $\xi_{XY}$ of the $K_S \to \pi^+\pi^-\pi^0$ amplitude. Using the parametrization of the neutral-kaon decay amplitudes given in Eqs. (59), at each point of the Dalitz plot, we define the asymmetry

$$\begin{aligned} A_\xi(X,Y,\tau) &= \frac{[\bar{R}(X,Y,\tau|X<0) + R(X,Y,\tau|X>0)] - [\bar{R}(X,Y,\tau|X>0) + R(X,Y,\tau|X<0)]}{[\bar{R}(X,Y,\tau|X<0) + R(X,Y,\tau|X>0)] + [\bar{R}(X,Y,\tau|X>0) + R(X,Y,\tau|X<0)]} \\ &= 2|X|\,\frac{\gamma - \xi_{XY}Y}{\alpha - \beta Y}\cos(\Delta m\tau)\mathrm{e}^{-(\Gamma_S-\Gamma_L)\tau/2} \ , \end{aligned} \tag{64}$$

where the rescattering phases and second-order terms in $X$ and $Y$ are neglected.

The asymmetries of Eq. (64) were folded with the $X$ and $Y$ resolutions determined with simulated data, and fitted simultaneously, with a likelihood fit, to the experimental asymmetries, constructed as usual from the corresponding summed weights of events:

$$A_\xi^{\mathrm{exp}}(X,Y,\tau) \approx (1 - \zeta_{\mathrm{B}}(X,Y,\tau))A_\xi(X,Y,\tau) \ ,$$

where $\zeta_{\mathrm{B}}(X,Y,\tau)$ is the parametrization of the total-background distribution as a function of the decay time $\tau$ and the Dalitz variables $X$ and $Y$, see Section 4.4. In this fit, $\gamma$ and $\xi_{XY}$ vary freely while $\alpha$ and $\beta$ are fixed to the experimental values of Ref. [117], see first column of Table 20. Table 16

Table 16
Summary of the systematic errors on $\gamma$ and $\xi_{XY}$

| Source | $\gamma$ | $\xi_{XY}$ |
|---|---|---|
| Pionic and kaonic background—amount and asymmetry in $X$ | $\begin{pmatrix} +0.20 \\ -0.06 \end{pmatrix}$ | $\begin{pmatrix} +0.31 \\ -0.05 \end{pmatrix}$ |
| $\Lambda(1115)$ background—amount and asymmetry in $X$ | $\begin{pmatrix} +0.12 \\ -0.32 \end{pmatrix}$ | $\begin{pmatrix} +0.05 \\ -0.28 \end{pmatrix}$ |
| Decay-time resolution | $+0.10$ | $+0.01$ |
| Regeneration | — | — |
| $\Delta m$ and $\Gamma_S$ | $\pm 0.01$ | — |
| $\alpha$ and $\beta$ | $\pm 0.03$ | $\pm 0.03$ |
| Total | $\pm 0.3$ | $\pm 0.3$ |

summarizes the systematic errors which affect the determination of $\gamma$ and $\xi_{XY}$, mostly from the same sources as $\lambda$. The uncertainties on the values of $\alpha$ and $\beta$ have a negligible effect. The final results for $\gamma$ and $\xi_{XY}$ are

$$\gamma = 3.3 \pm 0.4_{\text{stat}} \pm 0.3_{\text{syst}} \ ,$$

$$\xi_{XY} = 0.4 \pm 0.7_{\text{stat}} \pm 0.3_{\text{syst}} \ ,$$

with a statistical correlation of 8% between the two extracted parameters.

### 4.6.2. $K_L$ decay: the slope parameters

The slope parameters defined in Eq. (60) were extracted by fitting the energy dependence of the $K_L \to \pi^+\pi^-\pi^0$ events in the Dalitz plot. The Dalitz distribution was constructed from initial $K^0$ and $\bar{K}^0$ events in the decay-time interval between 2 $\tau_S$ and 24 $\tau_S$ so as to remove the $K_S$ component and the early decay-time background. To correct for the variation of the acceptance across the Dalitz plot and the background, the simulated distributions of $K_L$ decays to various channels were parametrized using orthogonal polynomials in $X$ and $Y$. Then a function of the form of Eq. (60) multiplied by the simulation acceptance is fitted to the data.

The events were split into samples corresponding to disjoint decay-time intervals of 2 $\tau_S$ width where the acceptance is assumed not to depend on the decay time. These event samples were separately fitted to obtain the slope parameters as a function of the decay time and the results then averaged with a minimum-$\chi^2$ procedure. The results of the fit are shown in Fig. 28; the correlations between the slope parameters are small as indicated in Table 17. The systematic errors are summarized in Table 18. Contrary to the determination of $\eta_{+-0}$ and $\lambda$ which are based on asymmetries, the determination of the slope parameters depends crucially on the knowledge of the acceptance shape. However, the systematic errors related to the early decay-time background are negligible since only data with decay times above 2 $\tau_S$ are used in the analysis. The final results for the slope

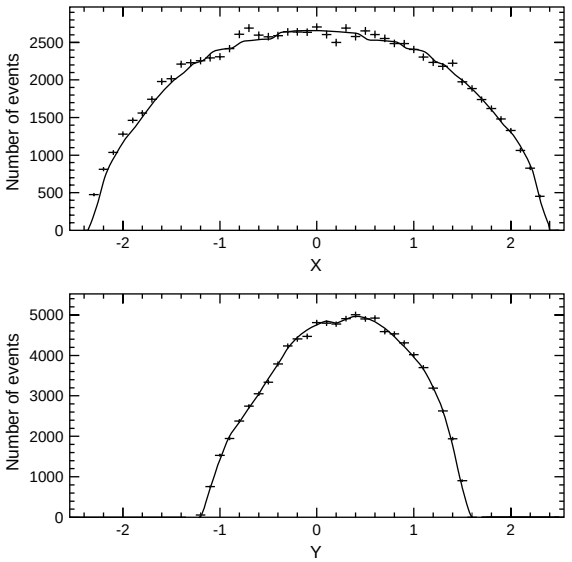


Fig. 28. $X$ and $Y$ distributions for $K_L$ decays to $\pi^+\pi^-\pi^0$ with a decay time greater than 2 $\tau_S$. The crosses indicate the data while the solid lines are calculated with the results of the slope-parameter fit.

Table 17
Correlation matrix for the slope parameters of the Dalitz plot

| | $g$ | $h$ | $j$ | $k$ | $f$ |
|---|---|---|---|---|---|
| $g$ | 1 | | | | |
| $h$ | +0.011 | 1 | | | |
| $j$ | −0.050 | +0.075 | 1 | | |
| $k$ | +0.003 | +0.031 | −0.017 | 1 | |
| $f$ | +0.066 | +0.060 | +0.055 | +0.005 | 1 |

Table 18
Summary of the systematic errors of the slope parameters for $K_L$ decays to $\pi^+\pi^-\pi^0$

| Source | $g$ $(10^{-3})$ | $h$ $(10^{-2})$ | $j$ $(10^{-3})$ | $k$ $(10^{-3})$ | $f$ $(10^{-3})$ |
|---|---|---|---|---|---|
| Acceptance shape | ±3.8 | ±1.4 | ±2.8 | ±2.3 | ±5.6 |
| Acceptance statistics | ±2.3 | ±0.1 | ±0.9 | ±0.5 | ±1.7 |
| Resolution in $X$ and $Y$ | ±0.5 | ±0.1 | ±0.6 | ±0.5 | ±1.0 |
| Total | 4.4 | 1.5 | 3.0 | 2.4 | 5.9 |

The uncertainties due to radiative corrections, primary-vertex normalization, semileptonic background and regeneration effects were all found to be negligible.

Table 19
The slope parameters of the $K_L$ decays to $\pi^+\pi^-\pi^0$: the values measured by CPLEAR are compared with other existing results

| | K experiments [117] | ChPT $\mathcal{O}(p^4)$ [117,118] | PDG'98 [78] | CPLEAR |
|---|---|---|---|---|
| $g$ | $0.67 \pm 0.01$ | 0.67 | $0.670 \pm 0.014$ | $0.682 \pm 0.007$ |
| $h$ | $0.08 \pm 0.01$ | 0.06 | $0.079 \pm 0.007$ | $0.061 \pm 0.015$ |
| $j$ | — | $1.1 \times 10^{-4}$ | $0.0011 \pm 0.0008$ | $0.001 \pm 0.004$ |
| $k$ | $0.01 \pm 0.04$ | 0.006 | $0.0098 \pm 0.0018$ | $0.010 \pm 0.003$ |
| $f$ | — | $3.7 \times 10^{-5}$ | — | $(4.5 \pm 6.4) \times 10^{-3}$ |

The values in the first two columns were obtained from the kaon decay amplitudes of Table 20, by using Eqs. (61) with $\mathrm{Re}(\varepsilon_L) = \delta_\ell/2$, where $\delta_\ell$ is the $K_L$ lepton-charge asymmetry as given in [78].

parameters are

$$g = 0.6823 \pm 0.0044_{\mathrm{stat}} \pm 0.0044_{\mathrm{syst}} ,$$

$$h = [6.1 \pm 0.4_{\mathrm{stat}} \pm 1.5_{\mathrm{syst}}] \times 10^{-2} ,$$

$$j = [1.0 \pm 2.4_{\mathrm{stat}} \pm 3.0_{\mathrm{syst}}] \times 10^{-3} ,$$

$$k = [1.04 \pm 0.17_{\mathrm{stat}} \pm 0.24_{\mathrm{syst}}] \times 10^{-2} ,$$

$$f = [4.5 \pm 2.4_{\mathrm{stat}} \pm 5.9_{\mathrm{syst}}] \times 10^{-3} .$$

The CPLEAR values are compared in Table 19 with the ones previously available. In general, good agreement with previous experiments is found, with an improvement in the determination of the parameter $g$ by a factor of two.

From the CPLEAR slope parameters and the value of $\alpha$ reported in Table 20, first column, we deduce, using Eq. (61), the values of the $K_L$ decay amplitudes $\beta$, $\xi$ and $\zeta$ which are reported in Table 20, last column, together with the values of $\gamma$ and $\xi_{XY}$ measured directly. These results are compared in Table 20, with the values given by either a phenomenological fit to all known kaon decay rates or ChPT calculations [117,118]. Our direct measurement of $\gamma$ and $\xi_{XY}$ is in agreement with these values and has a comparable uncertainty.

By using Eq. (62), with the above values of $\gamma$ and $\xi_{XY}$ the resulting $\mathrm{Re}(\lambda)$ can be compared with the measured one obtained when $\mathrm{Im}(\lambda)$ is fixed to zero. Both determinations of $\mathrm{Re}(\lambda)$ agree within the errors, confirming our understanding of the $X$ and $Y$ dependence on the background.

#### 4.6.3. Branching ratio of $\mathcal{CP}$-allowed $K_S$ decays to $\pi^+\pi^-\pi^0$

The ratio of the partial decay widths of $K_S$ and $K_L$ decays to $\pi^+\pi^-\pi^0$ ($\Gamma_S^{+-0}$ and $\Gamma_L^{+-0}$, respectively) is expressed as a function of the isospin components, $\alpha$, $\beta$ and $\gamma$, see Eqs. (59), if the amplitude $\xi_{XY}$ is neglected:

$$\frac{\Gamma_S^{+-0}}{\Gamma_L^{+-0}} = \frac{\int_\Omega |\mathscr{A}_S^{3\pi(\mathrm{CP}=+1)}(X,Y)|^2 \, \mathrm{d}X \, \mathrm{d}Y}{\int_\Omega |\mathscr{A}_L^{3\pi(\mathrm{CP}=-1)}(X,Y)|^2 \, \mathrm{d}X \, \mathrm{d}Y} = \gamma^2 \times \frac{I_{2,0}}{\alpha^2 I_{0,0} - 2\alpha\beta I_{0,1} + \beta^2 I_{0,2}} . \tag{65}$$

Table 20
Summary of the values of the neutral-kaon decay amplitude components appearing in Eqs. (59)

| | K expts. [117] | ChPT [117] | ChPT [118] | PDG'98 [78] | CPLEAR |
|---|---|---|---|---|---|
| $\alpha$ | $+84.3 \pm 0.6$ | | $+84.2$ | — | — |
| $\beta$ | $-28.1 \pm 0.5$ | | $-28.1$ | $-28.2 \pm 0.6$ | $-28.8 \pm 0.3$ |
| $\zeta$ | $-0.05 \pm 0.2$ | | $-0.6$ | $-0.08 \pm 0.2$ | $-0.5 \pm 0.4$ |
| $\xi$ | $-1.3 \pm 0.5$ | | $-1.4$ | $-1.3 \pm 0.2$ | $-1.8 \pm 0.4$ |
| $\gamma$ | $+2.6 \pm 0.3$ | | $+2.9$ | — | $+3.3 \pm 0.5$ |
| $\xi_{XY}$ | $-0.3 \pm 0.7$ | | $-0.1$ | — | $+0.4 \pm 0.8$ |
| $\delta_1$ | — | — | 0.13 | — | — |
| $\delta_{1M}$ | — | — | 0.41 | — | — |
| $\delta_2$ | — | — | 0.047 | — | — |
| $\delta_2 - \delta_1$ | — | — | $-0.083$ | — | $-0.33 \pm 0.29$ |

For comparison, earlier values are reported in the first three columns. They result from fits to all known charged-and neutral-kaon decay rates using either Eqs. (59) (first column from left) or chiral perturbation theory (ChPT) calculations (second and third columns). In the last two columns, the values of $\beta$, $\zeta$ and $\xi$ were computed using Eqs. (61), $\alpha = +84.3 \pm 0.6$, and the slope parameters measured in earlier experiments [78] and by CPLEAR; the values of $\gamma$ and $\xi_{XY}$ were instead directly measured by CPLEAR. The phase difference $(\delta_2 - \delta_1)$ was computed from the value of $\mathrm{Im}(\lambda)$ measured by CPLEAR, using Eq. (63) and the amplitude values given by ChPT.

In our numerical evaluation a better accuracy is achieved if we express $\gamma$ through $\mathrm{Re}(\lambda)$ by using Eq. (62). With this option, we obtain

$$\mathrm{BR}(\mathrm{K_S} \to \pi^+\pi^-\pi^0) = \frac{\Gamma_\mathrm{L}}{\Gamma_\mathrm{S}} \times \mathrm{BR}(\mathrm{K_L} \to \pi^+\pi^-\pi^0) \times \mathrm{Re}(\lambda)^2 \times \frac{I_{2,0}(\alpha^2 I_{0,0} - 2\alpha\beta I_{0,1} + \beta^2 I_{0,2})}{(\alpha I_{1,0} - \beta I_{1,1})^2} \ .$$

By taking the world average value for $\mathrm{BR}(\mathrm{K_L} \to \pi^+\pi^-\pi^0)$ [78], and the experimental values for $\alpha$ and $\beta$ (first column of Table 20), we arrive at the following numerical relation between the desired branching ratio and $\mathrm{Re}(\lambda)$:

$$\mathrm{BR}(\mathrm{K_S} \to \pi^+\pi^-\pi^0) = \mathrm{Re}(\lambda)^2 \times (3.24 \pm 0.06) \times 10^{-4} \ . \tag{66}$$

Using the above equation with the CPLEAR value of $\mathrm{Re}(\lambda)$ we finally obtain for the branching ratio of the $\mathscr{CP}$-conserving $\mathrm{K_S}$ decay to $\pi^+\pi^-\pi^0$

$$\mathrm{BR}(\mathrm{K_S} \to \pi^+\pi^-\pi^0) = \left( 2.5 \begin{matrix} +1.3 \\ -1.0 \end{matrix}^{\mathrm{stat}} \begin{matrix} +0.5 \\ -0.6 \end{matrix}^{\mathrm{syst}} \right) \times 10^{-7} \ ,$$

where the systematic error also includes a contribution from the uncertainties on the $\mathrm{K_L}$ isospin components. This result is currently the most precise determination of the $\mathscr{CP}$-conserving $\mathrm{K_S}$ decay rate to $\pi^+\pi^-\pi^0$ with small systematic errors, and it is in good agreement with previous measurements.

From our measured value of $\mathrm{Im}(\lambda)$, by using Eq. (63), we have obtained a limit on the rescattering phase difference $(\delta_2 - \delta_1)$. For this purpose we used the values of $\alpha$, $\beta$ and $\gamma$ from ChPT (Table 20) since only in that case were the rescattering phases taken into account. The term proportional to $\xi_{XY}$

could be neglected, and an uncertainty of $\pm\pi$ on $(\delta_2 - \delta_{1M})$ was assumed. Finally we have that at 90% CL

$$-46^\circ < (\delta_2 - \delta_1) < 9^\circ \ ,$$

where the confidence interval is mainly determined by the total uncertainty on the measured value of $\mathrm{Im}(\lambda)$.

### 4.7. $\pi^0\pi^0\pi^0$—*Measurement of* $Re(\eta_{000})$ *and* $Im(\eta_{000})$ *[10]*

In contrast to the $\pi^+\pi^-\pi^0$ final state, the $\pi^0\pi^0\pi^0$ state has a well-defined $\mathscr{CP}$ eigenvalue and the $\mathscr{CP}$-conserving $K_S \to \pi^0\pi^0\pi^0$ decay does not occur. The $\mathscr{CP}$-violation parameter $\eta_{000}$ is the ratio of $K_S$ to $K_L$ decay amplitudes for this final state, and is more accurately defined by Eq. (47): $\mathrm{Re}(\eta_{000})$ is a measure of $\mathscr{CP}$ violation in the mixing of neutral kaons, and $\mathrm{Im}(\eta_{000})$ is sensitive to a possible direct $\mathscr{CP}$ violation in the decay amplitudes.

The decay $K^0(\bar{K}^0) \to \pi^0\pi^0\pi^0 \to 6\gamma$ is selected by requiring two charged tracks that have been identified as a kaon and a pion, and six electromagnetic showers in the ECAL [6]. In order to determine the neutral-kaon decay time, the position of the annihilation vertex and the four-momentum of the neutral kaon are calculated from the track parameters of the charged kaon and pion, whereas the decay vertex of the neutral kaon along its direction of flight is determined from the six photon showers measured in the calorimeter. The average energies of the least and most energetic photons are $\approx 40$ and $\approx 250$ MeV, respectively. The reconstruction of the showers is provided by the shower-pattern recognition algorithm described in Ref. [6]. To suppress photons generated by secondary interactions of charged tracks in the calorimeter, showers are only accepted if their conversion point is at least 50 or 25 cm from the charged-kaon or -pion track extrapolation into the calorimeter, respectively.

The neutral-kaon decay time is determined by a full geometrical and kinematical reconstruction of the annihilation $\bar{p}p \to \bar{K}^0(K^0)K^\pm\pi^\mp$ and the neutral-particle cascade $K^0 \to \pi^0\pi^0\pi^0 \to 6\gamma$ through a constrained fit. This fit requires energy and momentum conservation, the missing mass at the annihilation vertex to equal the $K^0$ mass, and the $\gamma\gamma$ invariant masses of the three $\gamma\gamma$ pairs to equal the $\pi^0$ mass. The fit assumes that the six photons originate from a common point located on the flight direction of the neutral kaon, namely the unknown neutral-kaon decay vertex. As can be shown by simulation, the $K^0$ momentum and the precise measurement of the photon conversion points contribute most of the information required to find the neutral-kaon decay vertex. The photon energies are used in the fit in order to find the correct association of the six photons to the three intermediate neutral pions. This is achieved by application of the constrained fit to all 15 possible $\gamma\gamma$ pairings. The pairings with the lowest $\chi^2$ values are chosen. The directions of the showers are not used in the fit. Simulation also shows that the reconstructed neutral-kaon momentum is entirely determined by the charged-track information, and that the photons do not contribute additional useful information. Therefore the $\chi^2$ probability provided by the fit can be expressed as the sum of two almost uncorrelated probabilities: one related to the reconstruction of the $K^0$ missing mass determined by the charged particles ($\chi^2_{\mathrm{charged}}$), and one related to the reconstruction of the $\pi^0$ invariant masses determined by the six photons ($\chi^2_{\mathrm{neutral}}$). A cut at 10% on the $\chi^2_{\mathrm{neutral}}$-probability is used for event selection and for background reduction, but no cut is applied to the $\chi^2_{\mathrm{charged}}$-probability in order to allow for background studies with an unbiased missing-mass distribution.

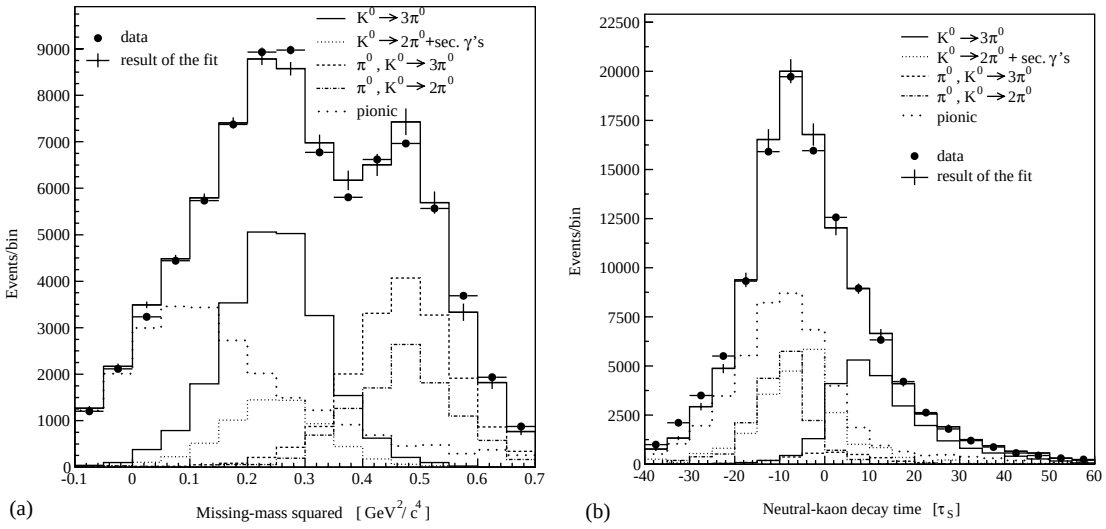


Fig. 29. (a) The measured missing-mass squared of $K^{\pm}\pi^{\mp}$ emerging from $\bar{p}p$ annihilation when selecting six showers in the ECAL. Only events with a neutral kaon detected within a decay-time interval of $-1$ to 20 $\tau_S$ are retained. Overlayed are the signal and background contributions resulting from the fit (see text). One can distinguish the signal events (which correspond to the neutral-kaon mass) from the kaonic-annihilation channels with an additional $\pi^0$ (which populate the high-mass region) and from the pionic annihilations (which contribute to the low-mass region). (b) The measured neutral-kaon decay-time distribution in the missing-mass squared interval 0.15–0.35 GeV$^2/c^4$. Overlayed are the signal and background contributions resulting from the fit (see text). At positive decay times most of the events are signal events, while events reconstructed at negative decay times are mainly background.

The decay-time resolution of signal events is determined from simulation and varies from 4.2 to 4.8 $\tau_S$ (RMS) between 0 and 20 $\tau_S$. Because of the finite decay-time resolution, the reconstructed decay time for signal events can become negative. Therefore, events populating the decay-time region below zero also contribute to the decay-rate time asymmetry.

Sources of background are the kaonic annihilation channels $\bar{p}p \to \bar{K}^0(K^0)K^{\pm}\pi^{\mp}\pi^0$, the pionic annihilation channel $\bar{p}p \to \pi^+\pi^- + n\pi^0$ $(n \geqslant 0)$ with a charged pion mistaken for a charged kaon, and the neutral-kaon decay $K^0 \to \pi^0\pi^0 \to 4\gamma$ with two additional photons that originate from the strong interaction or the decay of the accompanying charged particles in the calorimeter.

The number of $K^0(\bar{K}^0) \to \pi^0\pi^0\pi^0$ events and the contribution of background to the data are determined from the reconstructed decay-time distribution and from the $K^{\pm}\pi^{\mp}$ missing-mass spectrum, by fitting reference distributions for signal and background to the measured ones. The reference distributions are obtained from simulations of the signal and of the background with neutral-kaon decays. For the pionic-annihilation background these distributions are obtained from data by studying the energy-loss distribution of the charged particles in the inner scintillator of the particle-identification detector. The proportion of signal to background events in the data is determined from a simultaneous fit of the reference distributions to the measured missing-mass and decay-time distributions, leaving the number of events for each contribution as a free parameter in the fit.

Figs. 29(a) and (b) show the measured missing-mass and decay-time distributions, respectively. The measured distributions are compared with the result of the fit. Also shown are the individual

Table 21
Contributions of signal and background to the final data sample in the decay time interval $-1$ to 20 $\tau_S$ and within a missing-mass square interval of 0.15–0.35 GeV$^2/c^4$

| | Contribution (%) |
|---|---|
| *Signal* | |
| $\bar{p}p \to \bar{K}^0(K^0)K^\pm\pi^\mp$; $\bar{K}^0(K^0) \to \pi^0\pi^0\pi^0$ | $50.0 \pm 0.8$ |
| *Background* | |
| $\bar{p}p \to \bar{K}^0(K^0)K^\pm\pi^\mp\pi^0$; $\bar{K}^0(K^0) \to \pi^0\pi^0\pi^0$ | $4.9 \pm 0.2$ |
| $\bar{p}p \to \bar{K}^0(K^0)K^\pm\pi^\mp\pi^0$; $\bar{K}^0(K^0) \to \pi^0\pi^0$ | $3.7 \pm 0.2$ |
| $\bar{p}p \to \bar{K}^0(K^0)K^\pm\pi^\mp$ + photons; $\bar{K}^0(K^0) \to \pi^0\pi^0$ | $16.5 \pm 0.3$ |
| $\bar{p}p \to \pi^+\pi^- + n\pi^0$ $(n \geqslant 0)$ | $24.9 \pm 0.5$ |

The quoted errors are statistical.

contributions of signal and background. The correlation coefficients between the signal and the different background contributions given by the fit vary between 0.04 and 0.32. Those for the background channels relative to each other vary between 0.02 and 0.68. The biggest correlation is observed between the backgrounds from pionic annihilations and from secondary interactions generating photons.

In the $K^\pm\ \pi^\mp$ missing-mass spectrum of Fig. 29a one can distinguish the signal events (which correspond to the neutral-kaon mass) from the kaonic annihilation channels with an additional $\pi^0$ (which populate the high-mass region) and from the pionic annihilations (which contribute to the low-mass region). In order to reject background, only events in the missing-mass square interval of 0.15–0.35 GeV$^2/c^4$ are accepted. In the decay-time distribution (Fig. 29b), most of the events at positive decay times are signal events, while events reconstructed at negative decay times are mainly background. In order to retain most of the signal events and to reject a significant amount of background, a decay-time interval of $-1$ to 20 $\tau_S$ is selected. The events $K^0(\bar{K}^0) \to \pi^0\pi^0\pi^0$ with an additional $\pi^0$ are treated as background (wrong measurement of decay time). Kaon decays that are accompanied by additional photons from secondary interactions are suppressed, by requiring that the minimal $\gamma\gamma$ invariant mass of all possible $\gamma\gamma$ combinations be larger than 12 MeV$/c^2$. Table 21 summarizes the contributions of signal and background to the final data sample, in a missing-mass square interval of 0.15–0.35 GeV$^2/c^4$ and a decay-time interval of $-1$ to 20 $\tau_S$.

Selecting the missing-mass square region of 0.15–0.35 GeV$^2/c^4$, a total of 17 300 $K^0(\bar{K}^0) \to \pi^0\pi^0\pi^0$ events were reconstructed in the decay-time interval $-1$ to 20 $\tau_S$. The successive analysis followed the procedure used for the $\pi^0\pi^0$ decays, see Section 4.3. Measured decay-rate asymmetries of the type of Eq. (51b) were constructed in intervals of the neutral-kaon momentum, with summed weights computed from regeneration weights alone.

The values of $\mathrm{Re}(\eta_{000})$ and $\mathrm{Im}(\eta_{000})$ were extracted from a likelihood fit comparing the measured asymmetries with the following phenomenological expression:

$$A_{000}^{\exp}(\tau) = \frac{\alpha\xi - 1}{\alpha\xi + 1} - 2[\mathrm{Re}(\eta_{000})\cos(\Delta m\tau) - \mathrm{Im}(\eta_{000})\sin(\Delta m\tau)]e^{-(1/2)(\Gamma_S - \Gamma_L)\tau}\ . \tag{67}$$

Here $\alpha = [1 + 4\,\mathrm{Re}(\varepsilon_S)]$, while $\xi$ is again the normalization factor of the primary $K\pi$ pair (see Section 3.1).

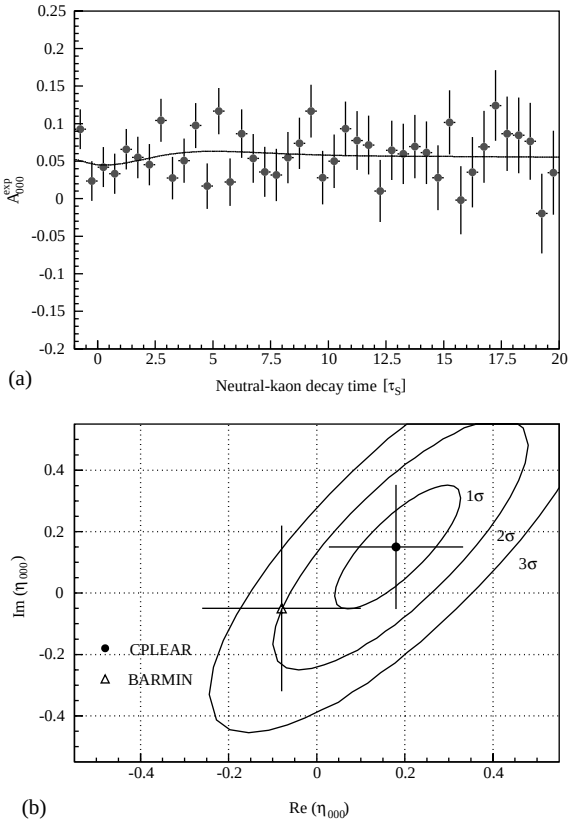


Fig. 30. (a) The measured decay-rate asymmetry $A_{000}^{exp}$. The solid line shows the result of the fit of Eq. (67) to the data (•), taking into account the decay-time resolution, and the background contributions as listed in Table 21. (b) The contour plot for Re($\eta_{000}$) and Im($\eta_{000}$) obtained in this analysis; the error bars represent the statistical and systematic uncertainties added in quadrature. For comparison, the result of Barmin et al. [119] is also shown; their error bars are statistical.

The measured asymmetry is shown in Fig. 30a as a function of the decay time, together with the result of the fit. The fit takes into account the parametrized decay-time resolution, and the background contributions as listed in Table 21. The $\alpha\xi$ values were left as free parameters in the fit; the tagging efficiency was assumed to be the same for all kaonic annihilation channels. The relative contribution of pionic background to the $K^0$ and $\bar{K}^0$ signal is determined from the study of the energy-loss distribution in the scintillator and is fixed to $1.18 \pm 0.02$.

The contributions to the systematic uncertainties in the determination of Re($\eta_{000}$) and Im($\eta_{000}$) are summarized in Table 22. We note the following.

- The resolution in reconstructing the neutral-kaon decay time. To evaluate the systematic errors in the values of Re($\eta_{000}$) and Im($\eta_{000}$) the width of the resolution function has been increased by 10% compared to the one extracted from the simulation. Furthermore, possible deviations in the decay-time dependence of the resolution function from the simulation have been considered by fitting the asymmetry with a resolution function of 5 $\tau_S$ (RMS) for all decay times. The effect of different parametrizations of the resolution function has been studied, and found to be negligible.

Table 22
Summary of the systematic errors on Re($\eta_{000}$) and Im($\eta_{000}$)

| Source | Re($\eta_{000}$) | Im($\eta_{000}$) |
|---|---|---|
| $\bar{K}^0(K^0)$ decay-time resolution | 0.01 | 0.01 |
| Amount of background in $K^0 + \bar{K}^0$ | 0.02 | 0.02 |
| Difference in background contribution to $K^0$ and $\bar{K}^0$ | 0.05 | 0.01 |
| Regeneration | $\ll 0.01$ | $\ll 0.01$ |
| $\Delta m$, $\tau_S$ and $\tau_L$ | $\ll 0.01$ | $\ll 0.01$ |
| Total | 0.06 | 0.03 |

- The amount of background contributing to the sum of $K^0$ and $\bar{K}^0$. Systematic uncertainties in the amount of signal and background in the data were estimated by comparing the results from the simultaneous fit with the level of signal and background obtained from independent fits of the reference distributions to the measured missing-mass and decay-time distributions. The proportions of signal and background obtained from the different fits agree within better than 3%. The amount of pionic annihilations was also estimated from a study of the energy-loss distribution of the charged particles in the scintillators, and gives a value that is 7% smaller than the result of the fit. The systematic errors on Re($\eta_{000}$) and Im($\eta_{000}$) were determined by varying the amount of signal and background from kaon decays by $\pm 3\%$, and by reducing the pionic annihilations by 7% compared to the mean values given in Table 21, taking into account their correlations. Uncertainties in simulating the missing-mass and decay-time reference distributions for the neutral-kaon background decays are small and introduce a negligible error on Re($\eta_{000}$) and Im($\eta_{000}$).
- The relative contribution of background to the $K^0$ and $\bar{K}^0$ signal can be different from the relative tagging efficiency of $K^0$ and $\bar{K}^0$. The tagging efficiency and the relative contribution of each background channel have been determined from simulation for the kaon decays. The values are all compatible within better than 5% and in agreement, within statistical errors, with the $\alpha\xi$ value resulting from the asymmetry fit. The relative contribution of pionic background to the $K^0$ and $\bar{K}^0$ signal was determined from the study of the energy-loss distribution in the scintillator S1 and yields $1.18 \pm 0.02$. The systematic errors on Re($\eta_{000}$) and Im($\eta_{000}$) are evaluated by varying the relative contribution of background to $K^0$ and to $\bar{K}^0$ within $\pm 5\%$ for each background channel.

Our final result is

$$\mathrm{Re}(\eta_{000}) = 0.18 \pm 0.14_{\mathrm{stat}} \pm 0.06_{\mathrm{syst}} \ ,$$

$$\mathrm{Im}(\eta_{000}) = 0.15 \pm 0.20_{\mathrm{stat}} \pm 0.03_{\mathrm{syst}} \ ,$$

with $\alpha\xi = 1.10 \pm 0.03_{\mathrm{stat}}$. The result of the fit is shown as a solid line in Fig. 30a. The correlation coefficient between Re($\eta_{000}$) and Im($\eta_{000}$) given by the fit is 0.79. The correlations of $\alpha\xi$ with Re($\eta_{000}$) and Im($\eta_{000}$) are $-0.09$ and $-0.56$, respectively.

This is the first determination of $\eta_{000}$ using the rate asymmetry of initially pure $\bar{K}^0$ and $K^0$ decaying to $\pi^0\pi^0\pi^0$. We have obtained an improved sensitivity for $\eta_{000}$ compared to the previous measurement [119], as shown in Fig. 30b. We note that this result does not depend on assumptions on $\mathscr{CPT}$ invariance.

By fixing $\mathrm{Re}(\eta_{000})$ to $\mathrm{Re}(\varepsilon) = 1.635 \times 10^{-3}$ [78] in the fit, we obtain

$$\mathrm{Im}(\eta_{000}) = -0.05 \pm 0.12_{\mathrm{stat}} \pm 0.05_{\mathrm{syst}} \ .$$

Using the definition of $\eta_{000}$ and $\mathrm{BR}(K_L \to \pi^0\pi^0\pi^0) = (21.12 \pm 0.27)\%$ from Ref. [78], an upper limit for the branching ratio of the $K_S \to \pi^0\pi^0\pi^0$ decay is deduced to be

$$\mathrm{BR}(K_S \to \pi^0\pi^0\pi^0) < 1.9 \times 10^{-5}$$

at the 90% confidence level, which is an improvement by a factor of two compared to the measurements of Ref. [119].

### 4.8. $\mathscr{CP}$ summary and conclusions for the pionic channels

Departures from $\mathscr{CP}$ invariance were searched for in the neutral-kaon decay rates to $\pi\pi$ and $\pi\pi\pi$, by directly comparing the decay rates of $\mathscr{CP}$-conjugated states, $K^0$ and $\bar{K}^0$. To this purpose the experiment relied on tagging the strangeness of $K^0$ and $\bar{K}^0$ produced through $\bar{p}p$ annihilation, in contrast to the methods based on $K_L$ and (regenerated) $K_S$ beams generally used in the past (see however Ref. [82]).

As a principle, when $K^0$ and $\bar{K}^0$ decay to $\mathscr{CP}$-conjugated states (any $\mathscr{CP}$ eigenstate of a multipion system is $\mathscr{CP}$ self-conjugated) a difference between the corresponding rates is an unequivocal proof of $\mathscr{CP}$ violation: however the difference in itself does not discriminate between mixing ($|\Delta S| = 2$) and decay ($|\Delta S| = 1$) effects. The rate difference is due to the presence (with opposite sign for $K^0$ and $\bar{K}^0$) of a term whose behaviour with time depends on the strength of $\mathscr{CP}$ violation through the parameter $\eta_{\pi\pi}$ (or $\eta_{\pi\pi\pi}$), see Section 2.2.

CPLEAR has measured the whole set of these parameters contributing to their knowledge in various ways. The importance of precision measurements of $\eta_{+-}$ and $\eta_{00}$ nowadays lies in the crucial role these parameters play in indirect tests of $\mathscr{CPT}$ invariance, see Section 8.3, and of some basic principles, see Sections 9.1 and 9.3. $\mathscr{CP}$ violation with three-pion decays still remains to be demonstrated, but lowering the upper limits on $\eta_{+-0}$ and $\eta_{000}$ also improves the tests of $\mathscr{CPT}$ invariance.

For the $\pi\pi$ decay channels, the CPLEAR results are in agreement with the earlier results obtained with strangeness-untagged beams, see Fig. 22. The experiments measuring $\phi_{+-}$ together with $|\eta_{+-}|$, and $\phi_{00}$ together with $|\eta_{00}|$ rely either on a beam containing a known mixture of $K^0$ and $\bar{K}^0$ [86,88,91,104] or on a $K_L$ beam, regenerating in matter [87,89,90,92] or not [93]. Values of $|\eta_{+-}|$ and $|\eta_{00}|$ alone are obtained by measuring $K_L$ and $K_S$ branching ratios [85].

Of the two experiments measuring $\eta_{+-0}$, one [110] makes use of $K^0$ produced by a $K^+$ beam via charge exchange in a bubble chamber filled with liquid xenon, and the other [111] of a beam containing a mixture of $K^0$ and $\bar{K}^0$. For $\eta_{000}$, the other earlier values were obtained in the liquid-xenon bubble chamber [119]. Recently, at the $\phi$ factory of VPP-2M, tagged $K_S$ decays to $\pi^0\pi^0\pi^0$ have been searched for, pushing the upper limit of the branching ratio down to $1.4 \times 10^{-5}$ at 90% CL [120].

In summary we note the following.

- $\pi^+\pi^-$—CPLEAR $\phi_{+-}$ and $|\eta_{+-}|$ have errors slightly smaller than quoted by the two other best values [89,90]. The value of $\phi_{+-}$ is in good agreement with the superweak phase $\phi_{SW} = 43.50^\circ \pm 0.08^\circ$ [85], which is a test of $\mathscr{CPT}$ invariance, see Section 8.3.
- $\pi^0\pi^0$—CPLEAR $\phi_{00}$ and $|\eta_{00}|$ are the second best measurements currently available.
- $\pi^+\pi^-\pi^0$—CPLEAR results constitute the most precise determination of the real and imaginary parts of $\eta_{+-0}$. Compared to the published values of Barmin et al. [110] and Zou et al. (only $\mathrm{Im}(\eta_{+-0})$) [111], our errors are smaller by more than one order of magnitude and by a factor of four, respectively. Our sensitivity on the $\mathscr{CP}$-violating parameter, however, is still one order of magnitude away from the expected $\mathscr{CP}$-violation effect.
- $\pi^0\pi^0\pi^0$—The values obtained for $\mathrm{Re}(\eta_{000})$ and $\mathrm{Im}(\eta_{000})$ represent the best sensitivity to $\mathscr{CP}$ violation in this decay mode. These parameters provide an important experimental input to a test of $\mathscr{CPT}$ symmetry based on the Bell–Steinberger relation [30,52]. Prior to CPLEAR, the errors on these parameters were the limiting factor in this test as discussed in Section 8.3.

We have also obtained new results on the $K_L$ and $K_S$ decays to $\pi^+\pi^-\pi^0$ when $\mathscr{CP}$ is conserved.

- We have performed the most accurate determination of the branching ratio of the $K_S$ decay to $\pi^+\pi^-\pi^0$.
- By analysing the Dalitz-plot distributions of the sum of $\bar{K}^0$ and $K^0$ decays to $\pi^+\pi^-\pi^0$, we have extracted the amplitude components $\beta$, $\gamma$, $\xi$, $\xi_{XY}$ and $\zeta$ contributing to $K_S$ and $K_L$ decays. The observed values are in agreement with the world averages as well as with the predictions of chiral perturbation theory.

## 5. The semileptonic decay channels ($\mathscr{T}$ and $\mathscr{CPT}$)

The simultaneous comparison between $K^0$ and $\bar{K}^0$ behaviour with respect to decay rates is particularly powerful when decays to semileptonic decays are considered. The principle of some of the measurements then becomes straightforward, for instance for the establishment of $\mathscr{T}$ violation, as discussed in Section 2.1.

CPLEAR measured $e\pi\nu$ decays. The two strangeness states of the neutral kaons were tagged at production, as in the case of the pionic channels, taking advantage of the associate kaon-pair production in $\bar{p}p$ annihilation, and the final states were characterized by the two charge configurations $(e^+\pi^-)$ and $(e^-\pi^+)$. A typical $e\pi\nu$ event is displayed in Fig. 31, and the characteristics of the electron detection are shown in Fig. 32. The decay rates for the four possible types of decay were measured as a function of the decay time, and in order to minimize systematic errors three asymmetries were formed: $A_T$, $A_\delta$ and $A_{\Delta m}$. Two of the asymmetries, $A_T$ and $A_\delta$, flatten out at early decay times to a continuous level below 1%. The asymmetry $A_{\Delta m}$ instead shows a pronounced oscillatory behaviour.

The data analysis was performed along the same lines as the $\pi^+\pi^-$ analysis of Section 4.1. However, the following points deserved special care.

- The kinematics (three-body final states including a neutrino) was less constraining. As a result, to select the signal events and achieve background suppression, the identification of the final-state electron was necessary.

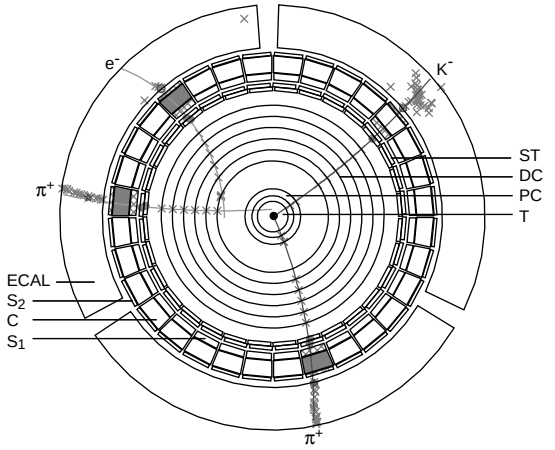


Fig. 31. Display of an event, $\bar{p}p$ (not shown) $\rightarrow K^- \pi^+ K^0$ with the neutral kaon decaying to $e^- \pi^+ \bar{\nu}$.

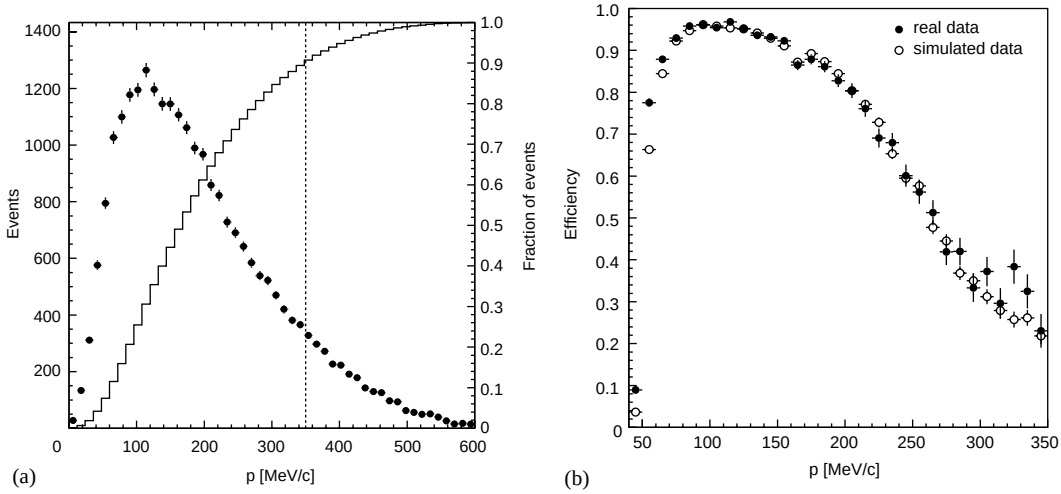


Fig. 32. Neutral-kaon decays to $e\pi\nu$. (a) Frequency density (•) and relative-frequency running sum (continuous line) of the electron momentum (simulated data). The dotted line indicates the cut position. (b) Electron identification efficiency as a function of momentum when $< 2\%$ of pions fake electrons, for real (•) and simulated (○) calibration data.

- The need for $e/\pi$ separation introduces a potential bias between $e^+\pi^-$ and $e^-\pi^+$ final states. The efficiency ratio of these final states demanded precise calibrations.
- The background/signal ratio was determined by simulation, and is displayed in Fig. 33a, while Fig. 33b shows the time distribution of the real and simulated data.
- The $K^0/\bar{K}^0$ initial ratio was determined using the $\pi^+\pi^-$ events collected at early decay time in the same data-taking periods. Thus, systematic errors were minimized, but at the price of introducing in the analysis the parameter $\mathrm{Re}(\varepsilon - \delta)$. This quantity cancels by construction in the $A_\delta$ asymmetry (it also cancelled in the $\pi^+\pi^-$ asymmetry), and has no impact in the measurement of $\Delta m$. However,

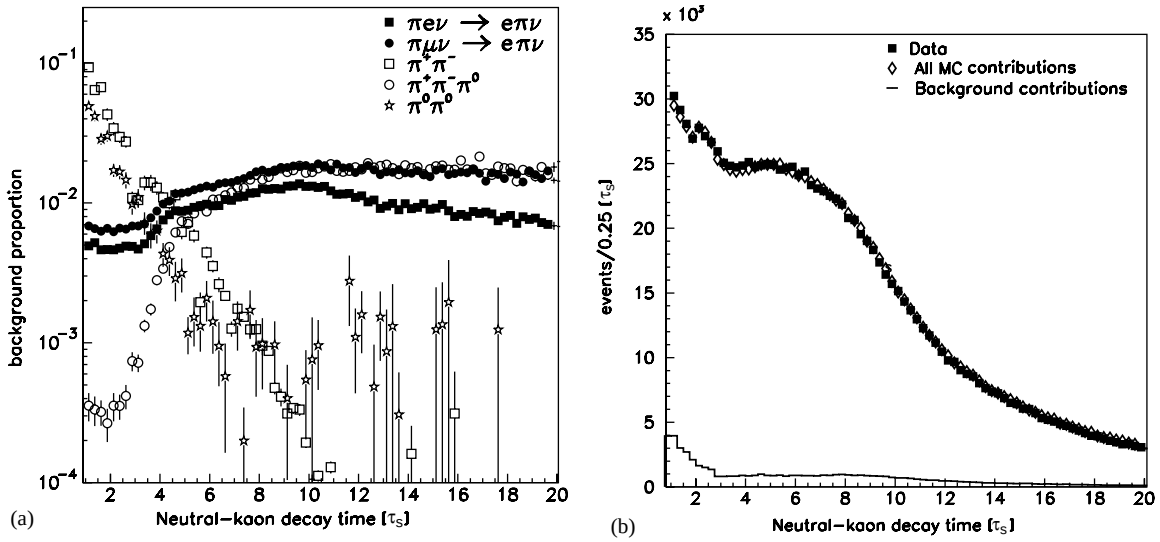


Fig. 33. (a) Proportion of events from various background channels relative to the e$\pi\nu$ signal. (b) Decay-time distribution for real data (squares) and simulated data (open diamonds). The expected background contribution is shown by the solid line.

this is not the case for the asymmetry $A_T$. Here a careful discussion of the physics consequences is needed.

- The asymmetry behaviours for $A_T$ and $A_\delta$ are not strongly time dependent, which renders the measurement more susceptible to normalization and efficiency effects, and less sensitive to the values of parameters such as $\Delta m$, $\Gamma_S$ and $\Gamma_L$. The asymmetry $A_{\Delta m}$ however shows a large dependence on time (as was the case for the asymmetry measured in the $\pi^+\pi^-$ decay channel), thus allowing the measurement of $\Delta m$ with high precision. The $\Delta m$ measurement is in turn sensitive to $\Gamma_S$ and to the absolute decay-time scale.
- The e$\pi\nu$ statistics was lower by a factor 50 compared to the $\pi^+\pi^-$ sample: most of the reduction occurred because the e$\pi\nu$ sample originates essentially from $K_L$, of which only 3% decay within the fiducial volume of the CPLEAR detector.

Finally, the systematic errors affecting our measurements were shown to be smaller than the statistical ones. The consistency of the results for the three asymmetries in the different data-taking periods is shown in Fig. 34. The following sources of systematic error have been investigated.

- Background level and charge asymmetry. The determination of the relative acceptances for various background contributions was performed using a Monte Carlo simulation. By changing the analysis cuts on real and simulated data, the upper limits within which these acceptances are known were estimated to be $\pm 10\%$. The error of the background charge asymmetry was estimated to be $0.03 \pm 0.01$.
- Normalization corrections. The normalization corrections, $\xi$ and $\eta$, are limited by the statistics available from calibration samples.

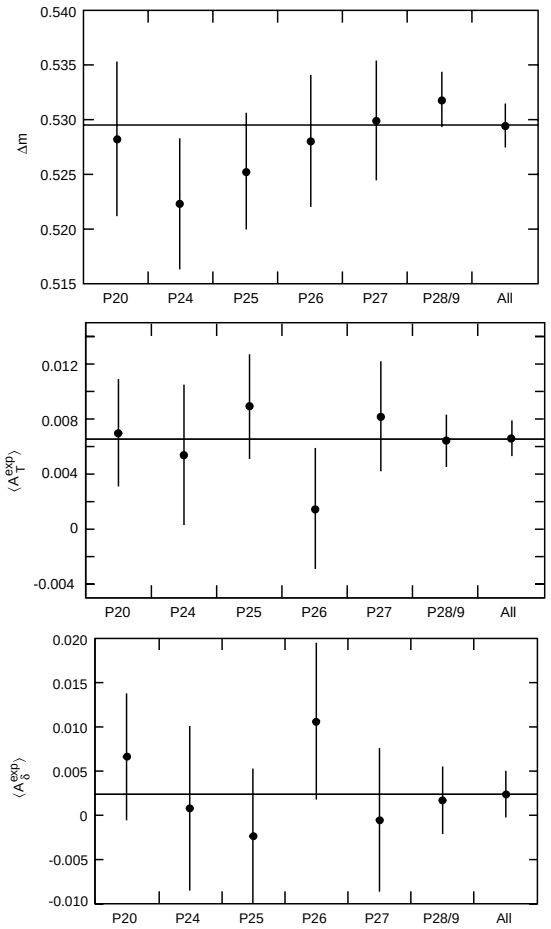


Fig. 34. $\Delta m$, $\langle A_{\mathrm{T}}^{\mathrm{exp}}\rangle$ and $\langle A_{\delta}^{\mathrm{exp}}\rangle$ for different data-taking periods (P20 and from P24 to P28/29) together with the final value.

- Regeneration correction. The evaluation of the systematic error resulting from the regeneration correction was performed by altering the $\Delta f$ values along the one-standard-deviation ellipses in the complex plane [$\mathrm{Re}(\Delta f)$, $\mathrm{Im}(\Delta f)$].
- Decay-time resolution. The decay-time resolution was determined from a Monte Carlo simulation. Its precision was estimated to be better than 10%, and affects only the measurement of $\mathrm{Re}(x_+)$ extracted from the $A_{\Delta m}$ asymmetry. The systematic error resulting from the decay-time resolution was estimated by folding the resolution distribution to the asymmetry under study.

The effects of the above contributions are summarized in Tables 23–26 for the $A_{\Delta m}$, $A_{\mathrm{T}}$ and $A_{\delta}$ analyses, respectively, together with the systematic errors arising from the phenomenological parameters used in the fit. The systematic errors were evaluated by allowing each error source to vary within its uncertainty in the fit procedure.

Table 23
Summary of systematic errors on the results from the $A_{\Delta m}^{\exp}$ asymmetry

| Source | Precision | $\Delta m$ ($10^7$ $\hbar$/s) | Re($x_+$) ($10^{-3}$) |
|---|---|---|---|
| Background level[a] | ±10% | ±0.2 | ±4.4 |
| Background asymmetry | ±1% | | |
| Normalization ($\alpha\xi$) | $\pm 3.4 \times 10^{-4}$ | | |
| and | | ±0.1 | ±0.1 |
| Normalization ($\eta$) | $\pm 2.0 \times 10^{-3}$ | | |
| Normalization ($\omega$) | $\pm(4\text{–}9) \times 10^{-4}$ | ±0.1 | — |
| Decay-time resolution[a] | ±10% | ±0.1 | ±0.3 |
| Absolute time-scale[a] | $\pm 2 \times 10^{-4}$ | ±0.1 | ±0.3 |
| Regeneration | Ref. [24] | — | — |
| $\tau_S = \hbar/\Gamma_S$ | $\pm 0.08 \times 10^{-12}$ s | ±0.1 | ±0.7 |
| Total | | ±0.3 | ±4.5 |

[a]A relative precision is given.

Table 24
The correlation coefficients from the $A_\delta$ fit

| | Re($\delta$) | Im($\delta$) | Re($x_-$) | Im($x_+$) |
|---|---|---|---|---|
| Re($\delta$) | 1 | 0.44 | −0.56 | +0.60 |
| Im($\delta$) | | 1 | −0.97 | +0.91 |
| Re($x_-$) | | | 1 | +0.96 |
| Im($x_+$) | | | | 1 |

Table 25
Summary of systematic errors on the results from the $A_\delta^{\exp}$ asymmetry

| Source | Precision | Re($\delta$) ($10^{-4}$) | Im($\delta$) ($10^{-2}$) | Re($x_-$) ($10^{-2}$) | Im($x_+$) ($10^{-2}$) |
|---|---|---|---|---|---|
| Background level[a] | ±10% | ±0.1 | ±0.1 | ±0.1 | ±0.1 |
| Background asymmetry | ±1% | ±0.2 | ±0.3 | ±0.2 | ±0.3 |
| Normalization ($\alpha\xi$) | $\pm 3.4 \times 10^{-4}$ | ±0.5 | ±0.03 | ±0.02 | ±0.03 |
| Normalization($\eta$) | $\pm 2.0 \times 10^{-3}$ | ±0.02 | ±0.03 | ±0.02 | ±0.03 |
| Decay-time resolution[a] | ±10% | Negligible | ±0.1 | ±0.1 | ±0.1 |
| Regeneration | Ref. [24] | ±0.25 | ±0.02 | ±0.02 | ±0.02 |
| Total | | ±0.6 | ±0.3 | ±0.3 | ±0.3 |

[a]A relative precision is given.

Table 26
Summary of systematic errors on the results from the $A_T^{exp}$ asymmetry

| Source | Precision | $\langle A_T^{exp}\rangle$ $(10^{-3})$ | $\mathrm{Im}(x_+)$ $(10^{-3})$ |
|---|---|---|---|
| Background level[a] | ±10% | ±0.03 | ±0.2 |
| Background asymmetry | ±1% | ±0.02 | ±0.5 |
| Normalization ($\xi$) | $\pm 4.3\times 10^{-4}$ | ±0.2 | ±0.1 |
| Normalization ($\eta$) | $\pm 2.0\times 10^{-3}$ | ±1.0 | ±0.4 |
| Decay-time resolution[a] | ±10% | Negligible | ±0.6 |
| Regeneration | Ref. [24] | ±0.1 | ±0.1 |
| Total | | ±1.0 | ±0.9 |

[a] A relative precision is given.

### 5.1. Measurement of $\Delta m$ (method b): the $A_{\Delta m}$ asymmetry [11,14]

The parameters of interest in this analysis become manifest when we write in the limit of negligible background:

$$A_{\Delta m}(\tau)=\frac{\cos(\Delta m\tau)-2\,\mathrm{Im}(x_-)\sin(\Delta m\tau)}{\cosh(\Delta\Gamma\tau/2)-2\,\mathrm{Re}(x_+)\sinh(\Delta\Gamma\tau/2)}\ . \tag{68}$$

After including the background rates, Eq. (68) folded with the decay-time resolution was fitted to the data $A_{\Delta m}^{exp}(\tau)$, see Eq. (51e), with $\Delta m$ and $\mathrm{Re}(x_+)$ as free parameters, and $\mathrm{Im}(x_-)=0$ (that is $\mathscr{CPT}$ invariance was assumed for possible $\Delta S\neq\Delta Q$ decay amplitudes).

- Since in the construction of $A_{\Delta m}$ all terms linear in the regeneration corrections cancel, these corrections are not needed, thus leading to no systematic error from that source.
- Again by the asymmetry construction, systematic errors arising from normalization factors are not important.
- Since $\Delta m$ is proportional to the frequency of the $K^0\rightleftharpoons\bar{K}^0$ oscillation, this measurement is very sensitive to the absolute time-scale precision.
- Folding the decay-time resolution distribution to the $A_{\Delta m}$ asymmetry results in a shift of $+1.3\times 10^7\ \hbar/\mathrm{s}$ for the value of $\Delta m$ and $-2.9\times 10^{-3}$ for the value of $\mathrm{Re}(x_+)$. The uncertainty on this correction was estimated to be ±10%.
- The $A_{\Delta m}$ asymmetry is sensitive to a possible correlation in the detection efficiencies of the primary charged kaon and the decay electron. This required a normalization factor $\omega$ for a part of the data with an overall correction for $\Delta m$ of $+0.6\pm 0.1\times 10^7\ \hbar/\mathrm{s}$.

The measured asymmetry, together with the fitted function, is displayed in Fig. 35. Fit residuals are shown in the inset. The starting point of the fit was determined according to the sensitivity of the asymmetry to the residual background. Our final results are the following:

$$\Delta m=(529.5\pm 2.0_{\mathrm{stat}}\pm 0.3_{\mathrm{syst}})\times 10^7\ \hbar/\mathrm{s}\ ,$$

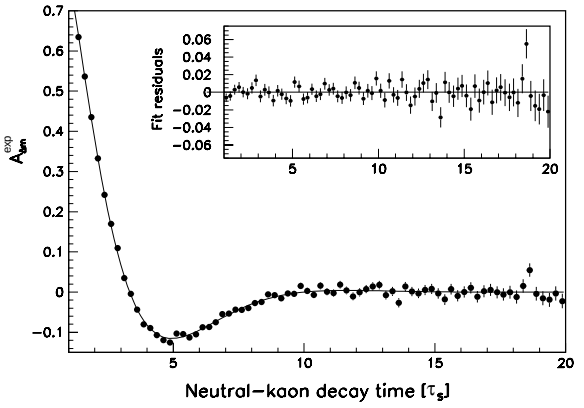


Fig. 35. The $A_{\Delta m}^{\exp}$ asymmetry versus the neutral-kaon decay time (in units of $\tau_S$). The solid line represents the result of the fit. Fit residuals are shown in the inset.

$$\mathrm{Re}(x_+) = (-1.8 \pm 4.1_{\mathrm{stat}} \pm 4.5_{\mathrm{syst}}) \times 10^{-3} \ ,$$

$$\chi^2/\mathrm{ndf} = 0.94, \quad \mathrm{ndf} = 606 \ .$$

The correlation coefficient between $\Delta m$ and $\mathrm{Re}(x_+)$ is equal to 0.40. This $\Delta m$ measurement is the most accurate single value contributing to the present world average [85], see Refs. [89,90,121–123]. The $\mathrm{Re}(x_+)$ measurement improves the present limit on a possible violation of the $\Delta S = \Delta Q$ rule by a factor three.

In Eq. (68) it is not possible to disentangle the two oscillating terms, which produce a correlation $> 0.99$ between $\Delta m$ and $\mathrm{Im}(x_-)$. If we assume $\Delta m = (530.1 \pm 1.4) \times 10^7\ \hbar/\mathrm{s}$, we obtain $\mathrm{Im}(x_-) = (-0.8 \pm 3.5) \times 10^{-3}$.

### 5.2. Measurement of $\mathscr{CPT}$-invariance: the $A_\delta$ asymmetry [13,14]

For this analysis we refer to Eq. (51d), and the fitting equation becomes, in the limit of negligible background,

$$A_\delta(\tau) = 4\,\mathrm{Re}(\delta) + 4\,\frac{\mathrm{Re}(\delta)\sinh(\Delta\Gamma\tau/2) + \mathrm{Im}(\delta)\sin(\Delta m\tau)}{\cosh(\Delta\Gamma\tau/2) + \cos(\Delta m\tau)} - 4\,\frac{\mathrm{Re}(x_-)\cos(\Delta m\tau)\sinh(\Delta\Gamma\tau/2) - \mathrm{Im}(x_+)\sin(\Delta m\tau)\cosh(\Delta\Gamma\tau/2)}{[\cosh(\Delta\Gamma\tau/2)]^2 - [\cos(\Delta m\tau)]^2} \ . \tag{69}$$

After including the background, Eq. (69) folded with the decay-time resolution was fitted to the data $A_\delta^{\exp}(\tau)$, with $\mathrm{Re}(\delta)$, $\mathrm{Im}(\delta)$, $\mathrm{Re}(x_-)$ and $\mathrm{Im}(x_+)$ as free parameters. The measured asymmetry $A_\delta^{\exp}$, together with the fitted function, is displayed in Fig. 36. We stress that the analysis of the $\pi^+\pi^-$ decay channel [7] gives exactly the quantity $\alpha\xi = (1 + 4\,\mathrm{Re}(\varepsilon_L))\xi$ which enters the asymmetry presented here, and we do not use the result of any external measurement for the quantity $\mathrm{Re}(\varepsilon_L)$. On average we have $\langle\alpha\xi\rangle = 1.12756 \pm 0.00034$. The $A_\delta$ asymmetry depends only weakly on $\eta$. The level of the background contributions remains below 2% of the signal. The regeneration corrections

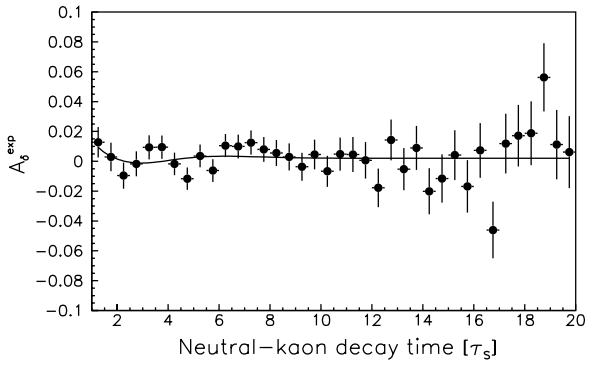


Fig. 36. The $A_\delta^{\exp}$ asymmetry versus the neutral-kaon decay time (in units of $\tau_S$). The solid line represents the result of the fit.

result in a shift of the $A_\delta^{\exp}$ value of the order of $0.3\times10^{-3}$. The systematic errors are shown in detail in Table 25: the main systematic error on $\mathrm{Re}(\delta)$ results from the uncertainty in the normalization factor $\alpha\xi$, while $\mathrm{Im}(\delta)$, $\mathrm{Re}(x_-)$ and $\mathrm{Im}(x_+)$ are mainly affected by the uncertainty in the background charge asymmetry. The dependence of the fit results on $\Delta m$, $\Gamma_S$ and $\Gamma_L$ errors is negligible. Our final results are the following:

$$\mathrm{Re}(\delta) = (3.0 \pm 3.3_{\mathrm{stat}} \pm 0.6_{\mathrm{syst}}) \times 10^{-4} ,$$

$$\mathrm{Im}(\delta) = (-1.5 \pm 2.3_{\mathrm{stat}} \pm 0.3_{\mathrm{syst}}) \times 10^{-2} ,$$

$$\mathrm{Re}(x_-) = (0.2 \pm 1.3_{\mathrm{stat}} \pm 0.3_{\mathrm{syst}}) \times 10^{-2} ,$$

$$\mathrm{Im}(x_+) = (1.2 \pm 2.2_{\mathrm{stat}} \pm 0.3_{\mathrm{syst}}) \times 10^{-2} ,$$

$$\chi^2/\mathrm{ndf} = 1.14, \quad \mathrm{ndf} = 604 .$$

The correlation coefficients of the fit are shown in Table 24. We note that $\mathrm{Re}(x_-)$ and $\mathrm{Im}(x_+)$ are compatible with zero, which is expected in the case where the $\Delta S = \Delta Q$ rule holds. When we fix $\mathrm{Re}(x_-) = \mathrm{Im}(x_+) = 0$ in the fit, we obtain

$$\mathrm{Re}(\delta) = (2.9 \pm 2.6_{\mathrm{stat}} \pm 0.6_{\mathrm{syst}}) \times 10^{-4} ,$$

$$\mathrm{Im}(\delta) = (-0.9 \pm 2.9_{\mathrm{stat}} \pm 1.0_{\mathrm{syst}}) \times 10^{-3} ,$$

that is a negligible change for $\mathrm{Re}(\delta)$ but an error of $\mathrm{Im}(\delta)$ smaller by an order of magnitude. The correlation coefficient is $-0.5$. In this case, the systematic error on $\mathrm{Re}(\delta)$ does not change while the systematic error on $\mathrm{Im}(\delta)$ becomes three times smaller.

### 5.3. Measurement of $\mathcal{T}$-violation: the $A_T$ asymmetry [12,14]

The $A_T$ asymmetry represents a direct comparison of $\mathcal{T}$-conjugated rates. For this analysis we refer to the asymmetry (51c). The measured asymmetry $A_T^{\exp}$ is shown in Fig. 37. Between 1 and

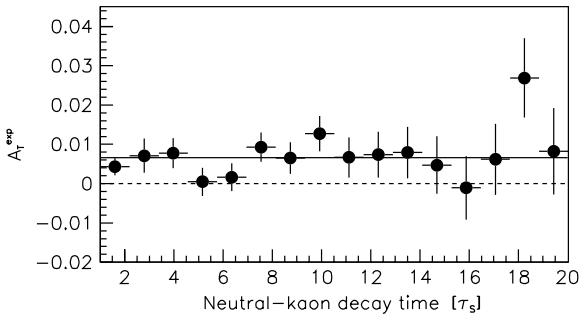


Fig. 37. Experimental demonstration of $\mathscr{T}$-violation: the asymmetry $A_T^{exp}$ versus the neutral-kaon decay time (in units of $\tau_S$). The positive values show that a $\bar{K}^0$ develops into a $K^0$ with higher probability than does a $K^0$ into a $\bar{K}^0$. The solid line represents the fitted average $\langle A_T^{exp}\rangle$.

20 $\tau_S$ the data points scatter around a constant offset from zero, the average being

$$\langle A_T^{exp}\rangle = (6.6 \pm 1.3) \times 10^{-3} \ ,$$

$$\chi^2/\mathrm{ndf} = 0.84, \quad \mathrm{ndf} = 607 \ .$$

For a more detailed analysis, the appropriate phenomenological expression was used. In the limit of negligible background, the fitting equation becomes

$$A_T(\tau) = 4(\mathrm{Re}(\varepsilon) - \mathrm{Re}(y) - \mathrm{Re}(x_-)) + 2\,\frac{\mathrm{Re}(x_-)(e^{-(1/2)\Delta\Gamma\tau} - \cos(\Delta m\tau)) + \mathrm{Im}(x_+)\sin(\Delta m\tau)}{\cosh(\frac{1}{2}\Delta\Gamma\tau) - \cos(\Delta m\tau)} \ . \tag{70}$$

With respect to Eq. (33), we note on the right-hand side an additional term $-2(\mathrm{Re}(x_-) + \mathrm{Re}(y))$. This term follows from the primary-vertex normalization procedure. Eq. (70) simplifies when $\mathscr{CPT}$ invariance in the $e\pi\nu$ decay amplitudes is assumed ($\mathrm{Re}(y)=0$ and $\mathrm{Re}(x_-)=0$). We allowed, however, for a possible violation of the $\Delta S = \Delta Q$ rule ($\mathrm{Im}(x_+) \neq 0$). The fitting procedure then contains only two parameters, $\mathrm{Re}(\varepsilon)$ and $\mathrm{Im}(x_+)$, both $\mathscr{T}$ violating. After including the background rates, Eq. (70) folded with the decay-time resolution was fitted to the data $A_T^{exp}(\tau)$. The final results are the following.

$$4\,\mathrm{Re}(\varepsilon) = (6.2 \pm 1.4_{stat} \pm 1.0_{syst}) \times 10^{-3} \ ,$$

$$\mathrm{Im}(x_+) = (1.2 \pm 1.9_{stat} \pm 0.9_{syst}) \times 10^{-3} \ ,$$

$$\chi^2/\mathrm{ndf} = 0.84, \quad \mathrm{ndf} = 606 \ .$$

The correlation coefficient between $4\,\mathrm{Re}(\varepsilon)$ and $\mathrm{Im}(x_+)$ is 0.46.

We observe clear evidence for $\mathscr{T}$ violation in the neutral-kaon mixing. $\mathrm{Im}(x_+)$ is compatible with zero. Thus, no $\mathscr{T}$ violation is observed in the semileptonic decay amplitude which violates the $\Delta S = \Delta Q$ rule, should this amplitude be different from zero. We note that $\mathrm{Im}(x_+)$ is given by the values of the asymmetry at early decay times while $4\,\mathrm{Re}(\varepsilon)$ is determined by the late decay-time values.

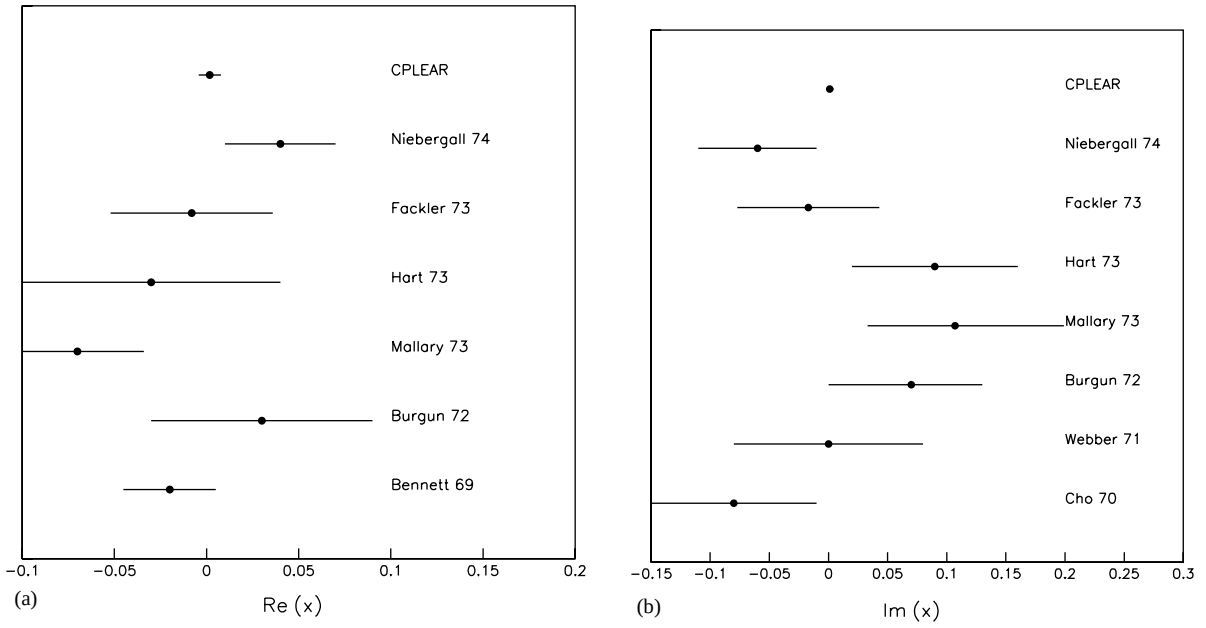


Fig. 38. Neutral-kaon decays to e$\pi\nu$: the parameters of the $\Delta S=\Delta Q$ rule, (a) Re($x$) and (b) Im($x$), measured by CPLEAR. The value of the earlier experiments with the smallest quoted errors [83,124] are also shown. $\mathscr{CPT}$ invariance is assumed, thus $\mathrm{Re}(x) \equiv \mathrm{Re}(x_+)$ and $\mathrm{Im}(x) \equiv \mathrm{Im}(x_+)$.

Therefore, the average $\langle A_{\mathrm{T}}^{\mathrm{exp}} \rangle$ between 1 and 20 $\tau_{\mathrm{S}}$ is essentially equal to $4\,\mathrm{Re}(\varepsilon)$. The systematic errors on $\langle A_{\mathrm{T}}^{\mathrm{exp}} \rangle$ also apply to $4\,\mathrm{Re}(\varepsilon)$ for the case of the two-parameter fit. We note that the secondary-vertex normalization $\eta$ is the dominant source of systematic error for this asymmetry. The decay-time resolution introduces a negligible change in $\langle A_{\mathrm{T}}^{\mathrm{exp}} \rangle$. The dependence of the fit on the error of $\Delta m$, $\Gamma_{\mathrm{S}}$ and $\Gamma_{\mathrm{L}}$ is negligible.

### 5.4. Measurement of $\Delta S \neq \Delta Q$ amplitudes

The $\Delta S=\Delta Q$ rule first postulated in 1958 [49] was for many years just an experimental fact, and its accuracy was determined by the experiment. The different asymmetries considered by CPLEAR were studied at first with separate analyses and different hypotheses on the parameters describing the $\Delta S \neq \Delta Q$ amplitudes, with and without $\mathscr{CPT}$ invariance. We summarize as follows.

- $A_{\Delta m}$ depends on $\mathrm{Re}(x_+)$ and $\mathrm{Im}(x_-)$: we assume $\mathrm{Im}(x_-)=0$.
- $A_{\delta}$ depends on $\mathrm{Re}(x_-)$ and $\mathrm{Im}(x_+)$: no assumption was made.
- $A_{\mathrm{T}}$ depends on $\mathrm{Im}(x_+)$ and $\mathrm{Re}(x_-)$ (and $\mathrm{Re}(y)$): we assume $\mathrm{Re}(x_-)=0$ (and $\mathrm{Re}(y)=0$).

The fit results are given in the corresponding sections. Earlier experiments [83,124] were always analysed assuming $\mathscr{CPT}$ invariance for the decay amplitudes, thus we compare their results with the CPLEAR values of $\mathrm{Re}(x)=\mathrm{Re}(x_+)$ from $A_{\Delta m}$, and $\mathrm{Im}(x)=\mathrm{Im}(x_+)$ from $A_{\mathrm{T}}$, see Fig. 38.

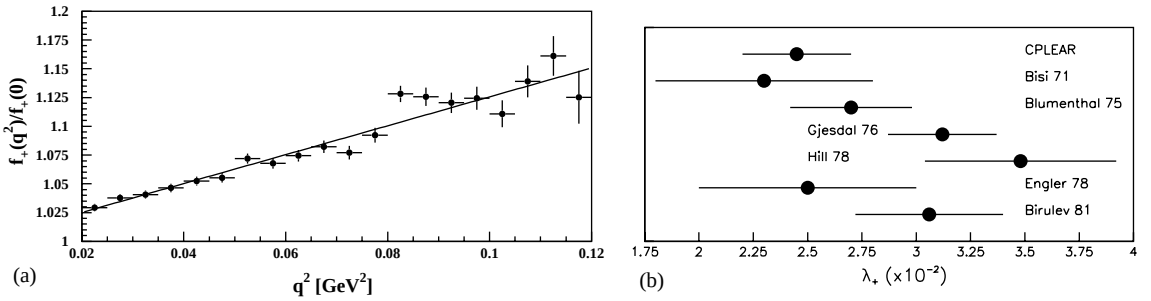


Fig. 39. Neutral-kaon decays to e$\pi\nu$: (a) the $q^2$ dependence of the form-factor $f_+$, normalized to $f_+(q^2=0)=1.0$, with the fit result (solid line) superimposed on the data points (•). (b) The value of the slope $\lambda_+$ (see text) is displayed, together with the values of the most accurate earlier experiments [125].

### 5.5. Measurement of the $q^2$ dependence of the $K^0_{e3}$ form factor [15]

This analysis is based on the $q^2$ dependence of the decay rates integrated over all lifetimes, where $q$ is the spatial component of the four-momentum transferred from kaon to pion. From the comparison of real and simulated data samples we obtained [15] $\lambda_+ = 0.0245 \pm 0.0012_{\text{stat}} \pm 0.0022_{\text{syst}}$, to be compared with the world-average value $\lambda_+ = 0.0300 \pm 0.0016$. The $q^2$ dependence of the form-factor is displayed in Fig. 39a, and shown to be linear. The addition of a quadratic term to $f_+(q^2)$ was investigated experimentally and found to be compatible with zero. The comparison with earlier experiments [125] is shown in Fig. 39b. Our result is in very good agreement with a recent calculation at order $p^6$ of Chiral Perturbation Theory [126].

### 5.6. $\mathcal{T}$ and $\mathcal{CPT}$ summary and conclusions for the e$\pi\nu$ channels

Departures from $\mathcal{T}$ and $\mathcal{CPT}$ invariance were searched for in the decay rates to $e^+\pi^-\nu$ and $e^-\pi^+\bar{\nu}$ of initially strangeness-tagged $K^0$ and $\bar{K}^0$. For this purpose convenient decay-rate asymmetries were formed. Fitting the phenomenological expressions of these asymmetries to the data allowed a variety of parameters to be determined, in particular the following.

- $A_T$—We have directly observed $\mathcal{T}$ violation in the neutral-kaon mixing matrix by comparing two $\mathcal{T}$-conjugated rates. The asymmetry $A_T$ was measured for the first time and is well compatible with $4\,\mathrm{Re}(\varepsilon)$. In the limit of $\mathcal{CPT}$ invariance in the semileptonic decay process, this measurement demonstrates a violation of time-reversal invariance in the evolution of neutral kaons into their antiparticles, independently of the validity of the $\Delta S = \Delta Q$ rule. Effectively it manifests the difference of $\mathcal{T}$-conjugated processes as the difference between the rate of oscillation from $K^0$ to $\bar{K}^0$ and from $\bar{K}^0$ to $K^0$. The question of the $\mathcal{T}$-odd effects, especially in relation to the KTeV result [127],where they might falsely be interpreted as the outcome of $\mathcal{T}$ violation, is dealt with in Refs. [73]. For the CPLEAR experiment, on the other hand, a theoretical discussion [128] shows that $\mathcal{CPT}$-violating effects in the decay which possibly could fake $A_T \neq 0$, concerning the kaon development, can be excluded.

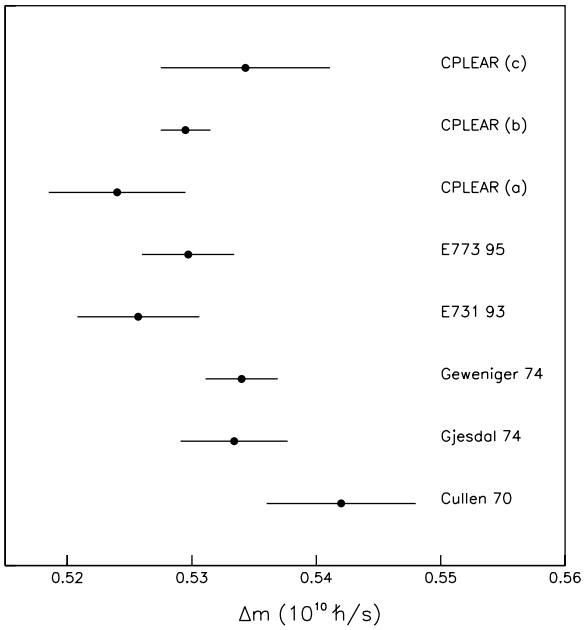


Fig. 40. The $K_L - K_S$ mass difference $\Delta m$ : the CPLEAR values obtained from the analysis of neutral-kaon decays (a) to $\pi^+\pi^-$ (Section 4.1) and (b) to $e\pi\nu$ are displayed together with the results from earlier experiments [89,90,121–123]. Of these, only the value of Gjesdal et al. [121] was obtained using semileptonic decays—as in CPLEAR (b) the decay amplitudes were assumed to be $\mathscr{CPT}$ invariant, and $\mathrm{Im}(x_-) \equiv 0$. The CPLEAR value (c) obtained using strong interactions as time markers (Section 7.1) is also shown.

- $A_\delta$—We have directly measured $\mathscr{CPT}$ invariance through the parameters $\mathrm{Re}(\delta)$ and $\mathrm{Im}(\delta)$. Again we underline the direct approach in contrast to an evaluation of $\mathrm{Im}(\delta)$ from various measurements, using the unitarity relation and resulting in an error smaller by two orders of magnitude [28]. It was the measurement of $\mathrm{Re}(\delta)$ which enabled us for the first time to set a limit on the $K^0 - \bar{K}^0$ decay-width difference, and to disentangle possible cancellation effects [29], see Section 8.3.
- $A_{\Delta m}$—From the asymmetry $A_{\Delta m}$ we obtained the best individual measurement for $\Delta m$, which is one of the fundamental parameters of the neutral-kaon system. The $\Delta m$ result is compared with previous experiments in Fig. 40.
- Decay amplitudes to $e\pi\nu$ and the $\Delta S = \Delta Q$ rule—This rule is now understood in a simple quark model where semileptonic strange decays are seen as $s \to u\ell^-\bar{\nu}$ (and charge-conjugated reaction) [68]. Our results on the $\Delta S = \Delta Q$ rule are compared with previous experiments in Fig. 38, all assuming $\mathscr{CPT}$ invariance for the decay amplitudes, i.e. $\mathrm{Re}(x_-) = \mathrm{Im}(x_-) = 0$: the improvement brought in by CPLEAR is impressive. However, the current limits are still too large with respect to the values expected in the Standard Model ($< 10^{-7}$) [129]. Our result on $\mathrm{Re}(x_-)$ is unique.
- Decay amplitudes to $e\pi\nu$ and $\mathscr{CPT}$ invariance—For the $\Delta S \neq \Delta Q$ amplitudes see above the value of $\mathrm{Re}(x_-)$; a limit on $\mathrm{Re}(y)$ could only be achieved in a global fit, see Section 8.2.
- Decay amplitudes to $e\pi\nu$ and form-factor slope—Our value for $\lambda_+$ has an error comparable to the best earlier experiments, as shown in Fig. 39, and is consistent with them within the errors.

## 6. The electromagnetic decay channels

### 6.1. Upper limit of the $BR(K_S \to e^+e^-)$ [16]

The decay $K_S \to e^+e^-$ is a flavour-changing neutral-current process, suppressed in the Standard Model and dominated by the two-photon intermediate state. Full event reconstruction together with $e/\pi$ separation in the calorimeter, and in the PID for momenta below 200 MeV/$c$, allowed powerful background rejection and high signal acceptance. A constrained fit was performed with the hypothesis of this decay, and both secondary tracks had to be recognized as electrons in the calorimeter by exploiting shower topology. The analysis of these data yields $BR(K_S \to e^+e^-) < 1.4 \times 10^{-7}$ at 90% CL, an improvement on the current experimental limit by a factor of 20 [16].

## 7. The strong interaction channels

### 7.1. Measurement of $\Delta m$ (method c) [26]

Very early, after the hypothesis of particle mixture had been advanced for $K^0$ and $\bar{K}^0$ [4], the change of strangeness content with time was predicted, as a consequence, for beams starting as pure $K^0$ or $\bar{K}^0$ [5]. Proposals followed on how to monitor the strangeness oscillations and measure the $K_L - K_S$ mass difference $\Delta m$, that is the oscillation frequency modulus $\hbar$. It was suggested that starting with a pure $K^0$ (or $\bar{K}^0$) beam, one could observe the building up of a $\bar{K}^0$ (or $K^0$) flux by measuring either weak decays to $e\pi\nu$ [39] or the products of strong interactions in a thin slab of material [40]. These suggestions were soon followed by the first experiments [40,130,131]. In another approach [79,132,133] it was shown that the intensity of the $K_S$ component transmitted through an absorber is a very sensitive function of the mean life $\tau_S$ and of the $K_L - K_S$ mass difference, and this led to the first of many variants of the regenerator method [134]. Later, this method provided results in the current range of accuracy [89,90,122,123] and even allowed the $\Delta m$ sign to be determined [98,100]. Comparable accuracy was obtained with the oscillation method coupled to the measurement of semileptonic decays in Ref. [121], and recently by CPLEAR [11].

The CPLEAR set-up, modified for the regeneration amplitude measurement, see Section 4.2, was also used to determine the $K_L - K_S$ mass difference by a method where neutral-kaon strangeness oscillations were monitored, both at the initial and final time, using kaon strong interactions, method (c), rather than semileptonic decays, method (b), thus requiring no assumptions on $\mathscr{CPT}$ invariance for the decay amplitudes.

For this measurement, the strangeness at the production was identified with the standard method of Section 3.1. In order to identify the strangeness at a later time $t = \tau$, we took advantage of the carbon absorber, shaped as a segment of a hollow cylinder, which had been added to the CPLEAR detector, see Fig. 17. Hence we measured the numbers of $K^0$ and $\bar{K}^0$ interacting with the absorber's bound nucleons in one of the following reactions:

$$K^0 + p \to K^+ + n, \quad \bar{K}^0 + n \to K^- + p, \quad \bar{K}^0 + n \to \pi^0 + \Lambda(\to \pi^- p) \ . \tag{71}$$

In the case of initial $K^0$, we denote by $N_+$ and $N_-$ the numbers of $K^0$ and $\bar{K}^0$ which are measured to interact at time $\tau$ in the absorber, and by $\bar{N}_+$ and $\bar{N}_-$ the corresponding numbers for initial $\bar{K}^0$.

These numbers $N_\pm$ and $\bar{N}_\pm$ are converted to the probabilities $\mathscr{P}_\pm$ and $\bar{\mathscr{P}}_\pm$ using the cross-sections of reactions (71) and the detection efficiencies of the relevant particles. However, all cross-sections and efficiencies cancel in the ratios $N_+/\bar{N}_+$ and $N_-/\bar{N}_-$, except for the detection/tagging efficiency of $\bar{\mathrm{K}}^0$ relative to $\mathrm{K}^0$ at the production. The latter is expressed by the ratio $\xi$ between the detection efficiencies of the accompanying charged $\mathrm{K}\pi$ pair, $\xi = \epsilon(\mathrm{K}^+\pi^-)/\epsilon(\mathrm{K}^-\pi^+)$:

$$\frac{N_+}{\bar{N}_+} = \frac{1}{\xi}\frac{\mathscr{P}_+}{\bar{\mathscr{P}}_+}, \quad \frac{N_-}{\bar{N}_-} = \frac{1}{\xi}\frac{\mathscr{P}_-}{\bar{\mathscr{P}}_-} \ . \tag{72}$$

If we compare the experimental asymmetry $A_{\Delta m}^{\exp}(\tau)$,

$$A_{\Delta m}^{\exp}(\tau) = \frac{N_+(\tau)/\bar{N}_+(\tau) - N_-(\tau)/\bar{N}_-(\tau)}{N_+(\tau)/\bar{N}_+(\tau) + N_-(\tau)/\bar{N}_-(\tau)} \ , \tag{73}$$

with the phenomenological asymmetry $A_{\Delta m}(\tau)$,

$$A_{\Delta m}(\tau) = \frac{\mathscr{P}_+(\tau)/\bar{\mathscr{P}}_+(\tau) - \mathscr{P}_-(\tau)/\bar{\mathscr{P}}_-(\tau)}{\mathscr{P}_+(\tau)/\bar{\mathscr{P}}_+(\tau) + \mathscr{P}_-(\tau)/\bar{\mathscr{P}}_-(\tau)} = \frac{2\cos(\Delta m\tau)\cosh(\frac{1}{2}\Delta\Gamma\tau)}{[\cosh(\frac{1}{2}\Delta\Gamma\tau)]^2 + [\cos(\Delta m\tau)]^2} \ , \tag{74}$$

the relative efficiency $\xi$ also cancels. On the right-hand side of Eq. (74) additional terms, quadratic in $\mathscr{T}$- and $\mathscr{CPT}$-violation parameters of the mixing matrix, are neglected as they were shown to be irrelevant in the fit.

The data for the present measurement are a subset of the data taken for the regeneration measurement [24] (see Section 4.2), recorded under the same detector and trigger conditions as for the $\mathscr{CP}$-violation measurement in the $\pi^+\pi^-$ decay channel, except for the presence of the absorber. The absorber thickness was such as to allow neutral-kaon interactions to be measured within the time interval 1.3–5.3$\tau_S$. About $5.6\times10^8$ triggers were recorded. Three sets of measured asymmetries were formed with the $N_\pm$ and $\bar{N}_\pm$ samples, depending on whether the negative strangeness in the final state was detected by the presence of a $\mathrm{K}^-$ or a $\Lambda$, or both. Each of these asymmetries was fitted with Monte Carlo simulations of Eq. (74) performed for values of $\Delta m$ in the range $(515–545)\times10^7\ \hbar/\mathrm{s}$. The simulations included the neutral-kaon momentum distributions, the $\mathscr{P}_\pm$ and $\bar{\mathscr{P}}_\pm$ probabilities, the secondary-vertex spatial resolutions, and a time resolution of $0.025\tau_S$ due to the uncertainty on the determination of the $\mathrm{K}^0$ momentum. The simulated asymmetries were compared with the experimental asymmetries, and the values of $\Delta m$ corresponding to the minimum $\chi^2$ were determined. Given the agreement between the $\Delta m$ values obtained with the two ways of tagging the strangeness of $\bar{\mathrm{K}}^0$, our final result is that given for the combined $(\mathrm{K}^- + \Lambda)$ sample, shown in Fig. 41b.

Various sources of systematic uncertainties were investigated as summarized in Table 27. Our final result is the following:

$$\Delta m = (534.3 \pm 6.3_{\mathrm{stat}} \pm 2.5_{\mathrm{syst}}) \times 10^7\ \hbar/\mathrm{s} \ .$$

This result is in good agreement with the current values [85]: $\Delta m = (530.0 \pm 1.2)\times10^7\ \hbar/\mathrm{s}$ (fit) and $\Delta m = (530.7 \pm 1.5)\times10^7\ \hbar/\mathrm{s}$ (average). Our measurement, though not improving on the current world-average error, has the merit of relying only on strong interactions to tag the kaon strangeness. Moreover, the only parameter of the neutral-kaon system which enters the measurement, apart from $\Delta m$, is the $\mathrm{K}_S$ mean lifetime. We conclude that this measurement of $\Delta m$ provides a valuable input for many $\mathscr{CPT}$ tests.

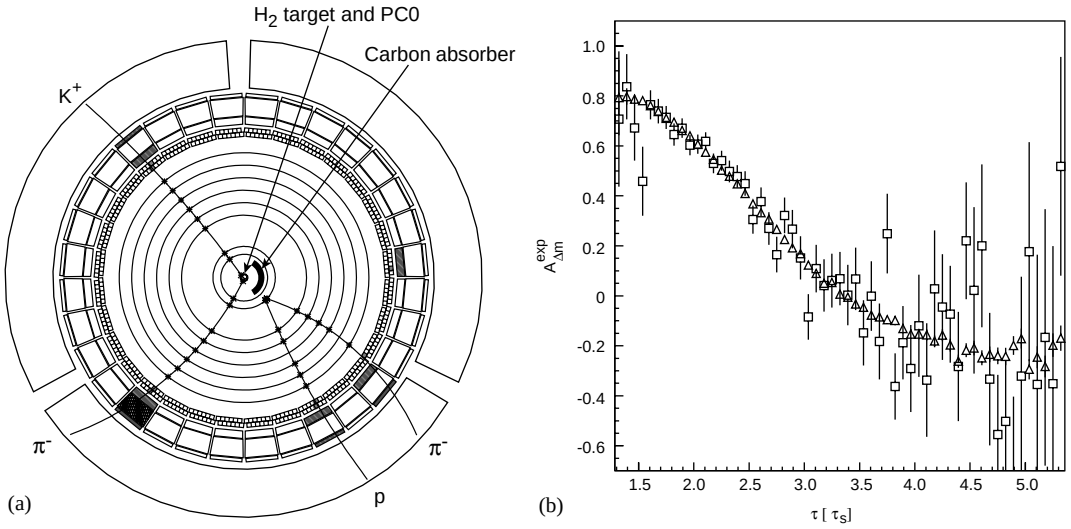


Fig. 41. (a) Display of an event (transverse view): the $K^+\pi^-$ pair produced in a $\bar{p}p$ annihilation together with a $\bar{K}^0$ is shown. The $\bar{K}^0$, interacting in the carbon absorber, produces a $\Lambda$ subsequently decaying to $p\pi^-$ (also shown). (b) $A^{\exp}_{\Delta m}(\tau)$: the data points (squares) of the $(K^- + \Lambda)$ sample are fitted with the simulated asymmetries (triangles), see text.

Table 27
Summary of the systematic errors on $\Delta m$ (method c)

| Source | $\Delta m$ ($10^7$ $\hbar$/s) |
|---|---|
| $\Gamma_S$ | 1.0 |
| Efficiencies | 0.5 |
| Monte Carlo | 1.5 |
| Binning and fit range | 0.5 |
| Selection criteria | 1.5 |
| Total | 2.5 |

## 8. Global evaluations

### 8.1. $\phi_{+-}$ and $\Delta m$ [27]

Given the different strong correlation of the measurement of $\phi_{+-}$ and $\Delta m$ for most of the experiments, averaging the measurements of $\phi_{+-}$ and $\Delta m$ independently is not the appropriate method. Better results are obtained if all the available experimental information, including correlation terms, is used to construct a global likelihood distribution $\mathscr{L}$ depending on the parameters $\Delta m$, $\phi_{+-}$ and $\tau_S$, as the product of individual likelihood distributions corresponding to the various experiments. The best estimates for the values of $\Delta m$, $\phi_{+-}$ and $\tau_S$ are then attained by maximizing $\mathscr{L}$.

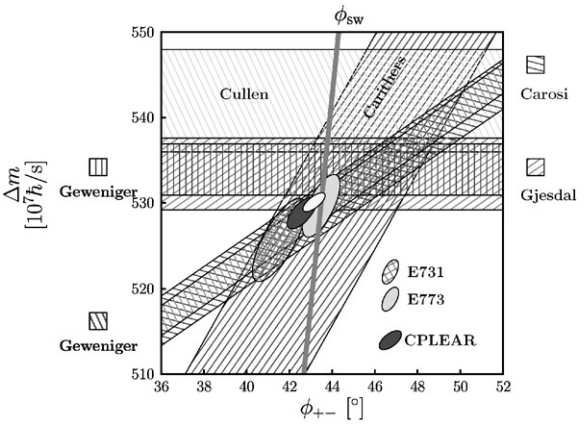


Fig. 42. The result of the global fit to $\phi_{+-}$ and $\Delta m$ measurements from different sources: the ellipse delimiting the white area is the one-standard-deviation contour plot. This fit updates the result of Ref. [27] by including the CPLEAR final results. The narrow stripe labelled $\phi_{SW}$ is the one-standard-deviation region around the line $2\Delta m = \Delta\Gamma \tan(\phi_{+-})$. The results of the individual measurements entering in the fit are also shown. For the earlier results, the inclined stripes refer to experiments measuring together $\phi_{+-}$ and $\Delta m$, from Refs. [86–88], while the horizontal stripes refer to measurements of $\Delta m$ alone, from Refs. [121–123]. The results from later experiments are displayed as regions of less than one standard deviation from their average ($\phi_{+-}$, $\Delta m$). The ellipses labelled E731 and E773 were computed using Refs. [89] and [90], respectively. The CPLEAR ellipse is a global fit to the CPLEAR results of Ref. [7] for $\Delta m$ together with $\phi_{+-}$, and from Refs. [14,26] for $\Delta m$ alone.

CPLEAR performed a first evaluation of this kind [27] taking into account the correlation between $\phi_{+-}$ and $\Delta m$ with the $\tau_S$ correlation handled in some approximation. The fit was recently repeated including the final CPLEAR results for $\phi_{+-}$ and $\Delta m$ (measured by method a), Section 4.1, and of $\Delta m$ measured by method b, Section 5.1, and method c, Section 7.1. For $\tau_S$, the updated average value given in Ref. [85] was used, $\tau_S = 89.40 \pm 0.09$ ps.

Fig. 42 shows the result of the global fit as the one-sigma white ellipse. The central values are $\phi_{+-} = (43.2 \pm 0.5)^\circ$ and $\Delta m = (530.2 \pm 1.2) \times 10^7\ \hbar/\text{s}$. The result of the fit to the values $\phi_{+-}$ and $\Delta m$ measured by CPLEAR is the one-sigma black ellipse with central values $\phi_{+-} = (42.7 \pm 0.7)^\circ$ and $\Delta m = (529.3 \pm 1.8) \times 10^7\ \hbar/\text{s}$. The values of $\phi_{SW}$ computed with the $\Delta m$ and $\tau_S$ values returned by these fits, and the average value of $\tau_L$ given in Ref. [85], were computed to be 43.51° and 43.47° for the global fit and CPLEAR alone, respectively, with errors of $\approx 0.1^\circ$.

### 8.2. $\mathcal{T}$ and $\mathcal{CPT}$ parameters constrained by the unitarity relation [28]

We have studied the constraints on the measured semileptonic asymmetries deriving from the Bell–Steinberger (or unitarity) relation [52,135,136]. The Bell–Steinberger relation relates all decay channels of neutral kaons to the parameters describing $\mathcal{T}$ and $\mathcal{CPT}$ non-invariance. With the present precision of the two-pion decay parameters, the dominant uncertainties arise from the three-pion and semileptonic decays. Moreover, the semileptonic decays enter the relation through the parameter Re($y$), describing $\mathcal{CPT}$ violation in semileptonic decays and as yet not measured. By improving the precision of the three-pion decay rates (Section 4) and measuring precisely the semileptonic decay

rates, CPLEAR made possible the determination of many parameters of the neutral-kaon system with unprecedented accuracy. We stress here that the values of these parameters were obtained free of theoretical assumptions, apart from unitarity, in contrast to previous analyses that are also based on the unitarity relation [137].

In the $K_S - K_L$ basis, the Bell–Steinberger relation [52] can be written as

$$-\mathrm{i}(\lambda_L^* - \lambda_S)\langle K_L|K_S\rangle = \sum \langle f|\mathscr{H}_{wk}|K_L\rangle^* \langle f|\mathscr{H}_{wk}|K_S\rangle \ , \tag{75}$$

where we sum over all the decay final states $f$. With the definitions of Eq. (36) the above equation becomes

$$\mathrm{Re}(\varepsilon) - \mathrm{i}\,\mathrm{Im}(\delta) = \frac{1}{2(\mathrm{i}\Delta m + \bar{\Gamma})} \times \sum \mathscr{A}_{fL}\mathscr{A}_{fS}^* \ . \tag{76}$$

The sum on the right-hand side of the above equation can be written as

$$\sum \mathscr{A}_{fL}\mathscr{A}_{fS}^* = \sum(|\mathscr{A}_{fS}|^2\eta_{\pi\pi}) + \sum(|\mathscr{A}_{fL}|^2\eta_{\pi\pi\pi}^*) + 2[\mathrm{Re}(\varepsilon) - \mathrm{Re}(y) - \mathrm{i}(\mathrm{Im}(x_+) + \mathrm{Im}(\delta))]|f_{\ell\pi\nu}|^2$$

with

$$|\mathscr{A}_{fS}|^2 = \mathrm{BR}_{\pi\pi}^S \Gamma_S \ ,$$
$$|\mathscr{A}_{fL}|^2 = \mathrm{BR}_{\pi\pi\pi}^L \Gamma_L \ ,$$
$$|f_{\ell\pi\nu}|^2 = \mathrm{BR}_{\ell\pi\nu}^L \Gamma_L \ .$$

Here BR stands for branching ratio, the upper index refers to the decaying particle and the lower index to the final state, $\eta_{\pi\pi}$ and $\eta_{\pi\pi\pi}$ are the $\mathscr{CP}$-violation parameters for neutral kaons decaying to two and three pions, respectively, and $\ell$ denotes electrons and muons. The radiative modes, like $\pi^+\pi^-\gamma$, are included in the corresponding parent modes [78]. Channels with $\mathrm{BR}_f^S$ (or $\mathrm{BR}_f^L \times \Gamma_L/\Gamma_S$) $< 10^{-5}$ do not contribute to Eq. (76) within the accuracy of the present analysis.

From Eq. (76) we obtain explicit expressions for the parameters $\mathrm{Re}(\varepsilon)$ and $\mathrm{Im}(\delta)$:

$$\begin{pmatrix} \mathrm{Im}(\delta) \\ \mathrm{Re}(\varepsilon) \end{pmatrix} = \frac{\Gamma_S}{2(\bar{\Gamma} - |f_{\ell\pi\nu}|^2)(\mu^2+1)} \begin{pmatrix} \mu & -1 \\ 1 & \mu \end{pmatrix} \times \begin{pmatrix} [1 - \gamma_{LoS}\mathrm{BR}_{\ell\pi\nu}^L]\mathrm{Re}(\eta_{\pi\pi}) + [-2\mathrm{BR}_{\ell\pi\nu}^L\mathrm{Re}(y) + \mathrm{BR}_{\pi\pi\pi}^L\mathrm{Re}(\eta_{\pi\pi\pi})]\gamma_{LoS} \\ [1 - \gamma_{LoS}\mathrm{BR}_{\ell\pi\nu}^L]\mathrm{Im}(\eta_{\pi\pi}) - [\mathrm{BR}_{\pi\pi\pi}^L\,\mathrm{Im}(\eta_{\pi\pi\pi}) + 2\mathrm{BR}_{\ell\pi\nu}^L\mathrm{Im}(x_+)]\gamma_{LoS} \end{pmatrix} \tag{77}$$

with

$$\mathrm{Re}(\eta_{\pi\pi}) = |\eta_{+-}|\cos(\phi_{+-})(1 - [(1-r) + r\sin(\Delta\phi)\tan(\phi_{+-})]\mathrm{BR}_{\pi^0\pi^0}^S) \ ,$$
$$\mathrm{Im}(\eta_{\pi\pi}) = |\eta_{+-}|\sin(\phi_{+-})(1 - [(1-r) - r\sin(\Delta\phi)\cot(\phi_{+-})]\mathrm{BR}_{\pi^0\pi^0}^S) \ ,$$
$$\mathrm{BR}_{\pi\pi\pi}^L\,\mathrm{Re}(\eta_{\pi\pi\pi}) = \mathrm{BR}_{\pi^+\pi^-\pi^0}^L\,\mathrm{Re}(\eta_{+-0}) + \mathrm{BR}_{\pi^0\pi^0\pi^0}^L\,\mathrm{Re}(\eta_{000}) \ ,$$
$$\mathrm{BR}_{\pi\pi\pi}^L\,\mathrm{Im}(\eta_{\pi\pi\pi}) = \mathrm{BR}_{\pi^+\pi^-\pi^0}^L\,\mathrm{Im}(\eta_{+-0}) + \mathrm{BR}_{\pi^0\pi^0\pi^0}^L\,\mathrm{Im}(\eta_{000}) \ ,$$

Table 28
Values of the neutral-kaon system parameters used as input to the unitarity equations

| Parameter | Value | References |
|---|---|---|
| $\lvert\eta_{+-}\rvert$ | $(2.283 \pm 0.025) \times 10^{-3}$ | [7,78] |
| $\phi_{+-}$ | $43.6^\circ \pm 0.6^\circ$ | [7,78] |
| $\Delta m$ | $(530.2 \pm 1.5) \times 10^7\ \hbar/\mathrm{s}$ | see text |
| $\Delta\phi$ | $-0.3^\circ \pm 0.8^\circ$ | [88] |
| $r = \dfrac{\lvert\eta_{00}\rvert}{\lvert\eta_{+-}\rvert}$ | $0.9930 \pm 0.0020$ | [78] |
| $\mathrm{Re}(\eta_{+-0})$ | $(-2 \pm 8) \times 10^{-3}$ | [9] |
| $\mathrm{Im}(\eta_{+-0})$ | $(-2 \pm 9) \times 10^{-3}$ | [9] |
| $\mathrm{Re}(\eta_{000})$ | $0.08 \pm 0.11$ | [10,110] |
| $\mathrm{Im}(\eta_{000})$ | $0.07 \pm 0.16$ | [10,119] |
| $\mathrm{BR}^{\mathrm{S}}_{\pi^0\pi^0}$ | $(31.39 \pm 0.28)\%$ | [78] |
| $\mathrm{BR}^{\mathrm{L}}_{\pi^+\pi^-\pi^0}$ | $(12.56 \pm 0.20)\%$ | [78] |
| $\mathrm{BR}^{\mathrm{L}}_{\pi^0\pi^0\pi^0}$ | $(21.12 \pm 0.27)\%$ | [78] |
| $\mathrm{BR}^{\mathrm{L}}_{\ell\pi\nu}$ | $(65.95 \pm 0.37)\%$ | [78] |
| $\tau_{\mathrm{S}}$ | $(89.34 \pm 0.08) \times 10^{-12}$ s | [78] |
| $\tau_{\mathrm{L}}$ | $(5.17 \pm 0.04) \times 10^{-8}$ s | [78] |

and

$$\mu = \frac{2\Delta m}{2(\bar{\Gamma} - |f_{\ell\pi\nu}|^2)}, \quad \gamma_{\mathrm{LoS}} = \frac{\Gamma_{\mathrm{L}}}{\Gamma_{\mathrm{S}}}, \quad r = \frac{|\eta_{00}|}{|\eta_{+-}|}, \quad \Delta\phi = \phi_{00} - \phi_{+-}\ .$$

Table 28 summarizes the experimental values of the parameters to be entered on the right-hand side of Eq. (77). The value of $\Delta m$ in Table 28 results from experiments [78] which do not assume $\mathscr{CPT}$ invariance in the decay (regeneration experiments). We note that experimental data exist for all the parameters related to two- and three-pion decays, $\eta_{\pi\pi}$ and $\eta_{\pi\pi\pi}$, which contain all the information required for the present analysis, including decay amplitudes. For the semileptonic decays we lack the measurement of the parameter $\mathrm{Re}(y)$, while for the parameter $\mathrm{Im}(x_+)$ the only existing measurement comes from CPLEAR, Section 5.

However, the parameters $\mathrm{Re}(y)$ and $\mathrm{Im}(x_+)$, together with $\mathrm{Re}(\varepsilon)$, $\mathrm{Im}(\delta)$, $\mathrm{Re}(\delta)$, and $\mathrm{Re}(x_-)$, do enter in the following two semileptonic asymmetries:

$$\frac{\bar{R}_+ - R_-[1 + 4\mathrm{Re}(\varepsilon_{\mathrm{L}})]}{\bar{R}_+ + R_-[1 + 4\mathrm{Re}(\varepsilon_{\mathrm{L}})]} = 2(\mathrm{Re}(\varepsilon) - \mathrm{Re}(y) + \mathrm{Re}(\delta)) + 2\,\frac{\mathrm{Im}(x_+)\sin(\Delta m\tau) - \mathrm{Re}(x_-)\sinh(\Delta\Gamma\tau/2)}{\cosh(\Delta\Gamma\tau/2) - \cos(\Delta m\tau)}\ , \tag{78}$$

and

$$\frac{\bar{R}_- - R_+[1 + 4\,\mathrm{Re}(\varepsilon_{\mathrm{L}})]}{\bar{R}_- + R_+[1 + 4\,\mathrm{Re}(\varepsilon_{\mathrm{L}})]} = 2(-\mathrm{Re}(\varepsilon) + \mathrm{Re}(y) + \mathrm{Re}(\delta))$$

Table 29
The correlation coefficients for the parameters $\mathrm{Im}(x_+)$, $\mathrm{Re}(y)$, $\mathrm{Re}(\delta)$, $\mathrm{Re}(x_-)$, $\mathrm{Re}(\varepsilon)$ and $\mathrm{Im}(\delta)$

| | $\mathrm{Im}(x_+)$ | $\mathrm{Re}(y)$ | $\mathrm{Re}(\delta)$ | $\mathrm{Re}(x_-)$ | $\mathrm{Re}(\varepsilon)$ | $\mathrm{Im}(\delta)$ |
|---|---|---|---|---|---|---|
| $\mathrm{Im}(x_+)$ | — | −0.624 | −0.555 | 0.651 | −0.142 | 0.075 |
| $\mathrm{Re}(y)$ | | — | 0.279 | −0.997 | −0.159 | −0.075 |
| $\mathrm{Re}(\delta)$ | | | — | −0.349 | 0.039 | −0.051 |
| $\mathrm{Re}(x_-)$ | | | | — | 0.060 | 0.109 |
| $\mathrm{Re}(\varepsilon)$ | | | | | — | −0.256 |
| $\mathrm{Im}(\delta)$ | | | | | | — |

Table 30
Summary of the systematic errors arising from the CPLEAR semileptonic data

| Source | $\mathrm{Im}(x_+)$ $(10^{-3})$ | $\mathrm{Re}(y)$ $(10^{-3})$ | $\mathrm{Re}(\delta)$ $(10^{-4})$ | $\mathrm{Re}(x_-)$ $(10^{-3})$ | $\mathrm{Re}(\varepsilon)$ $(10^{-5})$ | $\mathrm{Im}(\delta)$ $(10^{-5})$ |
|---|---|---|---|---|---|---|
| Background level | ±0.1 | ±0.1 | ±0.1 | ±0.1 | 0 | 0 |
| Background asymmetry | ±0.4 | ±0.2 | ±0.2 | ±0.2 | ±0.1 | ±0.1 |
| $\alpha\xi$ | 0 | ±0.1 | ±0.5 | ±0.1 | 0 | 0 |
| $\eta$ | ±0.02 | ±0.5 | ±0.02 | ±0.02 | 0 | 0 |
| Decay-time resolution | ±0.1 | ±0.1 | 0 | ±0.1 | 0 | 0 |
| Regeneration | ±0.1 | ±0.1 | ±0.25 | ±0.1 | 0 | 0 |
| Total | ±0.5 | ±0.6 | ±0.6 | ±0.3 | ±0.1 | ±0.1 |

$$+\frac{[4\,\mathrm{Re}(\delta)+2\,\mathrm{Re}(x_-)]\sinh(\Delta\Gamma\tau/2)+[2\,\mathrm{Im}(x_+)+4\,\mathrm{Im}(\delta)]\sin(\Delta m\tau)}{\cosh(\Delta\Gamma\tau/2)+\cos(\Delta m\tau)}\,. \tag{79}$$

Using as constraint the Bell–Steinberger relation, Eq. (77), and the $K_L$ charge asymmetry $\delta_\ell$, the determination of the parameters $\mathrm{Re}(\varepsilon)$, $\delta$, $\mathrm{Im}(x_+)$, $\mathrm{Re}(x_-)$ and $\mathrm{Re}(y)$ is possible. For $\delta_\ell$ we use the value from Ref. [78]:

$$\delta_\ell = 2\,\mathrm{Re}(\varepsilon) - 2\,\mathrm{Re}(\delta) - 2\,\mathrm{Re}(y) - 2\,\mathrm{Re}(x_-) = (3.27 \pm 0.12)\times 10^{-3}\,. \tag{80}$$

For the analysis of the asymmetries in Eqs. (78) and (79), we use the normalization procedure described in Ref. [13].

The values of Table 28 were used in the fit; all known correlations among these quantities were taken into account. From the fit we obtained a value of $\chi^2/\mathrm{ndf} = 1.09$ with the correlation coefficients between the various parameters shown in Table 29. The contribution to the final errors arising from systematic effects in the CPLEAR semileptonic data were determined in the same way as in Section 5, and are summarized in Table 30. Our final result, assuming only unitarity, is

$$\mathrm{Re}(\varepsilon) = (164.9 \pm 2.5_{\mathrm{stat}} \pm 0.1_{\mathrm{syst}})\times 10^{-5}\,,$$

$$\mathrm{Im}(\delta) = (2.4 \pm 5.0_{\mathrm{stat}} \pm 0.1_{\mathrm{syst}})\times 10^{-5}\,,$$

and

$$\mathrm{Re}(\delta) = (2.4 \pm 2.7_{\mathrm{stat}} \pm 0.6_{\mathrm{syst}}) \times 10^{-4} \ ,$$

$$\mathrm{Re}(y) = (0.3 \pm 3.0_{\mathrm{stat}} \pm 0.6_{\mathrm{syst}}) \times 10^{-3} \ ,$$

$$\mathrm{Im}(x_+) = (-2.0 \pm 2.6_{\mathrm{stat}} \pm 0.5_{\mathrm{syst}}) \times 10^{-3} \ ,$$

$$\mathrm{Re}(x_-) = (-0.5 \pm 3.0_{\mathrm{stat}} \pm 0.3_{\mathrm{syst}}) \times 10^{-3} \ .$$

Our results on $\mathrm{Re}(\varepsilon)$ and $\mathrm{Im}(\delta)$ are almost one order of magnitude more accurate than those of a previous similar analysis [135] owing to improvements in the accuracy of various measurements where CPLEAR has made significant contributions. The fact that $\mathrm{Re}(\varepsilon)$ and $\mathrm{Im}(\delta)$ are essentially determined through the Bell–Steinberger relation allows $\mathrm{Re}(y)$ to be obtained explicitly: a result which could not be achieved from semileptonic data alone. Moreover, the present analysis yields accuracies for the parameters $\mathrm{Im}(x_+)$ and $\mathrm{Re}(x_-)$ which are about one order of magnitude better than those in Section 5, while the accuracy on the parameter $\mathrm{Re}(\delta)$ is comparable with that reported in Section 5.

Table 29 shows a strong anticorrelation between the values of $\mathrm{Re}(x_-)$ and $\mathrm{Re}(y)$ given by the fit. If we consider their sum we find

$$\mathrm{Re}(y + x_-) = (-0.2 \pm 0.3) \times 10^{-3} \ . \tag{81}$$

This quantity appears in the asymptotic value of the time-reversal asymmetry $A_{\mathrm{T}}$ measured by CPLEAR (see Section 5.3). The present result confirms that the possible contribution to this asymmetry from $\mathscr{CPT}$-violating decay amplitudes is negligible.

The error on $\mathrm{Re}(\varepsilon)$ and $\mathrm{Im}(\delta)$ is dominated by the error on $\eta_{000}$. The CPLEAR accuracy on $\eta_{+-0}$ is such that its contribution to the error becomes negligible. If we assume that there is no $I = 3$ decay amplitude in the three-pion decay, it follows that $\eta_{+-0} = \eta_{000}$ and our analysis yields

$$\mathrm{Re}(\varepsilon) = (165.0 \pm 1.9) \times 10^{-5} \ ,$$

$$\mathrm{Im}(\delta) = (-0.5 \pm 2.0) \times 10^{-5} \ ,$$

thus reducing the errors on the parameters $\mathrm{Re}(\varepsilon)$ and $\mathrm{Im}(\delta)$ by a factor of two, while the correlation coefficient reduces to $-0.003$.

### 8.3. $\mathrm{K}^0 - \bar{\mathrm{K}}^0$ *mass and decay-width differences [29]*

The $\mathscr{CPT}$ theorem [48], which is based on general principles of the relativistic quantum field theory, states that any order of the triple product of the discrete symmetries $\mathscr{C}$, $\mathscr{P}$ and $\mathscr{T}$ should represent an exact symmetry. The theorem predicts, among other things, that particles and antiparticles have equal masses and lifetimes. The $\mathscr{CPT}$ symmetry has been tested in a variety of experiments (see for example Ref. [85]) and remains to date the only combination of $\mathscr{C}$, $\mathscr{P}$ and $\mathscr{T}$ that is observed as an exact symmetry in nature. On the other hand, there is some theoretical progress related to string theory which may allow a consistent theoretical framework including violation of $\mathscr{CPT}$ to be constructed [138].

The $K^0 - \bar{K}^0$ mass and decay-width differences may be obtained as the differences between the diagonal elements of the neutral-kaon mass and decay matrices,

$$m_{\bar{K}^0} - m_{K^0} = M_{\bar{K}^0\bar{K}^0} - M_{K^0K^0}, \quad \gamma_{\bar{K}^0} - \gamma_{K^0} = \Gamma_{\bar{K}^0\bar{K}^0} - \Gamma_{K^0K^0} \ .$$

In Refs. [78,88] the mass difference between $K^0$ and $\bar{K}^0$ was evaluated as

$$m_{\bar{K}^0} - m_{K^0} \approx \frac{2\Delta m|\eta|(\frac{2}{3}\phi_{+-} + \frac{1}{3}\phi_{00} - \phi_{SW})}{\sin(\phi_{SW})} \ . \tag{82}$$

We recall that $\phi_{+-}$ and $\phi_{00}$ are the phases of the parameters $\eta_{+-}$ and $\eta_{00}$ describing $\mathscr{CP}$ violation in the two-pion decay channel ($|\eta| = |\eta_{+-}| \approx |\eta_{00}|$), and $\phi_{SW}$(superweak phase) $\equiv \arctan(2\Delta m/\Delta\Gamma)$. Here we would like to stress that Eq. (82) contains the assumption of $\mathscr{CPT}$ invariance in the decay of neutral kaons and neglects some of the contributions from decay channels other than two-pion. [3]

These limitations were overcome in the CPLEAR evaluation by taking advantage of the values of the $\mathscr{CPT}$-violation parameters Re($\delta$) and Im($\delta$), obtained by applying the unitarity (or Bell–Steinberger) relation (Section 8.2).

The parameter $\delta$ is conveniently represented in the complex plane [70] by the projections along the $\phi_{SW}$ axis ($\delta_{\|}$) and its normal ($\delta_{\perp}$):

$$\delta_{\|} = \frac{1}{4}\frac{\Gamma_{K^0K^0} - \Gamma_{\bar{K}^0\bar{K}^0}}{\sqrt{\Delta m^2 + (\Delta\Gamma/2)^2}} \quad \text{and} \quad \delta_{\perp} = \frac{1}{2}\frac{M_{K^0K^0} - M_{\bar{K}^0\bar{K}^0}}{\sqrt{\Delta m^2 + (\Delta\Gamma/2)^2}} \ . \tag{83}$$

The quantities $\delta_{\|}$ and $\delta_{\perp}$ can be expressed as functions of the measured quantities Re($\delta$), Im($\delta$) and $\phi_{SW}$ as

$$\begin{aligned} \delta_{\|} &= \mathrm{Re}(\delta)\cos(\phi_{SW}) + \mathrm{Im}(\delta)\sin(\phi_{SW}) \ , \\ \delta_{\perp} &= -\mathrm{Re}(\delta)\sin(\phi_{SW}) + \mathrm{Im}(\delta)\cos(\phi_{SW}) \ , \end{aligned} \tag{84}$$

and allow in turn the $K^0 - \bar{K}^0$ decay-width and mass differences to be determined as

$$\begin{aligned} \Gamma_{K^0K^0} - \Gamma_{\bar{K}^0\bar{K}^0} &= \delta_{\|} \times \frac{2\Delta\Gamma}{\cos(\phi_{SW})} \ , \\ M_{K^0K^0} - M_{\bar{K}^0\bar{K}^0} &= \delta_{\perp} \times \frac{\Delta\Gamma}{\cos(\phi_{SW})} \ . \end{aligned} \tag{85}$$

Thus the evaluation of the $K^0 - \bar{K}^0$ mass and decay-width differences is straightforward, once the $\mathscr{CPT}$-violation parameters Re($\delta$) and Im($\delta$) are known.

From unitarity [52], or from Eq. (7b), it follows that the elements of the $\Gamma$-matrix are given by the products of the $K^0$ and $\bar{K}^0$ ($|\Delta S| = 1$) decay amplitudes to all real final states $f$, with

$$\Gamma_{K^0K^0} = \sum \mathscr{A}_f^* \mathscr{A}_f, \quad \Gamma_{\bar{K}^0\bar{K}^0} = \sum \bar{\mathscr{A}}_f^* \bar{\mathscr{A}}_f, \quad \Gamma_{K^0\bar{K}^0} = \Gamma_{\bar{K}^0K^0}^* = \sum \mathscr{A}_f^* \bar{\mathscr{A}}_f \ , \tag{86}$$

where $\mathscr{A}_f$ and $\bar{\mathscr{A}}_f$ denote the $K^0$ and $\bar{K}^0$ decay amplitudes to a specified final state $f$. The elements of the M-matrix on the other hand are given by Eq. (7a) and contain the products of the ($|\Delta S| = 1$) transition amplitudes to all virtual states as well as a possible ($|\Delta S| = 2$) term which is linear in the

[3] However, see L. Wolfenstein in Ref. [78, p. 107]. The relation between $\phi_{+-}$, $\phi_{00}$ and $\phi_{SW}$ has a long history since the seminal paper of Wu and Yang [51]. For a more recent critical discussion see Ref. [139].

Table 31
Experimental values of $K_S$ and $K_L$ parameters [28,78] used in the present analysis

| Parameter | Value |
|---|---|
| $1/\Gamma_S$ | $(89.34 \pm 0.08) \times 10^{-12}\ \hbar^{-1}$s |
| $1/\Gamma_L$ | $(5.17 \pm 0.04) \times 10^{-8}\ \hbar^{-1}$s |
| $\Delta\Gamma$ | $(1117.4 \pm 1.0) \times 10^{7}\ \hbar$s$^{-1} = (7.355 \pm 0.007) \times 10^{-15}$ GeV |
| $\Delta m$ | $(530.2 \pm 1.5) \times 10^{7}\ \hbar$s$^{-1} = (3.490 \pm 0.010) \times 10^{-15}$ GeV |

transition amplitude. Thus $\mathscr{CPT}$ violation could manifest itself in first order in the M-matrix, but only in higher orders in the $\Gamma$-matrix.

By using for $\mathrm{Re}(\delta)$ and $\mathrm{Im}(\delta)$ the following values of Section 8.2,

$$\mathrm{Re}(\delta) = (2.4 \pm 2.8) \times 10^{-4}\ ,$$
$$\mathrm{Im}(\delta) = (2.4 \pm 5.0) \times 10^{-5}\ , \tag{87}$$

with a correlation coefficient of 5%, together with the values for $\Delta\Gamma$ and $\Delta m$ of Table 31, we obtain from Eqs. (84)

$$\delta_{\|} = (1.9 \pm 2.0) \times 10^{-4}\ ,$$
$$\delta_{\perp} = (-1.5 \pm 2.0) \times 10^{-4}\ , \tag{88}$$

and subsequently from Eqs. (85)

$$\Gamma_{K^0K^0} - \Gamma_{\bar{K}^0\bar{K}^0} = (3.9 \pm 4.2) \times 10^{-18}\ \mathrm{GeV}\ ,$$
$$M_{K^0K^0} - M_{\bar{K}^0\bar{K}^0} = (-1.5 \pm 2.0) \times 10^{-18}\ \mathrm{GeV}\ , \tag{89}$$

with a correlation coefficient of $-0.95$. Fig. 43 shows the error ellipses corresponding to $1\sigma, 2\sigma$ and $3\sigma$. Our result on the mass difference is a factor of two better than the one obtained with a similar calculation in Ref. [140]. We note that the improvement is mainly due to $\mathrm{Re}(\delta)$ now being known with a smaller error.

The error of $\mathrm{Re}(\delta)$ becomes even smaller if we assume $\mathscr{CPT}$-invariant decay amplitudes, that is $\Gamma_{K^0K^0} = \Gamma_{\bar{K}^0\bar{K}^0}$ or, equivalently, $\mathrm{Re}(\delta) = -\mathrm{Im}(\delta) \times \tan(\phi_{SW})$. In this case $\mathrm{Re}(\delta)$ can be determined by $\mathrm{Im}(\delta)$ and the parameter $\delta_{\perp}$ becomes $\delta_{\perp} = \mathrm{Im}(\delta)/\cos(\phi_{SW})$. The results for $M_{K^0K^0} - M_{\bar{K}^0\bar{K}^0}$ are shown in Table 32 depending on the values for $\mathrm{Im}(\delta)$ which are obtained from the unitarity relation under different conditions: (a) no restriction [28]; (b) equal $\mathscr{CP}$-violation parameters for the decay to $\pi^0\pi^0\pi^0$ and to $\pi^+\pi^-\pi^0$, i.e. $\eta_{000} = \eta_{+-0}$ [28]; (c) only the $\pi\pi$ decay channel contributes to the unitarity relation.

We shall now compare the method outlined above with the one leading to Eq. (82). With the notation of Section 2.2.2 for the two-pion decay amplitudes, we obtain from the $\eta_{+-}$ and $\eta_{00}$ definitions [70]

$$\eta_{+-} = \varepsilon - \delta + \left( \mathrm{i}\,\frac{\mathrm{Im}(A_0)}{\mathrm{Re}(A_0)} + \frac{\mathrm{Re}(B_0)}{\mathrm{Re}(A_0)} \right) + \varepsilon'\ , \tag{90a}$$

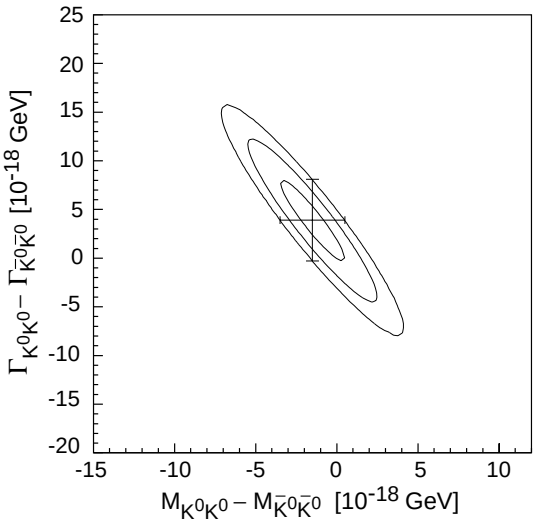


Fig. 43. The $K^0 - \bar{K}^0$ decay-width versus mass difference. The $1\sigma$, $2\sigma$ and $3\sigma$ ellipses are also shown.

Table 32
Mass difference assuming $\Gamma_{K^0K^0} - \Gamma_{\bar{K}^0\bar{K}^0} = 0$: values and modulus limits at 90% CL for different values of Im($\delta$) (see text)

| | Im($\delta$) ($10^{-5}$) | ($M_{K^0K^0} - M_{\bar{K}^0\bar{K}^0}$) ($10^{-19}$ GeV) | $\lvert M_{K^0K^0} - M_{\bar{K}^0\bar{K}^0}\rvert$ ($10^{-19}$ GeV) |
|---|---|---|---|
| (a) | $2.4 \pm 5.0$ | $3.3 \pm 7.0$ | $\leqslant 12.7$ |
| (b) | $-0.5 \pm 2.0$ | $-0.7 \pm 2.8$ | $\leqslant 4.8$ |
| (c) | $-0.1 \pm 1.9$ | $-0.1 \pm 2.7$ | $\leqslant 4.4$ |

$$\eta_{00} = \varepsilon - \delta + \left( \mathrm{i}\,\frac{\mathrm{Im}(A_0)}{\mathrm{Re}(A_0)} + \frac{\mathrm{Re}(B_0)}{\mathrm{Re}(A_0)} \right) - 2\varepsilon' \ , \tag{90b}$$

$$\varepsilon' = \frac{1}{\sqrt{2}} e^{\mathrm{i}(\delta_2 - \delta_0)} \frac{\mathrm{Re}(A_2)}{\mathrm{Re}(A_0)} \left( \mathrm{i} \left[ \frac{\mathrm{Im}(A_2)}{\mathrm{Re}(A_2)} - \frac{\mathrm{Im}(A_0)}{\mathrm{Re}(A_0)} \right] + \left[ \frac{\mathrm{Re}(B_2)}{\mathrm{Re}(A_2)} - \frac{\mathrm{Re}(B_0)}{\mathrm{Re}(A_0)} \right] \right) \ . \tag{90c}$$

The set of Eqs. (90) is visualized in Fig. 44. In this representation, according to the CPLEAR choice of $\phi_\Gamma = 0$ (Section 2.1) the parameter $\varepsilon$ has a phase equal to $\phi_{SW}$. We have also introduced the quantity $\Delta\phi = \mathrm{Im}(\Gamma'_{K^0\bar{K}^0})/\Delta\Gamma$ which stands for one-half the phase of the off-diagonal $\Gamma$-matrix element $\Gamma'_{K^0\bar{K}^0}$ corresponding to neutral kaons decaying to channels other than the two-pion ($I = 0$) state. From Eqs. (90) we obtain expressions for Im($\delta$), Re($\delta$) and, together with Eqs. (84), for $\delta_\perp$:

$$\mathrm{Im}(\delta) = \cos(\phi_{SW})|\eta_{+-}| \left( \phi_{SW} - \frac{2}{3}\,\phi_{+-} - \frac{1}{3}\,\phi_{00} \right) + \Delta\phi \ , \tag{91a}$$

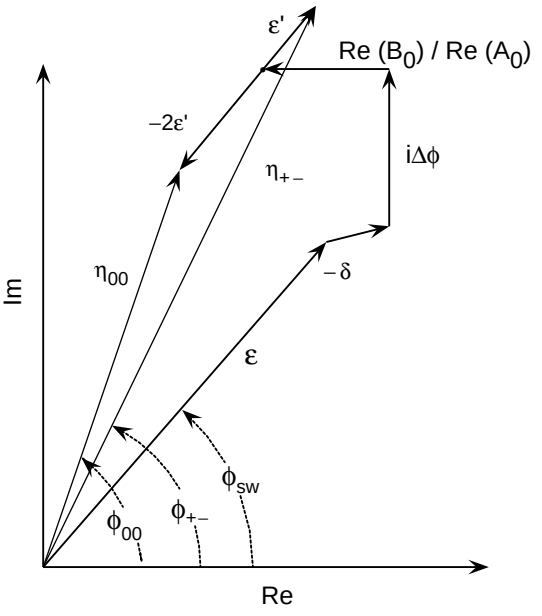


Fig. 44. $\mathscr{CP}$-, $\mathscr{T}$- and $\mathscr{CPT}$-violation parameters for neutral-kaon decays to $\pi^+\pi^-$.

$$\mathrm{Re}(\delta) = -\sin(\phi_{\mathrm{SW}})|\eta_{+-}| \left(\phi_{\mathrm{SW}} - \frac{2}{3}\,\phi_{+-} - \frac{1}{3}\,\phi_{00}\right) + \frac{\mathrm{Re}(B_0)}{\mathrm{Re}(A_0)}\ , \tag{91b}$$

$$\delta_\perp = |\eta_{+-}| \left(\phi_{\mathrm{SW}} - \frac{2}{3}\,\phi_{+-} - \frac{1}{3}\,\phi_{00}\right) + \Delta\phi\cos(\phi_{\mathrm{SW}}) - \frac{\mathrm{Re}(B_0)}{\mathrm{Re}(A_0)}\sin(\phi_{\mathrm{SW}})\ . \tag{91c}$$

Here, use is made of the fact that $|\eta_{+-}| \approx |\eta_{00}| \approx |\varepsilon|$. This approximation is no longer appropriate when computing $\delta_{\|}$ for which we obtain

$$\delta_{\|} \approx |\varepsilon| - |\eta_{+-}| + \Delta\phi\sin(\phi_{\mathrm{SW}}) + \frac{\mathrm{Re}(B_0)}{\mathrm{Re}(A_0)}\cos(\phi_{\mathrm{SW}})\ . \tag{92}$$

Owing to the lack of precise information on $|\varepsilon| - |\eta_{+-}|$, one evaluates only $\delta_\perp$ (and the mass difference), without any explicit consideration of $\delta_{\|}$ (and the decay-width difference). Finally, when the terms containing $\Delta\phi$ and $\mathrm{Re}(B_0)/\mathrm{Re}(A_0)$ are neglected[4] Eqs. (91) and (85) reduce to Eq. (82) and to case (c) of Table 32, leading to the limit $|\mathrm{M}_{\mathrm{K}^0\mathrm{K}^0} - \mathrm{M}_{\bar{\mathrm{K}}^0\bar{\mathrm{K}}^0}| \leqslant 4.4 \times 10^{-19}$ GeV (90% CL).

[4] The measurements of CPLEAR in semileptonic and $3\pi$ sectors have allowed stringent limits to be set on $\Delta\phi$. If one assumes the $I = 1$ decay amplitude to be dominant in the three-pion decay so that $\eta_{000} = \eta_{+-0}$, we obtain $\Delta\phi = (-5.8 \pm 8.1) \times 10^{-6}$ and $\delta_\perp = (-0.4 \pm 2.7) \times 10^{-5}$, while $\delta_\perp = (-0.0 \pm 2.6) \times 10^{-5}$ for $\Delta\phi = 0$. If one uses the measured value for $\eta_{000}$, the error on $\Delta\phi$ increases by an order of magnitude and becomes dominant in (91), provided that $\mathrm{Re}(B_0)/\mathrm{Re}(A_0)$ can be neglected. Without this last restriction, and using our evaluation of Eq. (95) the error of $\delta_\perp$ becomes as large as $\approx 2 \times 10^{-4}$.

With a similar approach, one could also simply use Eq. (90a) and neglect, in addition to $\Delta\phi$ and $\mathrm{Re}(B_0)/\mathrm{Re}(A_0)$, also the projection of $\varepsilon'$ along the normal to the $\phi_{\mathrm{SW}}$ axis, $\varepsilon'_\perp = |\eta_{+-}|(\phi_{+-} - \phi_{00})/3$—which means to neglect the real part of both $\mathscr{CPT}$-violating amplitudes $B_0$ and $B_2$, see Eq. (95). This procedure leads to a slightly lower limit, $|\mathrm{M}_{\mathrm{K}^0\mathrm{K}^0} - \mathrm{M}_{\bar{\mathrm{K}}^0\bar{\mathrm{K}}^0}| \leqslant 4.0 \times 10^{-19}$ GeV (90% CL).

The limit on the decay-width difference obtained from Eq. (89) is the result of a global evaluation of a possible violation of $\mathscr{CPT}$ in the decay. However, we may also give some information on the individual $\mathscr{CPT}$-violating decay amplitudes. For the semileptonic decays, the parameters $\mathrm{Re}(y)$ and $\mathrm{Re}(x_-)$, describing $\mathscr{CPT}$ violation in $\Delta S = \Delta Q$ and $\Delta S \neq \Delta Q$ transitions, respectively, and their sum, reported here for convenience, were already determined in Section 8.2:

$$\mathrm{Re}(y) = (0.3 \pm 3.1) \times 10^{-3} \ ,$$

$$\mathrm{Re}(x_-) = (-0.5 \pm 3.0) \times 10^{-3} \ ,$$

$$\mathrm{Re}(y + x_-) = (-2.0 \pm 3.0) \times 10^{-4} \ .$$

For the pionic decays, only the parameters $\mathrm{Re}(B_I)/\mathrm{Re}(A_I)$ are estimated. Without attempting a global fit to the data we perform this estimation by expressing the $\mathrm{K}^0 - \bar{\mathrm{K}}^0$ decay-width difference, according to its definition, as

$$\frac{\Gamma_{\mathrm{K}^0\mathrm{K}^0} - \Gamma_{\bar{\mathrm{K}}^0\bar{\mathrm{K}}^0}}{2\Gamma_{\mathrm{S}}} = \frac{\mathrm{Re}(B_0)}{\mathrm{Re}(A_0)} + \left|\frac{A_2}{A_0}\right|^2 \times \frac{\mathrm{Re}(B_2)}{\mathrm{Re}(A_2)} + \frac{\Gamma_{\mathrm{L}}}{\Gamma_{\mathrm{S}}}\left[\mathrm{BR}(\mathrm{K}_{\mathrm{L}} \to 3\pi)\frac{\mathrm{Re}(B_I)}{\mathrm{Re}(A_I)} - 2\,\mathrm{BR}(\mathrm{K}_{\mathrm{L}} \to \ell\pi\nu)\mathrm{Re}(y)\right] \ . \tag{93}$$

In Eq. (93), the left-hand side is determined from Eq. (89) to be $(2.6 \pm 2.9) \times 10^{-4}$. On the right-hand side, the last term is estimated to be $\approx 5 \times 10^{-6}$ with the values of the branching ratios from Ref. [78], $\mathrm{Re}(y)$ as given above, and the measured value of $\mathrm{Re}(\eta_{+-0})$ [9] considered as an upper limit for $\mathrm{Re}(B_1)/\mathrm{Re}(A_1)$. We are then left with the possible contributions to the decay-width difference from the two-pion decay channel.

Since $(\delta_2 - \delta_0) = -(42 \pm 4)^\circ$ [141], and $\phi_{\mathrm{SW}} = +(43.50 \pm 0.08)^\circ$ with the values of Table 31, we obtain as a good approximation from Eqs. (90)

$$\frac{1}{3}(\phi_{00} - \phi_{+-})|\eta_{+-}| = \frac{1}{\sqrt{2}}\frac{\mathrm{Re}(A_2)}{\mathrm{Re}(A_0)}\left[\frac{\mathrm{Re}(B_2)}{\mathrm{Re}(A_2)} - \frac{\mathrm{Re}(B_0)}{\mathrm{Re}(A_0)}\right] \ . \tag{94}$$

We estimate $\mathrm{Re}(A_2)/\mathrm{Re}(A_0) \approx |A_2/A_0| \approx 0.04479 \pm 0.00020$ [113], with $\mathrm{Re}(B_2)/\mathrm{Re}(A_2)$ and $\mathrm{Re}(B_0)/\mathrm{Re}(A_0) \ll 1$; we also take $|\eta_{+-}| = (2.283 \pm 0.025) \times 10^{-3}$ and $(\phi_{00} - \phi_{+-}) = (-0.3 \pm 0.8)^\circ$ [7,78]. By using these values for $\mathrm{Re}(A_2)/\mathrm{Re}(A_0)$, $|\eta_{+-}|$ and $(\phi_{00} - \phi_{+-})$ we obtain from Eq. (93)

$$0.002 \times \frac{\mathrm{Re}(B_2)}{\mathrm{Re}(A_2)} + \frac{\mathrm{Re}(B_0)}{\mathrm{Re}(A_0)} = (2.6 \pm 2.9) \times 10^{-4} \ ,$$

and from Eq. (94)

$$\frac{\mathrm{Re}(B_2)}{\mathrm{Re}(A_2)} - \frac{\mathrm{Re}(B_0)}{\mathrm{Re}(A_0)} = (-1.3 \pm 3.4) \times 10^{-4} \ ;$$

hence,

$$\frac{\mathrm{Re}(B_0)}{\mathrm{Re}(A_0)} = (2.6 \pm 2.9) \times 10^{-4}, \quad \frac{\mathrm{Re}(B_2)}{\mathrm{Re}(A_2)} = (1.3 \pm 4.5) \times 10^{-4} \ . \tag{95}$$

In conclusion, without any assumption, the $\mathrm{K}^0 - \bar{\mathrm{K}}^0$ mass and decay-width differences were shown to be consistent with $\mathscr{CPT}$ invariance within a few $10^{-18}$ GeV. This determination is based on the measurement of $\mathrm{Im}(\delta)$ and $\mathrm{Re}(\delta)$. The value of $\mathrm{Im}(\delta)$ results from a variety of measurements for pionic and semileptonic decay channels, many of which are from CPLEAR, while the value of $\mathrm{Re}(\delta)$ results essentially from the CPLEAR measurement of semileptonic decay-rate asymmetries [13]. In addition to the mass difference between $\mathrm{K}^0$ and $\bar{\mathrm{K}}^0$, owing to the $\mathrm{Re}(\delta)$ measurement, we are also able to evaluate for the first time the decay-width difference, and subsequently analyse it in terms of individual $\mathscr{CPT}$-violating decay amplitudes. The measurement of the decay-width difference relies mainly on the CPLEAR measurements of the semileptonic decay rates and the parameter $\mathrm{Re}(\delta)$ [13], also allowing possible cancellation effects to be disentangled. The ratio between $\mathscr{CPT}$-violating and $\mathscr{CPT}$-invariant amplitudes is shown to be smaller than a few times $10^{-3}$–$10^{-4}$ for a number of cases.

## 9. Measurements related to basic principles

### 9.1. Probing a possible loss of QM coherence [31]

The phenomenological framework of Section 2 is constructed, according to the QM of a closed system, on solutions of Eq. (5) which are pure states and evolve as such in time. Some approaches to quantum gravity [142] suggest that topologically non-trivial space–time fluctuations (space–time foam) entail an intrinsic, fundamental information loss, and therefore transitions from pure to mixed states [143]. The $\mathrm{K}^0 - \bar{\mathrm{K}}^0$ system is then described by a $2 \times 2$ density matrix $\rho$, which obeys

$$\dot{\rho} = -\mathrm{i}[\Lambda\rho - \rho\Lambda^\dagger] + \delta\Lambda\rho \ , \tag{96}$$

where $\Lambda$ is the $2 \times 2$ matrix of Eq. (6a), and the term $\delta\Lambda\rho$ induces a loss of quantum coherence in the observed system. In this context, the time evolution of the $\mathrm{K}^0 - \bar{\mathrm{K}}^0$ system allows for another nine parameters, in addition to the usual seven. Their measurability has been studied in Ref. [144]. Theoretical restrictions (in addition to those considered in Ref. [143]) on possible parameter values, based on the requirement that the solutions of Eq. (96) must *everywhere* result in positive probabilities, have been derived by the authors of Ref. [145]. They also point out the possibility to use the neutral-kaon system to test *complete positivity* of dynamical maps.

Here, we report the results obtained by CPLEAR [31] some time ago, with a partial statistics, for the parameters $\alpha$, $\beta$ and $\gamma$ (the six others were assumed to be zero). If different from zero, $\alpha$, $\beta$ and $\gamma$ would point to a loss of coherence of the wave function (and also to $\mathscr{CPT}$ violation). The decay-rate asymmetries [31] were fitted to data from the $\pi^+\pi^-$ and $\mathrm{e}\pi\nu$ decay channels, with the constraint of $|\eta_{+-}|$ and $\delta_\ell$ measured at long lifetimes [78], see Fig. 45. We obtained, as 90% CL limits, $\alpha < 4.0 \times 10^{-17}$ GeV, $\beta < 2.3 \times 10^{-19}$ GeV and $\gamma < 3.7 \times 10^{-21}$ GeV, to be compared with a possible order of magnitude of $\mathcal{O}(m_{\mathrm{K}}^2/m_{\mathrm{Planck}}) = 2 \times 10^{-20}$ GeV for such effects. An analysis of CPLEAR data based on Ref. [145], with six decoherence parameters, has been presented in Ref. [146].

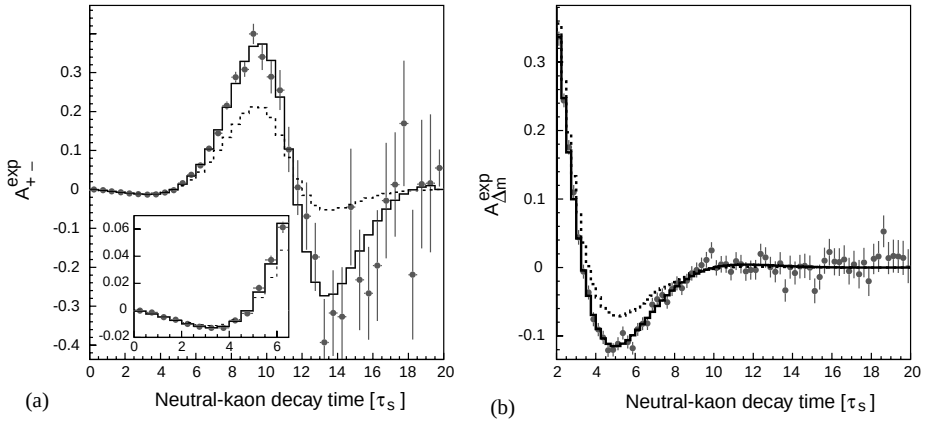


Fig. 45. The measured decay-rate asymmetries (partial statistics) (a) $A^{exp}_{\pm}$ (Section 4.1) and (b) $A^{exp}_{\Delta m}$ (Section 5.1) analysed to search for a possible loss of coherence of the neutral-kaon wave function. The solid lines are the result of our fit. The dashed lines represent the expected asymmetries with positive values of $\alpha$, $\beta$, $\gamma$, which are 10 times larger than the limits obtained.

### 9.2. *Testing the non-separability of the* $K^0\bar{K}^0$ *wave function [25]*

For this measurement, we selected pairs of $K^0\bar{K}^0$ produced, with a branching ratio of 0.07%, in the annihilation channel:

$$\bar{p}p \to K^0\bar{K}^0 \ . \tag{97}$$

The strangeness of the two neutral kaons is the analogous of the polarization in a two-photon system, more commonly used in EPR-type experiments. As a result of $K^0 - \bar{K}^0$ oscillations the individual strangeness is time-dependent. An EPR effect means that the measurement of the strangeness of one kaon at a given time predicts with certainty the strangeness state of the other unmeasured kaon at the same time. The two kaons, which have opposite strangeness when produced in (97), cannot appear in identical strangeness states at any equal proper times. The expected QM correlation for like- and unlike-strangeness final states $a$ and $b$, observed at times $t_a$ and $t_b$ respectively, is shown in Fig. 46a for the case of a $K^0\bar{K}^0$ pair with $J^{PC} = 1^{--}$ (93% of the cases [19]).

For this test, the strangeness was monitored by strong interaction in two absorbers near the target, see Fig. 46b, via the observation in the same event, at two different times, of a $\Lambda$ and a $K^+$ (unlike strangeness) or a $\Lambda$ and a $K^-$ or two $\Lambda$ (like strangeness).

The asymmetries of the yields for unlike- and like-strangeness events ($\Lambda K^+$ and $\Lambda K^-$) were measured for two experimental configurations C(0) and C(5), see Fig. 47a, corresponding to $\approx 0$ and 1.2 $\tau_S$ proper time differences between the two strangeness measurements, or path differences $|\Delta\ell|$ of $\approx 0$ and 5 cm. As shown in Fig. 47b, these asymmetries are consistent with the values predicted from QM, and therefore consistent with the non-separability hypothesis of the $K^0\bar{K}^0$ wave function. The non-separability hypothesis is also strongly favoured by the yield of $\Lambda\Lambda$ events. The probability of satisfying the separability hypothesis of Furry [147] is $< 10^{-4}$.

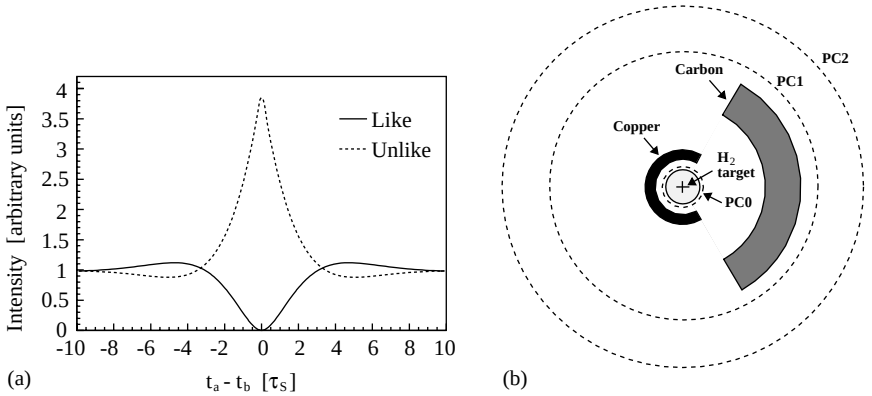


Fig. 46. (a) QM correlation for $J^{PC} = 1^{--}$ states; (b) expanded central region of the detector.

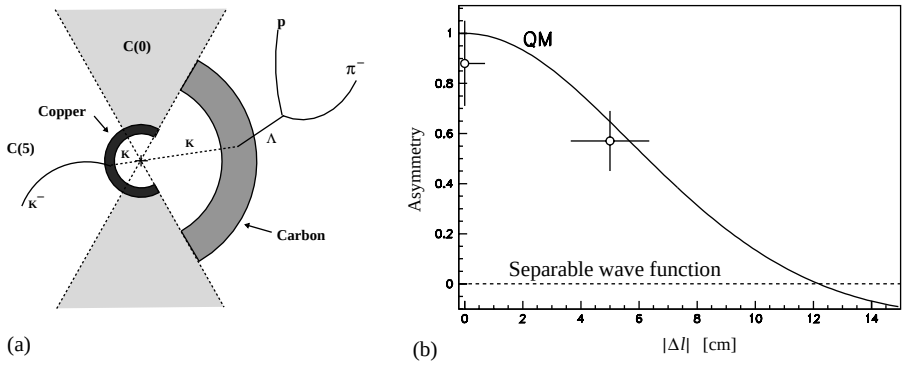


Fig. 47. (a) Conceptual sketch of the experiment (see text); (b) asymmetry of the measured $\Lambda K^{\pm}$ yields after background subtraction. The two points show the long distance correlation of the entangled kaons, in agreement with QM.

### 9.3. Test of the equivalence principle [32]

By considering the variations of the fitted values of $\phi_{+-}$ and $|\eta_{+-}|$ with the gravitational potential acting on the neutral kaons, CPLEAR has also made stringent tests of the equivalence principle for particles and antiparticles [32]. For the first time we searched for possible annual, monthly and diurnal modulations of the observables $\phi_{+-}$ and $|\eta_{+-}|$ that could be correlated with variations in astrophysical potentials. No such correlations were found within the CPLEAR accuracy. Data were analysed assuming effective scalar, vector and tensor interactions, and we concluded that the principle of equivalence between particles and antiparticles holds to a level of $(6.5, 4.3, 1.8) \times 10^{-9}$, respectively, for scalar, vector and tensor potential originating from the Sun with a range much greater than the Earth–Sun distance. Fig. 48 shows a compilation of the upper limits on $|g - \bar{g}|_J$, the gravitational coupling difference between $K^0$ and $\bar{K}^0$, as a function of the interaction range $r_J$ where $J = 0, 1, 2$ for scalar, vector and tensor potential, respectively.

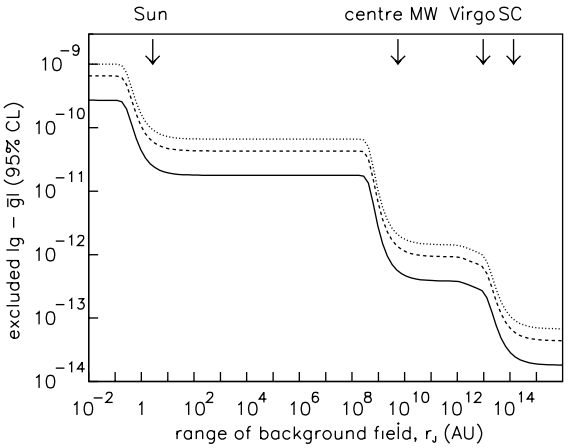


Fig. 48. Limits on the gravitational coupling difference between $K^0$ and $\bar{K}^0$, $|g-\bar{g}|_J$, obtained from the measured $K^0-\bar{K}^0$ mass difference as a function of the effective interaction range $r_J$, with $J=0,1,2$ for scalar, vector and tensor potential, respectively. Labels along the top indicate the distances to several astronomical bodies (Milky Way: MW, Shapley super-cluster: SC) measured in Astronomical Units (AU). The curves are upper limits shown separately for tensor (solid line), vector (dashed line) and scalar (dotted line) interactions.

## 10. Measurements related to the $\bar{p}p$ annihilation process

In general the cuts imposed by the trigger selection prevented, despite very high statistics, the precise study of the annihilation processes such as to bring a significant contribution to this field, nor was this necessary to achieve the main aim of the experiment. The annihilation study was limited to correct modelling of the simulation for the $K^0$ and $\bar{K}^0$ source and the annihilation sources of background. Nevertheless, new results were achieved by the measurement of the fraction of P-wave annihilation, $f_P$, for a hydrogen density not yet studied, and by the search of possible Bose–Einstein (BE) correlations within the four-pion and five-pion final states of the annihilation process.

### *10.1. Measurement of the fraction of P-wave annihilation [19]*

There were three measurements, two of which [17,18] used minimum-bias data taken for calibration purposes, and a third one a special trigger with no charged particle coming out of the target (PC0 in veto), and at least two charged tracks detected by the tracking device [19]. The results were branching ratios for some of the annihilation channels, or their ratio, and from these we extracted $f_P$. This quantity, which had been measured previously either for liquid or gaseous targets at normal pressure and temperature (or lower pressure), is known to depend on the target density because of the Stark effect favouring atomic S states at higher densities [148]. The values of $f_P$ obtained with minimum-bias data depend on external measurements, in contrast to the third measurement discussed below.

The reaction $\bar{p}p \to K_SK_S$ at rest occurs through the $^3P_0(J^{PC}=0^{++})$ and $^3P_2(J^{PC}=2^{++})$ initial states while the reaction $\bar{p}p \to K_SK_L$ at rest occurs only through the $^3S_1(J^{PC}=1^{--})$ state. The ratio $R=BR(\bar{p}p \to K_SK_S)/BR(\bar{p}p \to K_SK_L)$ therefore provides a measurement of the P- to S-wave relative

abundance. Two values were obtained: $R(27\text{ bar}) = 0.037 \pm 0.002$, and $R(15\text{ bar}) = 0.041 \pm 0.009$, from which we deduced $f_P = 0.45 \pm 0.06$ [19]. The measurement at 27 bar was essential for the analysis of the EPR experiment, see Section 9.2.

### *10.2. Search for Bose–Einstein correlations [20–22]*

Multipion systems are frequent results of $\bar{p}p$ annihilations. As any emission amplitude for identical bosons must be symmetrized, observable correlation effects can be expected for a pair of equal-charge pions if their momenta are equal, i.e. for vanishing relative momentum. Bose–Einstein (BE) correlations is the name often assigned to a very specific dynamic picture—the Hanbury-Brown–Twiss (HBT) mechanism [149]—linking the two-pion correlation function at small relative momentum to the space–time properties of the pion-emitting source, in particular its size [150–152].

At first interesting deviations from the stochastic HBT picture of BE correlations were observed in nucleon–antinucleon annihilation at rest; they are summarized in Ref. [20] together with the results of a first CPLEAR analysis performed on charged four-pion final states with criteria equivalent to those of previous analyses.

In a second approach a two-dimensional analysis for well defined pionic final states was performed. The phase-space factor was removed and the square of the amplitude for pion-pair emission was directly determined. The corresponding correlation functions were studied under kinematically controlled conditions and the distributions obtained confirmed that equal-charge two-pion correlations indeed peak at small relative momenta (or small invariant mass) [21]. However, the analysis performed on the five-pion channel [22] gave evidence that a fair amount of the observed correlation enhancement may be due to conventional resonance production amplitudes, rather than to BE effects. In order to clarify these topics more data and further investigations were required, both beyond the scope of CPLEAR.

## 11. Overview and conclusions

The CPLEAR experiment has performed studies of particle–antiparticle properties through a direct comparison of $K^0$ and $\bar{K}^0$ time evolutions. The use of $\bar{p}p$-annihilation channels $\bar{p}p \to K^{\mp}\pi^{\pm}K^0$ and $\bar{p}p \to K^{\pm}\pi^{\mp}\bar{K}^0$ and the detection of the charged particles, $K^{\mp}$ and $\pi^{\mp}$, has allowed the identification of the produced neutral kaon as a $K^0$ or as a $\bar{K}^0$ (strangeness tagging). This method has become practical due to the availabilty of intense beams of slow antiprotons. It implies furthermost detecting the low energy particles of the production and decay channels within a solid angle of $4\pi$, and in the presence of a large background.

Despite the abundant data already available on the neutral-kaon system and its symmetries, CPLEAR has improved significantly the knowledge of many of the parameters describing this system and possible violations of the symmetries.We have underlined in Sections 4.8 and 5.6 our contributions to the understanding of $\mathscr{CP}$, $\mathscr{T}$ and $\mathscr{CPT}$ symmetries in the neutral-kaon system. Appendix C contains a summary of selected results obtained through CPLEAR measurements.

$\mathscr{CP}$ violation was investigated by comparing $K^0$ and $\bar{K}^0$ decay rates to a common final state which was a $\mathscr{CP}$ eigenstate ($\pi\pi$ or $\pi\pi\pi$).

CPLEAR has improved the accuracy on the real and imaginary parts of the parameter $\eta_{+-}$ describing $\mathscr{CP}$ violation in the case of decay to $\pi^+\pi^-$ . These quantities enter sensitively into indirect tests of $\mathscr{T}$ and $\mathscr{CPT}$ symmetries based on the Bell–Steinberger unitarity relation.

The background associated with neutral pions and the limited energy resolution of the CPLEAR electromagnetic calorimeter rendered the measurements of decays to final states such as $\pi^0\pi^0$ very hard. Although CPLEAR has not observed $\mathscr{CP}$ violation in the case of decay to $\pi\pi\pi$, it has improved the limits on the parameters $\eta_{+-0}$ and $\eta_{000}$ by large factors. This had a great impact on the evaluation of the Bell–Steinberger unitarity relation, and thus on the errors of $\mathrm{Re}(\varepsilon)$ and $\mathrm{Im}(\delta)$.

The CPLEAR highlights are the direct tests of $\mathscr{T}$ and $\mathscr{CPT}$ violations. Strangeness tagging the neutral kaons at decay time in semileptonic decays, in addition to strangeness tagging at production, CPLEAR, for the first time through a rate comparison, has measured $\mathscr{T}$ violation and thus demonstrated that $\mathscr{CP}$ violation in mixing is related to $\mathscr{T}$ violation. Also for the first time, CPLEAR has measured $\mathrm{Re}(\delta)$, thus allowing a $\mathscr{CPT}$ test without assumptions. The same measurement determined $\mathrm{Im}(\delta)$, however with less precision than the indirect measurement through the Bell–Steinberger unitarity relation.

The CPLEAR measurements, together with the measurements of $\phi_{+-} - \phi_{00}$ and $\tau_S$ by other experiments, have provided sensitive tests on $\mathscr{CPT}$. In particular, by evaluating the Bell–Steinberger unitarity relation and by using it as a constraint in the semileptonic asymmetry fits, mass and decay-width differences of $K^0$ and $\bar{K}^0$ are compatible with zero and have errors of $2 \times 10^{-18}$ and $4.2 \times 10^{-18}$ GeV, respectively, without any assumption (e.g. on $\mathscr{CPT}$ invariance in decay). The parameters describing $\mathscr{CPT}$ violation in the decays to $\pi^+\pi^-$ and to $e\pi\nu$ were also determined (some by direct measurement as well).

The $K_L - K_S$ mass difference $\Delta m$ was measured with three methods, with different systematic and statistical errors. The results agree within the errors, thus probing the overall consistency of the experiment. Using $e\pi\nu$ decays the error is the smallest currently obtained for a $\Delta m$ single measurement.

The difference between the $K^0$ and $\bar{K}^0$ forward-scattering amplitudes in carbon was measured for the first time in such a low momentum range.

As a bonus, valuable measurements related to $\mathscr{CP}$-invariant neutral-kaon decays were performed (Dalitz-plot parameters and slope of the $K^0_{e3}$ form-factor).

Basic topics in quantum mechanics were investigated with success in relation to possible losses of coherence of the wave function, on the one hand with a dedicated analysis of our $\pi^+\pi^-$ and $e\pi\nu$ data samples, and on the other with a dedicated measurement.

It was often mentioned in the past that the $K^0 - \bar{K}^0$ system is a most convenient laboratory for the study of discrete symmetries. With the CPLEAR experiment we have made a full tour of this laboratory, and fully profited of the opportunities offered.

## Acknowledgements

This report is based on the work of the CPLEAR Collaboration: it recalls the measurements performed but also the ideas which took shape in many discussions. We are indebted to the many colleagues who successively contributed to the experiment.

We would like to thank the CERN LEAR staff for their support and co-operation, as well as the technical and engineering staff of our institutes. This work was supported by the following agencies: the French CNRS/Institut National de Physique Nucléaire et de Physique des Particules et Université de la Méditerranée, the French Commissariat à l'Energie Atomique, the Greek General Secretariat of Research and Technology, the Netherlands Foundation for Fundamental Research on Matter (FOM), the Portuguese National Board for Science and Technology (JNICT), the Ministry of Science and Technology of the Republic of Slovenia, the Swedish Natural Science Research Council, the Swiss National Science Foundation, the UK Particle Physics and Astronomy Research Council (PPARC), and the US National Science Foundation.

## Appendix A. Neutral-kaon system: some milestones

From the start the CPLEAR experiment was conceived to obtain as complete and precise a survey of the neutral-kaon system as possible. This gave us the chance to revisit with modern eyes the path taken since the histories of discrete symmetries and kaons became intertwined [33]. Thus, we like to recall here a few points which help to frame the present report and make clear, in the CPLEAR perspective, how CPLEAR built on past research.

- 1947: Two unusual events, a fork and a track making a marked angle, were observed in a cloud chamber exposed to cosmic rays [34]. For both events the mass was near 400 MeV. They were referred to as V-particles; the fork was most probably the first record of a neutral kaon decaying to two pions.
- 1953: Particles with a mass between the pion and the proton were named K mesons [35]. These mesons seemed to have very similar mean lives; moreover, two of the best known—the charged $\tau$ and the neutral $\theta$, decaying to three and two pions, respectively—had equal masses within 0.5 MeV: *It was difficult to believe that this was an accident…* [35]. The way was paved to a critical examination of the symmetries observed in particle physics.
- 1953: For the first time two V-particles were seen at an accelerator [36].
- 1953: The new particles were classified [37,38] in terms of isospin in an attempt to explain the large production cross-section of V-particles ($\approx 1\%$ of the pions) while their decays seemed to be suppressed by some selection rules: $(\mathrm{K}^+, \mathrm{K}^0)$ and $(\bar{\mathrm{K}}^0, \mathrm{K}^-)$ are doublets of isospin $I = 1/2$ with $I_3 = 1/2, -1/2$. Strong and electromagnetic interactions conserve isospin, but weak interactions do not, and in some decays $|\Delta I| = 1/2$. Within this context the idea of two neutral kaons, one being the antiparticle of the other, emerged.
- 1954: Gell-Mann and Pais, under the hypothesis of $\mathscr{C}$ conservation, consider $\mathrm{K}^0$ and $\bar{\mathrm{K}}^0$ to be mixtures of particles with definite mean lives [4]. Different proposals are put forward to distinguish $\mathrm{K}^0$ from $\bar{\mathrm{K}}^0$ experimentally [5,39,40]. In Ref. [39] the decaying particles are treated in much the same way as Weisskopf and Wigner had treated unstable nuclei and their line widths [41].
- 1955: Gell-Mann [37] and Nishijima [38] independently suggest that for the new particles the charge $Q$ is related to the third component of the isospin $I_3$ and to the baryon number $B$ by $Q = I_3 + S/2 + B/2$ where $S$ (strangeness) is a new quantum number to be conserved in strong and electromagnetic interactions, whereas $|\Delta S| = 1$ interactions are weak interactions. The invariance of these with respect to the $\mathscr{C}$ and $\mathscr{P}$ symmetries has not been contested yet.

- 1956: Lee and Yang publish their seminal paper on $\mathscr{P}$ non-conservation [42]. The experiments are quick to establish in January 1957 that $\mathscr{P}$ and $\mathscr{C}$ are violated in weak interactions; $\mathscr{CP}$, however, seems to hold [43–45]. Independently, Landau considers the possibility that 'combined parity' may not be conserved [46], and Lee et al. make a number of *Remarks on possible non-invariance under time reversal and charge conjugation* [47]. $\mathscr{CPT}$ symmetry is still considered untouchable [48].
- 1964: Cronin et al. demonstrate experimentally the breaking of $\mathscr{CP}$ invariance [50]. Soon afterwards, Wu and Yang [51] perform a phenomenological analysis of $\mathscr{CP}$ violation in the decay of $K^0$ and $\bar{K}^0$, including decay amplitudes and the unitarity concept, but assuming $\mathscr{CPT}$ symmetry. They introduce the phenomenological parameters $\eta_{+-} = \varepsilon + \varepsilon'$, $\eta_{00} = \varepsilon - 2\varepsilon'$, $\varepsilon = (p - q)/p$, and take into account $x$, the parameter describing the violation of the $\Delta S = \Delta Q$ rule. They consider four ways for violating $\mathscr{CP}$ (or $\mathscr{T}$): by interference of the main $\pi\pi$ decay mode ($I = 0$) with the $\pi\pi$ ($I = 2$) mode, the lepton mode, the $3\pi$ mode and/or the off-energy shell contributions to $K^0 - \bar{K}^0$ elements of the mass operator.
- 1965: Bell and Steinberger present relations based on unitarity which connect the decay amplitudes with the decrease of the kaon probability [52].
- Late 1965: Enz and Lewis give a phenomenological framework which is the first to contain in nuce the CPLEAR method [53].
- 1967: Sakharov suggests that at the very early times of our Universe matter transformed into antimatter and vice versa (barring baryon-number violation), and this process was not symmetric ($\mathscr{CP}$ violation), which accounts for the survival of matter over antimatter [54]. (At the time of the Big Bang matter and antimatter are supposed to be present in equal amounts, and to annihilate. As a consequence, the Universe would consist of photons, with only one proton in $10^{18}$ photons, that is about one billion times fewer protons than otherwise measured.)
- Within the next 10 years the experimental scenario was fixed, as summarized in the Nobel talks of 1980 [55]. In the same period, particle interactions were shown to preserve, or to break, other kinds of symmetry, which eventually led to the Standard Model.
- In the 1980s, while $\mathscr{CP}$ violation could be accommodated within the Standard Model and the known interactions [56–59], two main topics required further experimental work: the so-called *direct* $\mathscr{CP}$ violation [58] and $\mathscr{CPT}$ violation [60]. The CPLEAR programme [1] was set up in this context. It took advantage of the inception of the Low-Energy Antiproton Ring (LEAR) at CERN, a facility [2] particularly suitable to study the symmetries between matter and antimatter.

## Appendix B. CPLEAR and the Standard Model

For completeness we sketch in Fig. 49 some of the diagrams which describe at the quark level the processes studied by CPLEAR: they involve $|\Delta S| = 2$ transitions as in (a), and $|\Delta S| = 1$ transitions, as in (b)–(d). The evaluation of the parameters measured by CPLEAR in terms of these diagrams seems to be a difficult task. Whether it is at all possible conceptually is sometimes questioned [65], although in some cases one finds numerical agreement with the experimental results. We note, however, that the current form of the Standard Model excludes any $\mathscr{CPT}$ violation. Thus, $\mathscr{CPT}$ tests are also tests of the Standard Model.

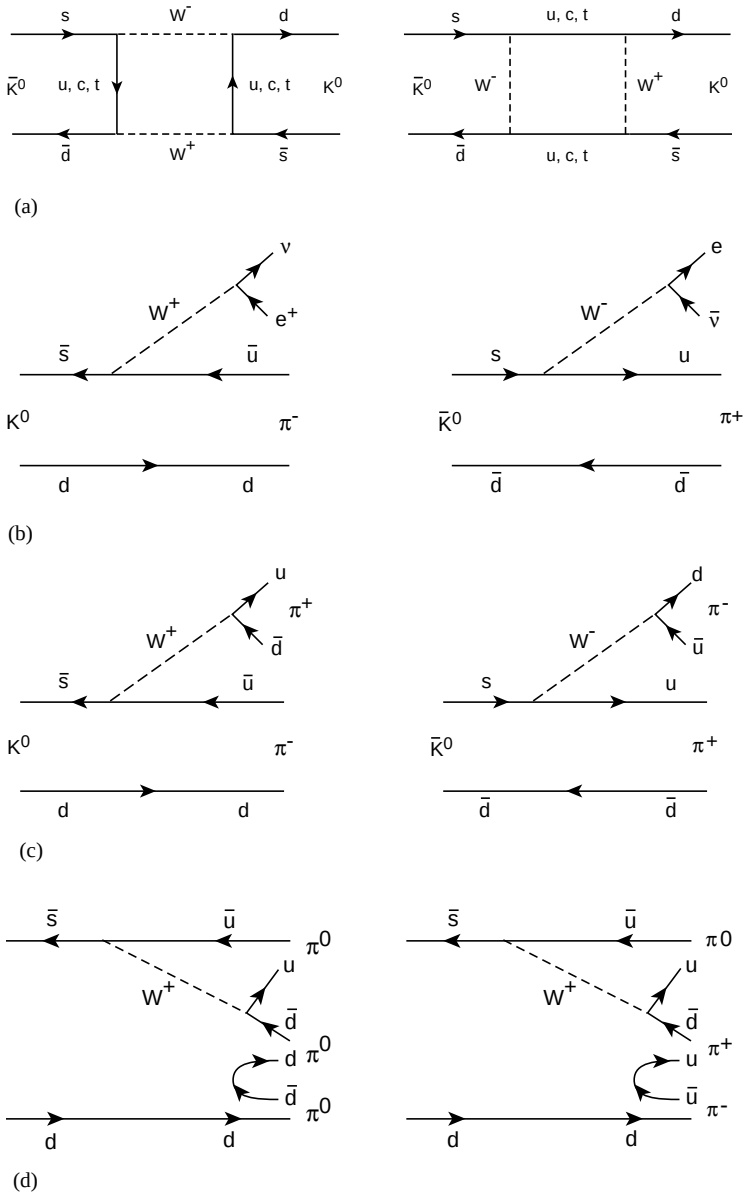


Fig. 49. The diagrams which describe (a) the oscillation $K^0 \leftrightharpoons \bar{K}^0$ and enter $\Delta m$ and $\varepsilon$ computations; (b) decays to $e\pi\nu$ and the $\Delta S = \Delta Q$ rule; (c) decays to $\pi^+\pi^-$; (d) decays to $\pi^0\pi^0\pi^0$ (left) and $\pi^+\pi^-\pi^0$ (right).

## Appendix C. Selected CPLEAR results

• $\mathscr{CP}$ violation

$K^0 \to \pi^+\pi^-$ Phys. Lett. B 458 (1999) 545

| | | |
|---|---|---|
| $\lvert\eta_{+-}\rvert = (2.264 \pm 0.023_{\text{stat}} \pm 0.026_{\text{syst}} \pm 0.007_{\tau_S}) \times 10^{-3}$ | | |
| $\phi_{+-} = 43.19^\circ \pm 0.53^\circ_{\text{stat}} \pm 0.28^\circ_{\text{syst}} \pm 0.42^\circ_{\Delta m}$ | | |
| $K^0 \to \pi^0\pi^0$ | | Phys. Lett. B 420 (1998) 191 |
| $\lvert\eta_{00}\rvert = (2.47 \pm 0.31_{\text{stat}} \pm 0.24_{\text{syst}}) \times 10^{-3}$ | | |
| $\phi_{00} = 42.0^\circ \pm 5.6^\circ_{\text{stat}} \pm 1.9^\circ_{\text{syst}}$ | | |
| $K^0 \to \pi^+\pi^-\pi^0$ | | Eur. Phys. J C5 (1998) 191 |
| $\text{Re}(\eta_{+-0}) = (-2 \pm 7_{\text{stat}}{}^{+4}_{-1\ \text{syst}}) \times 10^{-3}$ | | |
| $\text{Im}(\eta_{+-0}) = (-2 \pm 9_{\text{stat}}{}^{+2}_{-1\ \text{syst}}) \times 10^{-3}$ | | |
| $K^0 \to \pi^0\pi^0\pi^0$ | | Phys. Lett. B 425 (1998) 391 |
| $\text{Re}(\eta_{000}) = 0.18 \pm 0.14_{\text{stat}} \pm 0.06_{\text{syst}}$ | | |
| $\text{Im}(\eta_{000}) = 0.15 \pm 0.20_{\text{stat}} \pm 0.03_{\text{syst}}$ | | |
| • $\mathscr{T}$ violation | | |
| $\langle A_T^{\text{exp}} \rangle = (6.6 \pm 1.3_{\text{stat}} \pm 1.0_{\text{syst}}) \times 10^{-3}$ | | Phys. Lett. B 444 (1998) 43 |
| $\text{Re}(\varepsilon) = (1.65 \pm 0.33_{\text{stat}} \pm 0.25_{\text{syst}}) \times 10^{-3}$ | (direct) | Phys. Lett. B 444 (1998) 43 |
| $\text{Re}(\varepsilon) = (1.649 \pm 0.025) \times 10^{-3}$ | (unitarity) | Phys. Lett. B 456 (1999) 297 |
| • $\mathscr{CPT}$ symmetry | | |
| $\text{Re}(\delta) = (3.0 \pm 3.3_{\text{stat}} \pm 0.6_{\text{syst}}) \times 10^{-4}$ | (direct) | Phys. Lett. B 444 (1998) 52 |
| $\text{Im}(\delta) = (-1.5 \pm 2.3_{\text{stat}} \pm 0.3_{\text{syst}}) \times 10^{-2}$ | (direct) | Phys. Lett. B 444 (1998) 52 |
| $\text{Im}(\delta) = (2.4 \pm 5.0) \times 10^{-5}$ | (unitarity) | Phys. Lett. B 456 (1999) 297 |
| $M_{K^0K^0} - M_{\bar{K}^0\bar{K}^0} = (-1.5 \pm 2.0) \times 10^{-18}$ GeV | | Phys. Lett. B 471 (1999) 332 |
| $\Gamma_{K^0K^0} - \Gamma_{\bar{K}^0\bar{K}^0} = (3.9 \pm 4.2) \times 10^{-18}$ GeV | | Phys. Lett. B 471 (1999) 332 |
| • Other parameters of the neutral-kaon system | | |
| $\Delta m = (529.5 \pm 2.0_{\text{stat}} \pm 0.3_{\text{syst}}) \times 10^7 \hbar/\text{s}$ | | Phys. Lett. B 444 (1998) 38 |
| $\Delta m$ sign | | This report |
| $\text{Re}(x) = (-1.8 \pm 4.1_{\text{stat}} \pm 4.5_{\text{syst}}) \times 10^{-3}$ | | Phys. Lett. B 444 (1998) 38 |
| $\text{Im}(x) = (1.2 \pm 1.9_{\text{stat}} \pm 0.9_{\text{syst}}) \times 10^{-3}$ | | Phys. Lett. B 444 (1998) 43 |
| $\text{Re}(x_-) = (0.2 \pm 1.3_{\text{stat}} \pm 0.3_{\text{syst}}) \times 10^{-2}$ | | Phys. Lett. B 444 (1998) 52 |
| $\text{Im}(x_+) = (1.2 \pm 2.2_{\text{stat}} \pm 0.3_{\text{syst}}) \times 10^{-2}$ | | Phys. Lett. B 444 (1998) 52 |
| $\text{BR}(K_S \to \pi^+\pi^-\pi^0) = (2.5^{+1.3}_{-1.0\text{stat}}{}^{+0.5}_{-0.6\ \text{syst}}) \times 10^{-7}$ | | Phys. Lett. B 407 (1997) 193 |
| $\text{BR}(K_S \to e^+e^-) < 1.4 \times 10^{-7}$ | | Phys. Lett. B 413 (1997) 232 |
| Kaon scattering amplitudes in carbon (regeneration) | | Phys. Lett. B 413 (1997) 422 |
| • Other tests of fundamental physics | | |
| Test of quantum mechanics coherence | | Phys. Lett. B 364 (1995) 239 |
| EPR test with $\bar{p}p \to K^0\bar{K}^0$ | | Phys. Lett. B 422 (1998) 339 |
| Test of equivalence principle | | Phys. Lett. B 452 (1999) 425 |
| • $\bar{p}p$ annihilation | | |
| Bose–Einstein correlations | | Eur. Phys. J C6 (1999) 437 |
| P-wave annihilation | | Phys. Lett. B 403 (1997) 383 |

## References


[1] E. Gabathuler, P. Pavlopoulos, Strong and Weak CP violation at LEAR, in: U. Gastaldi, R. Klapisch (Eds.), Proceedings of the Workshop on Physics at LEAR with Low Energy Cooled Antiprotons, Erice, 1983, Plenum, New York, 1984, p. 747.

[2] S. Baird, et al., in: M. Comyn, et al. (Eds.), Proceedings of the 1997 Particle Accelerator Conference, Vancouver, IEEE, Piscataway, 1998, p. 982.

[3] R. Adler, et al., CPLEAR Collaboration, Nucl. Instr. Meth. A 379 (1996) 76.

[4] M. Gell-Mann, A. Pais, Phys. Rev. 97 (1955) 1387.

[5] A. Pais, O. Piccioni, Phys. Rev. 100 (1955) 1487.

[6] R. Adler, et al., CPLEAR Collaboration, Nucl. Instr. Meth. A 390 (1997) 293.

[7] A. Apostolakis, et al., CPLEAR Collaboration, A determination of the CP violation parameter $\eta_{+-}$ from the decay of strangeness-tagged neutral kaons, Phys. Lett. B 458 (1999) 545;
A. Apostolakis, et al., CPLEAR Collaboration, A detailed description of the analysis of the decay of neutral kaons to $\pi^+\pi^-$ in the CPLEAR experiment, Eur. Phys. J. C 18 (2000) 41.

[8] R. Adler, et al., CPLEAR Collaboration, Z. Phys. C 70 (1996) 211;
A. Angelopoulos, et al., CPLEAR Collaboration, Measurement of the $\mathscr{CP}$ violation parameter $\eta_{00}$ using tagged $\bar{K}^0$ and $K^0$, Phys. Lett. B 420 (1998) 191.

[9] R. Adler, et al., CPLEAR Collaboration, CPLEAR results on the CP parameters of neutral kaons decaying to $\pi^+\pi^-\pi^0$, Phys. Lett. B 407 (1997) 193;
A. Angelopoulos, et al., CPLEAR Collaboration, The neutral kaons decays to $\pi^+\pi^-\pi^0$: a detailed analysis of the CPLEAR data, Eur. Phys. J. C 5 (1998) 389.

[10] A. Angelopoulos, et al., CPLEAR Collaboration, Search for CP violation in the decay of tagged $\bar{K}^0$ and $K^0$ to $\pi^0\pi^0\pi^0$, Phys. Lett. B 425 (1998) 391.

[11] A. Angelopoulos, et al., CPLEAR Collaboration, Measurement of the $K_L - K_S$ mass difference using semileptonic decays of tagged neutral kaons, Phys. Lett. B 444 (1998) 38.

[12] A. Angelopoulos, et al., CPLEAR Collaboration, First direct observation of time-reversal non-invariance in the neutral-kaon system, Phys. Lett. B 444 (1998) 43.

[13] A. Angelopoulos, et al., CPLEAR Collaboration, A determination of the CPT violation parameter Re($\delta$) from the semileptonic decay of strangeness-tagged neutral kaons, Phys. Lett. B 444 (1998) 52.

[14] A. Angelopoulos, et al., CPLEAR Collaboration, $\mathscr{T}$-violation and $\mathscr{CPT}$-invariance measurements in the CPLEAR experiment: a detailed description of the analysis of neutral-kaon decays to e$\pi\nu$, Eur. Phys. J. C 22 (2001) 55.

[15] A. Apostolakis, et al., CPLEAR Collaboration, Measurement of the energy dependence of the form factor $f_+$ in $K^0_{e3}$, decay, Phys. Lett. B 473 (2000) 186.

[16] A. Angelopoulos, et al., CPLEAR Collaboration, An upper limit for the branching ratio of the decay $K_S \to e^+e^-$, Phys. Lett. B 413 (1997) 232.

[17] R. Adler, et al., CPLEAR Collaboration, Determination of the relative branching ratios for $\bar{p}p \to \pi^+\pi^-$ and $\bar{p}p \to K^+K^-$, Phys. Lett. B 267 (1991) 154.

[18] R. Adler, et al., CPLEAR Collaboration, Inclusive measurement of $\bar{p}p$ annihilation at rest in gaseous hydrogen to final states containing $\rho$ and $f_2$, Z. Phys. C 65 (1995) 199.

[19] R. Adler, et al., CPLEAR Collaboration, Experimental measurement of the $K_SK_S/K_SK_L$ ratio in antiproton annihilations at rest in gaseous hydrogen at 15 and 27 bar, Phys. Lett. B 403 (1997) 383.

[20] R. Adler, et al., CPLEAR Collaboration, Bose–Einstein correlations in antiproton–proton annihilations at rest, Z. Phys. C 63 (1994) 541.

[21] A. Angelopoulos, et al., CPLEAR Collaboration, M.P. Locher, V.E. Markushin, Direct determination of two-pion correlations for $\bar{p}p \to 2\pi^+2\pi^-$ annihilation at rest, Eur. Phys. J. C 1 (1998) 139.

[22] A. Apostolakis, et al., CPLEAR Collaboration, M.P. Locher, V.E. Markushin, Pion correlations and resonance effects in $\bar{p}p$ annihilation at rest to $2\pi^+2\pi^-\pi^0$, Eur. Phys. J. C 6 (1999) 437.

[23] W. Fetscher, et al., Regeneration of arbitrary coherent neutral kaon states: a new method for measuring the $K^0 - \bar{K}^0$ forward scattering amplitude, Z. Phys. C 72 (1996) 543.

[24] A. Angelopoulos, et al., CPLEAR Collaboration, Measurement of neutral kaon regeneration amplitudes in carbon at momenta below 1 GeV/c, Phys. Lett. B 413 (1997) 422.

[25] A. Apostolakis, et al., CPLEAR Collaboration, An EPR experiment testing the non-separability of the $\bar{K}^0K^0$ wave function, Phys. Lett. B 422 (1998) 339.
[26] A. Angelopoulos, et al., CPLEAR Collaboration, $K^0 \rightleftharpoons \bar{K}^0$ transitions monitored by strong interactions: a new determination of the $K_L - K_S$ mass difference, Phys. Lett. B 503 (2001) 49.
[27] A. Angelopoulos, et al., CPLEAR Collaboration, Evaluation of the phase of the $\mathscr{CP}$-violation parameter $\eta_{+-}$ and the $K_L - K_S$ mass difference from a correlation analysis of different experiments, Phys. Lett. B 369 (1996) 367.
[28] A. Apostolakis, et al., CPLEAR Collaboration, Determination of the $\mathscr{T}$- and $\mathscr{CPT}$-violation parameters in the neutral-kaon system using the Bell–Steinberger relation and data from CPLEAR, Phys. Lett. B 456 (1999) 297.
[29] A. Angelopoulos, et al., CPLEAR Collaboration, $K^0 - \bar{K}^0$ mass and decay-width differences: CPLEAR evaluation, Phys. Lett. B 471 (1999) 332.
[30] A. Angelopoulos, et al., CPLEAR Collaboration, M.P. Locher, V.E. Markushin, Dispersion relation analysis of the neutral kaon regeneration amplitude in carbon, Eur. Phys. J. C 10 (1999) 19.
[31] R. Adler, et al., CPLEAR Collaboration, J. Ellis, N.E. Mavromatos, D.V. Nanopoulos, Tests of $\mathscr{CPT}$ symmetry and quantum mechanics with experimental data from CPLEAR, Phys. Lett. B 364 (1995) 239.
[32] A. Apostolakis, et al., CPLEAR Collaboration, J. Ellis, N.E. Mavromatos, D.V. Nanopoulos, Tests of the equivalence principle with neutral kaons, Phys. Lett. B 452 (1999) 425.
[33] A. Pais, Inward Bound, Clarendon Press, Oxford, 1986.
[34] G.D. Rochester, C.C. Butler, Nature (London) (1947) 855.
[35] Congrès sur le rayonnement cosmique, Bagnères-de-Bigorres, July 1953, Proceedings unpublished, quoted by Ref. [33].
[36] W.B. Fowler, et al., Phys. Rev. 90 (1953) 1126;
W.B. Fowler, et al., Phys. Rev. 91 (1953) 1287.
[37] M. Gell-Mann, Phys. Rev. 92 (1953) 833;
M. Gell-Mann, A. Pais, Proceedings of the International Conference Glasgow, 1954;
M. Gell-Mann, Proceedings of the International Conference, Pisa, 1955, Nuovo Cimento Supp. 4 (1956) 848.
[38] T. Nakano, K. Nishijima, Prog. Theor. Phys. 10 (1953) 581;
K. Nishijima, Prog. Theor. Phys. 13 (1955) 285.
[39] S.B. Treiman, R.G. Sachs, Phys. Rev. 103 (1956) 1545.
[40] E. Boldts, D.O. Caldwell, Y. Pal, Phys. Rev. Lett. 1 (1958) 150;
W.F. Fry, R.G. Sachs, Phys. Rev. 109 (1958) 2212.
[41] V.F. Weisskopf, E.P. Wigner, Z. Phys. 63 (1930) 54;
V.F. Weisskopf, E.P. Wigner, Z. Phys. 65 (1930) 18.
[42] T.D. Lee, C.N. Yang, Phys. Rev. 104 (1956) 254.
[43] C.S. Wu, E. Ambler, R.W. Hayward, D.D. Hopper, R.P. Hudson, Phys. Rev. 105 (1957) 1413.
[44] R.L. Garwin, L. Lederman, M. Weinreich, Phys. Rev. 105 (1957) 1415.
[45] J.I. Friedman, V.L. Telegdi, Phys. Rev. 105 (1957) 1681.
[46] L. Landau, Nucl. Phys. 3 (1957) 127.
[47] T.D. Lee, R. Oehme, C.N. Yang, Phys. Rev. 106 (1957) 340.
[48] J.S. Bell, Proc. Royal Soc. A 231 (1955) 479;
G.L. Lüders, Ann. Phys. 2 (1957) 1;
R. Jost, Helv. Phys. Acta 30 (1957) 409.
[49] R.P. Feynman, M. Gell-Mann, Phys. Rev. 109 (1958) 193.
[50] J.H. Christenson, J.W. Cronin, V.L. Fitch, R. Turlay, Phys. Rev. Lett. 13 (1964) 138.
[51] T.T. Wu, C.N. Yang, Phys. Rev. Lett. 13 (1964) 360.
[52] J.S. Bell, J. Steinberger, Weak interactions of kaons, in: R.G. Moorhouse, et al., (Eds.), Proceedings of the Oxford International Conference on Elementary Particles, Rutherford Laboratory, Chilton, 1965, p. 195.
[53] C.P. Enz, R.R. Lewis, Phys. Lett. 16 (1965) 72;
C.P. Enz, R.R. Lewis, Helv. Phys. Acta 38 (1965) 860.
[54] A.D. Sakharov, JETP 5 (1967) 24.
[55] V.L. Fitch, Rev. Mod. Phys. 53 (1981) 367;
J.W. Cronin, Rev. Mod. Phys. 53 (1981) 373.
[56] M. Kobayashi, T. Maskawa, Prog. Theor. Phys. 48 (1972) 199.

[57] J. Ellis, M.K. Gaillard, D.V. Nanopoulos, Nucl. Phys. B 109 (1976) 213.
[58] F.J. Gilman, M.B. Wise, Phys. Lett. B 83 (1979) 83.
[59] C. Jarlskog, Z. Phys. C 29 (1985) 481.
[60] V.V. Barmin, et al., Nucl. Phys. B 247 (1984) 283.
[61] P.K. Kabir, The CP Puzzle, Academic Press, London, 1968.
[62] T.D. Lee, Particle Physics and Introduction to Field Theory, Harwood, Chur, 1981.
[63] R.G. Sachs, The Physics of Time Reversal, University of Chicago Press, Chicago, 1987.
[64] O. Nachtmann, Elementary Particle Physics, Springer, Berlin, 1990.
[65] E. Leader, E. Predazzi, An Introduction to Gauge Theories and Modern Particle Physics, Vol. 2, Cambridge University Press, Cambridge, 1996.
[66] M. Skalsey et al. (Eds.) Time Reversal, Ann Arbor, 1991, AIP Conference Proceedings, Vol. 270, AIP, New York, 1993.
I.B. Khriplovich, S.K. Lamoreaux, CP Violation without Strangeness, Springer, Berlin, 1997.
[67] G. Castelo Branco, L. Lavoura, J.P. Silva, CP Violation, Clarendon Press, Oxford, 1999.
[68] I.I. Bigi, A.I. Sanda, CP Violation, Cambridge University Press, Cambridge, 2000.
[69] R. Jacob, R.G. Sachs, Phys. Rev. 121 (1961) 350;
R.G. Sachs, Ann. Phys. 22 (1963) 239.
[70] C.D. Buchanan, et al., Phys. Rev. D 45 (1992) 4088.
[71] L. Maiani, CP and CPT violation in neutral kaon decays, in: L. Maiani, et al. (Eds.), The Second DAΦNE Physics Handbook, INFN, Frascati, 1995, p. 3.
[72] P.K. Kabir, Phys. Rev. D 2 (1970) 540, see also:
A. Aharony, Lett. Nuovo Cimento 3 (1970) 791.
[73] L. Alvarez-Gaumé, et al., Phys. Lett. B 458 (1999) 347;
L. Alvarez-Gaumé et al., Direct $\mathscr{T}$-violation measurements and $\mathscr{T}$-odd effects in decay experiments, in: Proceedings of XXXIVth Rencontres de Moriond on Electroweak Interactions and Unified Theories, Les Arcs, 1999.
[74] L. Wolfenstein, Int. J. Mod. Phys. E 8 (1999) 501.
[75] L. Wolfenstein, Phys. Rev. Lett. 83 (1999) 911.
[76] C. Zemach, Phys. Rev. 133 (1964) 1201.
[77] W. Grimus, Fortschr. Phys. 36 (1988) 201.
[78] C. Caso, et al., Particle Data Group, Eur. Phys. J. C 3 (1998) 1.
[79] M.L. Good, Phys. Rev. 106 (1957) 591.
[80] K. Kleinknecht, Fortschr. Phys. 21 (1973) 57.
[81] P.H. Eberhard, F. Uchiyama, Nucl. Instr. Meth. A 350 (1994) 144.
[82] D. Banner, et al., Phys. Rev. D 7 (1973) 1989.
[83] F. Niebergall, et al., Phys. Lett. B 49 (1974) 103.
[84] Determination of the position accuracy in CPLEAR, Internal Note, CPLEAR/DET/96-03, October 1996.
[85] D.E. Groom, et al., Particle Data Group, Eur. Phys. J. C 15 (2000) 1.
[86] C. Geweniger, et al., Phys. Lett. B 48 (1974) 487.
[87] W.C. Carithers, et al., Phys. Rev. Lett. 34 (1975) 1244.
[88] R. Carosi, et al., Phys. Lett. B 237 (1990) 303.
[89] L.K. Gibbons, et al., E731, Phys. Rev. Lett. 70 (1993) 1199.
[90] B. Schwingenheuer, et al., E773, Phys. Rev. Lett. 74 (1995) 4376.
[91] J.H. Christenson, et al., Phys. Rev. Lett. 43 (1979) 1213.
[92] S.H. Aronson, et al., Phys. Rev. Lett. 48 (1982) 1306.
[93] D.P. Coupal, et al., Phys. Rev. Lett. 55 (1985) 566.
[94] For higher energy data on regeneration in carbon see: K.-F. Albrecht et al., Nucl. Phys. B 93 (1975) 237;
W.C. Carithers, et al., Phys. Rev. Lett. 34 (1975) 1240;
J. Roehrig, et al., Phys. Rev. Lett. 38 (1977) 1116.
[95] R. Baldini, A. Michetti, LNF-96/008(IR) (1996), unpublished.
[96] D.V. Bugg, et al., Phys. Rev. 168 (1968) 1466.
[97] R.A. Krauss, et al., Phys. Rev. C 46 (1992) 655;
see also R. Weiss, et al., Phys. Rev. C 49 (1994) 2569.

[98] W.A.W. Melhop, et al., Phys. Rev. 172 (1968) 1613.
[99] A. Engler, Prog. Nucl. Phys. 11 (1970) 271.
[100] D.G. Hill, et al., Phys. Rev. D 4 (1971) 7.
[101] O. Behnke, Ph.D. Thesis, ETH-IPP Zürich, Nr. 11969, 1996.
[102] J.C. Chollet, et al., Phys. Lett. B 31 (1970) 658 (values are quoted as in [85]).
[103] B. Wolff, et al., Phys. Lett. B 36 (1971) 368 (values are quoted as in [85]).
[104] J.H. Christenson, et al., Phys. Rev. Lett. 43 (1979) 1209.
[105] M. Woods, et al., E731, Phys. Rev. Lett. 60 (1988) 1695.
[106] L.K. Gibbons, et al., E731, Phys. Rev. Lett. 70 (1993) 1203.
[107] G. Barr, et al., NA31, Phys. Lett. B 317 (1993) 233.
[108] A. Lai, et al., NA48, Eur. Phys. J. C 22 (2001) 231.
[109] A. Alavi-Harati, et al., KTeV, presented at KAON-01, Pisa, June 2001;
see also A. Alavi-Harati, et al., Phys. Rev. Lett. 83 (1999) 22.
[110] V.V. Barmin, et al., Nuovo Cimento A 85 (1985) 67.
[111] Y. Zou, et al., Phys. Lett. B 329 (1994) 519.
[112] Y. Zou, et al., Phys. Lett. B 369 (1996) 362.
[113] T.J. Devlin, J.O. Dickey, Rev. Mod. Phys. 51 (1979) 237.
[114] L.-F. Li, L. Wolfenstein, Phys. Rev. D 21 (1980) 178.
[115] S. Fajfer, J.M. Gerard, Z. Phys. C 42 (1989) 425.
[116] H.-Y. Cheng, Phys. Lett. B 238 (1990) 399.
[117] J. Kambor, et al., Phys. Lett. B 261 (1991) 496.
[118] G. D'Ambrosio, et al., Phys. Rev. D 50 (1994) 5767;
G. D'Ambrosio, et al., Phys. Rev. D 51 (1995) 3975(E).
[119] V.V. Barmin, et al., Phys. Lett. B 128 (1983) 129.
[120] M.N. Achasov, et al., Phys. Lett. B 459 (1999) 674.
[121] S. Gjesdal, et al., Phys. Lett. B 52 (1974) 113.
[122] M. Cullen, et al., Phys. Lett. B 32 (1970) 523.
[123] C. Geweniger, et al., Phys. Lett. B 52 (1974) 108.
[124] S. Bennett, et al., Phys. Lett. B 29 (1969) 317;
Y. Cho, et al., Phys. Rev. D 1 (1970) 3031;
B.R. Webber, et al., Phys. Rev. D 3 (1971) 64;
G. Burgun, et al., Nucl. Phys. B 50 (1972) 194;
M.L. Mallary, et al., Phys. Rev. D 7 (1973) 1953;
J.C. Hart, et al., Nucl. Phys. B 66 (1973) 317;
O. Fackler, et al., Phys. Rev. Lett. 31 (1973) 847.
[125] V. Bisi, et al., Phys. Lett. B 36 (1971) 533;
R. Blumenthal, et al., Phys. Rev. Lett. 34 (1975) 164;
G. Gjesdal, et al., Nucl. Phys. B 109 (1976) 118;
D.G. Hill, et al., Phys. Lett. B 73 (1978) 483;
A. Engler, et al., Phys. Rev. D 18 (1978) 623;
V. Birulev, et al., Nucl. Phys. B 182 (1981) 1.
[126] P. Post, K. Schilcher, Eur. Phys. J. C 25 (2002) 427.
[127] A. Alavi-Harati, et al., KTeV, Phys. Rev. Lett. 84 (2000) 408.
[128] J. Ellis, N. Mavromatos, Comments on CP, T and CPT violation in neutral kaon decays, in: L.V. Telegdi, K. Winter (Eds.), Festschrift for L.B. Okun, Phys. Rep. 320 (1999) 341.
[129] C.O. Dib, B. Guberina, Phys. Lett. B 255 (1991) 113.
[130] V.L. Fitch, P.A. Piroue, R.B. Perkins, Nuovo Cimento 22 (1961) 1160.
[131] U. Camerini, et al., Phys. Rev. 128 (1962) 362.
[132] K.M. Case, Phys. Rev. 103 (1956) 1449.
[133] M.L. Good, Phys. Rev. 110 (1958) 550.
[134] F. Muller, et al., Phys. Rev. Lett. 4 (1960) 418;
R.H. Good, et al., Phys. Rev. 124 (1961) 1223.

[135] K.R. Schubert, et al., Phys. Lett. 31B (1970) 662.
[136] K. Winter, in: Proceedings of the International Conference on Elementary Particles, Amsterdam, North-Holland, Amsterdam, 1971, p. 333.
[137] see for instance G.B. Thomson, Y. Zou, Phys. Rev. D 51 (1995) 1412.
[138] J. Ellis, N.E. Mavromatos, D.E. Nanopoulos, Int. J. Mod. Phys. A 11 (1996) 1489.
[139] L. Lavoura, Mod. Phys. Lett. A 7 (1992) 1367.
[140] E. Shabalin, Phys. Lett. B 369 (1996) 335.
[141] E. Chell, M.G. Olsson, Phys. Rev. D 48 (1993) 4076.
[142] S. Hawking, Commun. Math. Phys. 87 (1982) 395.
[143] J. Ellis, J.S. Hagelin, D.V. Nanopoulos, M. Srednicki, Nucl. Phys. B 241 (1984) 381.
[144] H.-J. Gerber, Phys. Rev. Lett. 80 (1998) 2969.
[145] F. Benatti, R. Floreanini, Nucl. Phys. B 488 (1997) 355.
[146] F. Benatti, R. Floreanini, Phys. Lett. B 401 (1997) 337.
[147] W.H. Furry, Phys. Rev. 49 (1936) 393.
[148] C.J. Batty, Nucl. Phys. A 601 (1996) 425.
[149] R. Hanbury-Brown, R.Q. Twiss, Phil. Mag. 45 (1954) 633.
[150] G. Goldhaber, et al., Phys. Rev. Lett. 3 (1959) 181;
G. Goldhaber, et al., Phys. Rev. 120 (1960) 300.
[151] G. Cocconi, Phys. Lett. B 49 (1974) 459.
[152] G.I. Kopylov, M.Y. Podgoretskii, Sov. J. Nucl. Phys. 19 (1974) 215.